INFORMATION TO USERS

This manuscript has been reproduced from the microfilm master. UMI films the text directly from the original or copy submitted. Thus, some thesis and dissertation copies are in typewriter face, while others may be from any type of computer printer.

The quality of this reproduction is dependent upon the quality of the copy submitted. Broken or indistinct print, colored or poor quality illustrations and photographs, print bleedthrough, substandard margins, and improper alignment can adversely affect reproduction.

In the unlikely event that the author did not send UMI a complete manuscript and there are missing pages, these will be noted. Also, if unauthorized copyright material had to be removed, a note will indicate the deletion.

Oversize materials (e.g., maps, drawings, charts) are reproduced by sectioning the original, beginning at the upper left-hand corner and continuing from left to right in equal sections with small overlaps.

Photographs included in the original manuscript have been reproduced xerographically in this copy. Higher quality 6" x 9" black and white photographic prints are available for any photographs or illustrations appearing in this copy for an additional charge. Contact UMI directly to order.

Bell & Howell Information and Learning
300 North Zeeb Road, Ann Arbor, MI 48106-1346 USA
800-521-0600

Stochastic J-Integral and Reliability of Composite Laminates based on a Computational Methodology combining Experimental Investigation, Stochastic Finite Element Analysis and Maximum Entropy Method

Lakshmi Vara Prasad Pondugala

A thesis
in
The Department
of
Mechanical Engineering

Presented in Partial Fulfillment of the Requirements
for the
Degree of Master of Applied Science
at
Concordia University
Montreal, Quebec, Canada

June, 2000

Abstract

Stochastic J-Integral and Reliability of Composite Laminates based on a Computational Methodology Combining Experimental Investigation, Stochastic Finite Element Analysis and Maximum Entropy Method

L. Vara Prasad Pondugala

The present thesis concerns itself with the stochastic fracture behavior and the reliability of laminated composites. A computational approach combining the Stochastic Finite Element Method (SFEM), the Maximum Entropy Method (MEM), and experimental investigation has been developed. Using this approach, the fracture parameters including the Stress Intensity Factor (SIF), the Energy Release Rate (ERR) and the *J*-Integral have been determined based on the experimental data for the properties of the composite material. The material parameters and the fracture parameters have been quantified in terms of the respective mean values, the standard deviations, the coefficients of variation, and the true analytical probability distributions. For this purpose, the analytical distributions are obtained using the maximum entropy method. The fracture behavior of laminates made of the NCT 301 graphite-epoxy composite material has been studied and further, a parametric study encompassing the effects of the laminate configuration, the number of stochastic simulations, the geometrical parameters of the laminate, and the crack length has been conducted. Relevant design aspects are synthesized based on the parametric study. The significance of the *J*-Integral in more accurately describing and quantifying the stochastic characteristics of fracture behavior than the *ERR* and the *SIF* is established. The formulation for the reliability analysis for the probabilistic design of laminates has been developed based on the interference theory of mechanical reliability. The formulation has been applied for the case of stress-based fracture criterion and demonstrated for the orthotropic laminates made of NCT 301 graphite-epoxy composite material. For this purpose, the fracture toughness values of the orthotropic laminate are obtained from the in-plane fracture toughness tests using Single Edge Notched (SEN) tension specimens of the laminate. Aspects related to the reliability-based probabilistic design are highlighted. Further, the effects of loading on the reliability of the orthotropic laminates are evaluated.

To all those who have spent innumerable

hours of their valuable time

in research for the betterment and safety of all.

Acknowledgements

I wish to express my gratitude and indebtedness to my supervisor, Dr. Rajamohan Ganesan for his care, encouragement, guidance and devoting his valuable time for me always inspite of his busy schedule. I also wish to express here that Dr. Ganesan has been my constant source of inspiration for the past one and half years.

I would like to acknowledge the financial support provided by the Quebec Government (through FCAR program) and Concordia University (through FRDP program). I would like to sincerely thank them for their support. Further, I would also like to thank Prof. S.V.Hoa for his encouragement and interest. The facilities at the Concordia Center for Composites (CONCOM) have been extensively used in the experimental part of the present thesis.

I would like to thank my friend Zaki-ul Haque for his suggestions and help in manufacturing composite laminates. I wish to express my appreciation of Mr. John Elliott's time and his help in the present thesis. I also wish to thank Paul and Ming without whom the test wouldn't have been a success. The cooperation of the work-shop people – Brian and Alex is sincerely appreciated. I also wish to thank my roommates, Sam and Rama Raju, and my friends, Kiran, Krishan Mohan, Bobby, Bhanu, Hari, Jeet, Reddy, Ravi, Sanjeev, Sahambi and Vijay for their understanding and cooperation. I would also like to thank my friend, Devabhaktuni Vijaya K., for his valuable suggestions and patient discussions during the past two years.

Table of Contents

List of Tables

List of Figures

Nomenclature

SIF, K_I, K_{II}, K_{III}	Stress intensity factors (in various modes)
K_{IC}	Fracture toughness
ERR, G	Energy release rate
G_C	Critical value of the ERR
J_C	Critical value of the J-integral
θ	Measure of counter clockwise angle in degrees
σ	Normal stress
τ	Shear stress
r	Radial distance
a	Crack length
Π	Potential energy
E	Young's modulus
G_I	ERR in opening mode
ν	Poisson's ratio
μ	Shear modulus
U	Strain energy
J	J-integral value
Γ	J-integral contour
$\{\varepsilon\}$	Strain vector
$\{n\}$	Components of the unit vector
$\{u \quad v\}^t$, $\{d\}$	displacement vector

$K^{(e)}$	Element stiffness matrix
$[K]$	Global stiffness matrix
[B]	Strain-nodal displacement matrix
N_i	Shape functions
$\{\sigma\}$	Stress vector
$[E]$	Elasticity matrix
γ	Shear strain
$[J]$	Jacobian matrix of transformation
Re	Real part
[a]	Compliance matrix
$[T]$	Transformation matrix
[A]	Axial stiffness matrix
C_{aa}	Covariance matrix
$\{f\}$	Global load vector
R_{aa}	Auto-correlation function
R	Reliability
t_{ply}	Thickness of each ply
u, v, w	The displacement components
ξ, η, ζ	Local coordinate axes
x, y, z	Global coordinate axes
$E^{\cdot}$	Effective Young's modulus
S	Entropy
$f(x)$	Maximum entropy probability density function

λ_i	Lagrangian constants
m	Number of moments

Chapter 1

Introduction

1.1 Fracture Mechanics in Mechanical Design

The phenomenon of failure by catastrophic crack propagation in structural components poses problems in mechanical design and analysis. The fracture behavior of a mechanical component, structure or material will depend on the stress level, presence of a flaw, material properties, and the mechanism by which the fracture proceeds to completion [1]. The driving need for methods that quantify the effects of cracks on the mechanical component's performance has led to the evolution and development of fracture mechanics. The field of fracture mechanics was virtually nonexistent prior to World War-II. Applications of fracture mechanics in industry are at present relatively common, as knowledge that was once confined to a few specialists is becoming more widespread.

Cracks may exist in all mechanical components and structures as basic defects in materials or they may be induced during manufacturing or during service. Therefore a fundamental requirement in fracture mechanics is some reliable means of assessing the stability of such cracks. In this respect, the most significant advance has been the introduction of the Stress Intensity Factor (SIF) and the Strain Energy Release Rate (G) as parameters for characterizing the onset of crack propagation. Also, the *J*-contour integral has enjoyed great success as a fracture characterizing parameter for both linear and nonlinear materials. By idealizing the elastic-plastic deformation as nonlinear elastic deformation, Rice [2] provided the basis for extending the fracture mechanics

methodology well beyond the validity limits of Linear Elastic Fracture Mechanics (*LEFM*).

Over the last few decades or so, the Finite Element Method (FEM) has been firmly established as a standard computational method for the solution of practical fracture problems. However, unless extremely fine meshes are employed, problems arise in accurately modeling the singular stress field in the vicinity of the crack tip. Therefore in order to be able to apply the finite element method to the efficient solution of fracture problems, certain adaptations and further developments must be made [3]. These range from simple procedures for extrapolation of the crack tip stress intensity factors to the development of special crack elements, which model the complete crack zone stress field in anisotropic materials. In addition, the existing approaches, which are predominantly deterministic, have to be modified so as to incorporate the inherent randomness in material and geometric parameters and in loadings.

1.2 Fracture of Metals and Composites

Synthetic composites distinguish themselves from conventional materials such as metals, ceramics or polymers by the fact that they consist of two, or more, physically distinct and mechanically separable materials. They can be made by mixing the constituent materials in such a way that the dispersion of one material in the other can be done in a controlled way so as to achieve optimum mechanical properties. Because of their complex microstructure the individual events of failure and final fracture can be complex too [4]. Fracture of the individual phases in the composite material can take place separately,

sequentially or simultaneously, depending on the type of loading, the external testing conditions, the particular microstructure of the composite and other factors.

In recent years there has been a tremendous interest in the fracture behavior of polymers and composite materials [5]. One reason for this is the increasing use of polymers and composites in structural components in aircraft, automotive, sporting and other industries.

The characteristic behavior of composite materials and their response to a tensile or compressive loading, however, are substantially different from that of metals. Whereas in metals, damage development under static loading exhibits only one primary failure mode, which is the initiation and propagation of one single crack (which can be described with simple fracture mechanics tools), composite materials exhibit a combination of different failure modes. They are the initiation and multiplication (and not propagation) of cracks, including transverse, longitudinal and angle-ply cracks in the matrix along fibers, delaminations, fiber fracture and fiber/matrix interface debonding.

If the fracture of the composite laminates is considered from the point of view of Linear Elastic Fracture Mechanics (LEFM), the engineer will be concerned with two distinct aspects of design: (1) the prediction of the stress intensity factor, which depends on the applied stress in addition to the laminate configuration and specimen geometry; (2) the experimentally determined value of the critical stress intensity factor, which defines the onset of crack propagation as occurring when the stress intensity factor is equal or greater than the critical stress intensity factor.

Due to the different nature of composite materials, different from that of homogeneous isotropic materials, the stress analysis of composite structures is more complex [6-7] and inherently three-dimensional [8]. Due to the inherent complexities, no exact solution for most of the problems has been found and the finite element method is usually employed to provide numerical solutions.

1.3 Randomness in Fracture Behavior

The parameters of any mechanical or structural system possess a random variation as a function of space and/or time. The randomness in fracture parameters encompasses the uncertainties involved at the design and manufacturing stages, as well as the uncertain nature of the operating conditions. At the design stage, randomness is present in the test data regarding material strength values, elastic constants, engineering constants, damage parameters, and the material properties pertinent to the service life. The randomness in material properties significantly affects the functioning of the mechanical component and is unavoidable even with the best quality control measures.

Tests on a single material specimen or structure yield a definite value for each material parameter such as the elastic constant, engineering constant and damage parameter. But when a number of specimens are tested, (i) the parameter values randomly fluctuate from specimen to specimen, (ii) within the same structure itself, the values of any parameter display an uncertain spatial variation, (iii) due to environmental degradation the parameters have uncertain fluctuations. The sample to sample variation, spatial

fluctuations within the structure, structure to structure variations, and variations due to environmental effects in strength, deterioration, deformation and damage parameters of most of the present day engineering materials are random [9]. This is particularly the case with fiber reinforced composite materials. Variations in fiber size, fiber volume fraction, fiber orientation, void content, matrix properties, interfaces and thickness of lamina are always present and unavoidable. As a result, the elastic constants, engineering constants and deformation parameters of fiber reinforced composite materials possess a random variation [10].

1.4 Reliability-based Probabilistic design

During the past few years engineers and designers have been increasingly concerned with problems of mechanical design under parameter uncertainty and adequacy (reliability). Such concerns indicate that a critical re-evaluation of the foundation of mechanical design is needed. According to Freudenthal [11], "Careful and rigorous analysis may be largely deprived of their merits if the accuracy of results is diluted by the employment of empirical multipliers – selected rather arbitrarily on the basis of considerations not always rational or even relevant." Obviously, one needs to select some suitable measures of performance in order to be able to compare various technological improvements and to assess the performance of mechanical systems. One such measure of performance can be the reliability of the mechanical system. Reliability can be defined as, "*the capability of the product (or a system or a service) to perform the expected job under the specified conditions of use over an intended period of time.*"

The stochastic nature of the design variables is usually ignored in conventional practice, as is demonstrated by the efforts made to find out representative unique values such as minimum guaranteed values, limit loads or ultimate loads. The conventional approach in design process may be compared to a kind of worst-case analysis. The maxima of loading and the minima of strength are treated not only as representative of design situations, but also of simultaneous occurrence. This is the basis on which the unknown parameters are computed. The nature of the variability of nominal stress and of the stress factors that effect nominal strength, and of the strength factors that effect component strength, explains the existence of stress and strength distributions. The safety factor concept completely ignores the facts of variability that result in different reliabilities for the same safety factor.

Reasons for employing the probabilistic approach can be summarized as follows:

1) The variable nature of parameters – encountered in the practical situations.
2) Variability – the particular domain of probability theory and statistics.
3) The need for a rational approach in design and analysis.
4) The economy suggested by uniform reliability.

The practical results achieved by employing probabilistic methods in design are as follows:

1) It is possible to quantify the adequacy.
2) Results in optimum design by avoiding over-design.
3) Ensures uniform reliability.

1.5 Literature Review

The earliest recorded investigations into the phenomenon of fracture would appear to be Leonardo da Vinci's [12] study of the variation of failure strength in wires of different lengths and of the same diameter. This size effect was also studied in iron bars by Lloyd and Hodkinson [12] and also in glass rods and fibers by Anderegg [12]. Weibull [13] demonstrated using statistical techniques that these size effects were due to internal flaws in the material. The first attempt with a mathematical approach to fracture mechanics was by Inglis [12] in 1913. By analyzing the case of an elliptical hole in a plate under uniform tensile stress, he showed that the maximum stress occurs at the apex of the major axis. The results obtained by Inglis were rationalized by Griffith [12] who applied energy conservation principles to the case of a centrally cracked glass plate. Griffith's approach does not involve the distribution of stresses around the crack tip. Furthermore, the energy approach is strictly applicable to brittle materials only, but Irwin [13] and Orowan [14] have suggested extensions to Griffiths' expressions which account for limited plastic deformation in the vicinity of the crack tip.

Conventional fracture mechanics deals with homogeneous and isotropic materials and has been widely used because many of the practically useful materials belong to this category. The same is true, of course, for stress analysis in general, and most elasticity texts contain only a passing reference to anisotropy. The notable exceptions to this have been the works generated as a result of efforts to design load bearing structures made of wood [15]. The use of fiber reinforced composites to make laminates and also the design of plywood have produced a considerable literature and in particular the text by

Lekhnitskii [16] which employed a development of the well-known Muskhelishvili [17] complex-number form of stress function analysis to produce a wide range of solutions to problems of practical importance. In more recent times, many computer codes have been developed employing finite elements and boundary integrals, which will give solutions for anisotropic materials.

Fracture mechanics has been investigated in some details for wood [18] and found to be a very useful tool for design purposes. In spite of this, the use of fracture mechanics analysis for composites has been rather limited. In the early days, Chen [19] applied the finite-difference method to predict the stress field around an edge crack in unidirectional laminates under uniaxial tension. Lakshminarayana [7] presented a computationally efficient finite element model that can provide accurate numerical solutions to the problem of a semi-circular edge-notch in a finite size laminated composite plate under uniaxial tension. In his study cross-ply and angle-ply composite laminates were under consideration and the formulated element was based on the equivalent single layer two-dimensional theory.

The defects which may lead to premature delamination in composites may arise from microcracks and cavities formed during composite manufacturing or from in-service damage caused by impact loading. Extensive research has therefore been reported on the interlaminar fracture testing of various composite materials. The majority of the works [20-23] have been concerned with the delamination and the interlaminar fracture energy, G_c, of unidirectional laminates evaluated through the application of linear elastic fracture

mechanics. Whitcomb [24] performed a parametric study of postbuckled through-width deleminations on laminated coupons. In his study, a two dimensional finite element analysis was developed to calculate stress distributions and strain energy release rates for various delamination lengths, delamination depths, applied loads and lateral deflections.

In-service composite structures are susceptible to bolted joint failure where through-the-thickness cracks often develop in the laminate. Due to the complexity of the problem, efficient and accurate analysis techniques have not yet been fully developed. Analysis techniques have been proposed for predicting the failure of bolted connections in laminated composites [25-29]. A finite element analysis of single and two-hole bolted joints in fiber reinforced plastic was performed by Wong [30]. In his study, two dimensional plane stress four-node constant-strain quadrilateral elements are used to model pin-loaded laminated plates made of carbon fiber reinforced plastic (CFRP) and glass fiber reinforced plastic (GFRP) composites. Only one element has been used in the through-thickness direction, and further, the in-plane stresses in each ply have been obtained using laminate theory. Kurt and Paul [31] predicted bolt joint failure in generally orthotropic laminated composite plates which fail in the tension mode. The analysis is based on fracture mechanics concepts applied to a pseudo-flaw which is related to the physical cracking of the laminate at the joint.

Composite materials are extremely notch sensitive. The presence of cracks in structural components drastically reduces their load carrying capacity. For this reason, the issue of

predicting composite residual strength in the presence of stress enhancers such as cracks has been an important research problem in the composites community.

A vast amount of experimental literature is available on the notched strength behavior of different composite systems. Several strength-based and fractures mechanics-based models have been proposed in the literature to predict the notched response of composite laminates under uniaxial tensile loading. The popular models, e.g., those by Whitney and Nuismer [32], Waddoups *et al* [33], Pipes *et al* [34] and Karlak [35], etc. are based on a characteristic distance concept. These models have been successfully used to predict laminate strength in the presence of notches and holes. A comprehensive review of these models has been done by Awerbuch and Madhukar [36]. An alternative approach to predicting notched strength of a class of laminates is presented by Rajesh and Sun [37]. In their study, fracture behavior of fiber-dominated center-notched AS4/3501-6 graphite/epoxy laminates is investigated and the results indicate that a constant value of fracture toughness K_Q of a laminate, is an in-situ or effective material property. Guofang [38] describes and discusses experiments on the fracture strengths and crack propagation of some aligned fiber-reinforced materials. Aronsson and Backlund [39] predicted strength of composites with through-the-thickness cracks using a model called the Damage Zone Model (DZM). Failure strength and damage mechanisms of E-glass/epoxy laminates under in-plane biaxial compressive deformation have been investigated by Wang and Darrell [40].

In the field of fracture mechanics, the Stress Intensity Factor (SIF) is an important parameter for predicting fracture strength and fatigue lives. This factor contains information on the stress field, crack size and geometry of the cracked material. Analytical solutions for stress intensity factors of cracked finite bodies are not readily available and are often difficult to obtain. Thus numerical techniques e.g., the boundary element method, the finite element method, boundary collocation method are widely used in computing stress intensity factors. For isotropic materials, the necessary stress intensity factors for finite size sheets are often available from the literature. However, for orthotropic or composite materials, little is known about stress intensity factors for finite size laminates.

Many research efforts have focused on the calculation of stress intensity factor. One of the most important and efficient methods is based on the use of weight functions [2] to obtain the desired stress intensity factors. Lee [41] employed a finite element method with virtual crack extension technique to find the weight function of SIF for cracked composite laminates. Ruijia and Reddy [42] used the finite element alternating method to find out the stress intensity factors and weight functions for semi-elliptical cracks. The Boundary Force Method (BFM), a form of an indirect boundary element method, has been used by Tan and Bigelow [43] to analyze composite laminates that contain a hole and cracks to find out stress intensity factors. Nairn [44] used the shear-lag model to solve the crack tip stress concentrations in double-edge notch and center-notch unidirectional composites of finite width. From the stress-state solution, expressions are derived for strain energy release rate due to crack propagation through the fibers and due

to crack propagation parallel to the fibers. Case *et al* [45] presented an approximate analysis to predict the stress concentrations in composites containing a single fiber fracture. Crack tip stress intensity factor in finite anisotropic plates is analyzed by Snyder and Cruse [46]. The stress intensity factor and energy release rates are determined for cracked orthotropic sheets with riveted stiffeners by Yeh [47]. Mandell *et al* [48] calculated the stress intensity factor for single edge notched, double edge notched, and double cantilever beams. In their study, they were using a two-dimensional hybrid stress finite element analysis. Phillips [49] measured critical stress intensity factor and fracture surface energies for a series of [0/90] carbon fiber reinforced epoxy and carbon fiber reinforced glass composites. Victor and Efthimios [50] presented a simple, yet accurate, approach for the determination of the stress intensity factors in three-dimensional cracked anisotropic bodies modeled with quadratic isoparametric elements.

More sophisticated models for material behavior are being incorporated into fracture mechanics analyses. While plasticity was the important concern in the 1960s, more recent works have gone a step further incorporating time-dependent nonlinear behavior such as viscoelasticity and viscoplasticity. Fracture mechanics has been used (and sometimes abused) in the characterization of composite materials. Recent trends in fracture research suggest that there are two alternative approaches to fracture analysis: the energy criterion and the stress intensity approach. The energy approach suggests that crack extension (fracture) occurs when the energy available for crack growth is sufficient to overcome the resistance of the material. While Griffith [12] was the first to propose the energy criterion

for characterizing fracture, Irwin [14] is primarily responsible for developing the present version of this new approach.

Rice [2] applied deformation plasticity (i.e., nonlinear elasticity) to the analysis of a crack in a nonlinear material. He showed that the nonlinear energy release rate, *J*-integral, could be written as a path independent line integral. He further showed that the value of this integral is equal to the energy release rate in a nonlinear elastic body that contains a crack. Hutchinson [51], Rice and Rosengren [52] also showed that the *J*-integral uniquely categorizes crack tip stresses and strains in nonlinear materials. Read [13] has measured the *J*-integral in test panels by attaching an array of strain gages in a contour around the crack tip.

Many efforts were aimed at the estimation of the *J*-integral. McMeeking [53] proposed that the area under the load-deflection curve can be used to determine the *J*-integral in cracked elastic-plastic specimens under large scale yielding. New formulae have been suggested. The results of this method for a compact tension specimen have been found to be superior to those obtained from the well established Merkle-Corten [53] formula. Derbalian [54] put forth efficient analytical procedures for estimating the *J*-integral for characterizing the crack growth in inelastic conditions. Klepaczko [55] came up with a novel procedure for determining the critical value of the *J*-integral at high loading rates. This procedure provides a better understanding by means of a more accurate analysis of the frictional effects that occur between the loaded wedge and the Wedge-Loaded Compact Tension specimen (*WLCT*). In addition, a unique procedure has been developed

to measure the coefficient of Coulomb friction in the real environment of fracture K_{IC} or J_{IC} tests.

Over the past decade many researchers have come up with different methods for the evaluation of the *J*-integral for several standard models. Zahoor [56] came up with a *J*-integral solution for the compact tension specimen. While previously presented analyses were based on full ligament yielding, deeply cracked specimen or limit load, he derived a *J*-integral solution that does not require such assumptions. Zahoor [57] also derived formulae for evaluating the *J*-integral and crack-associated displacement for the case of a notched round bar in tension. The specialty of these formulae is that the *J*-integral can be evaluated from single load-displacement record obtained as a part of the fracture toughness test. Zahoor [58] further derived a *J*-integral solution for a three point bend specimen for the case when the crack length/plate width ratio (*a/W*) is greater than 0.2. He also presented a solution for normalizing the load-displacement curve. Lubarda [59] presented a simple representation of the energy release rate or the *J*-integral for the case of a two-dimensional crack subjected to elastic conditions. Precise estimates of the stress intensity factors for the Griffith and edge cracks have been made by using a convenient representation of the *J*-integral and asymptotic crack-tip fields, without recourse to the solutions of the corresponding boundary value problems. Joyce and Smudz [60] developed a common test method for fracture mechanics testing from which all the major fracture mechanics parameters could be evaluated based on a single test or a series of tests using one specimen geometry and the *J*-integral method. Faucher [61] developed equations to calculate the *J*-integral from the area under the load-displacement curve

obtained with center-cracked and double-edge-notched tension specimens. Analytical expressions were also derived to calculate the crack length from unloading compliance. Fracture testing on compact tension (CT) and three point bend (3PB) specimens is preceded by fatigue precracking. Nevertheless, crack front curvature was not taken into account in numerical modeling of fracture toughness testing procedures. Niksihkov, Heerens and Hellmann [62] performed elasto-plastic finite element analysis on CT and 3PB specimens with crack fronts of different curvatures and determined the *J*-integral. It has been observed that the variations in the crack front curvature that are within the limits specified by the test standards, to a certain extent effect the so-called η factor employed for the determination of the experimental value of the *J*-integral using the area under the force versus displacement curve. Apart from evaluating the fracture resistance of metals significant work has been done in the area of non-metals such as paper, nylon, etc. which have been used for other applications. Yuhara and Kortschot [63] developed a simplified method for evaluating the *J*-integral for paper sheets. Westerlind, Carlsson and Andersson [64] used the *J*-integral approach for characterizing the fracture toughness of liner board. Crouch and Huang [65] used the *J*-integral technique to characterize the toughness of two rubber toughned nylons under impact loading conditions.

The material parameters used for fracture mechanics analysis should be independent of size and geometry. This being the case, these parameters can be employed in the analytical and numerical investigations of cracked components. Roos and Eisele [66] determined the material characteristic values in elastic-plastic fracture mechanics by means of *J*-integral crack resistance curves. In this work special attention has been paid

to the transferability of the characteristic values from laboratory specimens to the real world structures.

Finite Element Method (FEM) is one of the most effective numerical analysis tools in the engineering and physical sciences. It is a widely accepted mathematical technique for the numerical solution of partial differential equations. The fundamental idea underlying this method is to replace the continuous function by a piecewise polynomial approximation. Tian and Swanson [67] conducted a finite element analysis to investigate the fracture behavior of carbon/epoxy laminates containing internal cut fibers. Ko [68]described finite element microscopic stress analysis of cracked composite systems. The cracked composite systems are modeled with triangular and trapezoidal ring finite elements using NASTRAN® finite element computer program. Heppler, Frisken and Hansen [69] employed a finite element analysis employing a high precision linear elastic fracture element to determine the stress intensity factors (Mode I) associated with a prescribed laminate and a given length-to-specimen width ratio (L/W) for rectangular specimen subjected to uniaxial tension loading with a center crack. They also investigated the mixed mode fracture of rectilinear anisotropic plates using higher order finite elements [70]. A finite element based micromechanical failure analysis was developed by Zhu and Sankar [71]. A compact finite element formulation based on singularity transformation is presented by Yeh [72] and is used to analyze the stress singularity at the boundary-layer of an interface between adjacent layers in a laminated composite. The composite is subjected to uniform axial extension in the plane of the layers. Chen and Yang [73] developed a simple yet efficient formulation for a symmetrically laminated composite

plate finite element and also adopted some highly efficient numerical algorithms using stand-alone desktop microcomputers for structural analysis and design. Nassehi *et al* [74] described a mathematical model for the analysis of the influence of interlayers on the stress distribution around cylindrical fibers. The model is based on the Galerkin finite element technique in conjunction with a penalty method. Thomas *et al* [75] presented a simple method for the analysis of fracture propagation in orthotropic materials based on finite element modeling. In their study, several theories of fracture propagation in anisotropic materials are reviewed with regard to their application to various materials. It is shown that isoparametric quarter-point elements can be used to obtain accurate stress intensity factors using orthotropic displacement correlation equations. Tasu and Plunkett [76] presented a finite element analysis of progressive failure for laminated FRP plates subjected to in-plane loading. In their paper the proper mesh size for this analysis model has been investigated and the ultimate strength of composite laminates is predicted and compared with published experimental results in order to demonstrate the validity of this finite element computational model.

A fundamental problem in predicting the failure of a laminated composite material is the determination of the load at which an existing crack will begin to propagate as well as the direction of crack growth. A number of theories have been proposed to predict the direction of crack growth in anisotropic materials. Among them are the tensor polynomial criterion [77], the minimum strain energy density criterion [78] and the normal stress ratio criterion [79]. Kadi and Ellyin [80] investigated the problem of predicting the crack extension behavior of a center-notched unidirectional graphite/epoxy coupon. The

material under investigation has been assumed to be elastic, homogeneous and anisotropic. They have also introduced a criterion based on the critical strain energy [81] to accurately predict the crack extension behavior in unidirectional composites within the elastic crack analysis.

The possibility of the application of Mode I and Mode II fracture mechanics to the characterization of the glass fiber/epoxy matrix interface has been studied by Krawczak and Pabiot [82]. Sih and Chen [83] applied the concept of fracture mechanics to analyze the brittle fracture of unidirectional composites. The analytical prediction has been based on the so-called S_c-theory. Gu [84] investigated the fracture behavior of continuous alumina fiber reinforced epoxy composites under compression at two different temperatures. Effects of fiber orientation, stacking sequence and temperature on failure mechanisms of the composite material are analyzed. William [85] introduced a failure criterion for composite materials based upon the strain invariant of finite elasticity.

Probabilistic modeling in conjunction with micromechanics fracture of composites is a promising approach for the prediction of failure and reliability characteristics of composites. It takes into account inevitable variations in properties of the constituents as well as the scatter of composite structural parameters. Ovchinskii [86], Stock, *et al* [87], and Fukuda [88] carried out the probabilistic analysis of composite strength and effective properties using the Monte Carlo simulation technique. The simulation procedure required extensive computational resources for any new set of structural parameters and properties of the constituents.

Composites have inherent scatter in elastic and strength properties. A probabilistic model utilizing random material characteristics to predict damage evolution in orthotropic laminated composites is presented by Dzenis *et al* [89], Joshi and Frantziskonis [90] and Larder [91]. A stochastic simulation model for the growth of multiple matrix cracks in composite laminates subjected to both static and fatigue loads is presented by Wang *et al* [92]. In their study the simulation model is based on the general concepts of the classical fracture mechanics in conjunction with an effective flaw distribution as a basic ply property. Cassenti [93] investigated the probabilistic static failure of composite materials. Probabilistic failure strength analysis of graphite/epoxy cross-ply composite laminates has been performed by Fukunaga and Chou [94]. This paper treats the failure characteristics of [0/90/0] and [90/0/90] cross ply laminates based upon the statistical strength analysis. The stress redistributions at the failure of the 90° ply are analyzed using a shear-lag model.

The well-known probabilistic theories for the tensile strength of unidirectional composites have been proposed by Rosen [95] and Zweben [96] and further developments have been reported in detail by different authors [97-101]. These models give us a satisfactory strength estimation when the composite failure is predominantly affected by the stochastic strength distribution of reinforcement fibers but are not suitable when there are other competing fracture micromechanisms.

The analysis of structures, whether subjected to random or deterministic external loads, has been developed mainly under the assumption that the structure's parameters are deterministic quantities. In a significant number of circumstances, this assumption is not valid, and the probabilistic aspects of the structure need to be taken into account. The necessity to account for random effects in determining the response of a mechanical system is due, in general, to three different sources: random external loadings, random boundary conditions, and random material parameters. In the last twenty years the powerful finite element method has undergone various new developments to incorporate these random effects, and is now termed as Stochastic Finite Element Method (SFEM). The developments in this field are reviewed by Contreras [102], Vanmarcke, *et al* [103], Benaroya and Rehak [104], Yamazaki, Shinozuka and Dasgupta [105], Ostoja-Starzewski [106], and Vanmarcke [107]. The stochastic finite element method is capable of dealing with random structural properties described by random fields very efficiently. Recent developments, such as the weighted integral technique [108-110], provide an accurate and consistent transition from continuous type random fields to discrete type stochastic finite elements.

Ramu and Ganesan [111] developed a new finite element method to analyze the structures with more than one parameter behaving in a stochastic manner using the Galerkin weighted residual method. The stochastic finite element analysis based on the local averages of random vector fields is formulated by Zhu, Ren, and Wu [112] for static, eigenvalue, and stress intensity factor problems. Jensen, and Iwan [113] presented a method for the dynamic analysis of linear systems with uncertain parameters to

stochastic excitation. Liu, Belytschko, and Mani [114] studied the application of the SFEM in elastic/plastic dynamics with random material properties in details. Ghanem, and Spanos [115] proposed a new method for the solution of problems involving material variability. The material property is modeled as a stochastic process. The method makes use of a convergent orthogonal expansion of the process. Ganesan, Sankar, and Ramu [116] developed a stochastic finite element method to solve the more general non-self-adjoint eigenvalue problems. Shinozuka, Kako, and Tsurui [117] developed a method for the estimation of the structural reliability when a structure is subjected to loads that can be idealized in terms of a Gaussian random vector process. Ramu and Ganesan[118] analyzed the free vibrational characteristics of a beam-column, which is having randomly varying Young's modulus and mass density and subjected to randomly distributed axial loading. In their study, Hamilton's principle is used to formulate the problem using stochastic FEM. Ren, Elishakoff, and Shinozuka [119] proposed a new version of finite element method for the mean and covariance functions of the displacement for bending of beams with spatially random stiffness based on the variational principles. Sankar, Ramu, and Ganesan [120] derived the sensitivities of SIF and COD of cracked structural systems to fluctuations in material property values and external loadings. In their study, a Taylor series expansion is used to express the SIF and COD in terms of averaged values. Sankar, Ramu, and Ganesan [121] described an effective method for integrating the concepts of probabilistic structural mechanics with the finite element analysis for dynamic systems.

The successful application of the mechanics of composites for achieving safer and reliable designs is hindered by the inherent uncertain distributions of material and geometric properties. In recent years, composite structures involving random material properties have been studied by many researchers. Among them Liaw and Yang [122] developed a 16-dof quadrilateral stochastic laminated thin-plate element and a solution procedure within the framework of stochastic finite element method. Ganesan and Hoa [123] presented the stress analysis of composite structures with stochastic parameters. Nakagiri, Takabatake, and Tani [124] presented a methodology of stochastic finite element method applied to the uncertain eigenvalue problem of linear vibration which arises from the fluctuation of the overall stiffness due to uncertain variation of the stacking sequence of composite laminates. Engelstad and Reddy [125] developed a probabilistic finite element analysis procedure for laminated composite shells. In their study, a total Lagrangian finite element formulation, employing a degenerated three-dimensional laminated composite shell element with the full Green-Lagrange strains and first-order shear deformable kinematics, is used. Chang and Yang [126] formulated a geometrically nonlinear stochastic thin-plate finite element to study the reliability of fiber-reinforced laminated plates with structural uncertainties under random in-plane loads. Slattery [127] developed a stochastic model of damage progression in unidirectional laminates of advanced composite materials. The modeling involves two steps: a micro-mechanical simulation of the degradation of a small cell of the composite and a random-damage finite element simulation of material failure.

Many efforts have been directed at devising a widely acceptable test method for obtaining the fracture toughness of composite materials. Unfortunately to this date a method could not be devised for the experimental determination of all composite materials. The measurement of valid plain strain fracture toughness values for particulate reinforced metal matrix composites (*MMCs*) is an important step in the process of developing useful products manufactured from these materials. With years of research, many researchers have reported values for the fracture toughness which show a considerable amount of scatter due to the problems with the test method or from variations in the micro-structures. Roebuck and Lord [128] have examined the procedures for plane strain fracture toughness tests on a number of particulate reinforced aluminum alloy metal matrix composites. Kageyama [129] came forth with a new method for evaluating the in-plane fracture toughness of carbon-epoxy composites. Interlaminar fracture is of serious concern in designing with fiber composites. Delaminations in composite laminates can exist as manufacturing flaws or can be created due to coalescence of small voids, foreign object impact or peculiar stress fields near edges, holes, joints and attachments. Sailendra [130] reported the results from approximate and exact stress analysis for elastic stress and displacement fields in two interlaminar mode-II fracture test specimens. End-notched flexure tests for laminates and interlaminar composites have also been studied in detail. Closed form solutions for energy release rates procedures have been suggested for fitting compliance versus delamination length data.

Precise knowledge of the dynamic fracture mechanics parameters for materials is essential for the fail-safe design of structural components subjected to rapid and/or impact loading. Although there exists standard test methods (ASTM E399; ASTM E813 – for metals/isotropic materials) for determining the fracture toughness parameters K_{IC} and J_{IC} under quasi-static loading, simple and reliable test procedures for characterizing such parameters under dynamic loading have not yet been established. Yokoyama [131] described a novel impact bend test procedure for determining the dynamic fracture initiation toughness, K_{Id}, at a loading rate (stress intensity factor rate), K_I, of the order of 10^6 MPa$\sqrt{m}$/sec. The dynamic stress intensity factor history for the bend specimen is evaluated by means of a dynamic finite element technique. Kumar, Hirth, Hoagland and Feng [132] suggested a test procedure for measuring the mixed mode I-III fracture toughness. A three-dimensional (3-D) finite element model of the modified compact specimen to validate the analytical procedure is also described. Ceramics have been applied to structural components such as gas turbine and reciprocal engines because of their lightweight and stability when compared to metals, particularly at high temperatures. Under such applications, they are often subjected to multi-axial stress states. Ono and Kaji [133] investigated a mixed-mode fracture of structural ceramics under bi-axial stress state by using an anticlastic bending test using the controlled surface flaw technique. This test enables the study of fractures under pure mode-I, pure mode-II or any combination of mode-I and mode-II loading. Shivakumar, Crews and Vishnu [134] developed a modified mixed-mode bending test apparatus to measure the delamination fracture toughness and fatigue delamination growth rates of laminated

composites. The new test apparatus is compact, lightweight and has very few attachments.

High temperature, high pressure reactor pressure vessels used in the petroleum refineries and/or nuclear power stations require a fracture–safe analysis for their safe operation as the materials used may suffer toughness degradation during service. Iwadate, Tanaka and Takemata [135] proposed a method for predicting the toughness degradation of Cr-Mo steels during long term service using the parameter such as the J factor. Empirical methods for predicting the fracture toughness, K_{IC}, and the transition curves of chemical pressure vessel steels have been presented. All fracture toughness specimens, be it for static or for dynamic testing, should have a fatigue crack of certain length formed in them prior to testing. This is to ensure a sharp crack ahead of the notch tip. Sriharsha, Anantharaman, Chatterjee, and Pandey [136] presented an interactive computer program that accepts material properties and specimen dimensions as program inputs. The output of the program when plotted graphically suggests an easy and practical precracking procedure adhering to the *ASTM* standards.

Studies on the reliability of the static strength of fibrous composites can be classified into three groups: 1) studies that investigate experimentally the factors that effect the variation or the scatter of the strength using a number of specimens, 2) studies that analyze the variation of the strength theoretically using micro-mechanical models, 3) studies that analyze the reliability of the strength of unidirectional and laminated composites using a macroscopic failure criterion and fundamental data on the variations of the strengths

along the principal directions. The strength and stiffness of composite materials change remarkably by changing the kinds, volume contents and orientations of the reinforcing fibers and stacking sequences. Therefore, the optimum material design can be performed under a given loading condition. Mitsunori, Yoshisada, Tetsuo and Shaowen [137] have presented a method to evaluate the reliability of unidirectional fibrous composites under any plane stress condition, and the effects of various factors on the reliability are investigated. It has been found that the orientation angle that results in the maximum reliability and the optimum angle that corresponds to the design criterion vary with the variation in the applied stress in some cases. It has been found that the optimum fiber orientations of unidirectional composite materials under probabilistic loading conditions are found to be different from those under deterministic loading conditions. Mitsunori, Yoshisada, and Tetsuo [138] also proposed a simple and intuitive method called the interior tangent ellipsoid (*ITE*) method for the optimum design of composites under the action of loads with variations. Shaowen, Mitsunori and Yoshisada [139] presented a discussion on the optimum design of multiaxially laminated fibrous composites under probabilistic conditions of loads and material conditions. The first-ply failure criterion is adopted for conducting the reliability analysis. Mitsunori, Yoshisada and Nobuhiko [140] have presented a discussion on the optimum fiber orientation angles of multiaxial laminates based on reliability analysis. The probabilistic properties of the applied loads and the elastic constants of the ply material are discussed from the viewpoint of reliability and optimum design. The effects of the correlation between various random variables on the reliability and reliability-based design of composite plates subjected to buckling have been discussed by Nozomu, Shaowen and Yoshisada [141], and the reliability has been

maximised in terms of the mean ply orientation angles. The study shows that reliability-based design ignoring correlation is sometimes less safe than even a deterministic buckling load maximization design when random variables are correlated. By viewing the composite lamina as a homogeneous solid whose directional strengths are random variables, Thomas and Wetherhold [152] proposed some physically plausible phenomenological rules for the redistribution of load after a lamina has failed within the confines of a laminate. Using a non-interactive criterion for demonstration purposes, laminate reliabilities are calculated assuming previously established load sharing rules for the redistribution of the load as the failure of the laminae occurs. Cohen [143] presented a composite vessel design approach that is based on the reliability and the probabilistic failure strength distribution concepts. This method is based on fiber strain-strength interference reliability theory. The fiber statistical strength distribution is analyzed using the Weibull distribution function.

1.6 Scope and Objectives of the Thesis

A better understanding of the fracture behavior of composite laminates leads to a reliable design and safer operation of mechanical components. This can be achieved if the fracture parameter employed in the design is capable of adequately and more accurately characterizing the fracture behavior of composite laminates. Since the randomness in the material and fracture properties is inherent and unavoidable, (i) the fracture behavior of composite laminates has to be quantified based on a stochastic approach, (ii) a methodology for quantifying the reliability of composite laminates has to be developed, (iii) this methodology should be able to take into account the test data on material and

fracture failure parameters and more importantly, the true probability distributions of these parameters, and be able to combine these with the stochastic finite element analysis of the laminates, and (iv) the fracture parameter employed in the design should be able to adequately and more accurately characterize the fracture behavior of composite laminates, incorporate the above mentioned inherent variability, and provide us with a reliable prediction of the fracture behavior.

From the literature survey, it can be observed that (a) research work that can identify and establish such a reliable design parameter has not so far been conducted, and (b) research work that can address the above mentioned objectives has not been conducted so far. The present thesis work considers the above-mentioned objectives. Three fracture parameters, viz., the stress intensity factor (as obtained directly from the stress distribution), the strain energy release rate, and the *J*-Integral, have been considered and evaluated for their suitability to serve as the fracture parameter that has the above mentioned capabilities. Based on a combined experimental and stochastic finite element analysis methodology, the fracture behavior of (i) cross-ply laminates, (ii) quasi-isotropic laminates, and (iii) symmetric angle-ply laminates has been studied and quantified in terms of the above mentioned fracture parameters. In addition, the effects of various geometric, ply material and composite structural parameters on the fracture behavior are quantified. The methodology for quantifying the reliability of composite laminates that has the above-mentioned capabilities has been developed.

The thesis work aims (1) to develop a combined experimental and stochastic finite element analysis methodology for the fracture analysis of composite laminates that also incorporates the true probability distributions of material and fracture parameters, (2) to develop the associated computer program using the MATLAB® software, (3) to employ the developed stochastic finite element methodology to evaluate the stochastic characteristics of the fracture parameters of composite laminates, (4) to relatively evaluate through a detailed parametric study the effects of ply sequence, fiber orientation in lamina, etc. on the probabilistic fracture behavior of various composite laminates, (5) to find out an effective design parameter that can act as a true representative of the stress variations developed in the laminate, and (6) to devise a method for computing the reliability of composite laminates based on the true probability distributions of both the stress intensity factor and the fracture toughness.

Based on the parametric study, many important aspects regarding the design and reliability of laminates are obtained. The fracture parameters considered are the stress intensity factor, the strain energy release rate, and the J-integral under in-plane tensile loading. The experimental part involves the testing of laminate specimens for obtaining the fracture toughness data. For this purpose a total of 42 specimens are manufactured and tested. As for the ply material properties, the test data that have previously been obtained [144] are used. The objective here is not to repeat the time-consuming tests, rather to develop further applications of the available test data. Based on the test data, the true probability distribution of the fracture toughness has been obtained, and hence the

reliability is calculated. The isoparametric formulation using 8-node quadratic serendipity element is employed in the finite element analysis.

1.7 Organization of the Thesis

The present chapter provides a brief introduction and a literature survey regarding the probabilistic fracture behavior of composite laminates that was studied using finite element method. The scope and the objectives of the thesis have been provided in section 1.5.

In chapter 2, the basic concepts and mathematical expressions that are employed in the linear elastic finite element fracture analysis of two-dimensional problems are presented and summarized. The 8-node isoparametric element is used to model the mechanical component. A computer program using the MATLAB® software, which can perform the fracture analysis of mechanical components made of isotropic materials is developed, described and demonstrated.

In the first half of chapter 3, the salient aspects of linear elastic fracture mechanics of anisotropic materials are summarized. The concepts and equations that are employed in the fracture analysis of anisotropic plates are presented. The classical lamination theory of composite materials is also described in this chapter. The computer program, which is developed in chapter 2, is extended for composite laminates so as to evaluate the equivalent elastic constants and the stress intensity factor. In the latter half of chapter 3, the aspects of probabilistic fracture analysis that incorporates the spatial variability of

material properties of composite laminates are described. The spatial variabilities are modeled as two-dimensional homogeneous stochastic fields [105]. Also the developed computer program is modified for calculating the mean value, standard deviation and coefficient of variation of the stress intensity factor and that of the energy release rate of cracked composite laminates. Example applications are provided.

In chapter 4, the parametric study, encompassing the effects of variabilities in the material properties on the fracture parameters of different composite laminates, is presented. Useful conclusions as to the probabilistic characteristics of the fracture of composite laminates and their behavior are provided.

In chapter 5, the detailed procedure of manufacturing and fracture testing of composite laminates to determine sample random values of the fracture toughness data is summarized. The Maximum Entropy Method (*MEM*) that is employed for obtaining the true probability distributions from a set of sample data is presented with all the analytical details. The mathematical formulation for calculating the reliability of the laminate using the true probability distributions of the stress intensity factor and fracture toughness that are obtained using the *MEM* has been described. Finally, the variation of the reliability with change in the applied load has been determined and presented.

The thesis ends with chapter 6, which provides the conclusions of the present thesis work and some recommendations for future work.

Chapter 2

LEFM of Isotropic Plates

2.1 Introduction

Cracks are present in all engineering structures. They may exist as basic defects in the constituent materials or they may be induced during the manufacturing or during the service life due to fatigue. In order to assess the stability of cracks, the most significant development in *Fracture Mechanics* has been the introduction of the fracture parameters such as the Stress Intensity Factor (*SIF*), the Energy Release Rate (*ERR*) and the *J*-integral. In order to use the above parameters in examining the stability of crack growth, one also needs to have a complete understanding of the stress and strain fields at the crack-tip. Unfortunately, closed form solutions exist only for very few basic and relatively simple cases and therefore, in order to apply fracture mechanics to practical situations, one needs to resort to numerical methods for approximate solutions.

The Finite Element Method (*FEM*) can be used to yield the most accurate solutions, however extremely fine meshes need to be used. Extrapolation techniques and use of special elements for modeling the singularity of the crack-tip also become inevitable. In the present thesis, the Linear Elastic Fracture Mechanics (*LEFM*) Theory has been used along with the *FEM*. The application to isotropic materials and composites for a deterministic case has been described in the present chapter. In this chapter the basic aspects of *LEFM* and the relevant finite element formulation have been described in

detail. The corresponding program codes have been developed in MATLAB® for evaluating various fracture parameters. Applications have been demonstrated through few benchmark problems and the results have been validated. The computer program and its flow-chart have been detailed in this chapter.

2.2 Linear Elastic Fracture Mechanics (*LEFM*)

A brief summary of the basic concepts, terminology used in *LEFM* and their definitions are discussed in this section. A crack of any size and shape present inside a body can deform into any shape that depends on the external load being applied.

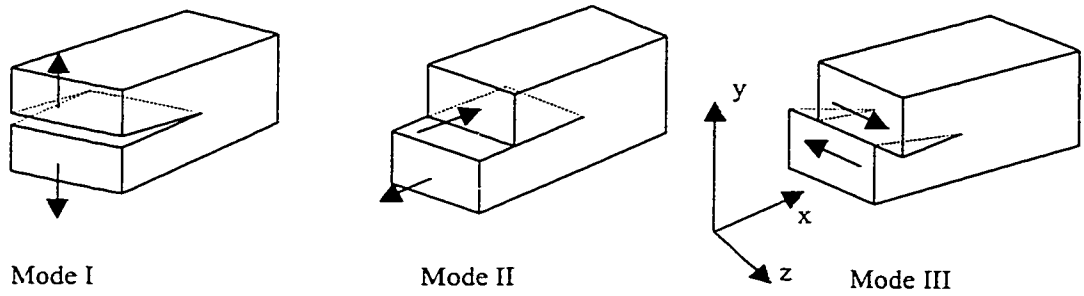

Figure 2.1 Modes of fracture failure

Opening Mode (Mode-I): In this mode, the two crack surfaces are pulled apart in the y-direction (a direction perpendicular to the surfaces of the crack) and the deformations are symmetric about the x-z and y-z planes.

Shearing Mode (Mode-II): In this mode, the two crack surfaces slide over each other in the x-direction and the deformations are symmetric about the x-y plane and skew-symmetric about the x-z plane.

Shearing Mode (Mode-III): In this mode, the crack surfaces slide over each other in the z-direction, and the deformations are skew-symmetric about the x-y and x-z planes.

While failure by fracture in mode-*I* is considerably dominant, the other two modes of fracture are less predominant. Even in composite materials, the most prominent mode of failure is by delamination, which is a kind of opening mode fracture failure. Hence, considerable attention has been paid to analytical and experimental determination of fracture parameters corresponding to mode-*I*. Though the modeling described in the present thesis can be extended to other modes of failure, the analyses and discussions are limited to mode-*I* type failure. A concise description of various fracture parameters is given below.

2.2.1 Stress Intensity Factor

The stresses at a point near the crack-tip, for an infinite plate with an edge-crack, subject to remote tensile stress can be represented as follows:

$$\sigma_x = \frac{K_I}{\sqrt{2\pi r}}\cos\left(\frac{\theta}{2}\right)\left[1-\sin\left(\frac{\theta}{2}\right)\sin\left(\frac{3\theta}{2}\right)\right] \tag{2.1}$$

$$\sigma_y = \frac{K_I}{\sqrt{2\pi r}}\cos\left(\frac{\theta}{2}\right)\left[1+\sin\left(\frac{\theta}{2}\right)\sin\left(\frac{3\theta}{2}\right)\right] \tag{2.2}$$

$$\tau_{xy} = \frac{K_I}{\sqrt{2\pi r}}\sin\left(\frac{\theta}{2}\right)\cos\left(\frac{\theta}{2}\right)\cos\left(\frac{3\theta}{2}\right) \tag{2.3}$$

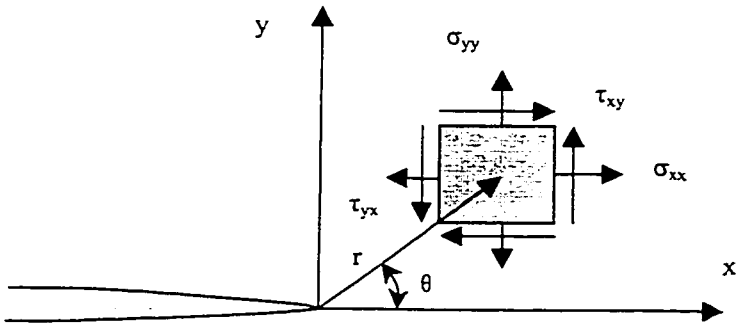

Figure 2.2 Stresses near the crack tip in an elastic material.

It can be observed that each stress component is proportional to a single parameter, K_I (the subscript, *I*, describes the mode of failure). If this parameter is known, the entire stress distribution around the crack-tip can be analytically determined with the help of the above closed form equations (2.1 – 2.3). This parameter completely characterizes the crack tip conditions in a linear elastic material, and is called the Stress Intensity Factor (*SIF*). The critical value of the *SIF* corresponding to the stresses at the crack tip at which the material failure occurs is called *Fracture Toughness*, K_{IC}. It is quite evident that the *SIF* is directly proportional to half the crack length, (a), and the stress component (σ) that tries to pull the crack faces apart (surface traction). Hence, the *SIF* can be written as

$$K_i = f(\sigma, a) \quad ; \quad i = I, II, III \tag{2.4}$$

The *SIF* for the above-described plate can be expressed as

$$K_I = \sigma\sqrt{\pi a} \quad ; \quad a \text{ is the crack length} \tag{2.5}$$

Failure occurs when the *SIF* equals the *Fracture Toughness*. K_I can be interpreted as the driving force for the crack propagation and K_{IC} as the resisting force for the crack growth. The K_{IC} is a basic material property and is independent of the geometry of the plate.

2.2.2 Strain Energy Release Rate

The energy approach states that the fracture occurs when the energy available for crack growth is sufficient to overcome the resistance of the material, which might be associated with the surface energy, plastic work, or any other type of energy dissipation associated with the propagating crack. For a linear elastic material, the *Energy Release Rate (ERR)* is defined as the rate of change of potential energy with the crack area. For an infinite

plate with a central crack of length $2a$ subjected to remote tensile stress, the *ERR* is given by

$$G_i = -\frac{d\Pi}{dA} = \frac{\pi\sigma^2 a}{E} \qquad ; \qquad i = I, II, III \tag{2.6}$$

where Π is the potential energy which is the sum of the internal strain energy and the work done by external forces, dA is the incremental increase in crack area, E is the Young's modulus, σ is the remotely applied stress and a is the half crack length. At fracture, $G_I = G_C$ in which G_C denotes the *critical ERR* obtained by the critical combination of stress and crack size at failure (denoted by σ_f and a_c respectively), given by

$$G_C = \frac{\pi\sigma_f^2 a_C}{E} \tag{2.7}$$

Using the same analogy as for *SIF*, G signifies the crack driving force whereas G_C denotes the material's resistance to fracture.

2.2.2.1 Relation between *SIF* and *ERR*:

For any structure, the *SIF* is related to the *ERR*, this relation being unique for each mode of failure. For mode-I type of failure, the *ERR* and *SIF* are related by

$$G_I = \frac{(\kappa+1)}{8\mu} K_I^2 \qquad where\ \kappa = \begin{cases} \dfrac{(3-\nu)}{(1+\nu)} & for\ plane\ stress \\ (3-4\nu) & for\ plane\ strain \end{cases} \tag{2.8}$$

in which ν represents the Poisson's ratio and μ represents the shear modulus of the material. Similarly, the relation between *SIF* and *ERR* for other modes of failure are given by replacing in equation (2.8) the respective modes of G_i and K_i. Whenever a

failure by fracture is a combination of two or more modes, the resulting *ERR* is just a sum of the *ERR*s in the constituent modes. Hence, for a mixed-mode fracture

$$G = \Sigma G_i \qquad ; \qquad i = I, II, III \tag{2.9}$$

2.2.3 The *J*-contour Integral

The *J*-contour integral has enjoyed great success as a fracture parameter for both linear as well as nonlinear materials. By idealizing elastic-plastic behavior as nonlinear elastic, the basis has been provided [145] for extending the fracture mechanics methodology well beyond the validity limits of *LEFM*. By applying the deformation plasticity theory (nonlinear elasticity) to nonlinear materials, Rice [145] showed that the nonlinear *ERR*, *J*, could be written as a path-independent integral. It has also been shown that the *J*-integral uniquely characterizes the crack tip stresses and strains in nonlinear materials. Thus the *J*-integral can be viewed as both an energy, as well as a stress intensity parameter.

2.2.3.1 Nonlinear Energy Release Rate, *J*

Rice [145] presented a path independent contour integral for the analysis of cracks. He showed that the value of this integral (which he termed as *J*), is equal to the *ERR* in a nonlinear elastic body that contains a crack. Equation (2.6) defines the *ERR* for linear materials. The same definition holds for nonlinear elastic materials, except that G is replaced by J:

$$J = -\frac{d\Pi}{dA} \tag{2.10}$$

where Π is the potential energy and A is the crack area. The potential energy Π is given by

$$\Pi = U - F \tag{2.11}$$

where U is the strain energy stored in the body and F is the work done by the external forces.

The *ERR*, denoted by G, is normally defined as the potential energy that is released from a structure when the crack grows in an elastic material. However, much of the strain energy absorbed by an elastic-plastic material is not recovered when the crack grows or the specimen is unloaded; a growing crack in an elastic-plastic material leaves a plastic wake as shown in Figure 2.3.

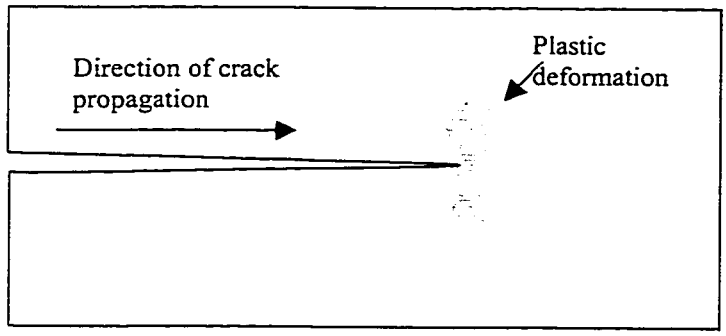

Figure 2.3 Crack growth leaving a plastic wake in an elastic-plastic material

Thus, the energy release rate concept has a different interpretation for elastic-plastic materials. Rather than defining the energy released from the body when the crack grows, Equation (2.10) relates J to the difference in energy *absorbed* by the structure with neighboring crack sizes.

2.2.3.2 *J* as a Path-Independent Line Integral

Consider an arbitrary counter-clockwise path (Γ) around the tip of a crack as shown in Figure 2.4. The J integral is given by [145]

$$J = \int_{\Gamma}\left(U\,dy - \mathrm{T}_i \frac{\partial u_i}{\partial x} ds \right) \tag{2.12}$$

in which U is the strain energy density

T_i is the traction vector

u_i is the displacement vector

ds an element of arc along the integration contour, Γ.

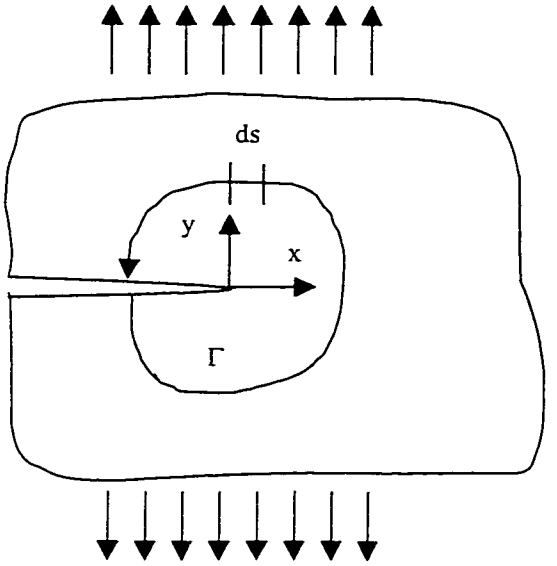

Figure 2.4 Arbitrary contour path for the J-integral

In the above, the strain energy density is defined as

$$U = \int_0^{\varepsilon_{ij}} \sigma_{ij}\, d\varepsilon_{ij} \tag{2.13}$$

where σ_{ij} and ε_{ij} are the stress and strain tensors respectively. The traction vector, T_i is a stress vector normal to the contour, representing the normal stresses acting on the boundaries of the free body diagram of the material inside the contour. The components of the traction vector are given by,

$$T_i = \sigma_{ij} n_j \tag{2.14}$$

where n_j represents the components of the unit vector normal to the contour, T_i at any point. Rice [145] showed that the value of the J integral is independent of the path of integration around the crack. Thus, the J integral is called as a path-independent integral.

It can be seen from Figure 2.4 that, as the contour Γ shrinks to a small portion around the crack tip (Γ_c), the second term in equation (2.12) reduces to zero and the equation can be expressed as

$$J = \int_{\Gamma_c} U \, dy \tag{2.15}$$

Thus J characterizes the energy stored at the crack tip and, due to the path-independence of J, the integral of equation (2.12) can be evaluated along a contour remote from this zone of singular behavior.

2.2.3.3 *J* as a Stress Intensity Parameter

For linear elastic situations and for each particular mode of deformation it can be shown that

$$G = J \tag{2.15}$$

Therefore, equation (2.8) can be rewritten as

$$J = \left(\frac{\kappa + 1}{8\mu}\right) K_i^2 \qquad ; \qquad i = I, II, III \tag{2.16}$$

In terms of the J integral the *SIF* for mode-I can be expressed as

$$K_I = \sqrt{\frac{8\mu J}{(1+\kappa)}} \tag{2.17}$$

2.3 Finite Element Formulation

In the following sub-sections, a description of all the relevant details of the finite element formulation for determining the parameters, *SIF*, *ERR* and *J*-integral, will be presented. The methods employed and the parameters that can be obtained form each of the methods are:

- Displacement Extrapolation Method : *SIF*
- Energy Release Rate Method (*ERRM*) : *ERR*, *SIF*
- J-Integral Method : *J* integral, *SIF*

2.3.1 Displacement Extrapolation Method

The analytical expressions for displacement variation along radial lines emanating from the crack tip are given by [3]

$$u = \frac{K_I}{4\mu}\sqrt{\frac{r}{2\pi}}\left[(2k-1)\cos\frac{\theta}{2} - \cos\frac{3\theta}{2}\right] - \frac{K_{II}}{4\mu}\sqrt{\frac{r}{2\pi}}\left[(2k+3)\sin\frac{\theta}{2} - \sin\frac{3\theta}{2}\right] \tag{2.18}$$

$$v = \frac{K_I}{4\mu}\sqrt{\frac{r}{2\pi}}\left[(2k+1)\sin\frac{\theta}{2} - \sin\frac{3\theta}{2}\right] + \frac{K_{II}}{4\mu}\sqrt{\frac{r}{2\pi}}\left[(2k-3)\cos\frac{\theta}{2} + \cos\frac{3\theta}{2}\right] \tag{2.19}$$

in which u and v represent the displacements along the x and y coordinate directions, K_I and K_{II} represent the *SIF*s for mode-*I* and mode-*II* failures respectively, μ is the shear modulus of the material, r is the radial distance of any point from the crack tip, k is a constant defined by equation (2.8) and θ is the polar angle between the x-axis and the line

obtained by joining the point to the crack tip. Simplifying the equations for the stress intensity factors, K_I and K_{II}, one gets

$$K_I \begin{bmatrix} (2k-1)\cos\frac{\theta}{2} - \cos\frac{3\theta}{2} \\ (2k+1)\sin\frac{\theta}{2} - \sin\frac{3\theta}{2} \end{bmatrix} = 4\mu\sqrt{\frac{2\pi}{r}}\begin{Bmatrix} u \\ v \end{Bmatrix} \tag{2.17}$$

$$K_{II} \begin{bmatrix} -(2k+3)\sin\frac{\theta}{2} - \sin\frac{3\theta}{2} \\ (2k-3)\cos\frac{\theta}{2} + \cos\frac{3\theta}{2} \end{bmatrix} = 4\mu\sqrt{\frac{2\pi}{r}}\begin{Bmatrix} u \\ v \end{Bmatrix} \tag{2.18}$$

Substituting for the values of r and the values of u or v obtained by finite element analysis (*FEA*), for the nodal points along a radial line emanating from the crack tip, a plot for K_I and K_{II} versus r can be obtained.

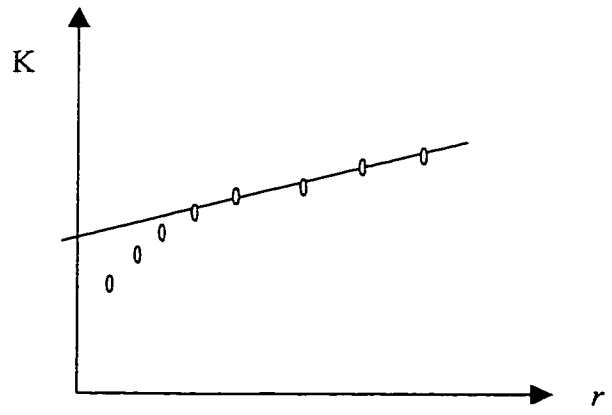

Figure 2.5 Evaluation of *SIF* by displacement extrapolation

Due to some non-linearity in the zone near the crack-tip, a few points in the plot

that are close to the crack tip can be neglected and the rest of the points obtained can be used for extrapolation. In the present case, θ was considered to be 180° and further, the *edge* nodal points (not the mid-side nodes) were used for extrapolation to the crack tip at $r = 0$. Both the conventional eight-node isoparametric elements as well as the quarter-point crack-tip singularity elements were used.

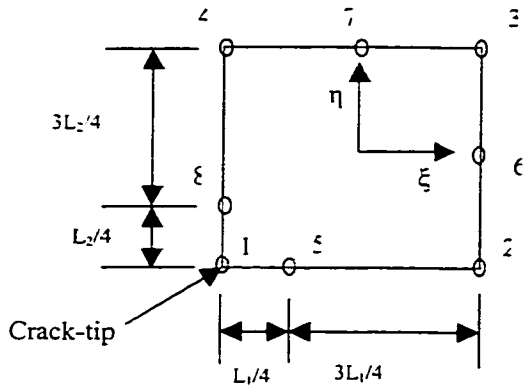

Figure 2.6 Quadratic isoparametric element with mid-side nodes at quarter points

The *SIF*s for the quarter-point quadratic isoparametric element are given by [3]

$$K_I \begin{bmatrix} (2k-1)\cos\frac{\theta}{2} - \cos\frac{3\theta}{2} \\ (2k+1)\sin\frac{\theta}{2} - \sin\frac{3\theta}{2} \end{bmatrix} = 4\mu\sqrt{\frac{2\pi}{L_1}} \begin{Bmatrix} 4u_5 - u_2 - 3u_1 \\ 4v_5 - v_2 - 3v_1 \end{Bmatrix} \tag{2.19}$$

$$K_{II} \begin{bmatrix} -(2k+3)\sin\frac{\theta}{2} - \sin\frac{3\theta}{2} \\ (2k-3)\cos\frac{\theta}{2} + \cos\frac{3\theta}{2} \end{bmatrix} = 4\mu\sqrt{\frac{2\pi}{L_1}} \begin{Bmatrix} 4u_5 - u_2 - 3u_1 \\ 4v_5 - v_2 - 3v_1 \end{Bmatrix} \tag{2.20}$$

in which L_1 represents the length of the edge 1-5-2. Using this element the stress singularities at the crack tip can be modeled, which is an advantage over using conventional elements in the finite element formulation.

2.3.2 Strain Energy Release Rate Method

Consider a crack of initial length a, which advances by an incremental amount δa, and thereby causing a release of strain energy δU. The *ERR* can be defined as,

$$G = \frac{\delta U}{\delta a} = \frac{U_2 - U_1}{a_2 - a_1} \tag{2.21}$$

in which the thickness is assumed to be unity and the crack is idealized to extend uniformly through the thickness. The *SIF* is related to the *ERR* by equation (2.8). The *ERR* is obtained by conducting two finite element analyses on a structure, the first time with the initial crack (*ERR* is equal to U_1, say) and the second analysis with a small increment δa in the crack length (*ERR* is equal to U_2, say). The strain energy released can be calculated from equation (2.21) and hence the *SIF* from equation (2.8). The strain energy in the two configurations can be evaluated as

$$U = \{d\}^t [K] \{d\} \tag{2.22}$$

or according to

$$U = \{d\}^t \{b\} \tag{2.23}$$

in which $\{d\}$, $[K]$ and $\{b\}$ represent the displacement vector, the global stiffness matrix and the global applied loading vector respectively.

2.3.3 J-Integral Method

The nonlinear energy release rate denoted by J and given by equation (2.12) is evaluated numerically along a contour selected according to the convenience of computation. In the present thesis, the path has been selected such that it always coincides with $\xi = \xi_p =$ constant, as shown in the figure below.

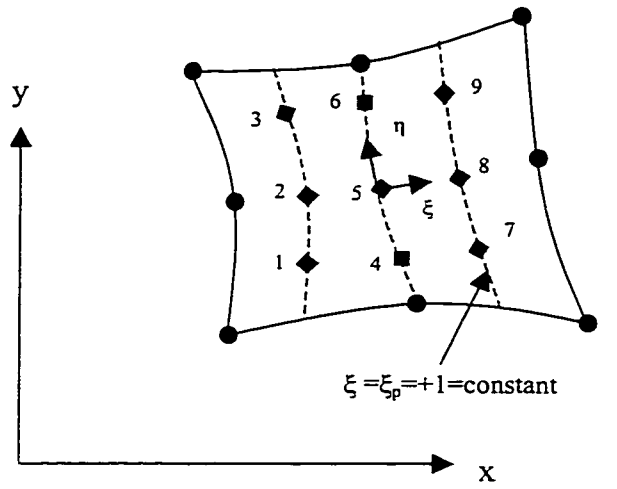

Figure 2.7 Gauss point numbering sequence

The first step in the numerical computation of the *J*-integral is to define the unit normal *n* to the contour Γ shown in Figure (2.4). In order to do this, two vectors A and B have been defined along ξ = *constant* and η = *constant*, and are given by

$$A^T = \left[\frac{\partial x}{\partial \eta}, \frac{\partial y}{\partial \eta}, 0\right] \quad ; \quad B^T = \left[\frac{\partial x}{\partial \xi}, \frac{\partial y}{\partial \xi}, 0\right] \tag{2.24}$$

The cross product of the vectors *A* and *B* gives the unit vector that is normal to these two vectors which is perpendicular to the plane of the element. This vector is given by

$$C^T = \left[0, 0, \left(\frac{\partial x}{\partial \eta}\frac{\partial y}{\partial \xi} - \frac{\partial y}{\partial \eta}\frac{\partial x}{\partial \xi}\right)\right] \tag{2.25}$$

Now, the vector normal to the contour Γ which is along the curve defined by ξ= *constant* is obtained by the cross product between vectors *C* and *A*, which is

$$D = CxA = \begin{Bmatrix} \frac{\partial y}{\partial \eta}\left(\frac{\partial y}{\partial \eta}\frac{\partial x}{\partial \xi} - \frac{\partial x}{\partial \eta}\frac{\partial y}{\partial \xi}\right) \\ \frac{\partial x}{\partial \eta}\left(\frac{\partial x}{\partial \eta}\frac{\partial y}{\partial \xi} - \frac{\partial y}{\partial \eta}\frac{\partial x}{\partial \xi}\right) \\ 0 \end{Bmatrix} = \begin{Bmatrix} D_1 \\ D_2 \\ 0 \end{Bmatrix} \tag{2.26}$$

Now, the unit vector is given by

$$n^T = [n_1 \quad n_2 \quad 0] = \left[\frac{D_1}{N} \quad \frac{D_2}{N} \quad 0\right] \quad ; \quad N = \sqrt{D_1^2 + D_2^2} \tag{2.27}$$

The elemental arc length, *ds* along the curve ξ=*constant* is given by

$$ds = \sqrt{dx^2 + dy^2} = \left\{\sqrt{\left(\frac{\partial x}{\partial \eta}\right)^2 + \left(\frac{\partial y}{\partial \eta}\right)^2}\right\} d\eta \quad ; \quad dy = \frac{\partial y}{\partial \eta} d\eta \tag{2.28}$$

For plane stress and plane strain cases, the strain energy density is given by

$$U = \left(\frac{1}{2}\right)\left[\sigma_{xx}\varepsilon_{xx} + 2\sigma_{xy}\varepsilon_{xy} + \sigma_{yy}\varepsilon_{yy}\right] \tag{2.29}$$

The traction vector T_i is given by,

$$T_i = \begin{Bmatrix} \sigma_{xx} n_1 + \sigma_{xy} n_2 \\ \sigma_{xy} n_1 + \sigma_{yy} n_2 \\ 0 \end{Bmatrix} \tag{2.30}$$

and $$\left[\frac{\partial u}{\partial x}\right]^t = \begin{Bmatrix} \frac{\partial u}{\partial x} & \frac{\partial v}{\partial x} & 0 \end{Bmatrix} \tag{2.31}$$

in which $$\frac{\partial(u,v)}{\partial x} = \sum_{i=1}^{n} \frac{\partial N_i^{(e)}}{\partial x}(u_i, v_i) \quad ; \quad \frac{\partial(u,v)}{\partial y} = \sum_{i=1}^{n} \frac{\partial N_i^{(e)}}{\partial y}(u_i, v_i) \tag{2.32}$$

where u_i and v_i are displacement components of the n nodes in the element. Substituting equations (2.27) through (2.31) in equation (2.12), one finally gets

$$J^{(e)} = \int_{-1}^{+1} \left\{ \begin{aligned} &\frac{1}{2}\left(\sigma_{xx} \frac{\partial u}{\partial x} + \sigma_{xy}\left(\frac{\partial u}{\partial y} + \frac{\partial v}{\partial x} \right) + \sigma_{yy} \frac{\partial v}{\partial y} \right) \\ &- \left[\begin{aligned} &\left(\sigma_{xx} n_1 + \sigma_{xy} n_2\right) \frac{\partial u}{\partial x} \\ &+ \left(\sigma_{xy} n_1 + \sigma_{yy} n_2\right) \frac{\partial v}{\partial x} \end{aligned} \right] \sqrt{\left(\frac{\partial x}{\partial \eta}\right)^2 + \left(\frac{\partial y}{\partial \eta}\right)^2} \end{aligned} \right\} d\eta = \int_{-1}^{+1} I \, d\eta \tag{2.33}$$

The numerical integration is achieved by

$$J^{(e)} = \sum_{q=1}^{NGAUS} I(\xi_p, \eta_q) W_q \tag{2.34}$$

in which *NGAUS* represents the order of Gaussian numerical integration and I is as described in equation (2.32), and is evaluated at the Gaussian sampling

points ξ_p and η_q, and W_q is the weighting factor corresponding to η_q. The J-integral is obtained by accumulating the contributions from all sampling points by equation (2.34) from the path ξ_p=constant through all the neighboring elements around the crack tip. This places restrictions on both the finite element mesh and the order of nodal numbering the elements through which the *J* contour(s) is to pass.

2.4 Finite Element Formulation of Isoparametric Elements

Most of the work in the present thesis has been limited to two-dimensional situations. Initially three-dimensional modeling has been done for the case of an isotropic material, in which twenty-node isoparametric elements have been used. But later on, the work has been limited to two dimensions and further, eight-node isoparametric elements have been used. All the relevant details regarding the 2-*D* and 3-*D* elements will be discussed in the following sub-sections.

2.4.1 The Eight-node Isoparametric Element

The internal nodes of an element do not contribute to the element connectivity. So, they can be condensed out and this helps in reducing the size of the stiffness matrices. These elements in which there are no internal nodes, are called serendipity elements.

The interpolation or shape functions for this element with local coordinates, ξ and η can be calculated [146] using the boundary conditions that any shape function, N_i equals one at node *i* and equals zero elsewhere i.e.,

$$N_i = \begin{cases} 1 & ; \quad i = i \\ 0 & ; \quad elsewhere \end{cases} \tag{2.35}$$

The nodal numbering and local co-ordinate system used for the present element are represented below.

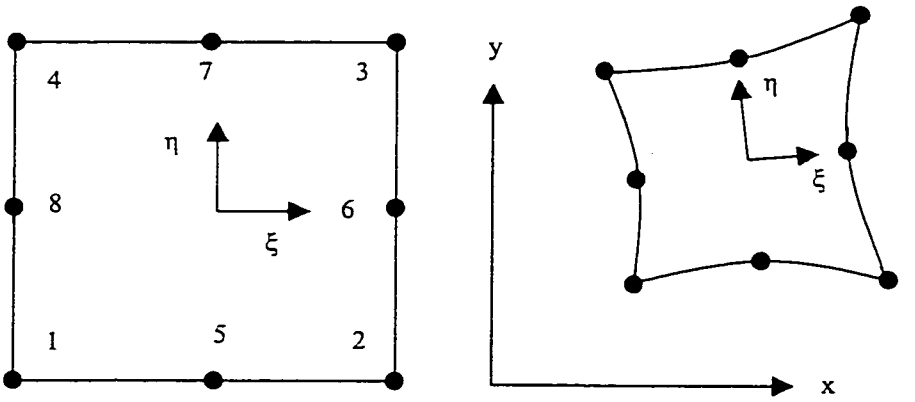

Figure 2.8 (a) Parent Element (b) Global Element

The shape functions for the eight-node element, which is used in the two-dimensional finite element analysis can be concisely presented as

$$N_i = \begin{cases} \frac{1}{4}(1+\xi\xi_i)(1+\eta\eta_i)(\xi\xi_i+\eta\eta-1) & ; \quad i=1,2,3,4 \\ \frac{\xi_i^2}{2}(1+\xi\xi_i)(1-\eta^2)+\frac{\eta_i^2}{2}(1+\eta\eta_i)(1-\xi^2) & ; \quad i=5,6,7,8 \end{cases} \tag{2.36}$$

2.4.1.1 Plane-Stress Case

This is the state of biaxial stress in a body in which the effect of the smallest dimension (usually called the thickness) is negligible. Hence, the stresses along the direction of the

thickness can be ignored. Considering only the x and y directions, the displacements and the strains can be expressed as

$$\{u\}=\begin{Bmatrix} u \\ v \end{Bmatrix} \quad and \quad \{\varepsilon\}=\begin{Bmatrix} \varepsilon_x \\ \varepsilon_y \\ \gamma_{xy} \end{Bmatrix} \tag{2.37}$$

respectively, in which

$$\{\varepsilon_x\}=\frac{\partial u}{\partial x} \quad ; \quad \{\varepsilon_y\}=\frac{\partial v}{\partial y} \quad ; \quad \{\gamma_{xy}\}=\frac{\partial u}{\partial y}+\frac{\partial v}{\partial x} \tag{2.38}$$

The stresses and strains are related by

$$\{\sigma\}=[E]\{\varepsilon\} \tag{2.39}$$

in which the matrix representing the stresses is given by

$$\{\sigma\}=\begin{Bmatrix} \sigma_x \\ \sigma_y \\ \tau_{xy} \end{Bmatrix} \tag{2.40}$$

For linear elastic conditions, the elasticity matrix (also called as the constitutive matrix or the stress-strain matrix), relating the strains to the stresses is given by

$$[E]=\frac{E}{(1-\nu^2)}\begin{bmatrix} 1 & \nu & 0 \\ \nu & 1 & 0 \\ 0 & 0 & \dfrac{(1-\nu)}{2} \end{bmatrix} \tag{2.41}$$

in which E and ν are the Young's modulus and the Poisson's ratio respectively.

2.4.1.2 Plane Strain Case

The plane strain stress state occurs in components where the thickness is quite

comparable to the other dimensions. Though the body is subjected to loads in a certain plane (say, x-y plane), the effect of the thickness on the stresses induced is quite considerable. Due to the Poisson effect, the out-of-plane normal stress is not zero even though the out-of-plane strain is zero.

For the case of plane strain one has the condition that $\varepsilon_{zz} = \gamma_{yz} = \gamma_{xz} = 0$ and hence the out-of plane normal stress is obtained as

$$\begin{aligned} \varepsilon_{zz} &= \frac{1}{E}\left[\sigma_{zz} - \nu\left(\sigma_{xx} + \sigma_{yy}\right)\right] = 0 \\ \Rightarrow \sigma_{zz} &= \nu\left(\sigma_{xx} + \sigma_{yy}\right) \end{aligned} \tag{2.42}$$

It should be noted that the normal stress $\sigma_{zz} \neq 0$ even though the corresponding normal strain $\varepsilon_{zz} = 0$. Using the value of σ_{zz} given by the equation (2.42), one gets

$$\varepsilon_{xx} = \frac{1}{E}\left[\sigma_{xx} - \nu\sigma_{yy} - \nu^2\left(\sigma_{xx} + \sigma_{yy}\right)\right] \tag{2.43}$$

$$\varepsilon_{yy} = \frac{1}{E}\left[\sigma_{yy} - \nu\sigma_{xx} - \nu^2\left(\sigma_{xx} + \sigma_{yy}\right)\right] \tag{2.44}$$

$$\gamma_{xy} = \frac{\tau_{xy}}{G} \tag{2.45}$$

$$\varepsilon_{zz} = 0 \tag{2.46}$$

Thus the elasticity matrix for the plane strain case is given as

$$[D] = \frac{E(1-\nu)}{(1+\nu)(1-2\nu)}\begin{bmatrix} 1 & \frac{\nu}{(1-\nu)} & 0 \\ \frac{\nu}{(1-\nu)} & 1 & 0 \\ 0 & 0 & \frac{(1-2\nu)}{2(1-\nu)} \end{bmatrix} \tag{2.47}$$

2.4.2 Twenty-node Isoparametric Element

The shape functions and the co-ordinate system for the twenty-node three dimensional isoparametric solid element are as represented below:

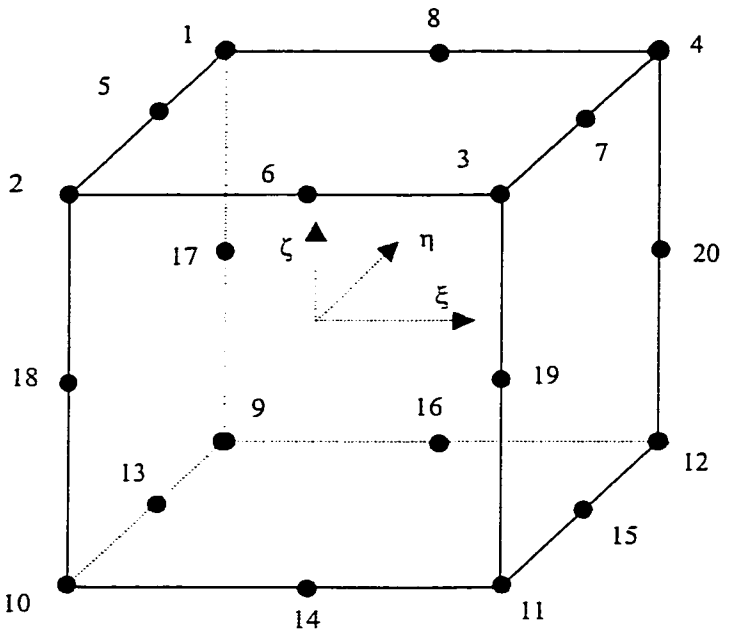

Figure 2.9 Twenty-node 3-D isoparametric solid element

Due to the following advantages of this particular element over other elements in the 3-D family, it has been selected for use in the present analysis:

- Capability to represent curved sides and edges.
- *Easily adaptable to fracture mechanics applications.*
- Ideal for non-linear formulations.

The only disadvantage of this element is:

- Decrease in accuracy with excessive shape distortion.

This might not be considered as a disadvantage as this disadvantage is inherent in any element belonging to the 3-D family of elements.

The shape functions for the above element are as follows:

$$N_5 = \frac{1}{4}(1-\xi^2)(1-\eta)(1+\zeta) \qquad N_{15} = \frac{1}{4}(1-\xi^2)(1+\eta)(1-\zeta)$$
$$N_6 = \frac{1}{4}(1+\xi)(1-\eta^2)(1+\zeta) \qquad N_{16} = \frac{1}{4}(1-\xi)(1-\eta^2)(1-\zeta)$$
$$N_7 = \frac{1}{4}(1-\xi^2)(1+\eta)(1+\zeta) \qquad N_{17} = \frac{1}{4}(1-\xi)(1-\eta)(1-\zeta^2)$$
$$N_8 = \frac{1}{4}(1-\xi)(1-\eta^2)(1+\zeta) \qquad N_{18} = \frac{1}{4}(1+\xi)(1-\eta)(1-\zeta^2)$$
$$N_{13} = \frac{1}{4}(1-\xi^2)(1-\eta)(1-\zeta) \qquad N_{18} = \frac{1}{8}(1+\xi)(1+\eta)(1-\zeta^2)$$
$$N_{14} = \frac{1}{4}(1+\xi)(1-\eta^2)(1-\zeta) \qquad N_{20} = \frac{1}{8}(1-\xi)(1+\eta)(1-\zeta^2)$$

$$N_1 = \frac{1}{8}(1-\xi)(1-\eta)(1+\zeta) - \frac{(N_5 + N_8 + N_{17})}{2}$$
$$N_2 = \frac{1}{8}(1+\xi)(1-\eta)(1+\zeta) - \frac{(N_5 + N_6 + N_{18})}{2}$$
$$N_3 = \frac{1}{8}(1+\xi)(1+\eta)(1+\zeta) - \frac{(N_6 + N_7 + N_{19})}{2}$$
$$N_4 = \frac{1}{8}(1-\xi)(1+\eta)(1+\zeta) - \frac{(N_7 + N_8 + N_{20})}{2}$$
$$N_9 = \frac{1}{8}(1-\xi)(1-\eta)(1-\zeta) - \frac{(N_{13} + N_{16} + N_{17})}{2} \qquad (2.48)$$
$$N_{10} = \frac{1}{8}(1+\xi)(1-\eta)(1-\zeta) - \frac{(N_{13} + N_{14} + N_{18})}{2}$$
$$N_{11} = \frac{1}{8}(1+\xi)(1+\eta)(1-\zeta) - \frac{(N_{14} + N_{15} + N_{19})}{2}$$
$$N_{12} = \frac{1}{8}(1-\xi)(+\eta)(1-\zeta) - \frac{(N_{15} + N_{16} + N_{20})}{2}$$

The element displacements can now be expressed as

$$\{u\}^{(e)} = [N]^{(e)}\{d\}^{(e)} \tag{2.49}$$

in which the matrix for the shape functions is given by

$$[N]^{(e)} = \begin{cases} \begin{bmatrix} N_1 & 0 & N_2 & 0 & \dots & \dots & N_8 & 0 \\ 0 & N_1 & 0 & N_2 & \dots & \dots & 0 & N_8 \end{bmatrix} \\ \textit{for eight node 2 - D isoparametric elements} \\ \\ \begin{bmatrix} N_1 & 0 & 0 & N_2 & 0 & 0 & \dots & \dots & \dots & N_{20} & 0 & 0 \\ 0 & N_1 & 0 & 0 & N_2 & 0 & \dots & \dots & \dots & 0 & N_{20} & 0 \\ 0 & 0 & N_1 & 0 & 0 & N_2 & \dots & \dots & \dots & 0 & 0 & N_{20} \end{bmatrix} \\ \textit{for twenty node 3 - D isoparametric elements} \end{cases} \tag{2.50}$$

and the displacement vector is given by

$$\{d\}^{(e)} = \begin{cases} \{u_1 \quad v_1 \quad u_2 \quad v_2 \quad \dots \quad \dots \quad u_8 \quad v_8\} \\ \textit{for eight node 2 - D isoparametric elements} \\ \\ \{u_1 \quad v_1 \quad w_1 \quad u_2 \quad v_2 \quad w_2 \quad \dots \quad \dots \quad \dots \quad u_{20} \quad v_{20} \quad w_{20}\}^t \\ \textit{for twenty node 3 - D isoparametric elements} \end{cases} \tag{2.51}$$

The strain matrix for 2-D finite element formulation can be expressed as

$$\{\varepsilon\}^{(e)} = \left\{ \frac{\partial u}{\partial x} \quad \frac{\partial v}{\partial y} \quad \left(\frac{\partial u}{\partial y} + \frac{\partial v}{\partial x} \right) \right\}^t = [B]^{(e)}\{d\}^{(e)} \tag{2.52}$$

in which the $[B]^{(e)}$ matrix relates the element nodal displacements to the element strains and is given by

$$[B]^{(e)} = \begin{bmatrix} \frac{\partial}{\partial x} & 0 \\ 0 & \frac{\partial}{\partial y} \\ \frac{\partial}{\partial y} & \frac{\partial}{\partial x} \end{bmatrix} [N]^{(e)} \tag{2.53}$$

In the case of 3-D finite element formulation, the strain matrix and the strain-displacement matrix are given by,

$$\{\varepsilon\}^{(e)} = \left\{ \frac{\partial u}{\partial x} \quad \frac{\partial v}{\partial y} \quad \frac{\partial w}{\partial z} \quad \left(\frac{\partial u}{\partial y} + \frac{\partial v}{\partial x}\right) \quad \left(\frac{\partial v}{\partial z} + \frac{\partial w}{\partial y}\right) \quad \left(\frac{\partial u}{\partial z} + \frac{\partial w}{\partial x}\right) \right\} = [B]^{(e)} \{d\}^{(e)} \tag{2.54}$$

$$[B]^{(e)} = \begin{bmatrix} \frac{\partial}{\partial x} & 0 & 0 \\ 0 & \frac{\partial}{\partial y} & 0 \\ 0 & 0 & \frac{\partial}{\partial z} \\ \frac{\partial}{\partial y} & \frac{\partial}{\partial x} & 0 \\ 0 & \frac{\partial}{\partial z} & \frac{\partial}{\partial y} \\ \frac{\partial}{\partial z} & 0 & \frac{\partial}{\partial x} \end{bmatrix} [N]^{(e)} \tag{2.55}$$

The derivatives of the shape functions are expressed in terms of the local co-ordinates

and they can be obtained by the chain rule of partial differentiation as

$$\frac{\partial N_i}{\partial \xi} = \frac{\partial N_i}{\partial x}\frac{\partial x}{\partial \xi} + \frac{\partial N_i}{\partial y}\frac{\partial y}{\partial \xi} \qquad \textit{and}$$
$$\frac{\partial N_i}{\partial \eta} = \frac{\partial N_i}{\partial x}\frac{\partial x}{\partial \eta} + \frac{\partial N_i}{\partial y}\frac{\partial y}{\partial \eta} \qquad (2.56)$$
$$\textit{for 2 - D}$$

$$\frac{\partial N_i}{\partial \xi} = \frac{\partial N_i}{\partial x}\frac{\partial x}{\partial \xi} + \frac{\partial N_i}{\partial y}\frac{\partial y}{\partial \xi} + \frac{\partial N_i}{\partial z}\frac{\partial z}{\partial \xi} \qquad \textit{and}$$
$$\frac{\partial N_i}{\partial \eta} = \frac{\partial N_i}{\partial x}\frac{\partial x}{\partial \eta} + \frac{\partial N_i}{\partial y}\frac{\partial y}{\partial \eta} + \frac{\partial N_i}{\partial z}\frac{\partial z}{\partial \eta} \qquad (2.57)$$
$$\frac{\partial N_i}{\partial \zeta} = \frac{\partial N_i}{\partial x}\frac{\partial x}{\partial \zeta} + \frac{\partial N_i}{\partial y}\frac{\partial y}{\partial \zeta} + \frac{\partial N_i}{\partial z}\frac{\partial z}{\partial \zeta}$$
$$\textit{for 3 - D}$$

The above expressions can be expressed in the matrix form as

$$\begin{Bmatrix} \frac{\partial N_i^{(e)}}{\partial \xi} \\ \frac{\partial N_i^{(e)}}{\partial \eta} \end{Bmatrix} = \begin{bmatrix} \frac{\partial x}{\partial \xi} & \frac{\partial y}{\partial \xi} \\ \frac{\partial x}{\partial \eta} & \frac{\partial y}{\partial \eta} \end{bmatrix}^{(e)} \begin{Bmatrix} \frac{\partial N_i^{(e)}}{\partial x} \\ \frac{\partial N_i^{(e)}}{\partial y} \end{Bmatrix} \qquad (2.57)$$

In the above, the matrix relating the derivatives of the shape functions with respect to the local co-ordinates to the derivatives of the shape functions with respect to the global co-ordinates is called as the *Jacobian* matrix of transformation and is denoted by $[J]$. Thus the *Jacobian* of transformation is given as,

$$[J]=\begin{bmatrix} J_{11} & J_{12} \\ J_{21} & J_{22} \end{bmatrix}=\begin{bmatrix} \frac{\partial x}{\partial \xi} & \frac{\partial y}{\partial \xi} \\ \frac{\partial x}{\partial \eta} & \frac{\partial y}{\partial \eta} \end{bmatrix}^{(e)} \quad for\ 2-D$$

and (2.58)

$$[J]=\begin{bmatrix} J_{11} & J_{12} & J_{13} \\ J_{21} & J_{22} & J_{23} \\ J_{31} & J_{32} & J_{33} \end{bmatrix}=\begin{bmatrix} \frac{\partial x}{\partial \xi} & \frac{\partial y}{\partial \xi} & \frac{\partial z}{\partial \xi} \\ \frac{\partial x}{\partial \eta} & \frac{\partial y}{\partial \eta} & \frac{\partial z}{\partial \eta} \\ \frac{\partial x}{\partial \zeta} & \frac{\partial y}{\partial \zeta} & \frac{\partial z}{\partial \zeta} \end{bmatrix}^{(e)} \quad for\ 3-D$$

The components of the Jacobian matrix are calculated using the shape functions and the nodal co-ordinates. For instance,

$$J_{11}=\frac{\partial x}{\partial \xi}=\sum_{i=1}^{Num.ofNodes}\frac{\partial N_i}{\partial \xi}x_i \tag{2.59}$$

Now the element stiffness matrix can be written as

$$K^{(e)}=\int_{V_{(e)}}\left[B^{(e)}\right]^T[E]\left[B^{(e)}\right]dV_{(e)} \tag{2.60}$$

in which

$$dV_{(e)}=\begin{cases} t\,|J|\,d\xi\,d\eta & for\ 2-D \\ |J|\,d\xi\,d\eta\,d\zeta & for\ 3-D \end{cases} \tag{2.61}$$

The stiffness matrix coefficient linking nodes i and j in any element *(e)* is given by

$$K_{ij}^{(e)} = \begin{cases} \sum_{r=1}^{NGAUS} \sum_{s=1}^{NGAUS} \left[B_{ir}^{(e)}\right]^t \left[E_{rs}^{(e)}\right] \left[B_{sj}^{(e)}\right] t \left|J^{(e)}\right| d\xi \, d\eta & \textit{for 2 - D} \\ \sum_{\zeta=1}^{NGAUS} \sum_{\eta=1}^{NGAUS} \sum_{\xi=1}^{NGAUS} \left[B^{(e)}\right]^t \left[E\right] \left[B^{(e)}\right] t \left|J^{(e)}\right| d\xi \, d\eta \, d\zeta & \textit{for 3 - D} \end{cases} \tag{2.62}$$

in which *NGAUS* represents the order of Gauss quadrature for numerical integration. The elements of the stiffness matrix of each element can be numerically evaluated as

$$K_{ij}^{(e)} = \sum_{q=1}^{NGAUS} \sum_{p=1}^{NGAUS} T\left(\xi_p, \eta_q\right)_{ij}^{(e)} W_p W_q \tag{2.63}$$

in which

$$T_{ij}^{(e)} = \sum_{r=1}^{NGAUS} \sum_{s=1}^{NGAUS} \left[B_{ir}^{(e)}\right]^t \left[E_{rs}^{(e)}\right] \left[B_{sj}^{(e)}\right] t \left|J^{(e)}\right| \tag{2.64}$$

and (ξ_p, η_q) represents a sampling position and W_p and W_q are the weighting factors. If q is the uniformly acting load along the edge of length L of an element (e), the nodal loads can be expressed as

$$\begin{Bmatrix} \textit{Equivalent load at the left node} \\ \textit{Equivalent load at the central node} \\ \textit{Equivalent load at the right node} \end{Bmatrix} = \frac{qL}{6} \begin{Bmatrix} 1 \\ 4 \\ 1 \end{Bmatrix} \tag{2.65}$$

2.5 Program Organization for FEA and Computation of Fracture Parameters

In the development of the program care has been taken to use *descriptive variable names* for every variable name for example, *nnode* represents the number of nodes in an element, *ndofn* represents the number of degrees of freedom per each node, and so on. The program has been divided into segments to take care of various tasks and each task has been designed to be performed by a single routine. The various tasks performed by the various routines are as follows:

✓ The master program	:	STIFPS
✓ Get all relevant input data	:	GETDAT & GETARR
✓ Establish nodal connectivity	:	ELCON
✓ Compute Elasticity matrix	:	MODPS
✓ Get Gaussian attributes	:	GAUSSQ
✓ Evaluate shape functions & their derivatives	:	SFR2
✓ Evaluate $[J]$, its inverse and $\lvert J \rvert$	:	JACOB2
✓ Evaluate $[B]$	:	BMATPS
✓ Assemble element stiffness matrices	:	ASMBLK
✓ Compute the load vector	:	LOADPS, FORCE
✓ Solve for nodal displacements	:	BCSOLVE
✓ Find the stresses at each gauss point	:	STREPS
✓ Calculate the *SIF* by *DEM*	:	EVALSIF1
✓ Calculate energy release rate	:	ERRCALC
✓ Calculate *SIF* by *ERRM*	:	EVALSIF2
✓ Calculate the *SIF* by J-Integral method	:	EVALJ

2.5.1 Flow Chart for the Main Program – STIFPS.m

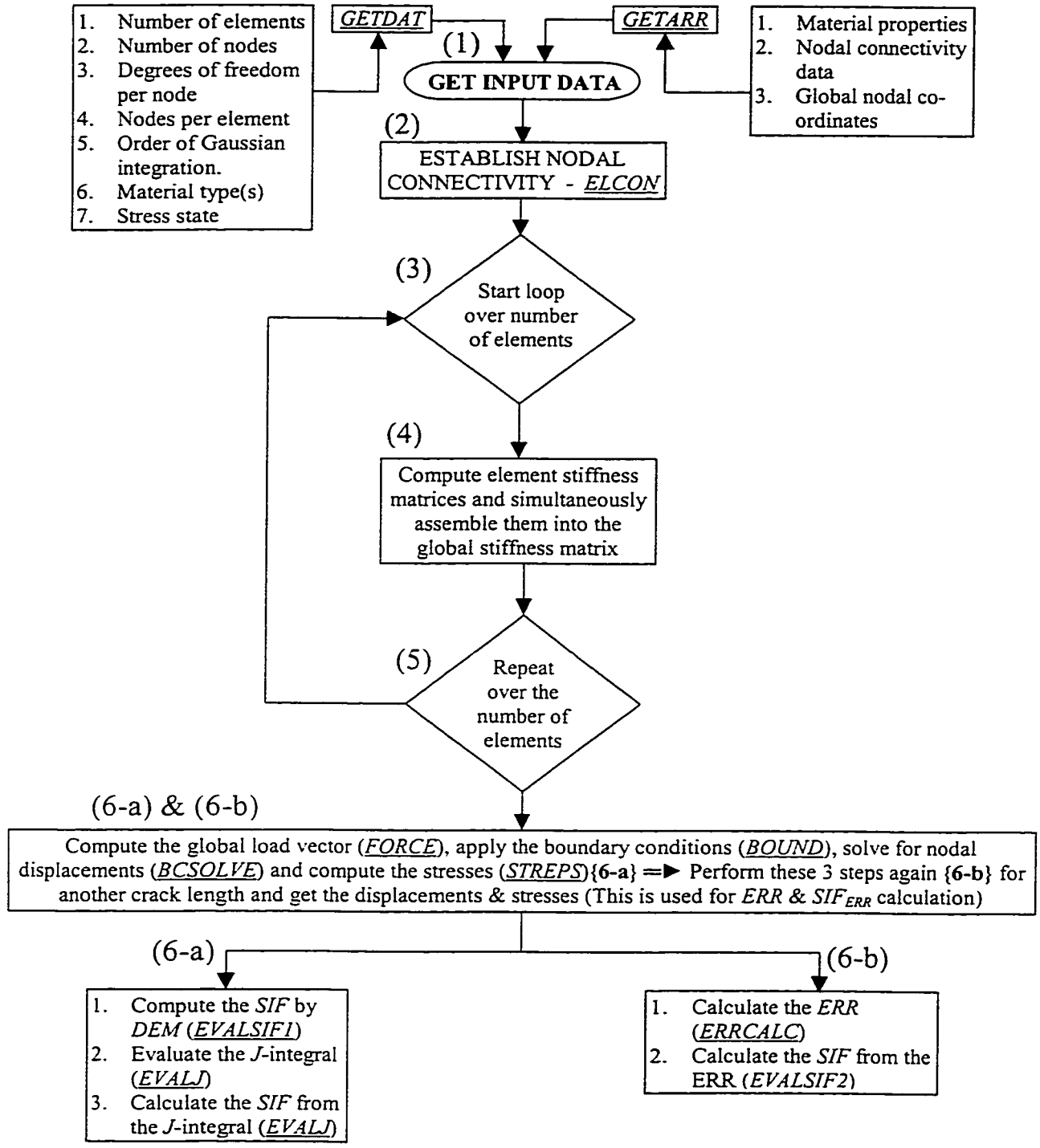

Figure 2.10 Flow chart for 2-D (& 3-D) FEA and computation of fracture parameters

2.5.2 Evaluation of Stiffness matrices for Numerically Integrated Isoparametric Elements (details of Step – 4 in Figure 2.10)

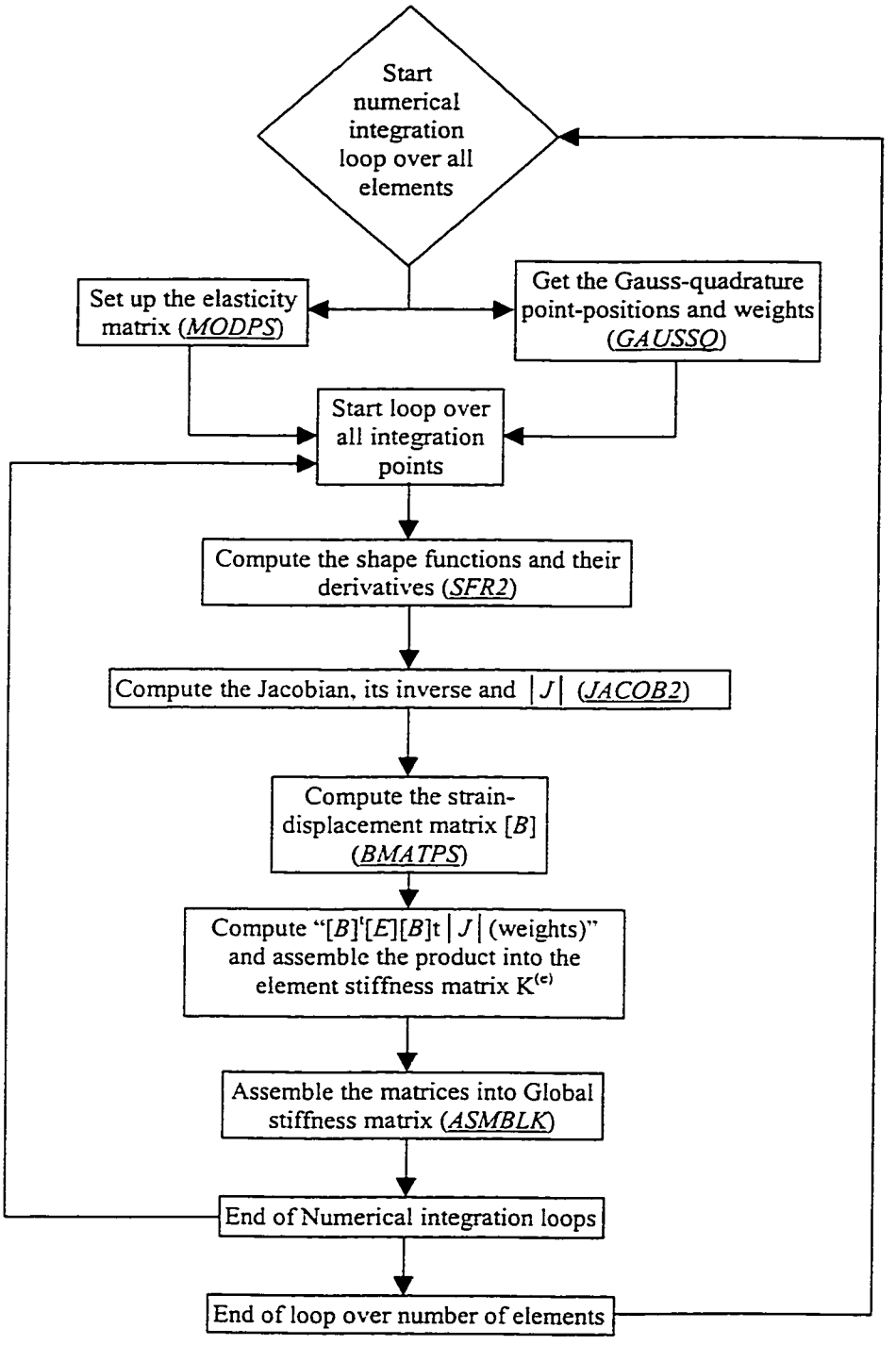

Figure 2.11 Flow chart for evaluation of element stiffness matrices

2.6 Sample Applications

The computer programs developed until now are demonstrated by the application to a standard linear elastic problem [3] and the results of the analyses are verified with the solutions given in Ref. [3]. It may be noted that the example problem and the numerical values for geometrical, structural and material parameters are exactly the same as in [3] wherein no specific units were used. The main objective here is to compare the results only. A plate with a central crack, subjected to uniformly distributed tensile loading is considered for analysis. The crack length is assumed to be 40% of the width of the plate. The material properties of the plate are assumed as: $E = 10{,}000$, $\nu = 0.3$ and the plate is assumed to be of unit thickness. The main reason for assuming the above material properties, geometry and comparing the results with those presented in Ref. [3] for the same problem is to make sure that the modeling is correct right from the beginning.

2.6.1 Results of Analysis

It must be noted that the displacements along the loaded edge and the displacements along the crack face are of primary importance since these are used for calculating the *ERR* and *SIF* by the Displacement Extrapolation Method. For the same problem described above, the displacements and the stresses have been calculated and presented in Ref. [3]. A comparison between the results obtained from the above-described finite element model and the results presented in [3] is also given in Table 2.1. It can be seen that the results match almost perfectly indicating that the modeling is correct. Also the finite element mesh that has been employed is shown below in Figure 2.12.

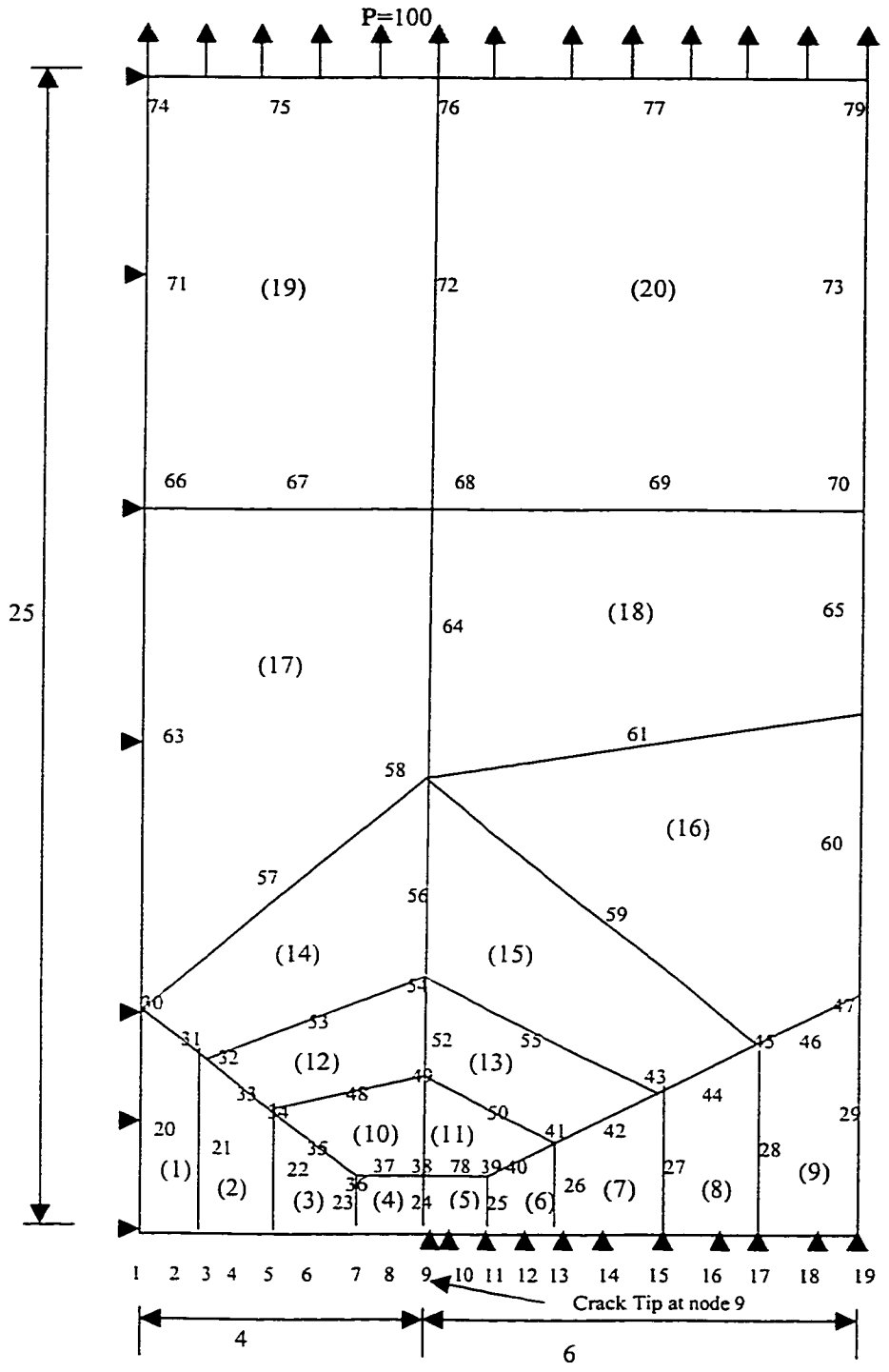

Figure 2.12 Finite element mesh for the center-cracked plate problem. All dimensions are in compatible units. (Please see section 2.6)

In the case of 3-D modeling, the same structure shown above has been used except that the thickness has been increased to 4. A similar mesh has been used with a single element used in the thickness direction. A comparison of the displacements of 2-D analysis and that given in Ref. [3] is presented below. Also presented is a comparison of the displacements obtained by 3-D analysis with those obtained from the standard ANSYS® software in which a different mesh was employed. *It must be noted here that the stresses and strains are obtained from the displacements* [3] *and will not be presented here, as the stresses and strains calculated would be correct once the displacements are correct.*

	Program Results		Results from Ref. [3]	
Node Number	u	V	u	v
1	0.000000	0.086136	0.000000	0.086136
2	-0.006984	0.085151	-0.006985	0.085151
3	-0.014354	0.081463	-0.014354	0.081463
4	-0.020902	0.075557	-0.020902	0.075557
5	-0.027502	0.066708	-0.027502	0.066708
6	-0.033251	0.055972	-0.033251	0.055972
7	-0.038510	0.039718	-0.038510	0.039718
8	-0.040344	0.026775	-0.040344	0.026775
9	-0.039981	0.000000	-0.039981	0.000000
74	0.000000	0.276943	0.000000	0.276943
75	-0.005959	0.276511	-0.005959	0.276511
76	-0.011833	0.276697	-0.011833	0.276697
77	-0.020950	0.276863	-0.020950	0.276863
79	-0.029706	0.276875	-0.029707	0.276875

Table 2.1 Comparison of displacements for nodes along the crack face (nodes :1-9) and along the loaded edge (nodes: 74-79)

A similar comparison has been done for the stresses (calculated based on the displacements) and have also been found to compare very well. Now a comparison of the displacements obtained from 3-D analysis is presented below.

Node Numbers	Program Results			
	u	v	w	
80	0.000000	0.084138	0.000000	Central nodes (along thickness) on the crack-face
81	-0.014884	0.079377	0.000000	
82	-0.028551	0.064471	0.000000	
83	-0.039076	0.038112	0.000000	
84	-0.039929	0.000000	0.000000	
107	0.000000	0.276509	0.000000	Central nodes at the loaded edge
108	-0.011855	0.276313	0.000000	
109	-0.029681	0.276467	0.000000	
1	0.000000	0.087923	0.006900	Front-face nodes along the crack-face
2	-0.006507	0.086876	0.006848	
3	-0.013371	0.083078	0.006392	
4	-0.019251	0.076827	0.005321	
5	-0.025085	0.067543	0.003232	
6	-0.029970	0.055761	0.000188	
7	-0.034094	0.038600	-0.004654	
8	-0.035615	0.025979	-0.008125	
9	-0.035899	0.000000	-0.011984	
74	0.000000	0.276552	-0.006190	Front-face nodes along the loaded edge
75	-0.005975	0.276108	-0.006101	
76	-0.011864	0.276281	-0.006031	
77	-0.020990	0.276455	-0.005989	
79	-0.029759	0.276479	-0.005863	

Table 2.2 Nodal displacements from 3-D analysis by the MATLAB® FEA program

Node Numbers	ANSYS Results			
	u	V	w	
193	0.000000	0.075686	0.000000	Central nodes (along thickness) on the crack-face
195	-0.021662	0.064853	0.000000	
196	-0.031795	0.000000	0.000000	
200	0.000000	0.272370	0.000000	Central nodes at the loaded edge
201	-0.005189	0.272350	0.000000	
202	-0.010440	0.272300	0.000000	
203	-0.015774	0.272280	0.000000	
204	-0.021167	0.272340	0.000000	
199	-0.026565	0.272450	0.000000	
97	0.000000	0.079260	0.007003	Front-face nodes along the crack-face
99	-0.009752	0.077281	0.006109	
100	-0.183150	0.067120	0.003341	
101	-0.023515	0.040974	-0.003137	
102	-0.028862	0.000000	-0.010007	
118	0.000000	0.272380	-0.005468	Front-face nodes along the loaded edge
127	-0.002593	0.272370	-0.005465	
126	-0.005199	0.272350	-0.005457	
125	-0.007812	0.272310	-0.005442	
124	-0.010449	0.272290	-0.005430	
123	-0.013108	0.272270	-0.005417	
122	-0.015778	0.272270	-0.005407	
121	-0.018475	0.272290	-0.005401	
120	-0.021172	0.272330	-0.005396	
119	-0.023875	0.272390	-0.005393	
108	-0.026573	0.272450	-0.005388	

Table 2.3 Nodal displacements obtained from the 3-D analysis by the ANSYS®

2.6.1.1 Fracture Parameters

(a) SIF by *Displacement Extrapolation Method*

It has been shown [3] that isoparametric elements yield the most accurate results by displacement extrapolation technique along the radial line corresponding to $\theta=180^{\circ}$. With the conventional 2-D eight node isoparametric elements, a *SIF* of 300 was obtained which is same as that obtained in Ref. [3], and which differs from the value of $K_I = 393.5$ given in Ref. [3] by approximately 23.8%. Upon use of ¼-point crack tip elements at elements 4 & 5 (described in section-2.3.1) a *SIF* of 377 was obtained by displacement extrapolation, with an error of approximately 4.2%.

It must be noted that the formulae employed for the evaluation of *SIF*, are appropriate for plane stress and plane strain cases only. So, the stresses induced in the 3-D structure were analyzed to find out which case they represent more closely. It has been observed that the stresses represent the plane stress case. So, all subsequent analyses are based on plane-stress behavior. The *SIF* obtained by displacement extrapolation is 300, which is same as that obtained in the 2-D case. Upon use of ¼-point crack tip elements the *SIF* was found to be 380, which is a somewhat better (error: 3.43%) prediction than that provided by the 2-D case.

Using the formulae for the plane-strain case and using conventional elements, a *SIF* of 325 was obtained by *DEM*. In the same case, a *SIF* of 392 (error: 0.4%) was obtained by using ¼-point crack tip elements.

(b) Strain Energy Release Rate Method

The crack increment is simulated by releasing the nodes in the finite element mesh. The crack is advanced by two different lengths [3] (obtained by releasing through one whole element each time) and, the *ERR* and *SIF* are calculated for the average of crack length each time. The *ERR* and *SIF* for the original crack length are obtained by extrapolating the above-obtained values to the original (average) crack length. In this case, a *SIF* of 386.7 (error: 1.7%) was obtained upon extrapolation. In the case of 3-D, a *SIF* of 392.95 (error: 0.014%) was obtained upon extrapolation.

(c) J-Integral Method

In this approach, the *J*-integral is evaluated along a contour path surrounding the crack tip. In the above mesh, three such element-paths can be noticed.

Path – 1: 8 – 15 – 14 – 1

Path – 2: 7 – 13 – 12 – 2

Path – 3: 6 – 11 – 10 – 3

And through each of the above element paths, three *J*-contours can be obtained, corresponding to $\xi = -1$, $\xi = 0$ and $\xi = +1$. Only the conventional isoparametric elements were employed.

The values of the *J*-integral and the *SIF* calculated using the *J* integral are listed below.

		J-integral	SIF	Error (%)
Path - 1				
	ξ=-1	14.835	385.160	2.12
	ξ=0	15.710	389.500	1.02
	ξ=+1	14.918	386.240	1.84
Path - 2				
	ξ=-1	14.754	384.110	2.38
	ξ=0	15.220	390.130	0.85
	ξ=+1	14.854	385.400	2.05
Path - 3				
	ξ=-1	13.760	370.930	5.73
	ξ=0	15.980	399.800	-1.60
	ξ=+1	14.430	379.800	3.48

Table 2.4 *J*-integral and *SIF* for various contours

From the above table, it can be observed that the slight variations in the *J* and *SIF* values increase as one approaches the crack tip, due to the limitations of the numerical solution technique.

2.7 Conclusions and Discussions

In this chapter, the concepts of *SIF*, *ERR* and *J*-integral in relation to Linear Elastic Fracture Mechanics (*LEFM*) of isotopic materials have been discussed in detail. Finite element analysis programs developed in MATLAB® for linear elastic analysis of structures made of isotropic materials were described and discussed in detail. Applications to specific standard problems (2-*D* and 3-*D*) were shown and the results (corresponding to various fracture parameters) obtained were verified [2]. This formulation will be extended in the subsequent chapters to anisotropic materials and stochastic problems respectively.

Chapter 3

Stochastic Finite Element Modeling and Analysis of Anisotropic Plates

3.1 Introduction

In the past few years, the applications of composite materials in various automotive, aerospace and biomedical structures have increased tremendously. The main advantages of composite materials over the conventional high strength metals are: high strength, high stiffness, low cost, long fatigue life (for a few composite materials, the fatigue strength remains unaltered with the number of cycles of operation), low density, high corrosion resistance, wear resistance, thermal and acoustic insulation, high specific stiffness and high specific strength. The most important aspect is the anisotropic and heterogeneous nature of the material. The ability to manufacture the laminates with different ply orientations and stacking sequences provides the designer and manufacturer with much freedom to achieve the optimum configuration for each specific application. With such wide range of applications for composite structures, it is essential for the analyst to have a thorough understanding of various mechanisms of failure of these materials, the most complex and least understood being the failure by fracture.

In the case of composite laminates, significant randomness in the material properties exists due to the variations in the distribution and arrangement of matrix and fiber. As a result, the material parameters obtained from any single test specimen are specific to that

particular sample and hence a probabilistic approach has to be followed in order to develop general models based on sample values. This approach can be used to get probabilistic parameters that represent the sample lot in general. Thus, when the Finite Element Analysis (*FEA*) is performed based on a stochastic approach, such that a stochastic description can be provided for both the material properties and the response of the laminate, the resulting *FEA* is called the Stochastic Finite Element Analysis.

The first few sections in the present chapter are devoted to:

(a) the various concepts of LEFM as applied to anisotropic materials

(b) the finite element fracture analysis of anisotropic materials

(c) the extension and adaptation of the MATLAB® program developed in chapter 2 so as to include the case of anisotropic materials, and

(d) illustrative applications on composite laminates

Further, the last few sections in this chapter are devoted to:

(a) incorporating the concepts of stochastic FEA into the program developed above in section (c), and

(b) determining various fracture parameters based on a probabilistic approach for the same illustrative applications discussed above in section (d)

3.2 Fracture Mechanics of Anisotropic Plates

For anisotropic materials, the complex analytic function theory [21] has been employed in stress analysis. The various fracture parameters (*SIF*, *ERR* and *J*-Integral) for a cracked anisotropic plate have been calculated based on the stress analysis results. The stresses at the crack tip in an anisotropic material in Mode-*I* are given by [3] Equations (3.1 – 3.3)

$$\sigma_x = \frac{K_I}{\sqrt{2\pi r}} \mathrm{Re}\left[\frac{\mu_1\mu_2}{(\mu_1-\mu_2)}\{\mu_2 F_2 - \mu_1 F_1\}\right] \tag{3.1}$$

$$\sigma_y = \frac{K_I}{\sqrt{2\pi r}} \mathrm{Re}\left[\frac{1}{(\mu_1-\mu_2)}\{\mu_1 F_2 - \mu_2 F_1\}\right] \tag{3.2}$$

$$\tau_{xy} = \frac{K_I}{\sqrt{2\pi r}} \mathrm{Re}\left[\frac{\mu_1\mu_2}{(\mu_1-\mu_2)}\{F_1 - F_2\}\right] \tag{3.3}$$

The stress components for an anisotropic material in Mode-*II* failure are given by

$$\sigma_x = \frac{K_{II}}{\sqrt{2\pi r}} \mathrm{Re}\left[\frac{1}{(\mu_1-\mu_2)}\{\mu_2^2 F_2 - \mu_1^2 F_1\}\right] \tag{3.4}$$

$$\sigma_y = \frac{K_{II}}{\sqrt{2\pi r}} \mathrm{Re}\left[\frac{1}{(\mu_1-\mu_2)}\{F_2 - F_1\}\right] \tag{3.5}$$

$$\tau_{xy} = \frac{K_{II}}{\sqrt{2\pi r}} \mathrm{Re}\left[\frac{1}{(\mu_1-\mu_2)}\{\mu_1 F_1 - \mu_2 F_2\}\right] \tag{3.6}$$

In the above equations, K_I and K_{II} are the stress intensity factors for Mode *I* and Mode *II* respectively, Re represents the real part of the function and further μ_1 and μ_2 are given by

$$\mu_{1,2} = \frac{i}{\sqrt{2}}\left[(\chi+\lambda)^{1/2} \pm (\chi-\lambda)^{1/2}\right] \quad \text{when } \chi > \lambda \tag{3.7}$$

$$\mu_{1,2} = \frac{1}{\sqrt{2}}\left[i(\chi+\lambda)^{1/2} \mp (\lambda-\chi)^{1/2}\right] \quad \text{when } \chi < \lambda \tag{3.8}$$

in which

$$\lambda^2 = \frac{a_{22}}{a_{11}} \qquad \text{and} \qquad \chi = \frac{(2a_{12}+a_{66})}{2a_{11}} \tag{3.9}$$

where a_{11}, a_{12}, a_{22} and a_{66} are the compliances as in

$$\varepsilon_x = a_{11}\sigma_x + a_{12}\sigma_y + a_{16}\tau_{xy} \tag{3.10}$$

$$\varepsilon_y = a_{21}\sigma_x + a_{22}\sigma_y + a_{26}\tau_{xy} \tag{3.11}$$

$$\gamma_{xy} = a_{61}\sigma_x + a_{62}\sigma_y + a_{66}\tau_{xy} \tag{3.12}$$

Due to the condition for symmetry, $a_{12} = a_{21}$, $a_{26} = a_{62}$ and $a_{16} = a_{61}$. In the case of an orthotropic material, the principal elastic directions are orthogonal to each other and further there is no coupling between deformations due to shear and normal stresses. In

that case $a_{16} = a_{26} = 0$. The orthotropic coefficients are given by

$$a_{11} = \frac{1}{E_1}, a_{22} = \frac{1}{E_2}, a_{66} = \frac{1}{G_{12}} \text{ and } a_{12} = -\frac{\nu_{12}}{E_{11}} = -\frac{\nu_{21}}{E_{22}} \tag{3.13}$$

The equations for the displacements in Mode *I* and Mode *II* are given by

$$u = \frac{K_I\sqrt{2\pi r}}{\pi}\mathrm{Re}\left[\frac{1}{(\mu_1 - \mu_2)}\left\{\frac{\mu_1 p_2}{F_2} - \frac{\mu_2 p_1}{F_1}\right\}\right] \tag{3.14}$$

$$v = \frac{K_I\sqrt{2\pi r}}{\pi}\mathrm{Re}\left[\frac{1}{(\mu_1 - \mu_2)}\left\{\frac{\mu_1 q_2}{F_2} - \frac{\mu_2 q_1}{F_1}\right\}\right] \tag{3.15}$$

$$u = \frac{K_I\sqrt{2\pi r}}{\pi}\mathrm{Re}\left[\frac{1}{(\mu_1 - \mu_2)}\left\{\frac{\mu_1 p_2}{F_2} - \frac{\mu_2 p_1}{F_1}\right\}\right] \tag{3.16}$$

$$v = \frac{K_I\sqrt{2\pi r}}{\pi}\mathrm{Re}\left[\frac{1}{(\mu_1 - \mu_2)}\left\{\frac{\mu_1 q_2}{F_2} - \frac{\mu_2 q_1}{F_1}\right\}\right] \tag{3.17}$$

in which

$$p_{1,2} = \mu_{1,2}^2 a_{11} + a_{12} - \mu_{1,2} a_{16} \tag{3.18}$$

$$q_{1,2} = \mu_{1,2} a_{1,2} + \left(\frac{a_{22}}{\mu_{1,2}}\right) - a_{26} \tag{3.19}$$

3.2.1 Stress Intensity Factor

The behavior of composite laminates with stress raisers such as cracks is of great interest to the designer because of the resulting strength and life reduction due to damage growth around these stress raisers. An expression for the stress distribution ahead of the crack shown below in Figure 3.1 is given by [2]

$$\sigma_y = \begin{cases} \dfrac{\sigma_{ap}|x|}{\sqrt{x^2 - a^2}} & ; \quad |x| > a \\ 0 & ; \quad |x| < a \end{cases} \tag{3.20}$$

in which

σ_y represents the stress at any point along the y-axis

σ_{app} represents the externally applied far-field stress and

a represents the semi-crack length.

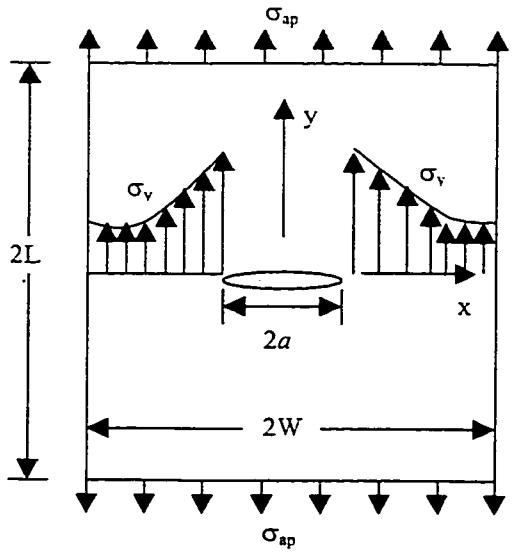

Figure 3.1 Composite laminate with a central crack under uniaxial tensile loading

By using the distance, r, from the crack tip, i.e., $r = |x\text{-}a|$, it can be seen that Equation (3.20) has singularities of type $r^{-1/2}$ at the crack tips and if r is sufficiently smaller than half the crack length, the stress σ_y is can be approximated by

$$\sigma_y = \frac{K_I}{\sqrt{2\pi r}} \tag{3.21}$$

where K_I is the stress intensity factor which in the case of a center crack in an infinite plate of very large width is given by

$$K_I = \sigma_{ap}\sqrt{\pi a} \tag{3.22}$$

In the case of a rectangular plate of finite length (2L) and width (2W) with a center crack (as shown in Figure 3.1), the *SIF* is given by

$$K_I = f\left(\frac{a}{W}, \frac{L}{W}\right)\sigma_{ap}\sqrt{\pi a} \tag{3.23}$$

in which $f\left(\frac{a}{W}, \frac{L}{W}\right)$ is a non-dimensional factor which is a function of the aspect ratios (a/W) and (L/W). From equations (3.20 – 3.23) it is quite evident that the finite geometry of the laminates as well as the type of externally applied loading have a bearing on the stresses distributed at the crack tip. The *SIF* is a parameter that quantifies the stress field around the crack tip which is a characteristic of the material.

3.2.2 Energy Release Rate

Under general loading conditions, the Energy Release Rate (*ERR*) for Mode *I* and Mode *II* can be given by [17]

$$G_I = K_I^2 a_{22}\left[\frac{(\chi+\lambda)^{1/2}}{\sqrt{2\lambda}}\right] \tag{3.24}$$

$$G_{II} = K_{II}^2 a_{11}\left[\frac{(\chi+\lambda)^{1/2}}{\sqrt{2\lambda}}\right] \tag{3.25}$$

3.2.3 *J* - Integral

It can be recalled from Equation (2.12) that the value of the *J*-integral is influenced by the stresses and the strains at various points through which the contour for the *J*-integral passes. Further, the stresses and strains are influenced by the type of material and the external loading conditions. Thus, for a set of given loading conditions the stresses and strains depend only on the type of material. Thus for composite laminates the *J*-integral evaluation depends only on the elasticity matrix. Further, the stress intensity factor can be calculated from Equation (3.24) by replacing G_I with J as

$$K_I = \sqrt{\frac{J\sqrt{2\lambda}}{a_{22}(\chi+\lambda)^{1/2}}} \tag{3.26}$$

In the next section, the evaluation of the elasticity matrix for composite laminates is discussed with all relevant details.

3.3 Elasticity Matrix for Composite Laminates

In the following few sections, the various aspects of laminate theory [115] that are relevant to the present thesis are discussed in sufficient detail.

3.3.1 Aspects of Laminate Theory

For a single unidirectional lamina in plane-stress situations, the strain-stress relations referred to the material axes are given by [147]

$$\begin{Bmatrix} \varepsilon_1 \\ \varepsilon_2 \\ \tau_6 \end{Bmatrix} = \begin{bmatrix} S_{11} & S_{12} & 0 \\ S_{12} & S_{22} & 0 \\ 0 & 0 & S_{66} \end{bmatrix} \begin{Bmatrix} \sigma_1 \\ \sigma_2 \\ \tau_6 \end{Bmatrix} = \begin{bmatrix} 1/E_1 & -\nu_{21}/E_2 & 0 \\ -\nu_{12}/E_1 & 1/E_2 & 0 \\ 0 & 0 & 1/G_{12} \end{bmatrix} \begin{Bmatrix} \sigma_1 \\ \sigma_2 \\ \tau_6 \end{Bmatrix} \tag{3.26}$$

In most practical cases, the material axes (1,2) do not coincide with the global or loading axes (x,y) as shown below in Figure (3.2).

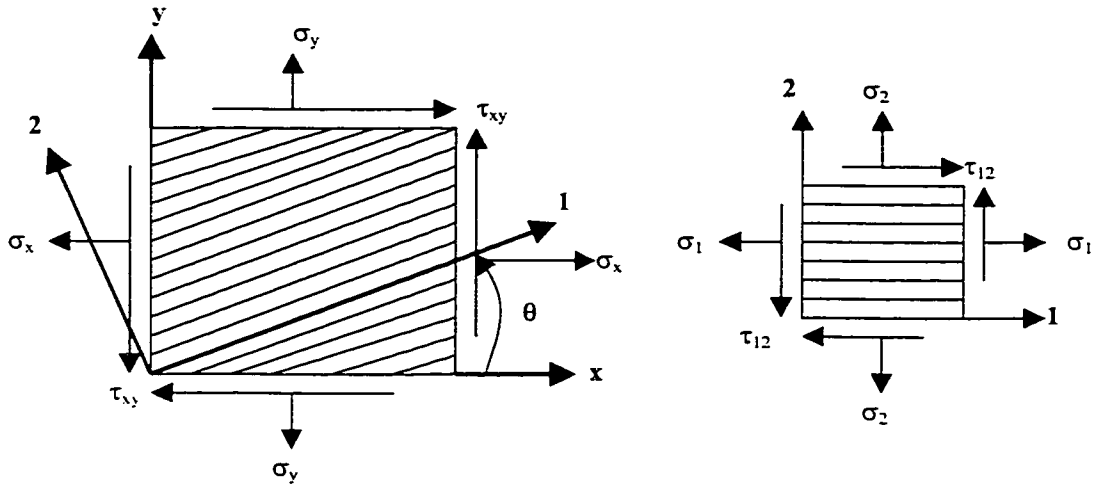

Figure 3.2 Stress components in an unidirectional ply referred to the local and global material axes

In such a case, the stress and strain components referred to the material axes can be expressed in terms of the global axes by

$$\begin{Bmatrix} \sigma_1 \\ \sigma_2 \\ \tau_6 \end{Bmatrix} = [T] \begin{Bmatrix} \sigma_x \\ \sigma_y \\ \tau_{xy} \end{Bmatrix} \tag{3.27}$$

$$\begin{Bmatrix} \varepsilon_1 \\ \varepsilon_2 \\ \gamma_{12}/2 \end{Bmatrix} = [T] \begin{Bmatrix} \varepsilon_x \\ \varepsilon_y \\ \gamma_{xy}/2 \end{Bmatrix} \tag{3.28}$$

In the above equations, the tensorial shear strain, ε_{xy} is used and is related to the engineering shear strain by

$$\varepsilon_{12} = \frac{\gamma_{12}}{2} \quad \text{and} \quad \varepsilon_{xy} = \frac{\gamma_{xy}}{2} \tag{3.29}$$

and the transformation matrix, $[T]$ in Equations (3.27 – 3.28) is given by

$$[T] = \begin{bmatrix} m^2 & n^2 & 2mn \\ n^2 & m^2 & -2mn \\ -mn & mn & \left(m^2 - n^2\right) \end{bmatrix} \tag{3.30}$$

in which m=cosθ and n=sinθ, and θ is the angle measured positive in the counterclockwise direction from the x-axis to the 1-axis as shown above in Figure (3.2). In terms of the global axes, the stress-strain relations are given by

$$\begin{Bmatrix}\sigma_x\\ \sigma_y\\ \tau_{xy}\end{Bmatrix}=\begin{bmatrix}\bar{Q}_{11} & \bar{Q}_{12} & \bar{Q}_{16}\\ \bar{Q}_{12} & \bar{Q}_{22} & \bar{Q}_{26}\\ \bar{Q}_{16} & \bar{Q}_{26} & \bar{Q}_{66}\end{bmatrix}\begin{Bmatrix}\varepsilon_x\\ \varepsilon_y\\ \gamma_{xy}\end{Bmatrix} \tag{3.31}$$

in which $\bar{Q}_{ij}$ are called the transformed reduced stiffnesses, and are defined by

$$\begin{aligned}
\bar{Q}_{11} &= Q_{11}m^4 + 2(Q_{12}+2Q_{66})n^2m^2 + Q_{22}n^4\\
\bar{Q}_{12} &= (Q_{11}+Q_{22}-4Q_{66})n^2m^2 + Q_{12}(n^4+m^4)\\
\bar{Q}_{16} &= (Q_{11}-Q_{12}-2Q_{66})nm^3 + (Q_{12}-Q_{22}+2Q_{66})n^3m\\
\bar{Q}_{22} &= Q_{11}n^4 + 2(Q_{12}+2Q_{66})n^2m^2 + Q_{22}m^4\\
\bar{Q}_{26} &= (Q_{11}-Q_{12}-2Q_{66})n^3m + (Q_{12}-Q_{22}+2Q_{66})nm^3\\
\bar{Q}_{66} &= (Q_{11}+Q_{22}-2Q_{12}-2Q_{66})n^2m^2 + Q_{66}(n^4+m^4)
\end{aligned} \tag{3.32}$$

3.3.2 Laminate Stiffness Matrix

The strains at any point in a laminate with reference to the mid-plane strains and the laminate curvatures are given by [147]

$$\begin{Bmatrix}\varepsilon_x\\ \varepsilon_y\\ \gamma_s\end{Bmatrix}=\begin{Bmatrix}\varepsilon_x^o\\ \varepsilon_y^o\\ \gamma_s^o\end{Bmatrix}+z\begin{Bmatrix}\kappa_x\\ \kappa_y\\ \kappa_s\end{Bmatrix} \tag{3.33}$$

and the stresses at any point in any layer k in the laminate are given by

$$\begin{Bmatrix} \sigma_x \\ \sigma_y \\ \tau_s \end{Bmatrix}_k = \begin{bmatrix} Q_{xx} & Q_{xy} & Q_{xs} \\ Q_{yx} & Q_{yy} & Q_{ys} \\ Q_{sx} & Q_{sy} & Q_{ss} \end{bmatrix}_k \begin{Bmatrix} \varepsilon_x^o \\ \varepsilon_y^o \\ \gamma_s^o \end{Bmatrix} + z \begin{bmatrix} Q_{xx} & Q_{xy} & Q_{xs} \\ Q_{yx} & Q_{yy} & Q_{ys} \\ Q_{sx} & Q_{sy} & Q_{ss} \end{bmatrix}_k \begin{Bmatrix} k_x \\ k_y \\ k_s \end{Bmatrix} \tag{3.34}$$

It can be seen from Equations (3.33 – 3.34) that the strains vary linearly and continuously through the thickness, while the stresses vary discontinuously because of the discontinuous variation of the transformed stiffness matrix $[Q]_{xy}$ from layer to layer.

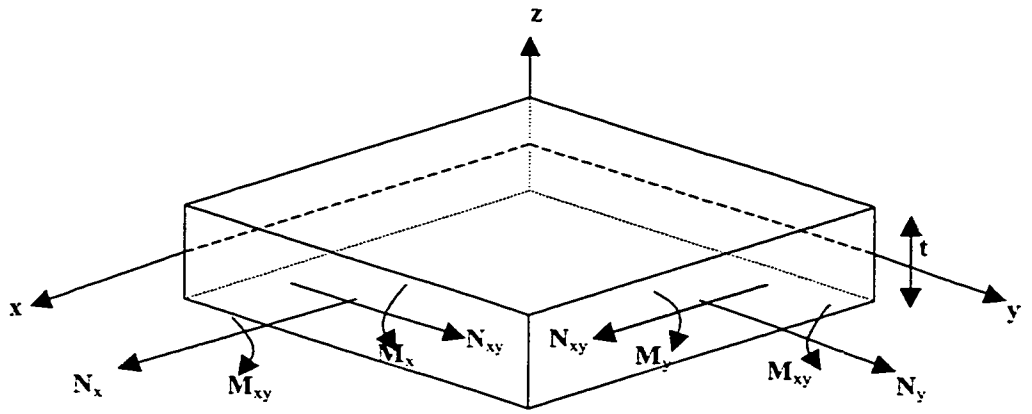

Figure 3.3 Element of a single layer with force and moment resultants

The net force and moment resultants of the stresses acting on a layer k of the laminate shown in Figure 3.3 are given by

$$N_x^k = \int_{-\frac{t}{2}}^{\frac{t}{2}} \sigma_x dz \qquad N_y^k = \int_{-\frac{t}{2}}^{\frac{t}{2}} \sigma_y dz \qquad N_{xy}^k = \int_{-\frac{t}{2}}^{\frac{t}{2}} \tau_{xy} dz \tag{3.35}$$

and

$$M_x^k = \int_{-\frac{t}{2}}^{\frac{t}{2}} \sigma_x z dz \qquad M_y^k = \int_{-\frac{t}{2}}^{\frac{t}{2}} \sigma_y z dz \qquad M_{xy}^k = \int_{-\frac{t}{2}}^{\frac{t}{2}} \tau_{xy} z dz \tag{3.36}$$

in which

z represents the coordinate variable of a point in the cross section and

t represents the ply thickness

In the case of a multilayer laminate the total force and moment resultants are obtained by summing the contributions from all layers. Thus for the laminate with *n* plies as shown in Figure (3.4), the force and moment resultants can be written as

$$\begin{Bmatrix} N_x \\ N_y \\ N_{xy} \end{Bmatrix} = \sum_{k=1}^{n} \int_{h_{k-1}}^{h_k} \begin{Bmatrix} \sigma_x \\ \sigma_y \\ \tau_{xy} \end{Bmatrix}_k dz \tag{3.37}$$

and

$$\begin{Bmatrix} M_x \\ M_y \\ M_{xy} \end{Bmatrix} = \sum_{k=1}^{n} \int_{h_{k-1}}^{h_k} \begin{Bmatrix} \sigma_x \\ \sigma_y \\ \tau_{xy} \end{Bmatrix}_k z dz \tag{3.38}$$

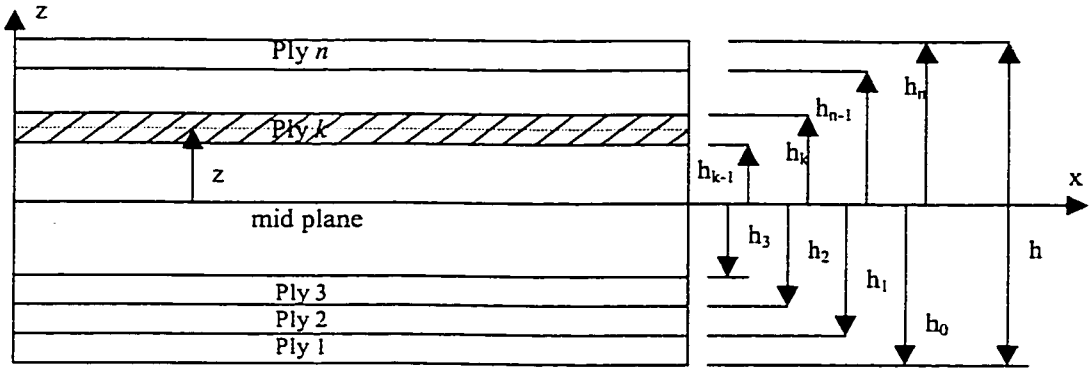

Figure 3.4 Multilayer laminate with coordinate notation for individual plies

Substituting Equation (3.34) in Equations (3.37-3.38) one can obtain

$$\begin{Bmatrix} N_x \\ N_y \\ N_{xy} \end{Bmatrix} = \sum_{k=1}^{n} \left\{ \begin{bmatrix} \bar{Q}_{11} & \bar{Q}_{12} & \bar{Q}_{16} \\ \bar{Q}_{12} & \bar{Q}_{22} & \bar{Q}_{26} \\ \bar{Q}_{16} & \bar{Q}_{26} & \bar{Q}_{66} \end{bmatrix}_k \begin{Bmatrix} \varepsilon_x^0 \\ \varepsilon_y^2 \\ \gamma_{xy}^0 \end{Bmatrix} \int_{h_{k-1}}^{h_k} dz + \begin{bmatrix} \bar{Q}_{11} & \bar{Q}_{12} & \bar{Q}_{16} \\ \bar{Q}_{12} & \bar{Q}_{22} & \bar{Q}_{26} \\ \bar{Q}_{16} & \bar{Q}_{26} & \bar{Q}_{66} \end{bmatrix}_k \begin{Bmatrix} k_x \\ k_y \\ k_{xy} \end{Bmatrix} \int_{h_{k-1}}^{h_k} z dz \right\} \quad (3.39)$$

and

$$\begin{Bmatrix} M_x \\ M_y \\ M_{xy} \end{Bmatrix} = \sum_{k=1}^{n} \left\{ \begin{bmatrix} \bar{Q}_{11} & \bar{Q}_{12} & \bar{Q}_{16} \\ \bar{Q}_{12} & \bar{Q}_{22} & \bar{Q}_{26} \\ \bar{Q}_{16} & \bar{Q}_{26} & \bar{Q}_{66} \end{bmatrix}_k \begin{Bmatrix} \varepsilon_x^0 \\ \varepsilon_y^2 \\ \gamma_{xy}^0 \end{Bmatrix} \int_{h_{k-1}}^{h_k} z dz + \begin{bmatrix} \bar{Q}_{11} & \bar{Q}_{12} & \bar{Q}_{16} \\ \bar{Q}_{12} & \bar{Q}_{22} & \bar{Q}_{26} \\ \bar{Q}_{16} & \bar{Q}_{26} & \bar{Q}_{66} \end{bmatrix}_k \begin{Bmatrix} k_x \\ k_y \\ k_{xy} \end{Bmatrix} \int_{h_{k-1}}^{h_k} z^2 dz \right\} \quad (3.40)$$

In the Equations (3.39-3.40) given above, the in-plane strains and curvatures refer to the entire laminate and are the same for all plies. Thus the strains and curvatures can be factored outside the summation sign as follows.

$$\{N\} = \left[\sum_{k=1}^{n} \left[\bar{Q} \right]_k \int_{h_{k-1}}^{h_k} dz \right] \{\varepsilon^0\} + \left[\sum_{k=1}^{n} \left[\bar{Q} \right]_k \int_{h_{k-1}}^{h_k} z dz \right] \{k\} \quad (3.41)$$

$$\{N\} = \left[\sum_{k=1}^{n} \left[\bar{Q} \right]_k \left(h_k - h_{k-1} \right) \right] \{\varepsilon^0\} + \left[\sum_{k=1}^{n} \left[\bar{Q} \right]_k \left(h_k^2 - h_{k-1}^2 \right) \right] \{k\} \quad (3.42)$$

$$\{N\} = [A]\{\varepsilon^0\} + [B]\{k\} \quad (3.43)$$

and

$$\{M\} = \left[\sum_{k=1}^{n}\left[\bar{Q}\right]_k \int_{h_{k-1}}^{h_k} z\,dz\right]\{\varepsilon^0\} + \left[\sum_{k=1}^{n}\left[\bar{Q}\right]_k \int_{h_{k-1}}^{h_k} z^2\,dz\right]\{k\} \tag{3.44}$$

$$\{M\} = \left[\sum_{k=1}^{n}\left[\bar{Q}\right]_k \left(h_k^2 - h_{k-1}^2\right)\right]\{\varepsilon^0\} + \left[\sum_{k=1}^{n}\left[\bar{Q}\right]_k \left(h_{k-1}^3 - h_k^3\right)\right]\{k\} \tag{3.45}$$

$$\{M\} = [B]\{\varepsilon^0\} + [D]\{k\} \tag{3.46}$$

in which

$$A_{ij} = \sum_{k=1}^{n} \bar{Q}_{ij}^{k}\left(h_k - h_{k-1}\right) \text{ (Axial stiffness)} \tag{3.47}$$

$$B_{ij} = \frac{1}{2}\sum_{k=1}^{n} \bar{Q}_{ij}^{k}\left(h_k^2 - h_{k-1}^2\right) \text{ (Axial-bending coupling stiffness)} \tag{3.48}$$

$$D_{ij} = \frac{1}{3}\sum_{k=1}^{n} \bar{Q}_{ij}^{k}\left(h_k^3 - h_{k-1}^3\right) \text{ (Bending stiffness)} \tag{3.49}$$

with $i,j = x, y, s$.

Thus the full form of the force-deformation relation of Equation (3.39) is

$$\begin{Bmatrix} N_x \\ N_y \\ N_{xy} \end{Bmatrix} = \begin{bmatrix} A_{11} & A_{12} & A_{16} \\ & A_{22} & A_{26} \\ symm & & A_{66} \end{bmatrix} \begin{Bmatrix} \varepsilon_x^0 \\ \varepsilon_y^0 \\ \gamma_{xy}^0 \end{Bmatrix} + \begin{bmatrix} B_{11} & B_{12} & B_{16} \\ & B_{22} & B_{26} \\ symm & & B_{66} \end{bmatrix} \begin{Bmatrix} k_x \\ k_y \\ k_{xy} \end{Bmatrix} \tag{3.50}$$

and the moment-deformation relation of Equation (3.40) is

$$\begin{Bmatrix} M_x \\ M_y \\ M_{xy} \end{Bmatrix} = \begin{bmatrix} B_{11} & B_{12} & B_{16} \\ & B_{22} & B_{26} \\ symm & & B_{66} \end{bmatrix} \begin{Bmatrix} \varepsilon_x^0 \\ \varepsilon_y^0 \\ \gamma_{xy}^0 \end{Bmatrix} + \begin{bmatrix} D_{11} & D_{12} & D_{16} \\ & D_{22} & D_{26} \\ symm & & D_{66} \end{bmatrix} \begin{Bmatrix} k_x \\ k_y \\ k_{xy} \end{Bmatrix} \tag{3.51}$$

The combined form of the Equations (3.50-3.51) is called the laminate constitutive equation and can be written as

$$\begin{Bmatrix} N_x \\ N_Y \\ N_{XY} \\ M_X \\ M_Y \\ M_{XY} \end{Bmatrix} = \left[\begin{array}{ccc:ccc} A_{11} & A_{12} & A_{16} & B_{11} & B_{12} & B_{16} \\ & A_{22} & A_{26} & & B_{22} & B_{26} \\ symm & & A_{66} & symm & & B_{66} \\ \hdashline B_{11} & B_{12} & B_{16} & D_{11} & D_{12} & D_{16} \\ & B_{22} & B_{26} & & D_{22} & D_{26} \\ symm & & B_{66} & symm & & D_{66} \end{array}\right] \begin{Bmatrix} \varepsilon_x^0 \\ \varepsilon_y^0 \\ \gamma_{xy}^0 \\ k_x \\ k_y \\ k_{xy} \end{Bmatrix} \tag{3.52}$$

3.3.3 Equivalent Elastic Constants

In-plane forces for symmetric laminates, for which the axial bending siffnesses B_{ij} are zero, can be written from Equation (3.50) as

$$\begin{Bmatrix} N_x \\ N_y \\ N_{xy} \end{Bmatrix} = \begin{bmatrix} A_{11} & A_{12} & A_{16} \\ A_{12} & A_{22} & A_{26} \\ A_{16} & A_{26} & A_{66} \end{bmatrix} \begin{Bmatrix} \varepsilon_x^0 \\ \varepsilon_y^0 \\ \gamma_{xy}^0 \end{Bmatrix} \tag{3.53}$$

Inversion of the Equation (3.53) gives

$$\begin{Bmatrix} \varepsilon_x^0 \\ \varepsilon_y^0 \\ \gamma_{xy}^0 \end{Bmatrix} = \begin{bmatrix} a_{11} & a_{12} & a_{16} \\ a_{12} & a_{22} & a_{26} \\ a_{16} & a_{26} & a_{66} \end{bmatrix} \begin{Bmatrix} N_x \\ N_y \\ N_{xy} \end{Bmatrix} \tag{3.54}$$

in which $[a]$ is the extensional laminate compliance matrix, which is the inverse of the corresponding stiffness matrix, $[A]$, as given below:

$$[a]=[A]^{-1} \tag{3.55}$$

The average laminate stresses can be defined as

$$\bar{\sigma}_x = \frac{N_x}{h}, \qquad \bar{\sigma}_y = \frac{N_y}{h}, \text{ and } \quad \bar{\tau}_{xy} = \frac{N_{xy}}{h} \tag{3.56}$$

in which h is the laminate thickness.

So Equation (3.54) can be rewritten in terms of average laminate stresses as

$$\begin{Bmatrix} \varepsilon_x^0 \\ \varepsilon_y^2 \\ \gamma_{xy}^0 \end{Bmatrix} = \begin{bmatrix} ha_{11} & ha_{12} & ha_{16} \\ ha_{12} & ha_{22} & ha_{26} \\ ha_{16} & ha_{26} & ha_{66} \end{bmatrix} \begin{Bmatrix} \frac{N_x}{h} = \bar{\sigma}_x \\ \frac{N_y}{h} = \bar{\sigma}_y \\ \frac{N_{xy}}{h} = \bar{\tau}_{xy} \end{Bmatrix} \tag{3.57}$$

A uniaxial stress σ_x produces the following strains

$$\varepsilon_x = \frac{1}{E_x}\sigma_x, \qquad \varepsilon_y = -\frac{\nu_{xy}}{E_x}\sigma_x, \text{ and } \quad \gamma_{xy} = -\frac{m_x}{E_x}\sigma_x \tag{3.58}$$

where E_x, ν_{xy}, and $m_x = -\dfrac{\gamma_{xy}}{\varepsilon_x}$ are the x-directional modulus, Poisson's ratio and shear coupling coefficient respectively.

In a similar manner, a uniaxial stress σ_y produces the following strains.

$$\varepsilon_x = -\frac{\nu_{yx}}{E_y}\sigma_y, \quad \varepsilon_y = \frac{1}{E_y}\sigma_y, \text{ and } \gamma_{xy} = -\frac{m_y}{E_y}\sigma_y \tag{3.59}$$

A pure shear stress τ_{xy} produces the following strains.

$$\varepsilon_x = -\frac{\tau_{xy}}{G_{xy}m_x}, \quad \varepsilon_y = -\frac{\tau_{xy}}{G_{xy}m_y}, \text{ and } \gamma_{xy} = \frac{\tau_{xy}}{G_{xy}} \tag{3.60}$$

By superposition of the three loadings σ_x, σ_y, and τ_{xy} the following strain-stress relation can be obtained in terms of engineering constants.

$$\begin{Bmatrix} \varepsilon_x \\ \varepsilon_y \\ \gamma_{xy} \end{Bmatrix} = \begin{bmatrix} \dfrac{1}{E_x} & -\dfrac{\nu_{yx}}{E_y} & -\dfrac{1}{G_{xy}m_x} \\ -\dfrac{\nu_{xy}}{E_x} & \dfrac{1}{E_y} & -\dfrac{1}{G_{xy}m_y} \\ -\dfrac{m_x}{E_x} & -\dfrac{m_y}{E_y} & \dfrac{1}{G_{xy}} \end{bmatrix} \begin{Bmatrix} \sigma_x \\ \sigma_y \\ \tau_{xy} \end{Bmatrix} \tag{3.61}$$

From symmetry considerations of the compliance matrix, the following equations are obtained.

$$\frac{\nu_{xy}}{E_x} = \frac{\nu_{yx}}{E_y}, \quad \frac{m_x}{E_x} = \frac{1}{G_{xy}m_x}, \text{ and } \frac{m_y}{E_y} = \frac{1}{G_{xy}m_y} \tag{3.62}$$

Comparison of equivalent strain-stress relations in Equation (3.57) and Equation (3.61) yields the following relations for equivalent engineering constants.

$$E_x = \frac{1}{ha_{11}}, \quad E_y = \frac{1}{ha_{22}}, \quad G_{xy} = \frac{1}{ha_{33}},$$

$$\nu_{xy} = -\frac{a_{12}}{a_{11}}, \quad \nu_{yx} = -\frac{a_{12}}{a_{33}}, \quad m_x = -\frac{a_{13}}{a_{11}}, \quad m_y = -\frac{a_{23}}{a_{22}} \tag{3.63}$$

The equivalent elasticity matrix [E] for a composite laminate can be calculated by inverting Equation (3.57) as

$$\begin{Bmatrix} \bar{\sigma}_x \\ \bar{\sigma}_y \\ \bar{\tau}_{xy} \end{Bmatrix} = \begin{bmatrix} ha_{11} & ha_{12} & ha_{16} \\ ha_{12} & ha_{22} & ha_{26} \\ ha_{16} & ha_{26} & ha_{66} \end{bmatrix}^{-1} \begin{Bmatrix} \varepsilon_x^0 \\ \varepsilon_y^2 \\ \gamma_{xy}^0 \end{Bmatrix} \tag{3.64}$$

Now comparing Equation (3.64) with Equation (2.39) in Chapter 2 (Section 2.4.1.1) for calculating the elasticity matrix [E], gives

$$[E] = \begin{bmatrix} ha_{11} & ha_{12} & ha_{16} \\ ha_{12} & ha_{22} & ha_{26} \\ ha_{16} & ha_{26} & ha_{66} \end{bmatrix}^{-1} \tag{3.65}$$

3.4 Flow chart for Computing the Elasticity matrix of Multidirectional Laminates

As has been noted earlier, the only difference in computing the fracture parameters of an isotropic material and an anisotropic material lies in the computation of the elasticity matrix. The flow chart for the computation of the elasticity matrix is as follows:

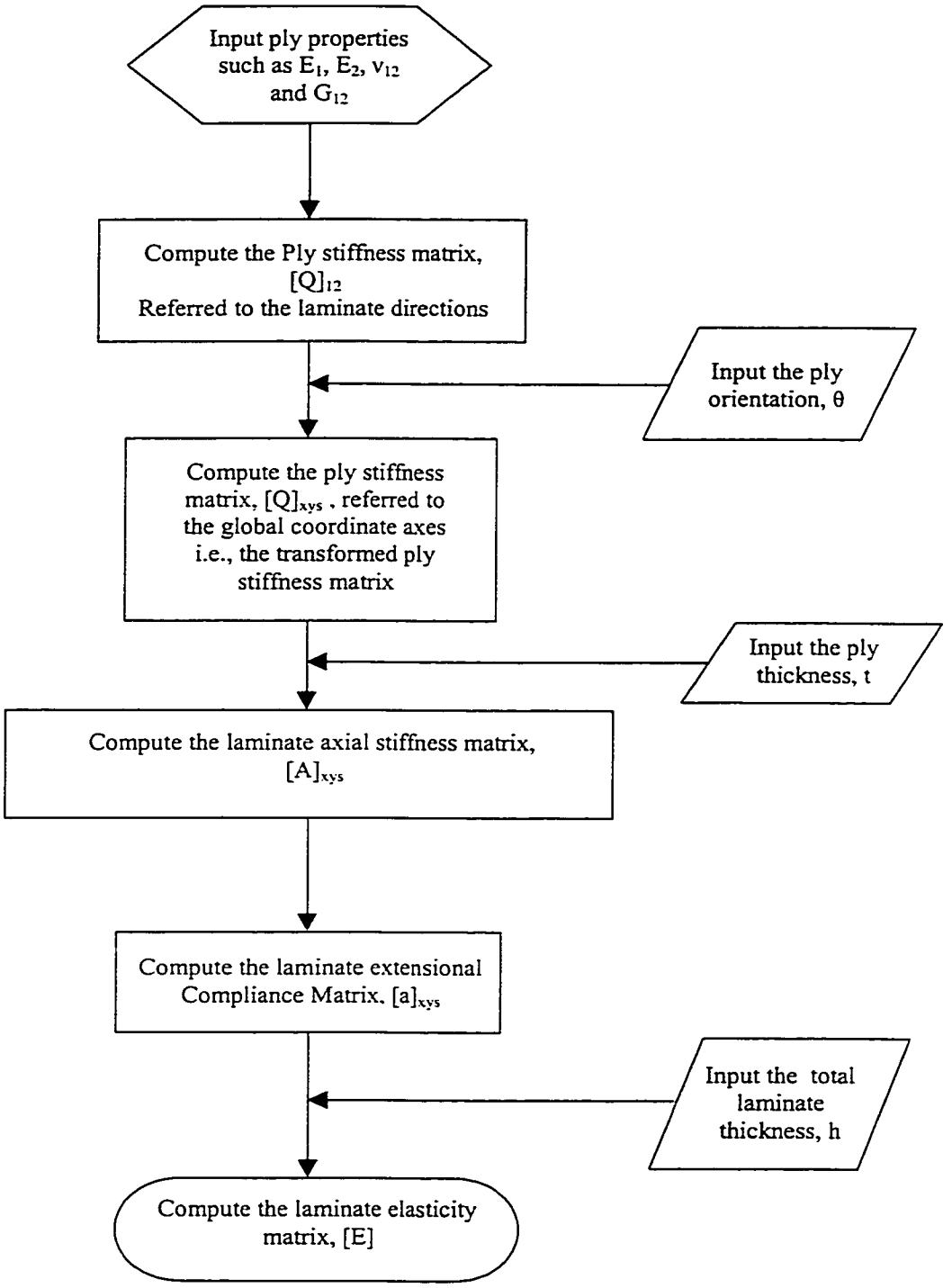

Figure 3.5 Flow chart showing the computational details for the elasticity matrix of multidirectional laminates

3.5 Illustrative Application

The program developed in the previous chapter is extended further in this chapter for applications to composite laminates will now be demonstrated through an example. The problem under consideration is a plate made of NCT 301 graphite-epoxy composite material with a configuration of $[0/90]_{5s}$ and having twenty plies. The mean values, standard deviations and coefficients of variation of the various material properties [144] for NCT 301 graphite-epoxy composite material are presented below in table 3.1.

	E_1 (GPa)	E_2 (GPa)	V_{21}	v_{12}	G_{12} (GPa)	Fiber direction failure load (N)	Matrix direction failure load (N)
Mean	129.43	7.99	0.0205	0.3322	4.28	18617.06	1257.89
Standard deviation	2.87	0.33	0.0021	0.0317	0.24	2789.09	169.34
Coefficient of variation	2.22	4.12	10.43	9.55	5.52	14.98	13.46

Table 3.1 Mean values, standard deviations and coefficients of variation of various material properties of NCT 301 graphite-epoxy composite material

The structure considered for analysis is a plate of width 240 mm and length 480 mm with a center crack of length 80 mm, subjected to an uniformly distributed load of magnitude 1.5 KN/mm which is approximately equal to 60% of the mean laminate strength [144]. Due to symmetry of the structure and the loading, only one-quarter of the structure is considered for analysis. The results of the analysis are presented below. The results are found to match very well with those obtained by using the standard ANSYS® software.

Again, only the displacements are provided, as the strains and further, the stresses are obtained from the displacements. The mesh employed is also shown below.

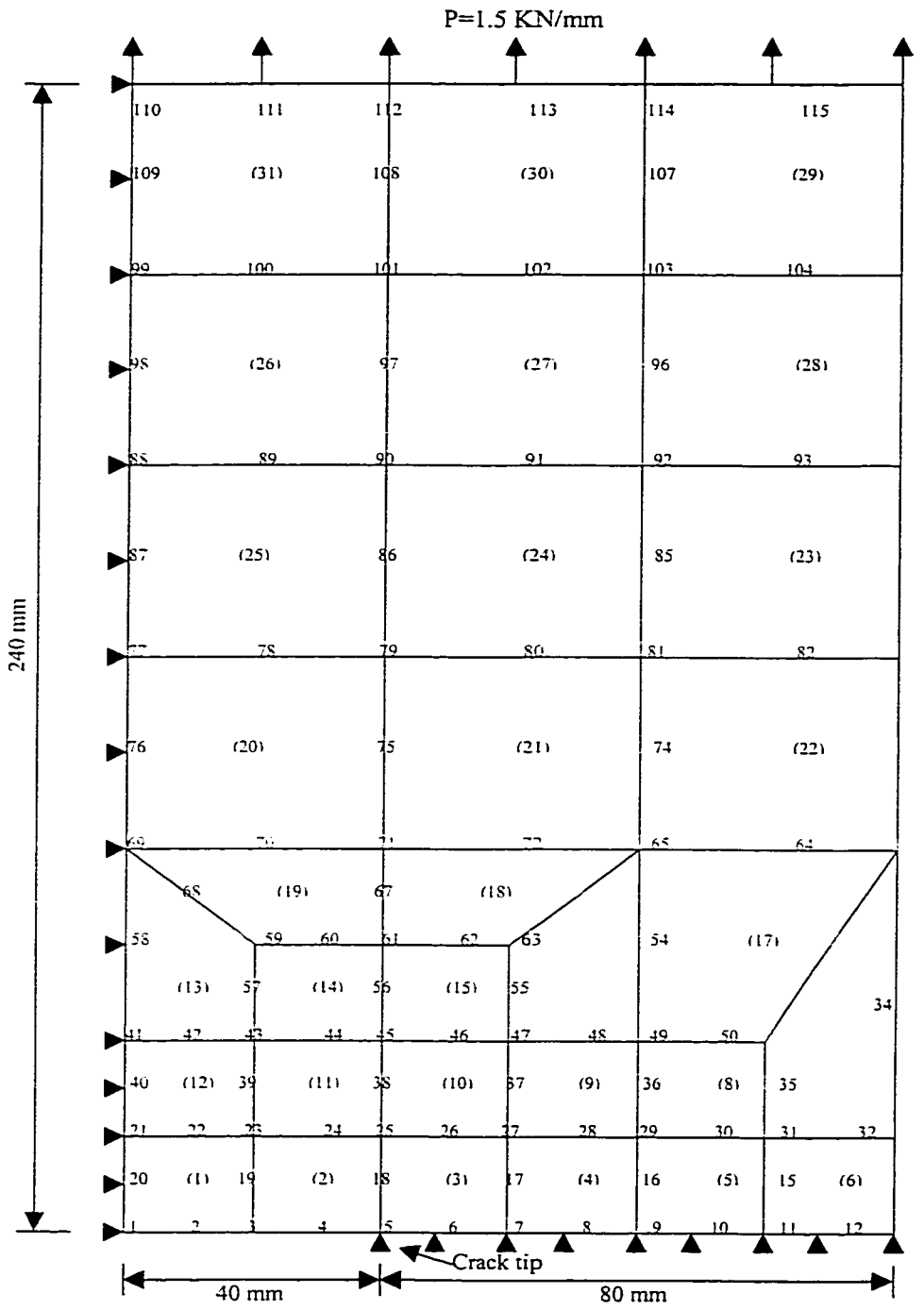

Figure 3.6 Finite element mesh for the center-cracked plate

Global Node Number		MATLAB® Program		ANSYS®	
		u (mm)	v (mm)	u (mm)	v (mm)
Crack Face	1	0.0000	1.5573	0.0000	1.5350
	2	-0.1010	1.5142	-0.1019	1.5712
	3	-0.1950	1.3096	-0.1967	1.2656
	4	-0.2590	1.0051	-0.2803	1.1040
	5	-0.2823	0.0000	-0.3244	0.0000
Loaded Edge	110	0.0000	2.8219	0.0000	2.8470
	111	0.0422	2.7600	0.0480	2.7830
	112	0.0759	2.6098	0.0872	2.6279
	113	0.0813	2.4445	0.0883	2.4588
	114	0.0768	2.3167	0.0802	2.3235
	115	0.0663	2.2407	0.0676	2.2475
	116	0.0550	2.1935	0.0540	2.1970

Table 3.2 Comparison of nodal displacements obtained by using the MATLAB® program and standard ANSYS® software.

It must be noted here that the mesh shown in Figure 3.6 was employed in order to compare the results of the analysis with those presented in an earlier work [144] and to verify if the analysis is correct. Due to some disadvantages such as being very coarse near the crack tip and also due to the absence of *element loops* around the crack tip, this mesh is inadequate for the evaluation of important fracture parameters such as *ERR* and the *J*-integral.

It is desired to evaluate the *J*-integral in a region close to the edges of the plate in order to find out the effect of stochastic variations in the material properties at the edges of the plate. Also, the stochastic variations of the stresses in the plate along a radial direction originating from the crack tip are kept track of, by evaluating the *J*-integral along various

contours selected through various element paths that are located at various distances from the crack tip. Hence a more sophisticated mesh is employed and is presented below in Figure 3.7. The various fracture parameters are evaluated and discussed below in the next few sections.

3.6 Evaluation of Fracture Parameters

In the next few sections, the fracture parameters such as *SIF*, *ERR* and *J*-integral are evaluated for NCT 301 graphite-epoxy laminate with a configuration of $[0/90]_{6s}$ (a/W = 0.333, W = 120 mm, L = 240 mm, tensile UDL = 1.5 KN/mm) and are presented.

3.6.1 Stress Intensity Factor

The stress intensity factor has been obtained by the following three methods [3]: *DEM*, *SERRM* and *J*-integral method. The *SIF* as obtained by the *DEM* is 52.24 MPa$\sqrt{m}$. The *SIF* as obtained by *SERRM* by releasing in Figure 3.7, elements 6 and 7 respectively, is 71.25 MPa$\sqrt{m}$. In the evaluation of the *J*-integral, various integration loops have been employed. The finite element mesh shown in Figure 3.7 has four loops:

Loop-1: 8 – 14 – 13 – 12 – 4

Loop-2: 9 – 17 – 16 – 15 – 3

Loop-3: 10 – 20 – 19 – 18 – 2

Loop-4: 11 – 25 – 30 – 35 – 40 – 43 – 42 – 41 – 36 – 31 – 26 – 21 – 1

Through each of the above loops three contours can be drawn corresponding to ξ=-1, ξ=0 and ξ=+1 for the evaluation of the *J*-integral. The *SIF* can be obtained from the *J*-integral by Equation (3.26).

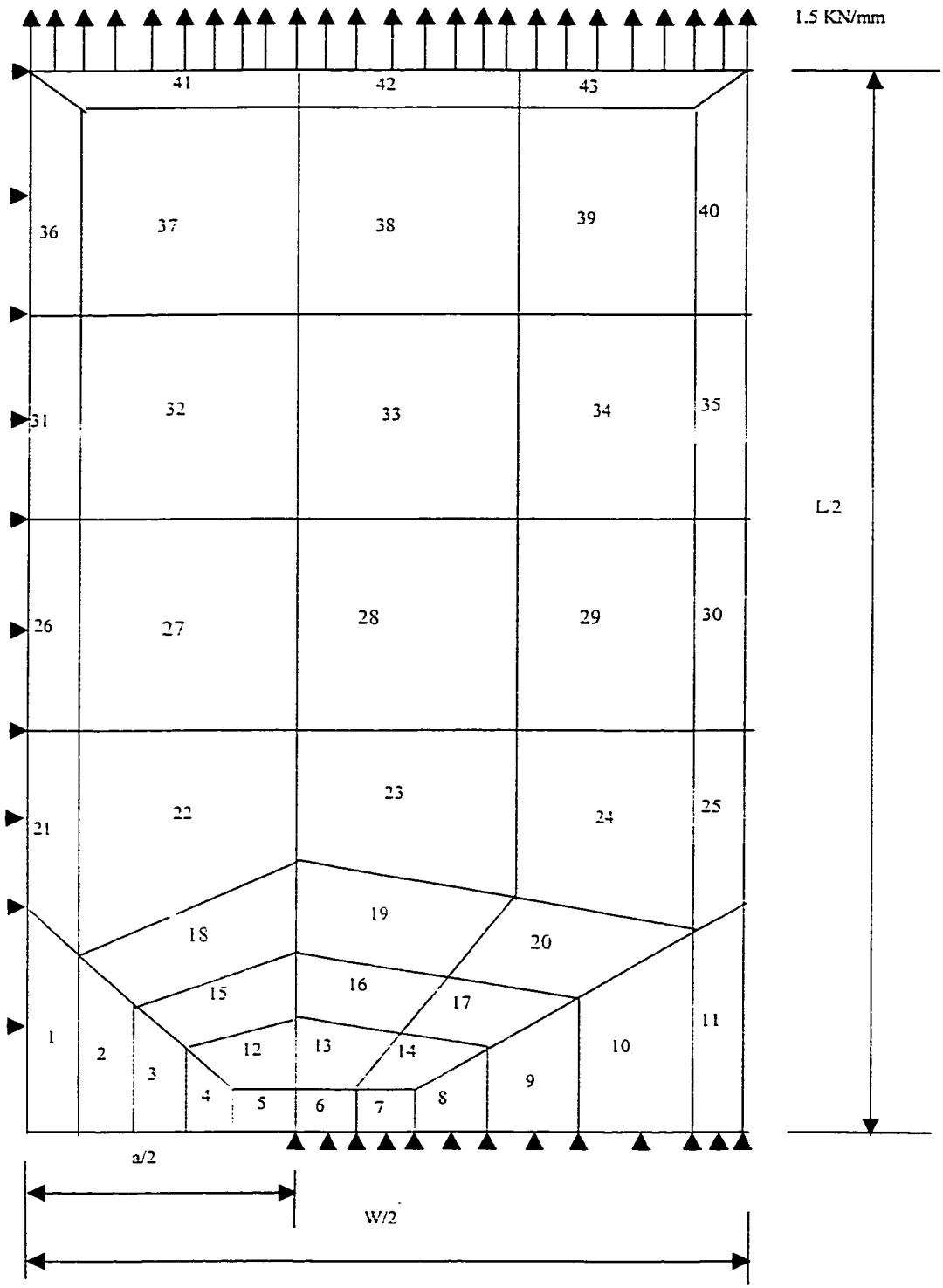

Figure 3.7 A finite element mesh appropriate for the evaluation of fracture parameters including *ERR* and *J*-integral

		J-integral (1.0e6 N-m/m^2)	SIF (MPa$\sqrt{m}$)
Path-1	ξ =-1	0.9417	70.16
	ξ =0	1.0152	72.84
	ξ=+1	0.9559	70.68
Path-2	ξ =-1	0.9661	71.06
	ξ =0	0.9815	71.62
	ξ =+1	0.9620	70.91
Path-3	ξ =-1	0.9645	70.99
	ξ =0	0.9690	71.17
	ξ =+1	0.9609	70.87
Path-4	ξ =-1	0.9628	70.94
	ξ =0	0.9634	70.96
	ξ=+1	0.9636	70.97

Table 3.3 Values of the *J*-integral and *SIF* for the various contours described in section 3.6.1.

3.6.2 Energy Release Rate

The *ERR* is obtained by extrapolating the values of energies released by advancing the crack through one whole element each time. In Figure 3.7 elements 6 and 7 are released one at a time. When element 6 is released, the energy released is equal to 224.49 N.m and further, when element 7 is released, the energy released is equal to 279.23 N.m. Now the average crack length is 55 mm, and the *ERR* is 1.1466 x 10^6 N.m/m^2. Similarly, the energy release rate obtained by releasing element 8 and having an average crack length of 62.5 mm is equal to 1.3365 x 10^6 N.m/m^2. By extrapolating the above *ERR* values to the crack tip, an *ERR* of 0.9567 x 10^6 N.m/m^2 has been obtained. Corresponding to this value of *ERR*, the *SIF* is calculated as 71.25 MPa$\sqrt{m}$.

3.6.3 *J* – Integral

The *J*-integral is numerically evaluated along the twelve contours described above in section 3.6.1 and the values of the *J*-integral are summarized in Table 3.3. It can be observed that the values of the *J*-integral compares very well with the value of the *ERR* and are almost equal to the *ERR*. The comparison also holds good for the values of the *SIF* obtained by *SERRM* and *J*-integral.

3.7 Stochastic Finite Element Analysis

Most modern mechanical systems possess high degree of structural complexity. Therefore, when their behavior is to be predicted under various loading and environmental conditions, advanced analytical and numerical techniques are required. In the case of composite laminates, significant randomness is present. This is due to the stochastic spatial variations of the properties of fibers, properties of the materials and properties at interfaces. In addition to the above, several variations exist in the fiber volume fraction, void contents, fiber orientation angles in various plies, thickness of the lamina, etc. due to significant variabilities that are introduced during the manufacturing processes. As a result, tests on a single material specimen provide a specific value for each material parameter and mechanical property. However, when a number of specimens are tested, different randomly distributed values are obtained for the same material property. Therefore, the analysis of laminates has to be performed based on a probabilistic approach. When finite element analysis is performed based on a stochastic approach such that a stochastic description can be provided for both the material parameters and the response of the laminates, the resulting FEA is termed as *Stochastic*

Finite Element Analysis (*SFEA*). The remainder of this chapter is devoted to the fracture analysis of composite laminates based on a stochastic approach.

3.8 Stochastic Field Modeling of Material Parameters

The spatial variations of material properties such as the Young's modulus, Poisson's ratio and shear modulus are considered to constitute in each case a two-dimensional homogeneous stochastic field. The fluctuating components $a(X)$ of a material property have a zero mean. For instance, the stochastic field of the Young's modulus in the fiber direction (E_1) is given below and a similar procedure is applicable to E_2, G_{12}, ν_{12}, ν_{21}, ply orientation angle and ply thickness.

$$E_1 = \bar{E}_1[1 + a(X)] \quad ; \quad E[a(X)] = 0 \tag{3.66}$$

The auto-correlation function is given by [85]

$$R_{aa}(\xi) = E[a(X)\,a(X+\xi)] \tag{3.67}$$

In the above, $X = [x, y]^t$ indicates the position vector and $\xi = [\xi_x, \xi_y]^t$ represents the separation vector between two points X and $(X + \xi)$. In practical cases each material property is considered to vary at each Gauss point. Thus, if n represents the number of finite elements present in the structure, and m represents the order of Gauss quadrature, then there are N (equal to $n*m$) material property values associated with the structure.

Consider only the fluctuating component of the homogeneous stochastic field, which is used to model the material property variations around the expected value. These N values $a_i = a(X_i)$ $(i = 1,2,3,...,N)$, are *correlated* random values with zero mean. Also X_i corresponds to the location of each Gauss point. Their correlation characteristics can be specified in terms of the covariance matrix C_{aa} of order N x N, whose ij^{th} component is given by

$$c_{ij} = Cov[a_i a_j] = E[a_i a_j] = R_{aa}(\xi_{ij}); \quad i,j = 1,...,N \tag{3.68}$$

in which $\xi_{ij} = (X_j - X_i)$ = the separation distance between the Gauss points i and j. Now a vector $a = [a_1 \quad a_2 \quad a_3 \quad ... \quad a_N]^t$ can be generated by

$$a = LZ \tag{3.69}$$

in which $Z = [Z_1 \quad Z_2 \quad Z_3 \quad ... \quad Z_N]^t$ is a vector consisting of N independent Gaussian random variables with zero mean and unit standard deviation, and L is a lower triangular matrix obtained by the Cholesky decomposition of the covariance matrix C_{aa}. Thus,

$$LL^t = C_{aa} \tag{3.70}$$

Once the Cholesky decomposition is accomplished, different sample vectors of a are easily obtained by generating different samples for the Gaussian random vectors Z.

The correlation properties of the stochastic field representing the fluctuating components of material properties are expressed using the Markov correlation model, also known as the First-order autoregressive model. The choice of this model in this work is due to its wide use in the literature [103].

3.9 Markov Model

The first order autoregressive correlation model or the Markov model is given by

$$R_{aa}(\xi) = \sigma_o^2 \exp\left[-\left(\frac{|\xi|}{d}\right)\right] \tag{3.71}$$

in which σ_o is the standard deviation of the stochastic field $a(X)$ and further d is a parameter called the correlation length, which is defined such that the correlation is negligible when d is large. The stochastic field $a(X)$ represents the deviatoric components of the material property with autocorrelation function as given in Equation (3.71). The stochastic field $a(X)$ for each Gauss point is represented by the value of a_g of $a(X)$ at the Gauss point X_g of the structure i.e., $a_g = a(X_g)$. The auto-correlation model given by the Markov model is presented below in Figure 3.8 for three different values of d = 10, 30 and 50 mm. From this figure it can be observed that the variations in the correlation with the separation distance, d have a similar trend (*concavity* of the graph) for all values of d. For instance, for a separation distance of 20, the correlation values for d = 10, 30 and 50 are 0.14, 0.51 and 0.69 respectively.

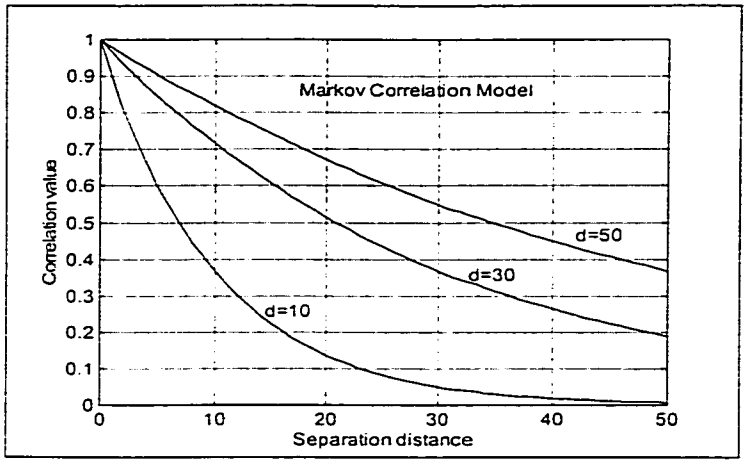

Figure 3.8 The first-order autoregressive correlation function for d = 10, 30 and 50

Considering for instance, that the distance between any two Gauss points (*i* and *j*) in the structure, the ij^{th} entry in the covariance matrix of any mechanical property, is given by Equations (3.68) and (3.71). Also the corresponding value for the standard deviation of the mechanical property is used in the Equation (3.71). This covariance matrix is symmetric and is different for each mechanical property. This covariance matrix is decomposed into upper and lower triangular matrices *U* and *L*. Considering the property, E_1, the column matrix *a* as in Equation (3.72) is generated by using the Equation (3.69).

The Young's modulus along the fiber direction can now be assumed to have distributions as given by the vector *a* and can be represented by

$$E_{1g} = E_{1m}(1 + a_g) \tag{3.72}$$

where E_{1g} is the value of the Young's modulus in the fiber direction at a Gauss point.

Moreover, E_{1m} is the mean value of the Young's modulus in the fiber direction and is taken from the Table 3.1. Similarly, the other material properties are represented by

$$\text{Young's modulus in the matrix direction, } E_{2g} = E_{2m}\left(1 + b_g\right) \tag{3.73}$$

$$\text{1-2 directional Poisson's ratio, } \nu_{12g} = \nu_{12m}\left(1 + c_g\right) \tag{3.74}$$

$$\text{Shear modulus, } G_{12g} = G_{12m}\left(1 + d_g\right) \tag{3.75}$$

in which E_{2m} is the mean value of the Young's modulus in the matrix direction and further, ν_{12m} and G_{12m} are the mean values of the 1-2 directional Poisson's ratio and the shear modulus respectively.

It should be noted here that the standard deviations of a_g, b_g, c_g and d_g represent the coefficients of variation of the material properties E_{1g}, E_{2g}, ν_{12g} and G_{12g}. Also the variation of the ply orientation angle, θ_g and the ply thickness t_g are evaluated in a manner similar to Equations (3.72 – 3.75) as

$$\theta_g = \theta_m\left(1 + e_g\right) \tag{3.76}$$

$$t_g = t_m\left(1 + f_g\right) \tag{3.77}$$

in which θ_m and t_m are the mean values of the ply orientation angle and ply thickness respectively. The assumption of Gaussian distribution implies the possibility of

generating negative values for the material properties. In order to avoid this difficulty, the values of the random variable, a_g, in the case of Monte-Carlo simulation are confined to the range

$$-1+\varepsilon \le a_g \le 1-\varepsilon \tag{3.78}$$

where ε is a very small perturbation parameter.

3.10 Programming the Stochastic Finite Element Analysis

Using the test data of the material properties provided in Table 3.1, the stochastic processes that correspond to the Young's moduli, Poisson's ratio and Shear modulus are determined according to Equations (3.72 – 3.75) and further, sample realizations at each Gauss point in the finite element mesh are obtained. Using the generated sample realizations of material properties at each Gauss point the stochastic elasticity matrix, $[E]$, is calculated for each Gauss point. The stochastic elasticity matrix generated thus is incorporated into the Equation (2.62) for the element stiffness matrix. The flow chart for computing the stochastic fields of the elastic constants is given below in Figure 3.9. This change is introduced as another routine (*RNDPROPS.m*) in the input file, *GETARR.m*. The rest of the programming logic details and control flow details are same as listed in Figures (2.10 – 2.11). Now the entire analysis is performed for 250 test specimens and the mean and standard values of various fracture parameters are computed. The reasons for using this specific number (250) are discussed in chapter 5.

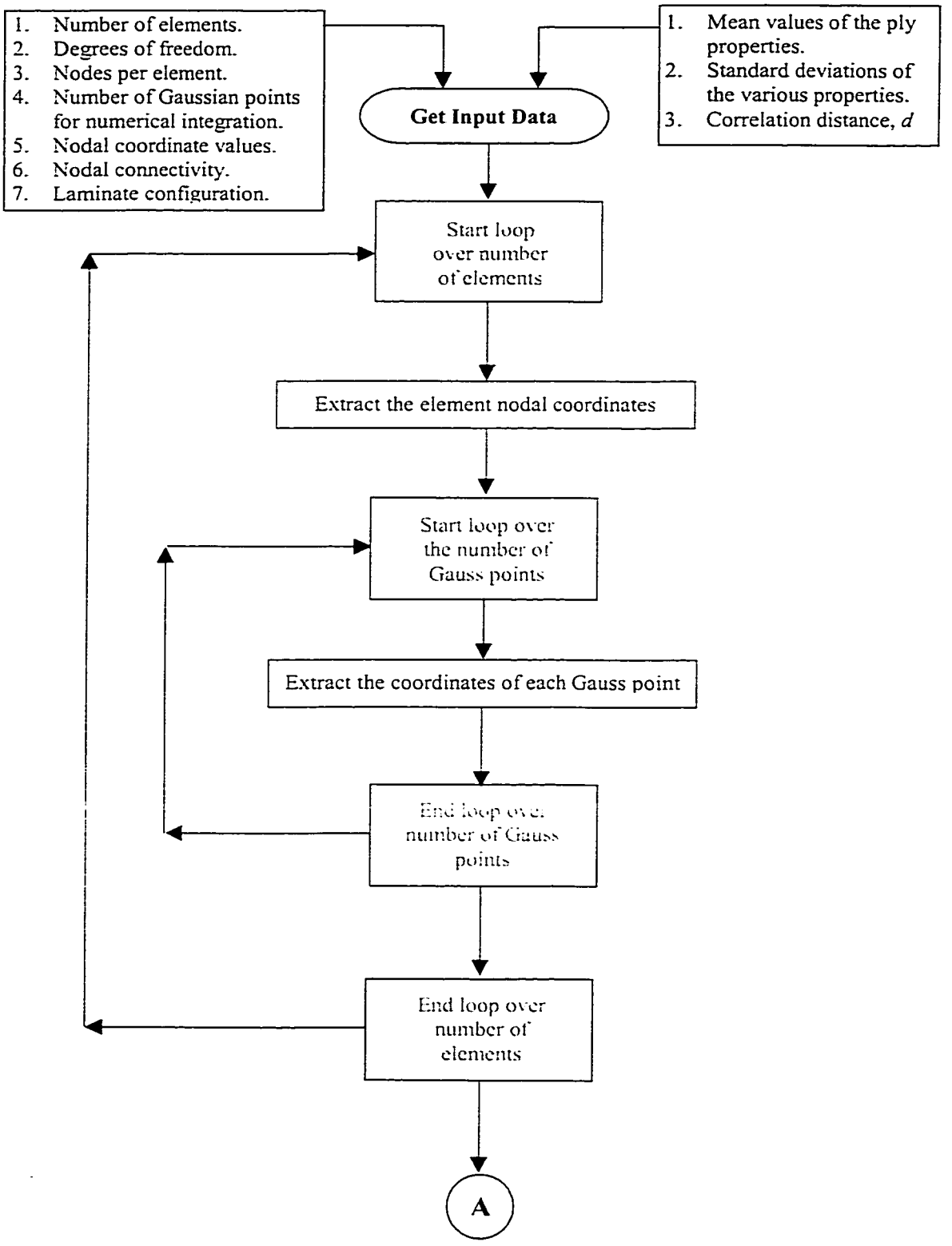
1. Number of elements.
2. Degrees of freedom.
3. Nodes per element.
4. Number of Gaussian points for numerical integration.
5. Nodal coordinate values.
6. Nodal connectivity.
7. Laminate configuration.
1. Mean values of the ply properties.
2. Standard deviations of the various properties.
3. Correlation distance, d
Get Input Data
Start loop over number of elements
Extract the element nodal coordinates
Start loop over the number of Gauss points
Extract the coordinates of each Gauss point
End loop over number of Gauss points
End loop over number of elements
A

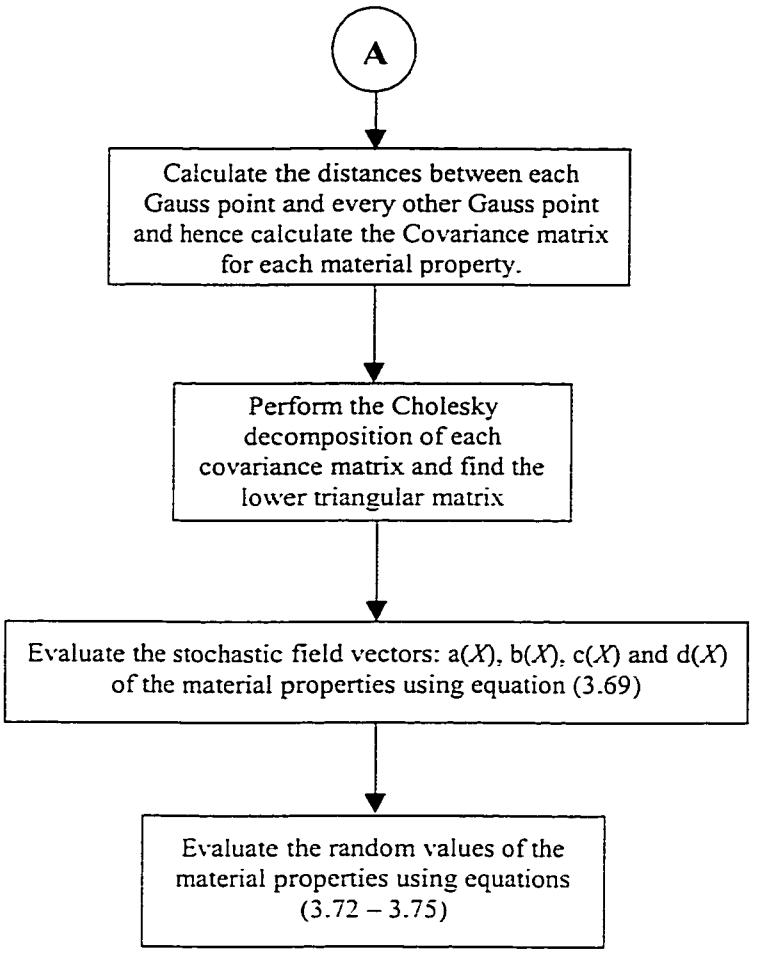

Figure 3.9 Flow chart used for the calculation of material properties based on stochastic field modeling

It must be noted here that, in order to make the program more understandable, each task has been assigned to a separate function. For example, *DISP_EXTRAP.m* and *ERR_EXTRAP.m* are two functions used to obtain the *SIF* and *ERR* by extrapolation techniques, whereas the function *ERRCALC.m* calculates the *ERR* each time an element is *released*. Also, the function *EVALJ.m* is used to evaluate the *J*-integral for the initial

boundary conditions and the functions *EVALSIF1.m*, EVALSIF3.m and EVALSIF4.m are used to evaluate the *SIF* by *DEM*, *ERRM* and *J*-integral method respectively.

3.11 Illustrative Application

The MATLAB® program developed in this chapter is now demonstrated through an application to a composite laminate with a configuration of $[0/90]_{6s}$ made of NCT 301 graphite-epoxy composite material. The structural geometry, the loading and the finite element mesh employed are the same as shown in Figure 3.7. The problem under consideration is the same as that considered in section 3.5 and in this case too, the crack-plate width ratio is taken as 0.33.

Using the test data on elastic constants of the composite material, presented in Table 3.1, the stochastic field realizations of all the material properties are obtained at each Gauss point using Equations (3.72 – 3.75). In the present thesis, a three-point Gaussian numerical integration is used as it gives the most accurate results. Considering any typical element in the structure (Figure 3.7), nine different sample realizations of each of the stochastic processes are generated corresponding to the nine Gauss points in the element. Considering a particular set of sample realizations generated for the entire structure, a sample realization for Gaussian points in elements 5 and 43, for the $[0/90]_{6s}$ laminate, is shown below in Figure 3.10.

Using these sample realizations of the material properties, the elasticity matrix, $[E]$, at each Gauss point is calculated according to Equation (3.47).

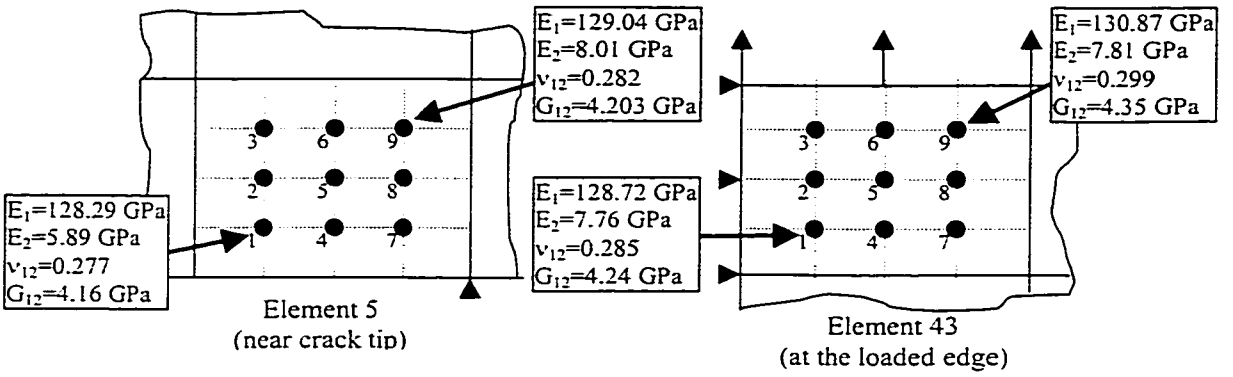

Figure 3.10 A set of sample realizations of elastic constants at different Gauss points in elements 5 (near the crack tip) and 43 (at the loaded edge)

Also presented below in Figure 3.11, are the sample variations of the Young's modulus along the fiber direction, with the distance of separation the Gauss points from each other.

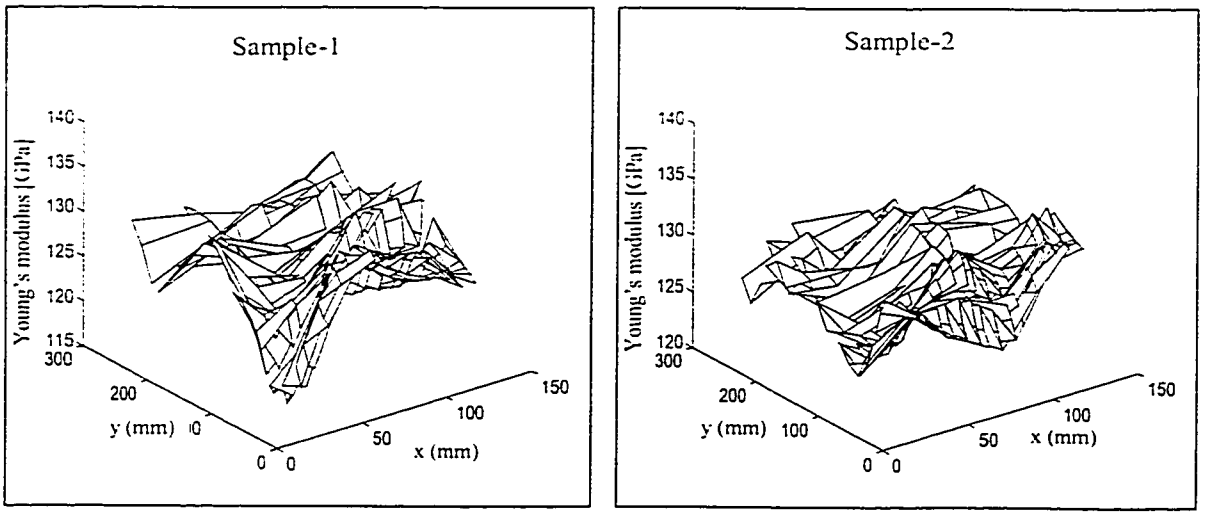

Figure 3.11 Simulated sample variations of the fiber direction Young's modulus

Using the generated sample realizations of elastic constants at each Gauss point, the stochastic laminate elasticity matrix [E] at the corresponding Gauss point is calculated according to Equation (3.65) in section 3.3.3.

A sample realization of the stochastic elasticity matrix [E] for a $[0/90]_{6S}$ laminate for the simulation that is the same as the one shown in Figure 3.10, is now shown in Figure 3..12.

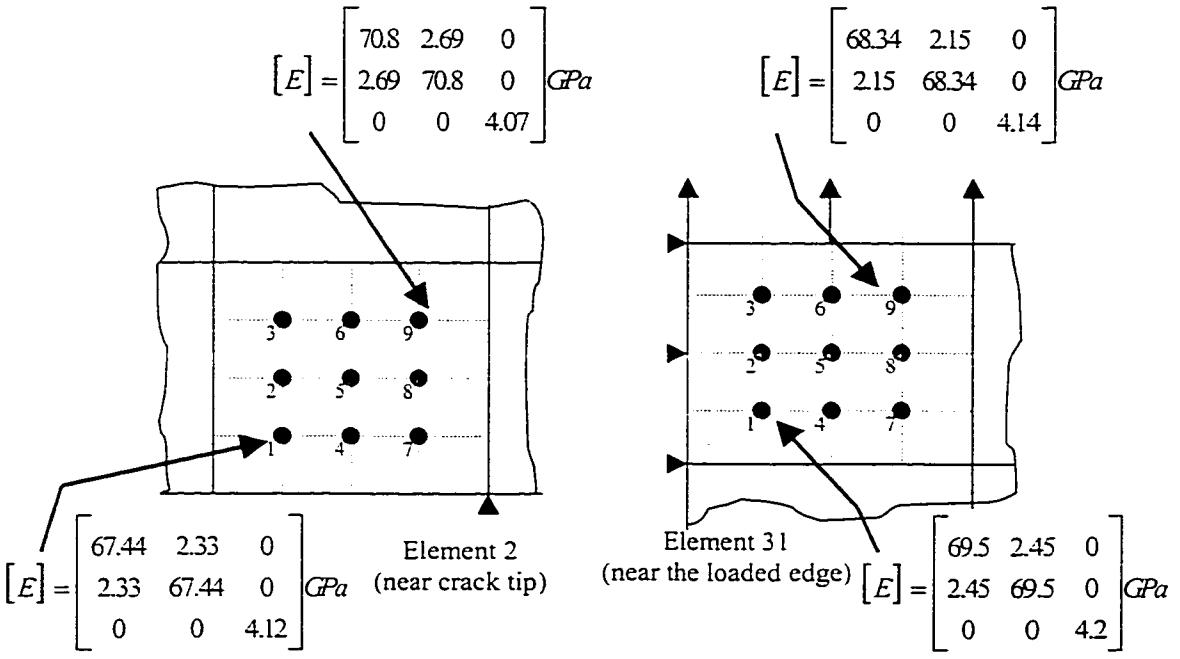

Figure 3.12 A set of sample realizations of the stochastic elasticity matrix at different Gauss points

With the above set of sample realizations for the material properties and elasticity matrices, the element stiffness matrices are computed according to Equation (2.60) and the global stiffness matrix for the structure can be obtained by

$$K = \sum_{ielem=1}^{NELEM} [k]^{(e)} \tag{3.79}$$

in which *NELEM* represents the number of elements in the entire structure and is equal to 43 in the present example. After obtaining the global stiffness matrix, the displacements are obtained by solving

$$[K]\{d\} = \{f\} \tag{3.80}$$

in which $\{d\}$ represents the displacement vector and $\{f\}$ represents the applied force vector. A set of sample displacements is listed below in Table 3.4.

Node Number	X-Displacement (u mm)	Y-Displacement (v mm)
1	0.0000	1.1740
2	-0.0299	1.1692
3	-0.0620	1.1510
4	-0.0932	1.1199
5	-0.1259	1.0728
6	-0.1578	1.0110
7	-0.1911	0.9309
8	-0.2241	0.8299
9	-0.2573	0.6807
10	-0.2757	0.4942
148	0.0000	2.1765
149	0.0403	2.1615
150	0.0666	2.0807
151	0.0697	1.9909
152	0.0597	1.9256
153	0.0474	1.9047
154	0.0372	1.9072

Table 3.4 A set of sample displacements at the crack flank and at the loaded edge

Using the displacements obtained above the strain energy is calculated as

$$Strain\ Energy = \frac{1}{2}\{d\}^t\{f\} \tag{3.81}$$

The *SIF* can be computed by using Equation (3.15). After obtaining the displacements, the strain energies and the *SIF*s, and the *SIF* at the crack tip can be obtained by extrapolation using the equation of a straight line as

$$Y = mX + c \tag{3.82}$$

in which X represents the radial distance from the crack tip along the $\theta = 180^\circ$ line and further, m and C are the slope and a constant (equal to the intercept on the Y axis when the value of X is equal to zero) respectively. In the above Equation (3.82), the slope, m, can be obtained as

$$m = \frac{K_2 - K_1}{a_2 - a_1} \tag{3.83}$$

and the value of C is the value of the *SIF* at the crack tip, which can be calculated as

$$C = K_1 - ma_1 \tag{3.84}$$

After performing 250 simulations (that is for 250 laminates), a set of 250 sample realizations are obtained for all the fracture parameters for each laminate: SIF_{DEM}, SIF_{SERRM}, $SIF_{J:1\text{-}12}$, *ERR* and J_1, J_2,...., J_{12} (corresponding to each of the twelve J contours). The mean values, standard deviations and coefficients of variation of these various fracture parameters are calculated and provided in Tables (3.5 – 3.7).

Stress Intensity Factor	Mean Value (MPa√m)	Standard Deviation (MPa√m)	Coefficient of Variation
DEM	51.302	3.531	0.069
ERRM	69.862	3.963	0.057

Table 3.5 Mean value, Standard deviation and Coefficient of variation of K_I for the $[0/90]_{6s}$ laminate determined by *DEM* and *ERRM*

ERR & J	Mean Values (x1.0e5 N-m/m2)	Standard Deviation (x1.0e5 N-m/m2)	Coefficient of Variation
ERR	9.211	1.061	0.115
J_1	9.374	1.219	0.130
J_2	10.049	1.312	0.131
J_3	9.505	1.231	0.129
J_4	9.602	1.253	0.130
J_5	9.741	1.278	0.131
J_6	9.571	1.251	0.131
J_7	9.588	1.257	0.131
J_8	9.636	1.267	0.132
J_9	9.551	1.253	0.131
J_{10}	9.520	1.263	0.133
J_{11}	9.512	1.262	0.133
J_{12}	9.512	1.264	0.133

Table 3.6 Comparison of the mean value, standard deviation and coefficient of variation values of *J*-integral obtained from various contours, and the *ERR*

Stress Intensity Factor corresponding to	Mean Value (MPa√m)	Standard Deviation (MPa√m)	Coefficient of Variation
J_1	69.848	4.536	0.065
J_2	72.318	4.716	0.065
J_3	70.337	4.549	0.065
J_4	70.693	4.607	0.065
J_5	71.201	4.666	0.066
J_6	70.578	4.609	0.065
J_7	70.638	4.628	0.066
J_8	70.813	4.652	0.066
J_9	70.503	4.619	0.066
J_{10}	70.416	4.661	0.066
J_{11}	70.386	4.660	0.066
J_{12}	70.353	4.668	0.066

Table 3.7 Values of the *SIF* obtained from various *J*-integral contours

3.12 Conclusions and Discussions

In the first half of this chapter, the various concepts of fracture mechanics (*LEFM*) as applied to anisotropic materials under plane stress state have been summarized. Also the computation of various fracture parameters has been demonstrated through an illustrative example. The analysis results for a deterministic case that are obtained from the MATLAB® program have been confirmed by using the standard ANSYS® software. In the latter half of this chapter, various concepts of stochastic formulation and their relevance with regard to the behavior of composite materials have been discussed. The stochastic finite element analysis formulation as applied to composite materials has been described in detail. An illustrative example problem is used to demonstrate the variations in material properties, and the variations in the various fracture parameters. Their mean

values, standard deviations and coefficients of variation have been determined and provided in Tables (3.5 – 3.7).

Chapter 4

Parametric Study of Stochastic Fracture Behavior of Composite Laminates

4.1 Introduction

The prediction of the values of various fracture parameters as well as their variations with the material and geometric parameters of the structure and applied loading is of much interest to the engineer. During design for a maximum load that a particular composite structure might be subjected to, while in operation, the engineer might have to take the help of standard data charts for obtaining the above-mentioned variations in various fracture parameters. These data are crucial to the engineer at various stages of the design and analysis process. In the present chapter, the variations of various fracture parameters and their probabilistic parameters (such as mean value, standard deviation and probability density function parameters) with the variations in the material and geometric parameters will be considered. The stochastic finite element analysis formulation for composite laminates described in the previous chapter is employed for the analysis of various types of composite laminates. The mean values and standard deviations of the *SIF*, *ERR* and *J*-integral are determined based on the *DEM*, the *ERRM* and the *J*-integral method, and then, they are represented in a graphical form. The analysis has been performed for the following three types of laminates:

a) Symmetric Cross-ply Laminate : $[0/90]_{6s}$

b) Quasi-isotropic Laminate : $[0/\pm45/90]_{3s}$

c) Symmetric Angle-Ply Laminate : $[\pm45]_{6s}$

The same geometric and ply material properties of the composite laminate considered in the earlier two chapters are also used in this chapter for determining the variations of various fracture parameters. The program logic shown previously in Figure 3.8 is employed here with a few modifications in order to reduce the amount of manual data input. In the final version of the MATLAB® program a couple of functions are added; they are *AUTOMESH.m* and *CALCLOADS.m*. The names are self-describing in the sense that the former is used to generate a finite element mesh automatically and the latter is used for calculating the nodal loads. For any given values of the ratios a/W and W/L, and any given plate geometry, the function *AUTOMESH.m* automatically generates a finite element mesh satisfying the given conditions. For a given uniformly distributed load, the function *CALCLOADS.m* calculates the work-equivalent nodal loads at the loaded edge.

4.2 Fracture Analysis of $[0/90]_{6s}$ NCT-301 Composite Laminate

First, the number of simulations for the stochastic analysis has been determined in order that the mean value of any fracture parameter does not change with further increase in the number of simulations. These results are presented below in Figure 4.1 in a graphical form. Also, the comparison between the *SIF* values that are obtained using the three methods, viz., *DEM*, *ERRM* and *J*-integral has been performed and represented below in a graphical form. The following results correspond to a crack length of 48 mm i.e., the *a/W* ratio is 0.4. In a similar manner, the comparison between the *J*-integral values obtained using various contours in the composite structure is shown. In all further analyses, the maximum value of the *J*-integral can be considered to be a critical factor in

design. Also for the same applied load the *J*-integral can be observed to have a stochastic variation, thus leading to a probabilistic design.

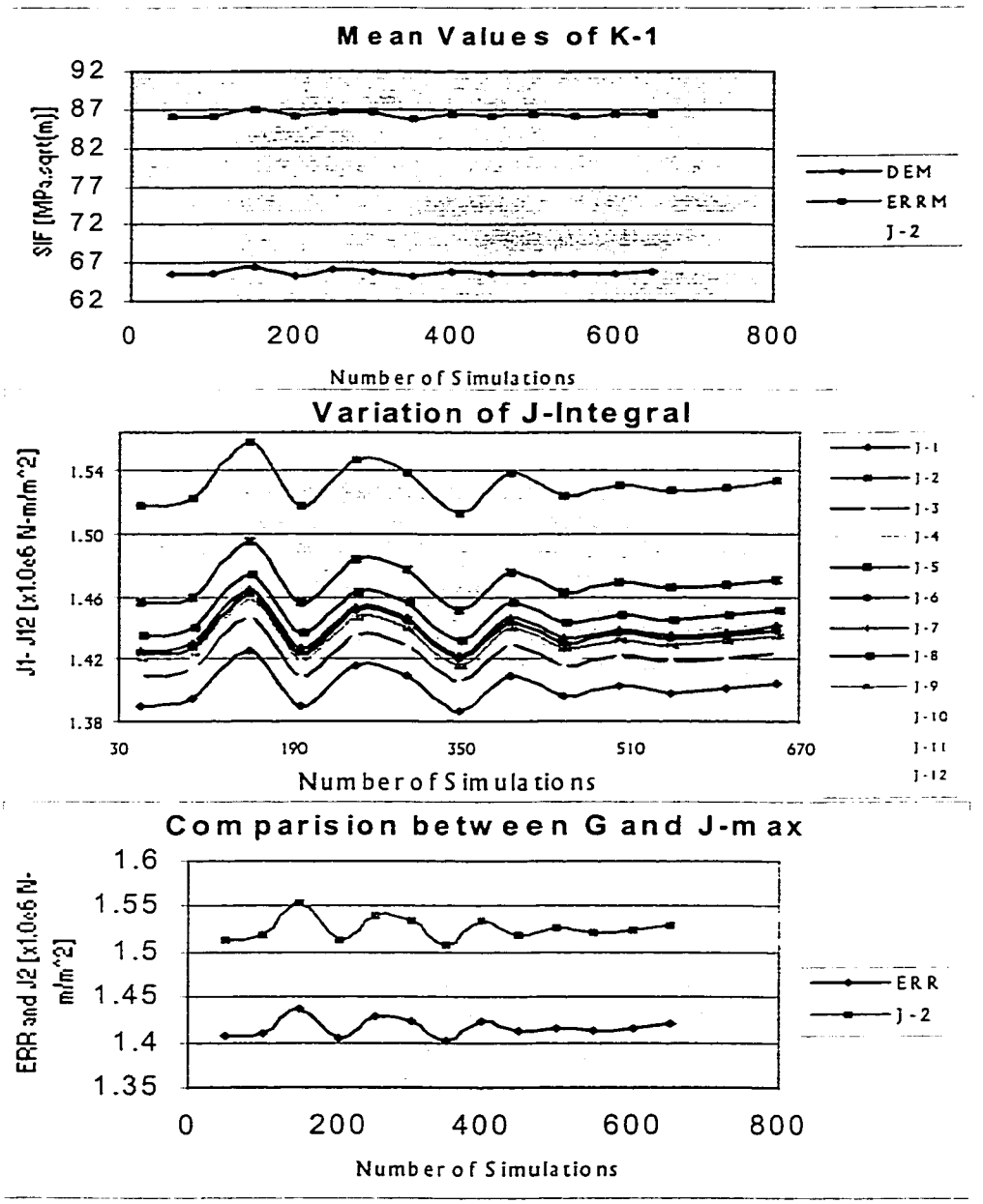

Figure 4.1 Fracture analysis of $[0/90]_{6s}$ laminate: (a) Variation of the mean values of *SIF* determined using by *DEM*, *ERRM* and *J*-integral method with the number of simulations. (b) Variation of the mean values of the *J*-integral with the number of simulations. (c) Comparison between the mean values determined using the *ERR* and maximum value of *J*-integral, i.e., J_2.

The influence of the number of simulations, within the range 50 - 650 on the probabilistic moments (mean value and standard deviation) of K_I has been studied. The variations in the mean values with the number of simulations have been presented above in Figure 4.1 and the variations in the standard deviation values with the number of simulations are presented below in Figure 4.2. From the above graph (Figure 4.1-a) it can be seen that the influence of the number of simulations on the variations of the mean values of K_I almost disappears after 450 simulations. This means that *after 450 simulations the SIF values obtained are almost constant*. Right from the beginning it can be seen that the mean value does not change quite considerably and fluctuations almost disappear later on. This information can be used in determining the number of specimens that have to be used in determining the average values of various fracture parameters, in a practical manner. The ultimate decision regarding the choice of the number of test specimens might however depend on other factors. It can also be observed that the *J*-integral method yields the maximum value of the *SIF*. Also, while the variations in the *SIF* is approximately 3% of the mean value the variations in the values of the *J*-integral and the *ERR* are approximately 2% of the mean value. Also from Figure 4.1-b it can be observed that the stochastic variations in the *J*-integral are very pronounced in the range: 50 – 450. The stochastic variations in the *J*-integral start to minimize after the number of simulations is equal to 450. Considering the fluctuations in the *J*-integral values with the average value of each *J*-integral as well as the computing time, the number of simulations is taken as 250. It can also be observed that J_2 yields the maximum value of all. A comparison between the maximum value of the *J*-integral (i.e. J_2) and the *ERR* is provided in Figure 4.1-c.

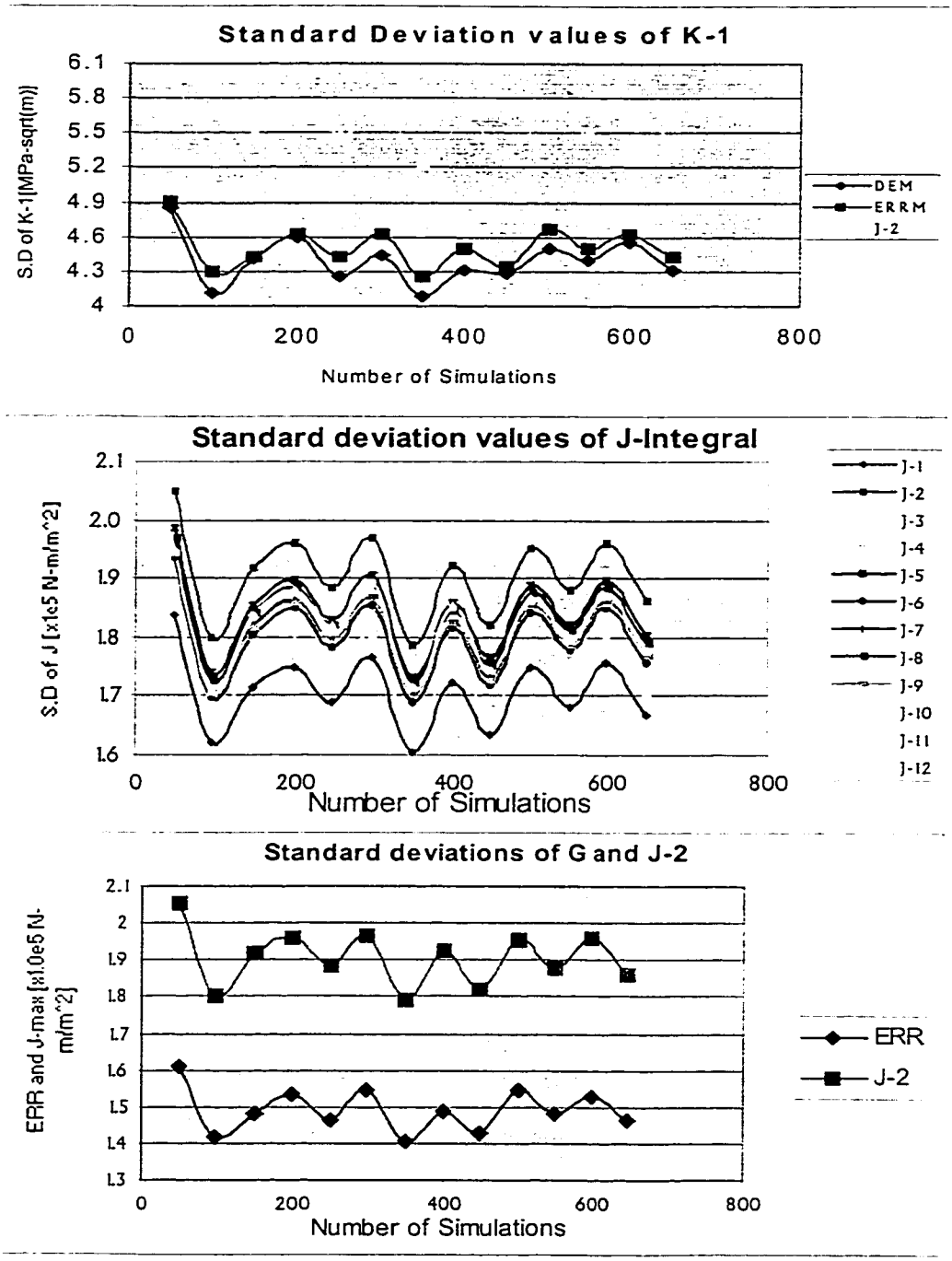

Figure 4.2 Fracture analysis of $[0/90]_{6s}$ laminate with the number of simulations: (a) Variation of the respective standard deviations of *SIF* values determined using *DEM*, *ERRM* and *J*-integral method with the number of simulations. (b) Variation of the standard deviations of the *J*-integral values with the number of simulations. (c) Comparison between the respective standard deviations of *ERR* and J_2.

From Figure 4.2 it can be seen that the influence of the number of simulations on the standard deviation values does not get reduced to the same order as that of the mean values, with increase in the number of simulations. However, the variations are maximum initially in the range 50–200, but get reduced comparatively after the number of simulations exceeds 250. This variation in standard deviation can be attributed to the stochastic behavior of the laminates. Due to the time considerations in the analysis and given the reduced variations in the mean values of the various fracture parameters, the number of simulations has been fixed at 250. It must be noted that the time taken for the analysis of 250 laminates is approximately around 8.5 hours on a standard 400 mega hertz Pentium class Windows NT 4.0 system. Other reasons for selecting 250 as the number of simulations based on the distribution of the sample values are further discussed in chapter 5. While it can be seen from Figure 4.1-a that the mean values of *SIF* obtained from J_2 and *ERR* are close to each other, the standard deviation values of *SIF* obtained from J_2 are much higher than those obtained from *ERR* and *DEM*. Also, the standard deviation values of J_2 are higher than the standard deviation values of the other *J*-integrals. Therefore, *J_2 can be considered as a critical factor in design as its variation is high for this particular case.*

4.2.1 Effect of the Crack Length – Plate Width Ratio on the SIF

In the following section, the variations of the mean values and standard deviations of the various fracture parameters with the variations in the crack length-plate width (*a/W*) ratio are discussed. It is widely believed that the crack length has a more pronounced effect on the variations of the *SIF* than the effects due to the length and width.

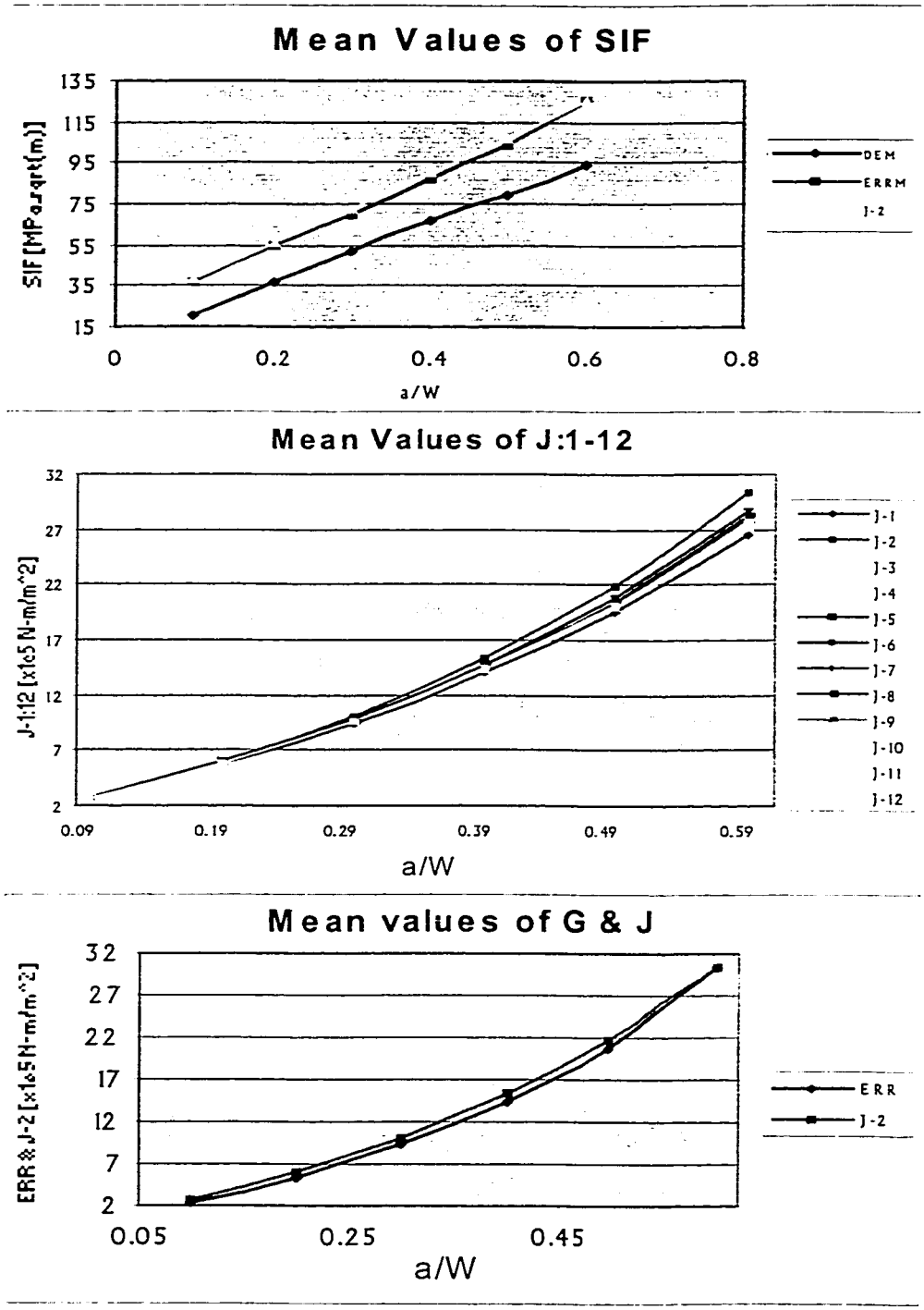

Figure 4.3 Fracture analysis of $[0/90]_{6s}$ laminate: (a) Variations of the mean values of *SIF* determined using *DEM*, *ERRM* and the *J*-max (J_2) with a/W ratio. (b)Variations of the mean values of J_1 - J_{12} with *a/W* ratio. (c) Comparison of the variations in the mean values of *ERR* and J_2 with *a/W* ratio.

From Figure 4.3-a it can be seen that the *SIF* values obtained using the *DEM*, *ERRM* and the maximum value of the *J*-integral follow an *almost* linear trend. It can also be noticed that the *SIF* obtained from the *DEM* follows a linear trend until *a/W* ratio is approximately equal to 0.45 and takes a slight decrease in slope and again increases in a linear manner. The *SIF* values obtained by *ERRM* are almost equal to the *SIF* values obtained from the maximum value of the *J*-integral (i.e. J_2) when the *a/W* ratio is almost equal to 0.6.

The stochastic variations in the mean values of the various *J*-integral values follow approximately a parabolic manner. Initially (at lower values of *a/W* ratio), all the *J*-integral contours are almost equal with values around 2.5×10^5 N-m/m^2. However, as *a/W* ratio increases the difference between the maximum and the minimum values of the *J*-integral increases to 3.5×10^5 N-m/m^2 when the *a/W* ratio is equal to 0.6. A comparison between the mean values of the *ERR* and the maximum value of the *J*-integral (i.e. J_2) are presented in Figure 4.3-c. At lower values of *a/W* the difference between the values of *ERR* and J_2 is very less. The difference between these two is almost zero when *a/W* ratio is equal to 0.55. Hence, *the ERRM and the maximum value of the J-integral give approximately the same values when a/W ratio is greater than 0.55.* Interestingly, this difference increases at intermediate values of *a/W* before it starts to decrease again.

From Figure 4.4, it can be observed that the stochastic variations in the standard deviation values of the *SIF* obtained by the *DEM*, *ERRM* and the maximum value of the *J*-integral (i.e. J_2) do not follow a linear trend as in the case of the mean values. Also, the standard deviation values of the *ERR* tend to drift away from those of J_2 as the *a/W* ratio increases. The variations in the standard deviation values of the various *J*-integral contours are similar to the variations in their respective mean values. A comparison between the standard deviation values of the *ERR* and the maximum value of the *J*-integral is provided below in Figure 4.4-c. In contrast to the variations in the mean values, the variations in the standard deviation values keep on increasing with an increase in the *a/W* ratio.

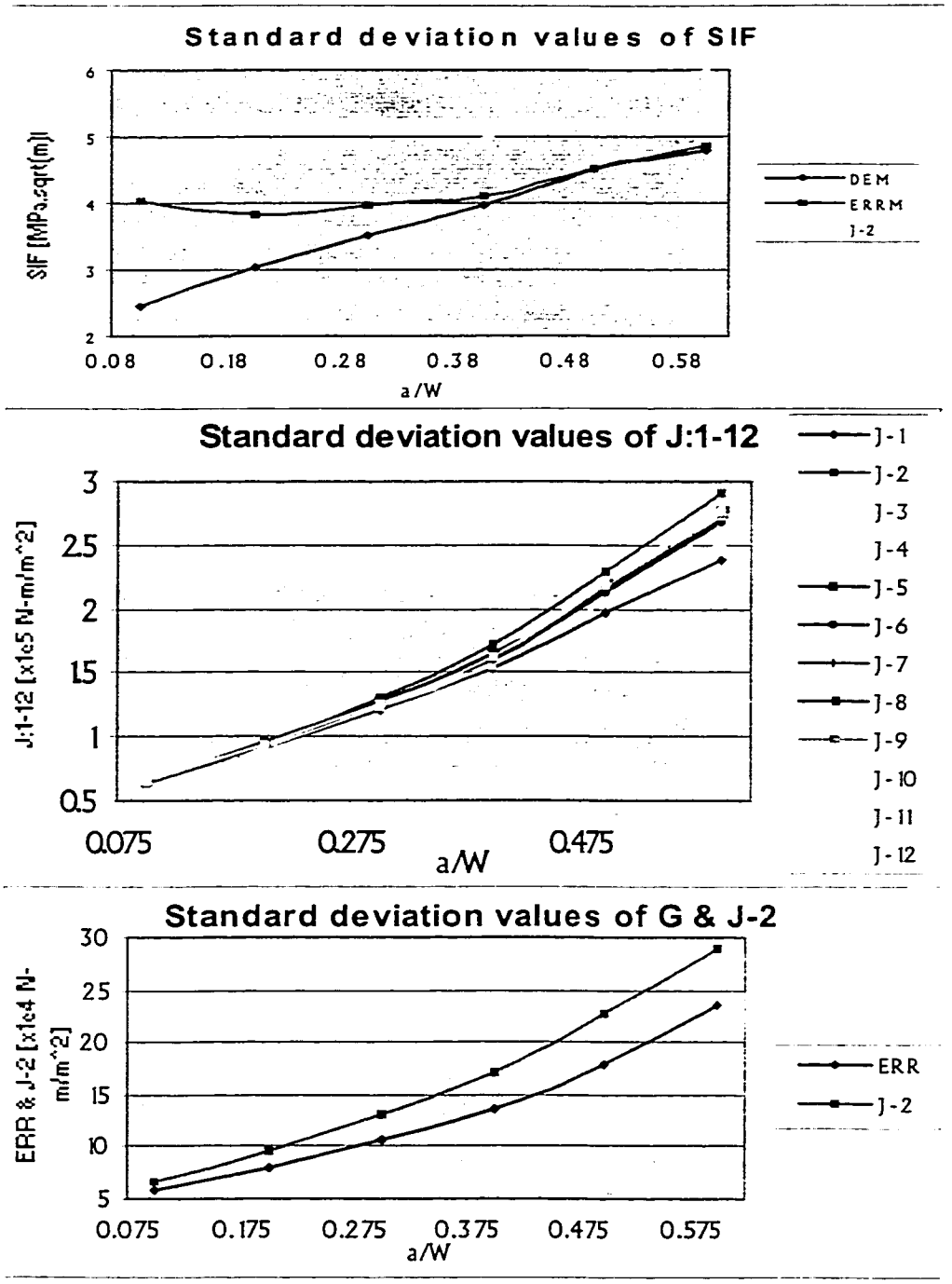

Figure 4.4 Fracture analysis of $[0/90]_{6s}$ laminate: (a) Variations of the standard deviations of *SIF* values determined using *DEM*, *ERRM* and *J*-max. (J_2) with *a/W* ratio. (b) Variations of the standard deviations of J_1 - J_{12} with *a/W* ratio. (c) Variations of the standard deviations of *ERR* and J_2 with a/*W* ratio.

In all the three cases that have been presented in Figures 4.3 – 4.4, it can be seen that the mean values as well as the standard deviation values increase with an increase in the length of the crack. *In general terms, the randomness in the fracture parameters increases with an increase in the crack length. Also, eventhough the ERRM and the maximum value of the J-integral yield approximately the same values of SIF, the variations of the J_2 as well as the SIF obtained from J_2 are more than the corresponding values obtained from ERRM.* Further, it can be observed that the standard deviations of the *SIF* are approximately around 5% of the respective mean values. In the case of the standard deviations of the *ERR* and *J*-integral values, the corresponding variations are found to be approximately around 10%. Further, it can be observed that the variations of the mean values of *SIF* with *a/W* ratio follow an almost linear relationship. With increase in the crack length, more clustering of the load flow lines can be assumed to occur around the crack tip and thus an increase in the *SIF* can be predicted. This aspect is authenticated in the Figure 4.3-a.

4.2.2 Effect of Finite Plate Size on the SIF

Just as the *SIF* is affected by the size of the crack, the finite geometry of the plate, i.e., the width and the length of the plate also affect the *SIF*. In general, the *SIF* may be expressed as

$$K_I = f_{iso}\left(\frac{a}{W}\right) f\left(\frac{a}{W}, \frac{W}{L}\right) \sigma\sqrt{\pi a} \qquad (4.1)$$

In the above equation, the factor that is responsible for deviating the value of the *SIF* from its *ideal* value as in the case of an infinite plate with a remotely acting stress can be represented as

$$f\left(\frac{a}{W},\frac{W}{L}\right)=f_1\left(\frac{a}{W}\right)f_2\left(\frac{W}{L}\right)=f_1 f_2 \tag{4.2}$$

and $f_{iso}\left(\frac{a}{W}\right)$ represents the normalized factor of an isotropic specimen. For a center cracked plate this factor is given by

$$f_{iso}\left(\frac{a}{W}\right)=\left[1-0.0025\left(\frac{a}{W}\right)^2+0.06\left(\frac{a}{W}\right)^4\right]\sqrt{sec\left(\frac{\pi a}{2W}\right)} \tag{4.3}$$

In the above Equation (4.2), it can be seen that, apart from the relative size of the crack, the relative sizes of the width and the length of the plate also have a bearing on the *SIF*.

In the second factor, $f_2\left(\frac{W}{L}\right)$, an increase in the width or a decrease in the length of the plate have the same effect of increasing the *W/L* ratio. However the resulting values of the second factor, i.e. f_2, may not be the same. Hence, the effects of the width and the length of the plate on the *SIF* have been investigated separately. Initially, the effect of the change in length (i.e., in f_2 of Equation (4.2), the width is kept constant at 120 mm and the length has been varied) on the *SIF* is studied and the results are presented below in Figures 4.5 – 4.6.

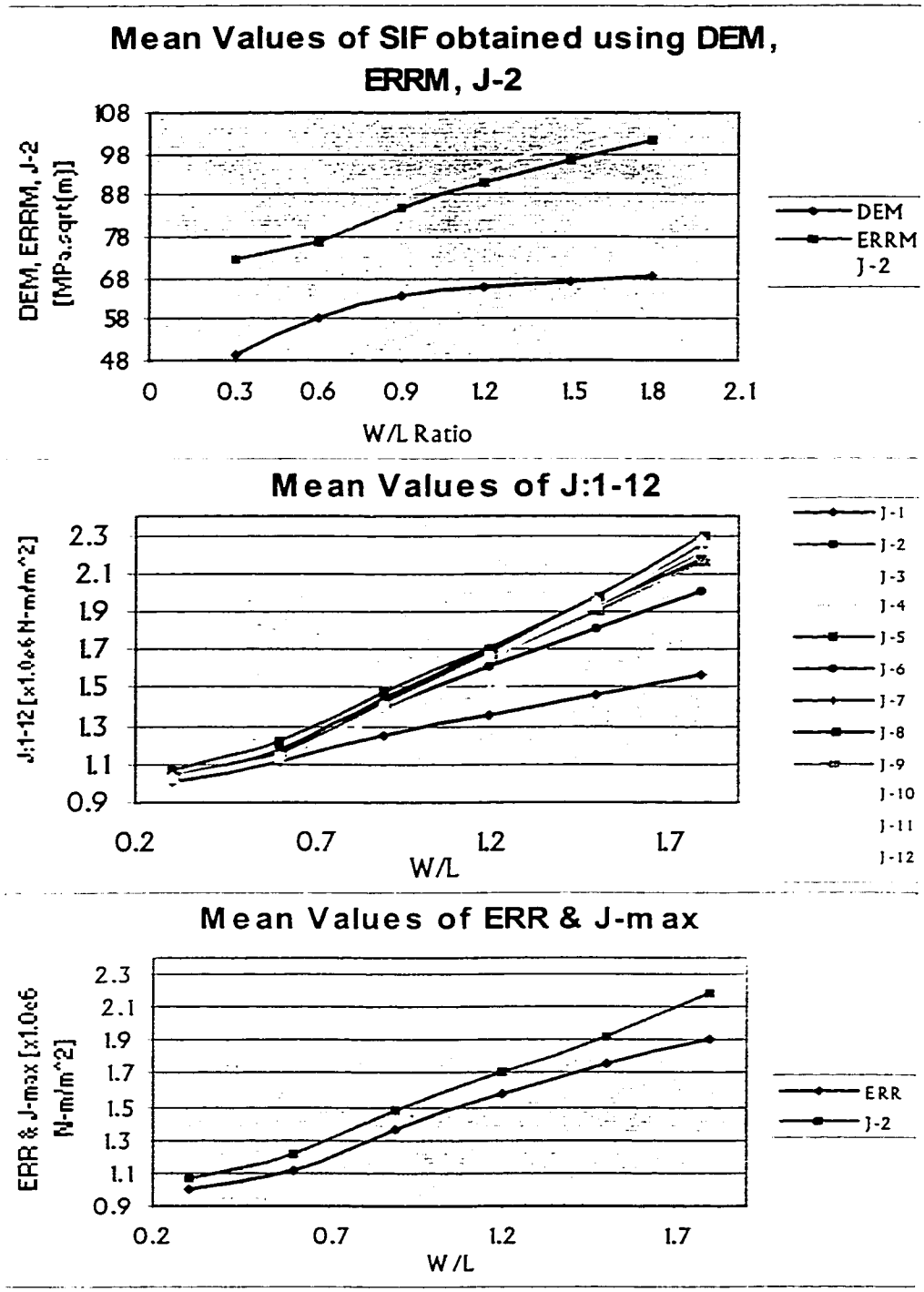

Figure 4.5 Fracture analysis of $[0/90]_{6s}$ laminate: (a) Variations of the mean values of *SIF* determined using *DEM*, *ERRM* and *J*-integral method with *W/L* ratio. (b) Variations of the mean values of J_1 - J_{12} with *W/L* ratio. (c) Comparison of the *ERR* with the maximum value of the *J*-integral.

It can be observed from Figure 4.5-a that the *SIF* increases with an increase in the *W/L* ratio i.e., with the decrease in the length of the plate the *SIF* increases. Initially, the *SIF* values obtained by the *DEM*, *ERRM* and *J*-integral (J_2) increase in a non-linear manner until the *a/W* ratio is equal to 1.0 and then onwards increases in a linear manner.

The stochastic variations in the various *J*-integral values with an increase in the *W/L* ratio are presented in Figure 4.5–b. It can be seen that the mean values of the *J*-integral (J_1 to J_{12}) increase non-linearly (in a parabolic manner) until a *W/L* ratio is almost equal to 0.5 and then starts to increase in a linear manner until the ratio *W/L* is equal to 1.8.

The comparison between the variations in the mean values of the *ERR* and the maximum value of the *J*-integral (i.e. J_2) is presented in Figure 4.5-c. The difference between the mean values of these two parameters is almost constant until the *W/L* ratio is 1.0 and then starts to increase gradually.

The effect of decreasing the length of the specimen on the standard deviation values of *SIF*, *ERR* and *J*-integral is presented below in Figure 4.6. An interesting pattern can be observed in the variations of the standard deviation; as shown in Figure 4.6, the standard deviation of *SIF* reduces with an increase in the *W/L* ratio, i.e., the standard deviation reduces with a decrease in the length of the specimen. The details are shown below in Figure 4.6.

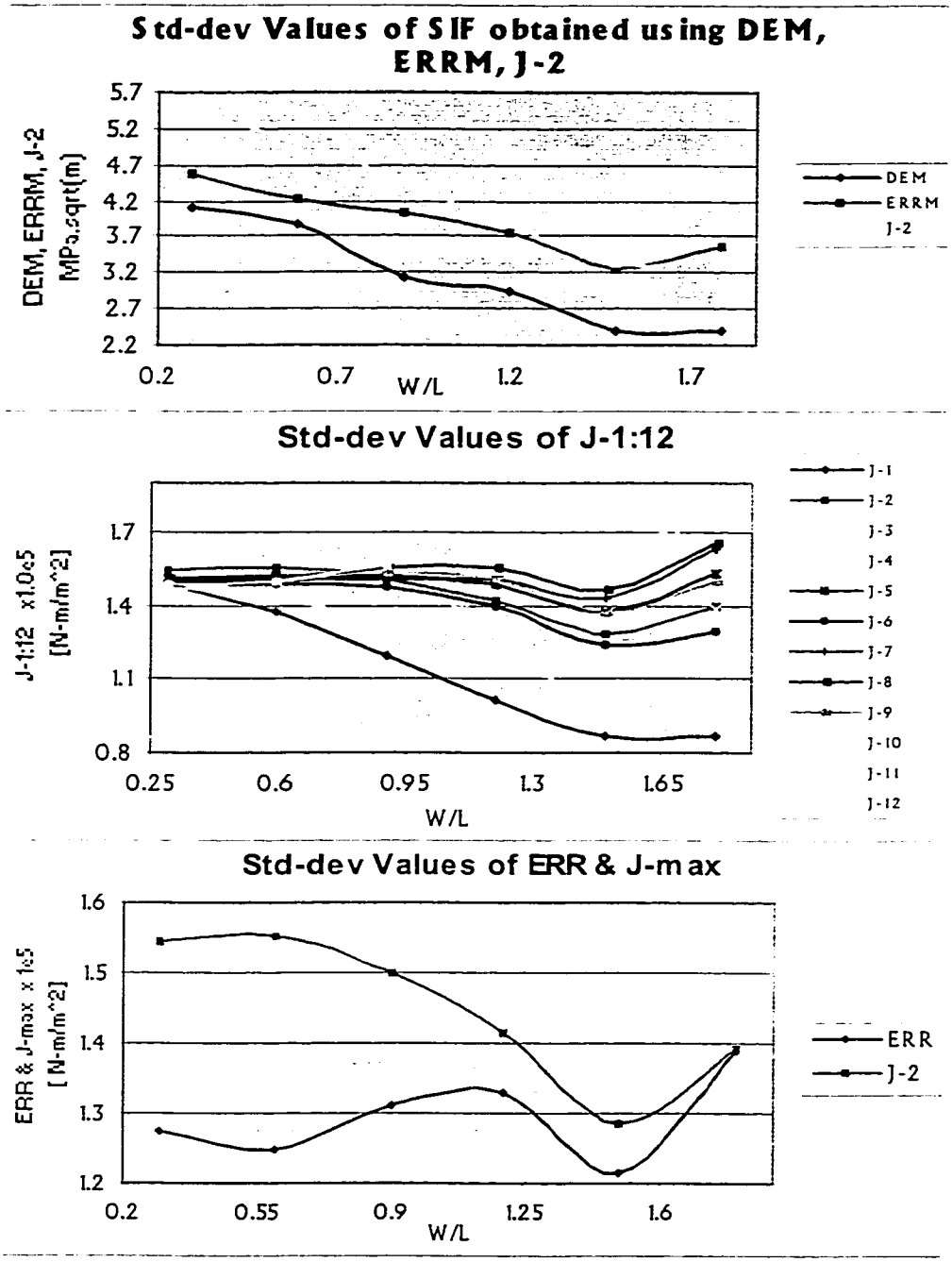

Figure 4.6 Fracture analysis of $[0/90]_{6s}$ laminate: (a) Variations of the standard deviation values of *SIF* with the plate length. (b) Variations of the standard deviation values of *J*-integral with the plate length. (c) Comparison of the standard deviation of *ERR* with that of the maximum value of *J*-integral.

A decrease in the standard deviation of the SIF with an increase in the plate length means that the sample values of the SIF are closer to the deterministic value. That is, the randomness in the fracture parameter, SIF, reduces with an increase in the plate length. *That is, as the dimension of the plate perpendicular to the crack surface is decreased, all the fracture parameters obtained using the three methods (DEM, ERRM and the J-integral method) are closer to their mean values.*

Also, the stochastic variations in the standard deviation values of *SIF* obtained by *DEM* and *ERRM* are high initially when the *W/L* ratio is equal to 0.3, and decrease gradually until a *W/L* ratio of 1.2 is reached. After this, the two values are almost equal and minor variations can be attributed to the stochastic behavior of the laminate. The variations in the standard deviation values of the various *J*-integral values initially are the same (when *W/L* ratio is almost equal to 0.3) but increase at higher values of the *W/L* ratio.

The variations in the standard deviation values of *ERR* and J_2 are shown in Figure 4.6-c. The difference between these two parameters keeps on decreasing with increase in the *W/L* ratio (decrease in the length of the laminate) and is almost equal when the *W/L* ratio is equal to 1.8.

Now, the effect of the change in the width of the plate on the *SIF* is investigated, and the observations are presented in Figures 4.7 – 4.8. In this case, the length of the plate is kept constant at 240 mm and the ratio, *W/L*, is increased by increasing the width of the plate.

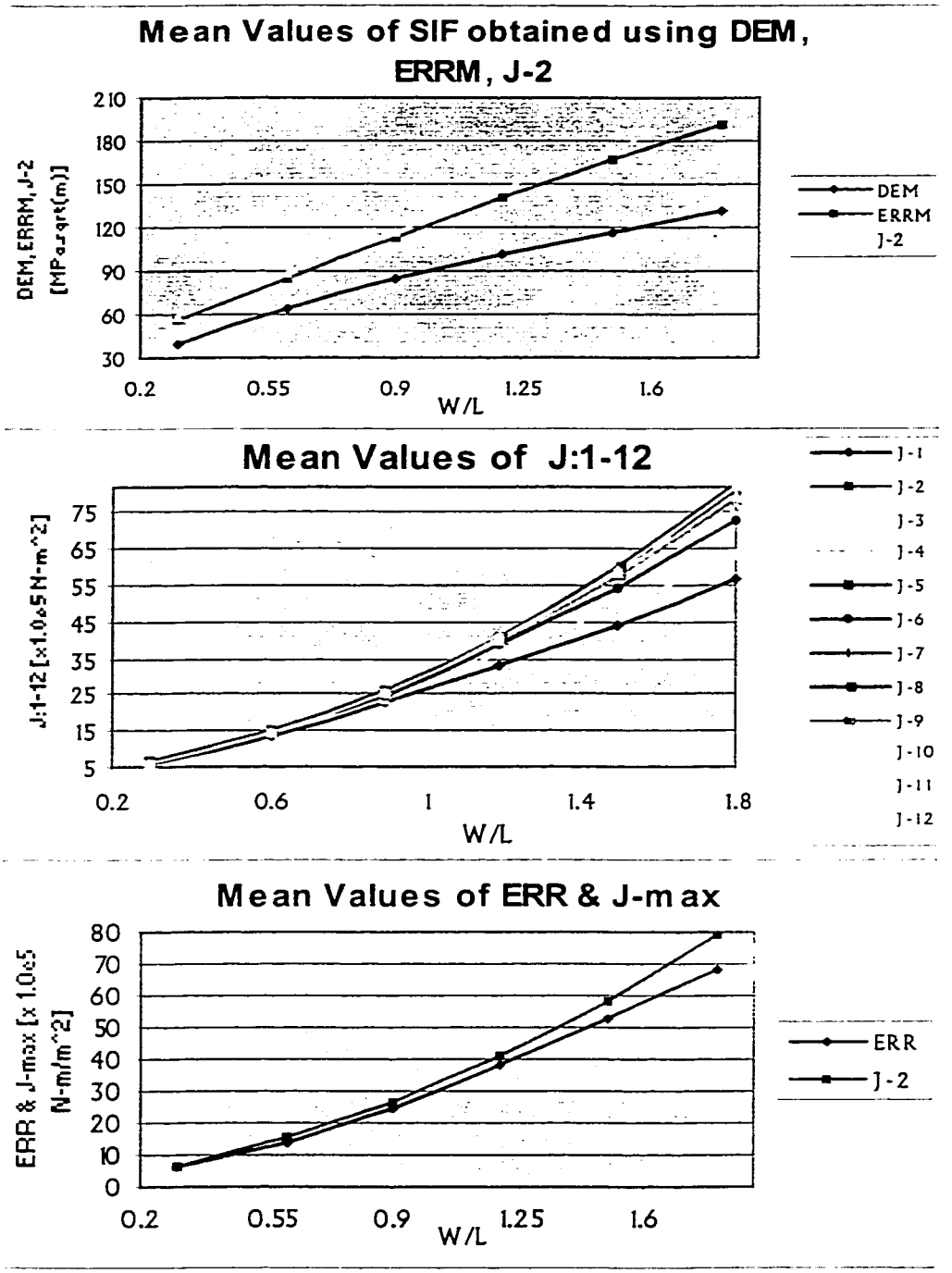

Figure 4.7 Fracture analysis of $[0/90]_{6s}$ laminate: (a) Variations of the mean values of the *SIF* with the width of the plate. (b) Variations of the *J*-integral values with the plate width. (c) Comparison between the values of *ERR* and the maximum value of *J*-integral.

It can be observed from Figure 4.7 that the *SIF* in this case increases almost linearly with an *increase* in the width of the plate. *It must be noted while the SIF increases linearly with an increase in the width of the plate, the same increases in a parabolic manner with a decrease in the length of the plate.* The J_2 values are maximum only until a *W/L* ratio of 1.4. However since J_2 represents the maximum value for a major portion of the graph, it is considered to be the maximum value of all the *J*-integral contours. Also from Figure 4.8, it can be seen that *the standard deviation values of J-integral and ERR also increase with an increase in the width of the specimen.* But the variations in the *SIF* with increase in the *W/L* ratio follow a stochastic manner. This behavior (depicted in Figures 4.5 – 4.8) is not entirely peculiar and a satisfactory reasoning can be offered. In the former situation the ratio, *W/L*, is varied by increasing the length of the plate. Here, as the length is increased the distance of the applied uniformly distributed load from the crack increases. This means that the *SIF* should approach the *SIF* for the case of a large plate loaded at its edge, which can be observed from the decreasing trend of the graph in Figure 4.5-a. Also, this means that the *SIF* approaches the ideal value and the variation (standard deviation) is also reduced as can be observed in Figure 4.6-a.

In the latter case of increase in the *W/L* ratio due an increase in the width of the plate, it can be assumed that each portion of the distributed load acting on the edge of the plate has its own portion of contribution to an *increase* in the *SIF* of the plate. With the increase in the width of the plate (while the length is constant), there is more load acting at the edges that contributes to the increase in the *SIF*. Hence, an increase in *SIF* can be predicted which is the same as observed in Figure 4.7-a.

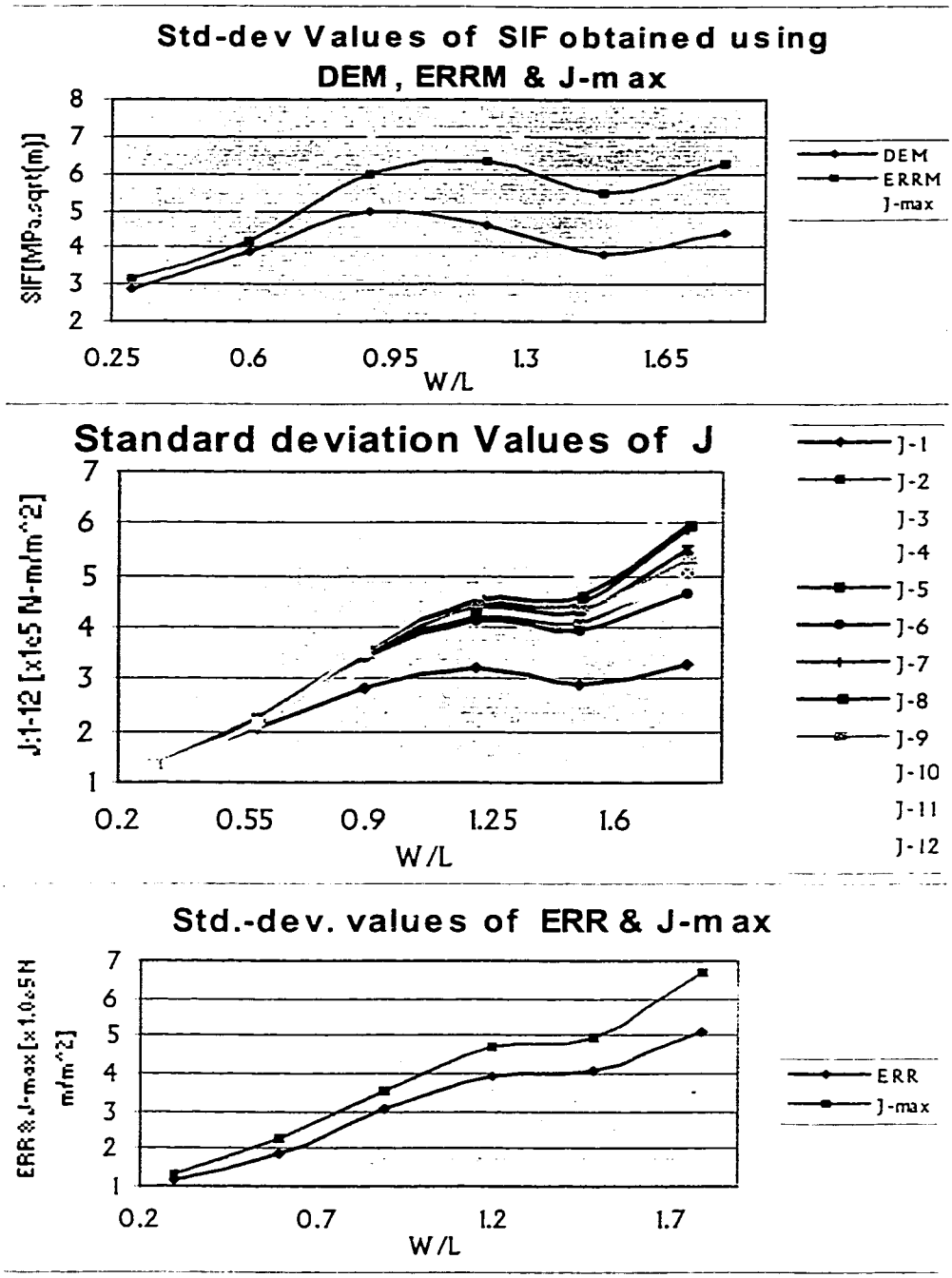

Figure 4.8 Fracture analysis of $[0/90]_{6s}$ laminate: (a) Variations of the standard deviation values of *SIF* with increase in the width of the plate. (b) Variations of the standard deviation values of *J*-integral with increase in the plate width. (c) Comparison of *ERR* with the maximum value of the *J*-integral.

4.3 Fracture Analysis of $[0/\pm45/90]_{3s}$ NCT-301 Composite Laminate

In this section, the effects of the crack length, the plate length and the width of the plate on the *SIF* of a quasi-isotropic plate are determined. Also, discussions will be put forth regarding the comparison of the behavior in the earlier case (cross-ply laminate) with that of the present one.

4.3.1 Effect of Crack Length - Plate Width Ratio on the SIF

In the following section, the variations of the mean values and standard deviations of the various fracture parameters with the crack-width (*a/W*) ratio are discussed. It can be observed from Figure 4.9-a that the variations in the mean values of the *SIF* obtained using the *DEM*, *ERRM* and the *J*-integral method increase approximately linearly with an increase in the *a/W* ratio. The *SIF* obtained from *ERRM* gives a higher approximate value of *SIF* than that obtained from the maximum value of the *J*-integral when the value of *W/L* exceeds 0.52. It can be observed from Figure 4.9-b that the mean values of the various *J*-integral values increase non-linearly in a parabolic manner. Of all the *J*-integral values, J_2 gives the maximum value. A comparison between the maximum values of *J*-integral (J_2) and the *ERR* is presented in Figure 4.9-c. Also, when the *a/W* ratio exceeds a value of 0.52, the *ERR* gives a higher approximation than the J_2. Also, from Figures 4.9-a and 4.9-c it can be observed that the difference between the *ERR* and the J_2 increases at a higher rate than the *SIF*. This is due to the fact that the *SIF* is proportional to the square root of the *ERR* and J_2.

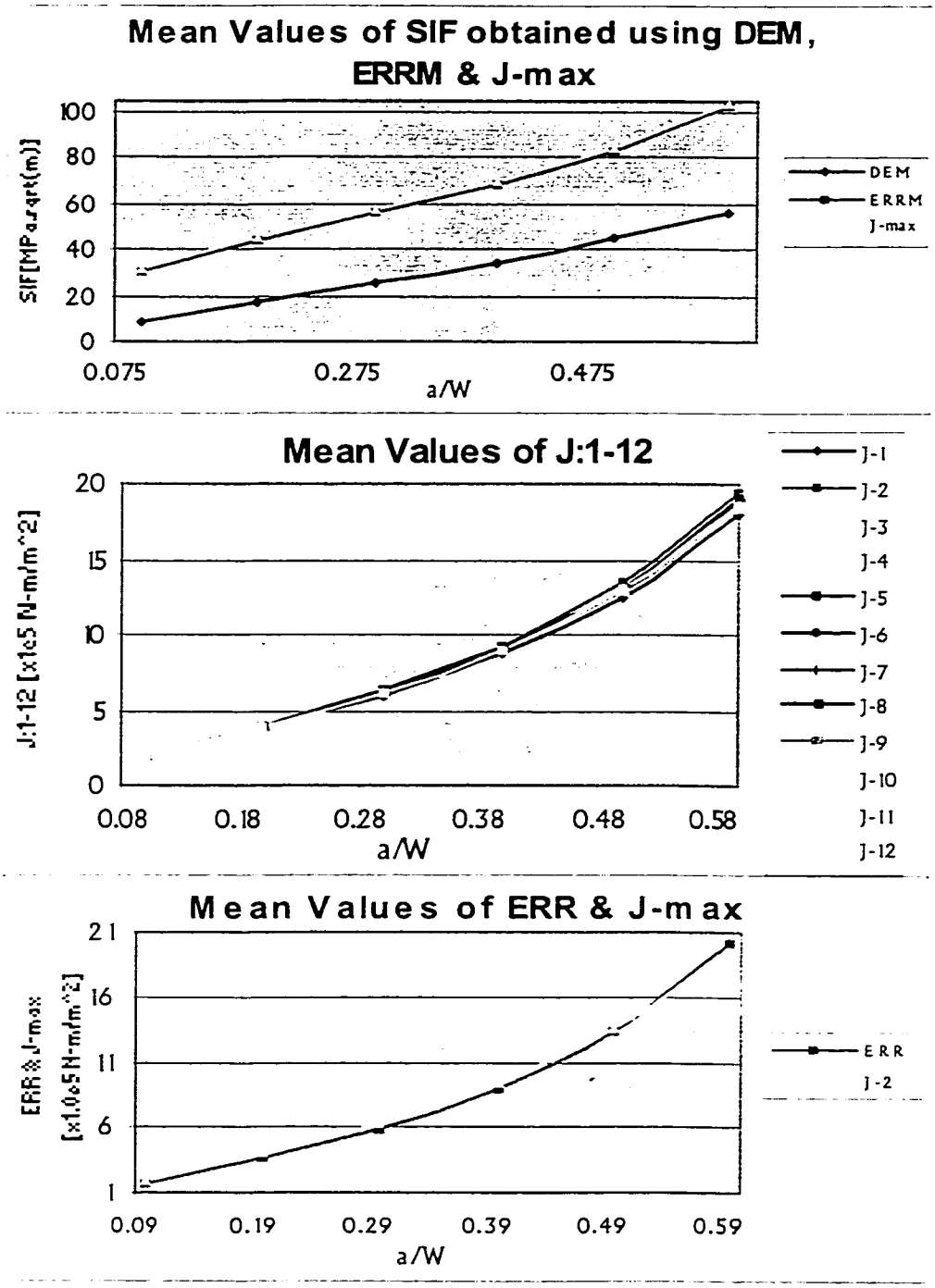

Figure 4.9 Fracture analysis of $[0/\pm45/90]_{3s}$ laminate: (a) Variations of the mean values of *SIF* with increase in the crack length. (b) Variations of the mean values of *J*-integral with increase in the crack length. (c) Comparison of *ERR* with the maximum value of *J*-integral.

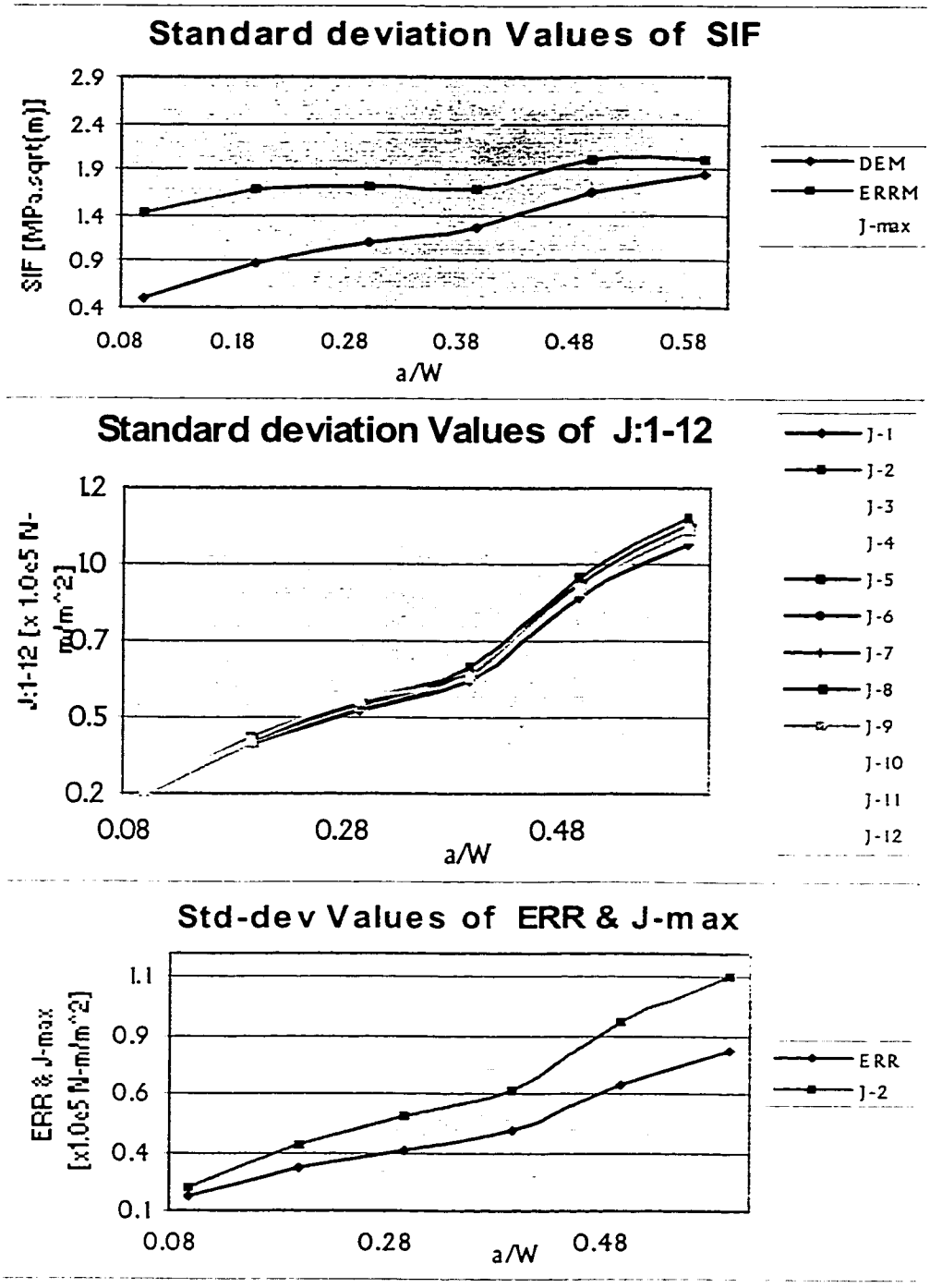

Figure 4.10 Fracture analysis of $[0/\pm45/90]_{3s}$ laminate: (a) Variations of the standard deviation values of *SIF* with increase in the crack length. (b) Variations of the standard deviation values of *J*-integral with increase in the crack length. (c) Comparison of the standard deviation of *ERR* with that of the maximum value of *J*-integral.

It can be observed from Figure 4.9 that in the cases of both the symmetric cross-ply laminate and the quasi-isotropic laminate, the *SIF* increases linearly with an increase in the crack length in the *a/W* ratio. In this case too the same reasoning offered earlier for the case of symmetric cross-ply or orthotropic laminate can be offered. As the crack length increases, the fracture parameters obtained using the *DEM*, *ERRM* and the maximum value of the *J*-integral increase. When the *a/W* ratio is more than approximately 0.5, the *ERRM* gives a higher estimate than J_2. The stochastic variations in the standard deviation values with the increase in the *a/W* ratio are presented above in Figure 4.10. Also, in the case of the variation of the standard deviation values, an increase in the values can be noted which is the same as in the previous case. In the present case, a *break point* can be noted when $a = (0.45)W$. The variations in the standard deviation values of the *SIF* continue to increase after this *break point* but start to decrease at higher values of crack length. In the case of the *J*-integral values the variations in the standard deviation values continue to increase with a decreasing slope except for the *break point* at $a=(0.45)W$. The same trend can be observed with the variations in the standard deviation values of *ERR*, but the difference between the variations in the standard deviation values of *ERR* and J_2 keep on increasing until *a/W* is equal to 0.6.

4.3.2 Effect of Finite Plate Size on the SIF

As in the previous case, the effects of the width of the plate as well as the length of the plate on the *SIF* have been investigated separately. Here too, initially the effect of the length of the plate on the *SIF* will be presented.

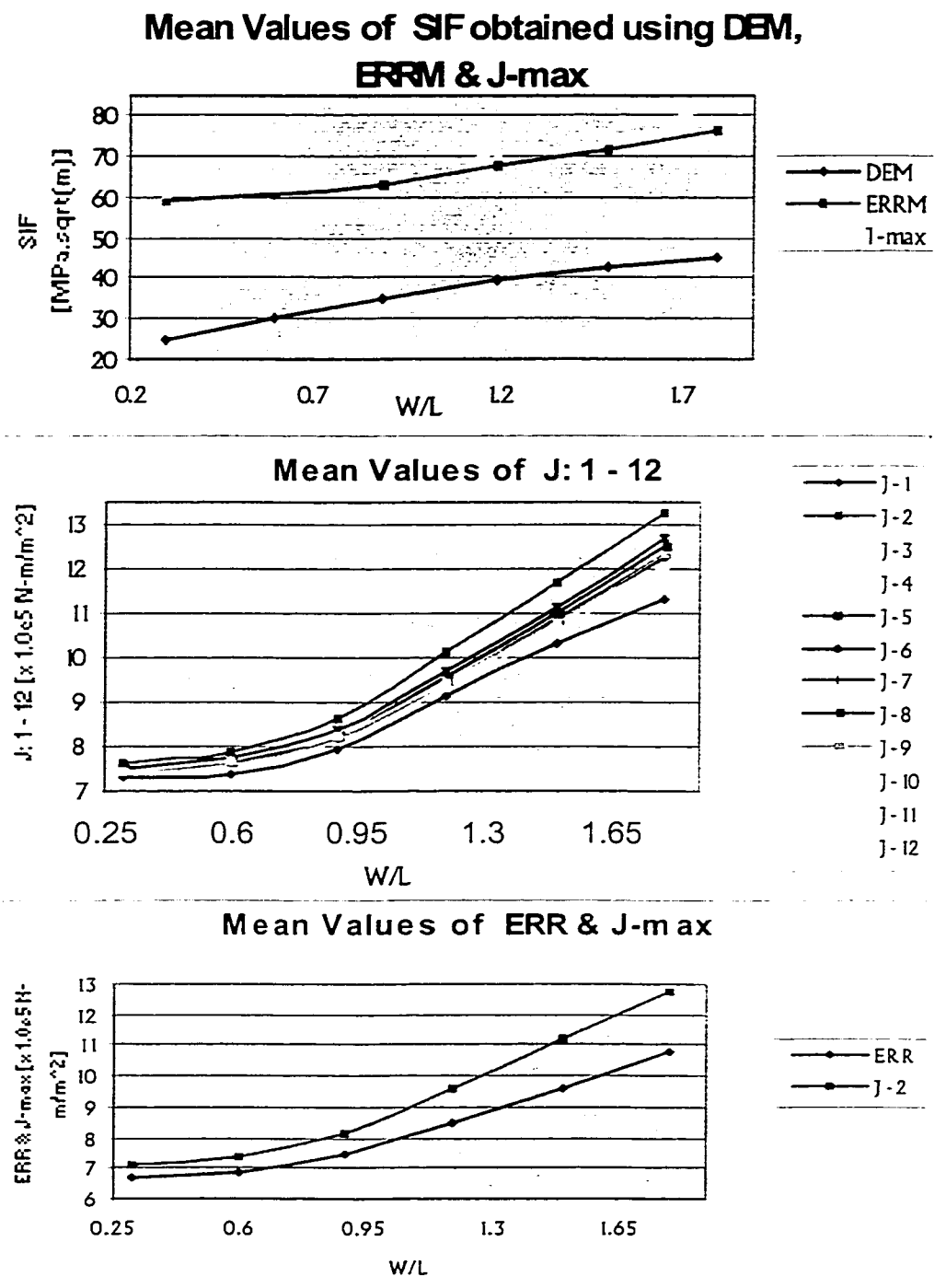

Figure 4.11 Fracture analysis of $[0/\pm45/90]_{3s}$ laminate: (a) Variations of the mean values of *SIF* with change in the length of the plate. (b) Variations of the mean values of *J*-integral with change in the length of the plate. (c) Comparison between the *ERR* and the maximum value of *J* (i.e. J_2).

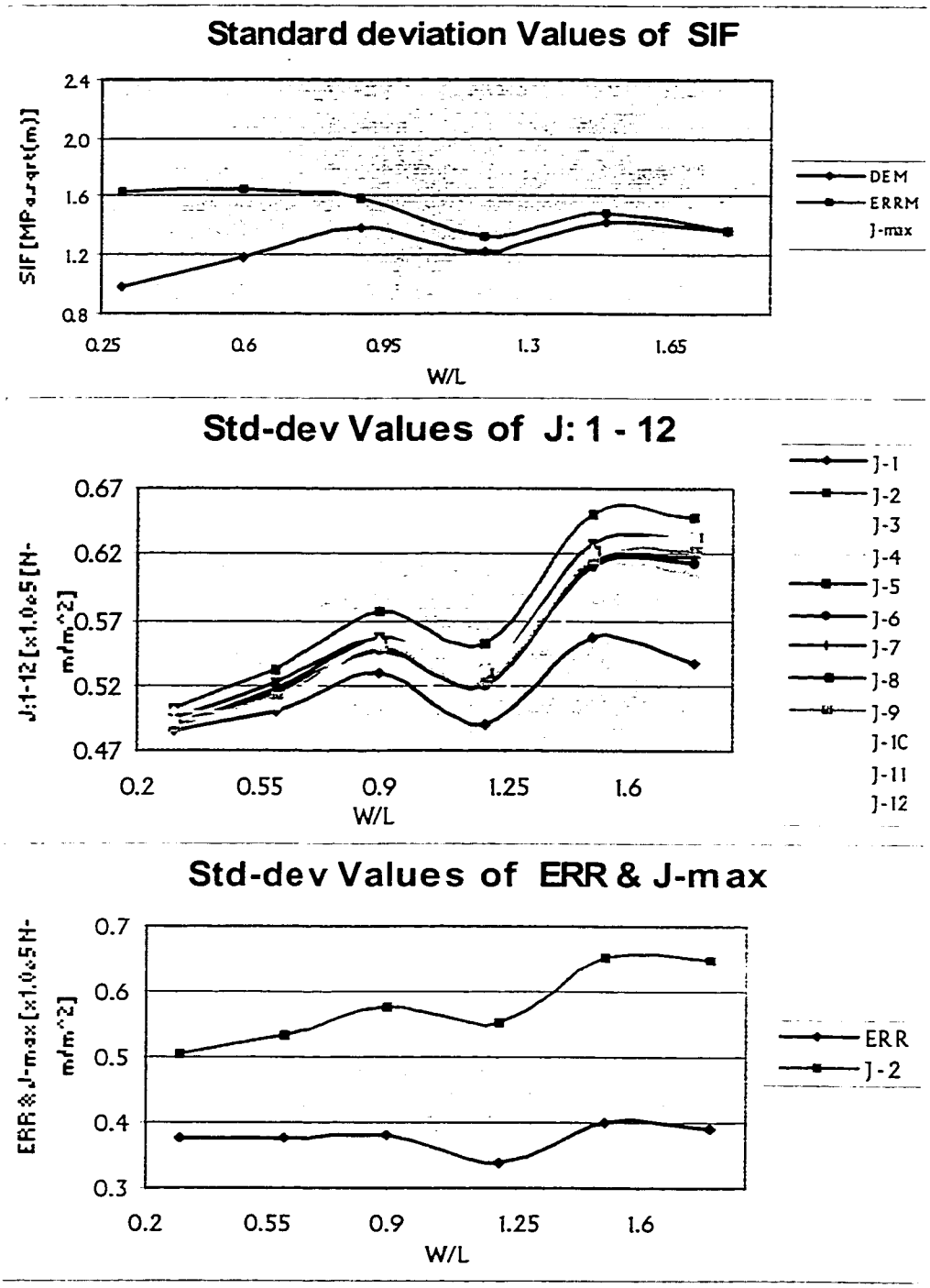

Figure 4.12 Fracture analysis of $[0/\pm45/90]_{3s}$ laminate: (a) Variations of the standard deviation values of *SIF* with change in the length of the plate. (b) Variations of the standard deviation values of *J*-integral with change in the length of the plate. (c) Comparison between the *ERR* and maximum value of *J* (i.e. J_2).

From Figure 4.5 it can be observed that the variation in the mean values of the *SIF* obtained using *DEM*, *ERRM* and the maximum value of the *J*-integral (J_2) is approximately linear after a *W/L* ratio of 0.8. Similarly, the maximum value of *J*-integral (J_2) and the *ERR* also increase linearly after a *W/L* ratio of 0.9, before which they increase in a parabolic manner. In the case of the standard deviation values for the quasi-isotropic laminate, the variations in the standard deviation values of the *SIF* remain fairly constant with a change in the length of the plate and this change can be attributed to the stochastic behavior of laminates. It must be noted here that while the mean values of the *SIF* increase in a parabolic and linear manner, the variations of the standard deviation values are almost linear with minor stochastic fluctuations. *While the ERRM yields values whose standard deviation doesn't change visibly with an increase in the crack length, the standard deviation of the values obtained from the maximum value of the J-integral(J_2) increases considerably.*

As in the case of orthotropic laminates, the variations of the standard deviation values of the *J*-integral values do not reduce with an increase in the *W/L* ratio. This trend can also be attributed to the quasi-isotropic behavior of this laminate configuration. From Figure 4.12-c it can be observed that while the standard deviation values of J_2 increase linearly, the variations of the standard deviation values are almost constant. But the standard deviation values of the *SIF* obtained from *ERRM* reduce slightly.

Now, the effect of the increase in the plate width on the mean values of various fracture parameters is presented below in Figures 4.13 and 4.14.

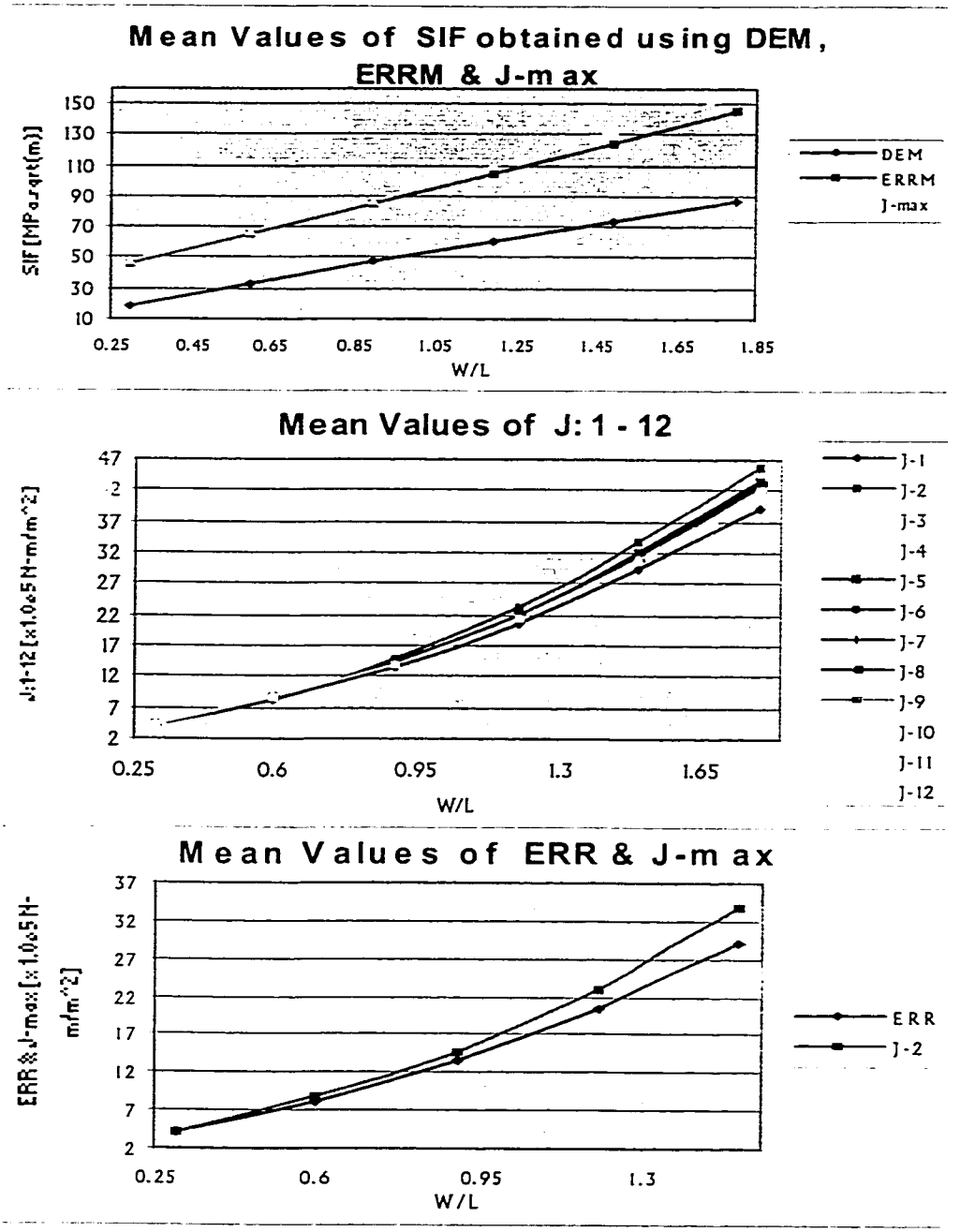

Figure 4.13 Fracture analysis of $[0/\pm45/90]_{3s}$ laminate: (a) Variations of the mean values of *SIF* with increase in the width of the plate. (b) Variations of the mean values of *J*-integral with increase in the plate width. (c) Comparison of the variations of the mean values of *ERR* and *J*-integral with increase in the plate width.

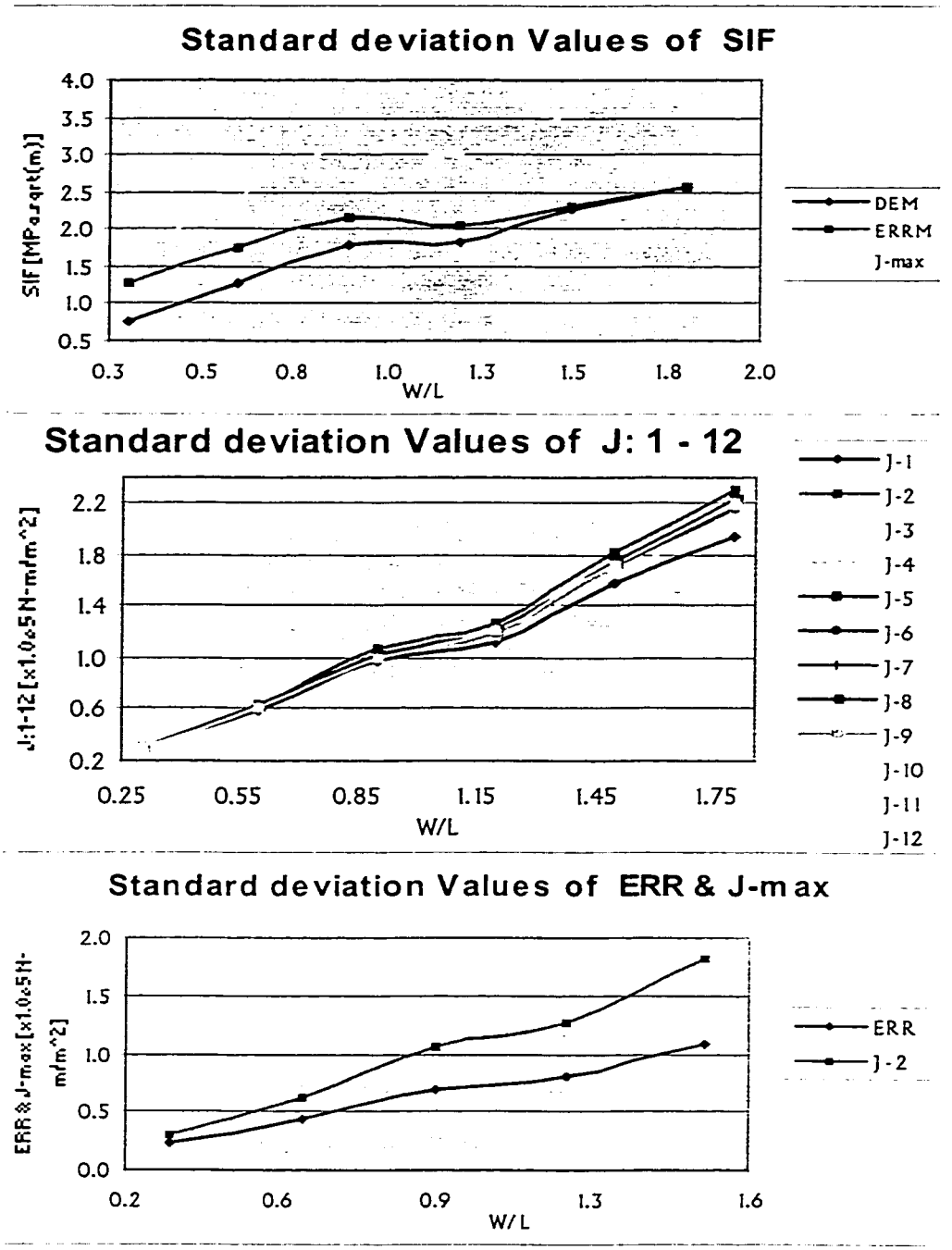

Figure 4.14 Fracture analysis of $[0/\pm45/90]_{3s}$ laminate: (a) Variations of the standard deviation values of *SIF* with increase in the plate width. (b) Variations of the standard deviation values of *J*-integral with increase in the plate width. (c) Comparison between the variations of standard deviations of *ERR* and J_2.

It can be inferred that the probabilistic behavior of the quasi-isotropic laminate is almost similar to the orthotropic laminate in this regard as the graphs obtained in Figures 4.7 and 4.13 are almost identical, except that in Figures 4.7-b and 4.7-c the maximum value of the stochastic *J*-integral is not given by J_2 all through the range of the *W/L* ratio. In the case of $[0/\pm45/90]_{3s}$, the maximum value of the *J*-integral is given by J_2. As can be seen from Figure 4.14, presented above, the increase in the standard deviation values in this case is almost similar to the case of an orthotropic laminate except that, in the present case, the increase is more rapid. Also, the variations in the standard deviation values (in the case Figure 4.8) of the *SIF* obtained from the maximum *J*-integral remains approximately constant after a *W/L* ratio of 0.9. Whereas in this case the standard deviation values keep on increasing throughout the range of *W/L* ratio except for a *break point* at a *W/L* ratio that is approximately equal to 0.9. As the width of the plate increases, the variations in the values of the fracture parameters also increase, and hence drifting away from the deterministic value. *It must be noted that while the graphs obtained are very similar, the individual values differ from each other quite substantially.*

4.4 Fracture Analysis of $[\pm45]_{6s}$ NCT-301 Composite Laminate

In this section, the effects of the crack length, the plate length and the width of the plate on the *SIF* of the $[\pm45]_{6s}$ laminate are determined. Also, discussions will be put forth regarding the comparison of the behavior in the earlier cases with the present one. In the following section, the variations of the mean values and standard deviations of the various fracture parameters with the plate geometry (*a/W* and *W/L*) are determined and further, the values are represented in a graphical form.

4.4.1 Effect of the Crack Length - Plate Width Ratio on the SIF

The variations in the mean values of the *SIF* values, *J*-integral values and *ERR* values with an increase in the *a/W* ratio are presented in Figure 4.15. Further the stochastic variations in the standard deviation values of the various fracture parameters are presented in Figure 4.16. It can be observed from Figures 4.15 and 4.16 that the trend of variations of the mean values of all the fracture parameters are the same as that in the case of orthotropic and quasi-isotropic laminates as described before in Figures 4.3 and 4.9. The mean values of the *SIF* obtained from the *ERR* and the maximum value of the *J*-integral (i.e. J_2) are almost equal when the *a/W* ratio is almost equal to 0.6, before which the *SIF* obtained from J_2 is maximum. Of all the mean values of the various *J*-integral values, the J_2 gives the maximum value of the *J*-integral. A comparison between the mean values of *ERR* and J_2 is provided in Figure 4.15-c. It can be observed that the values of these two parameters are almost equal throughout the entire range and converge at the *a/W* ratio of 0.6.

Similarly, a comparison of the standard deviations of the various fracture parameters with an increase in the crack length is represented below in Figure 4.16. It can be observed that the standard deviation increases almost parabolically for the *ERR* and J_2 except at a *break point* which is at the *a/W* ratio of 0.3. Also, the increase in the standard deviation of the *SIF* is almost linear. *The variations in the SIF and the J-integral values increase in a non-linear manner with an increase in the crack length.* The variations in the standard deviation values of the *SIF* values obtained from J_2 have the maximum values.

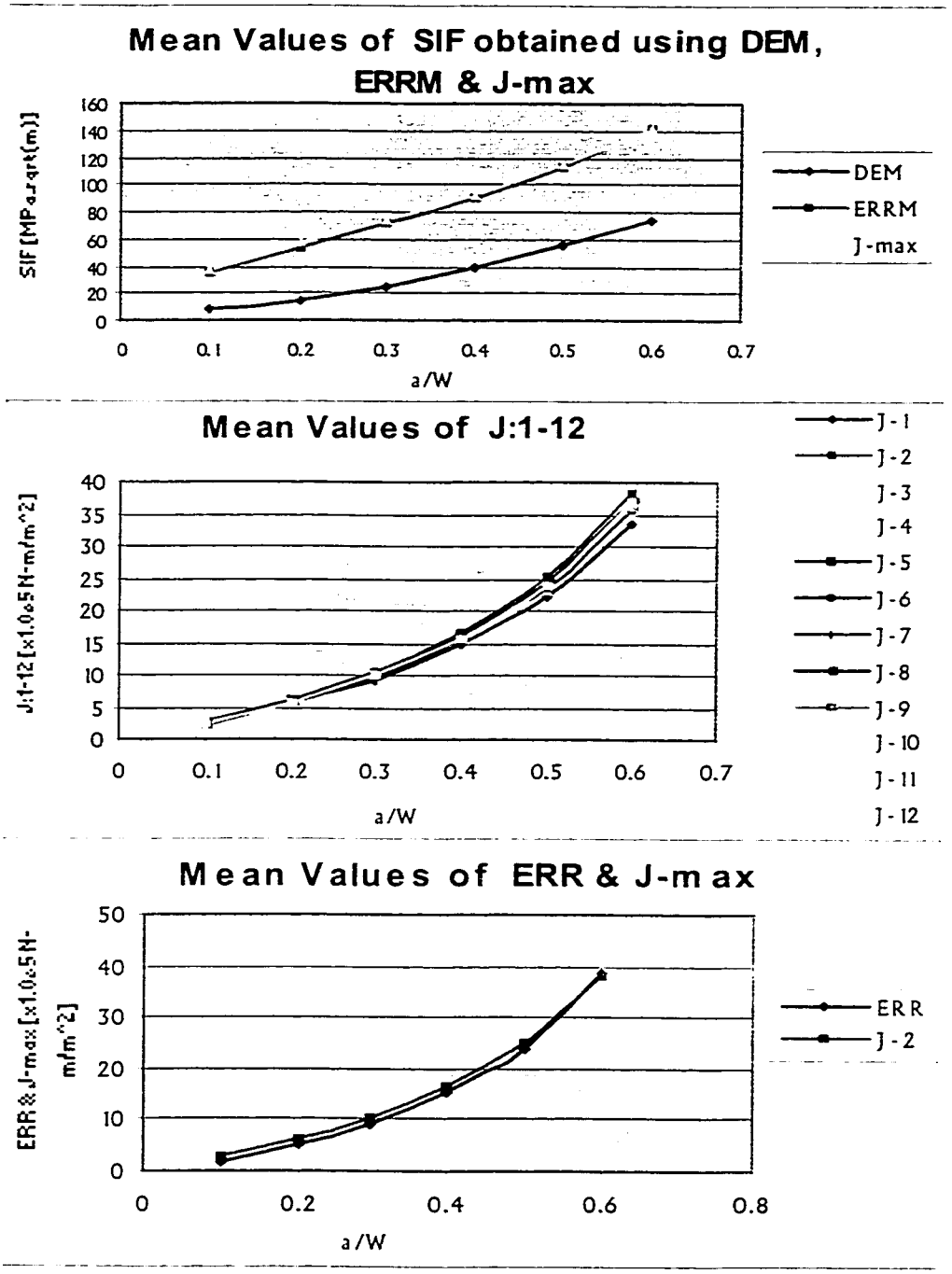

Figure 4.15 Fracture analysis of angle-ply ($[\pm 45]_{6s}$) laminate: (a) Variations of the mean values of the *SIF* with increase in the crack length. (b) Variations of the mean values of *J*-integral with increase in the crack length. (c) Comparison between the mean values of the *ERR* and maximum value of *J*-integral i.e., J_2.

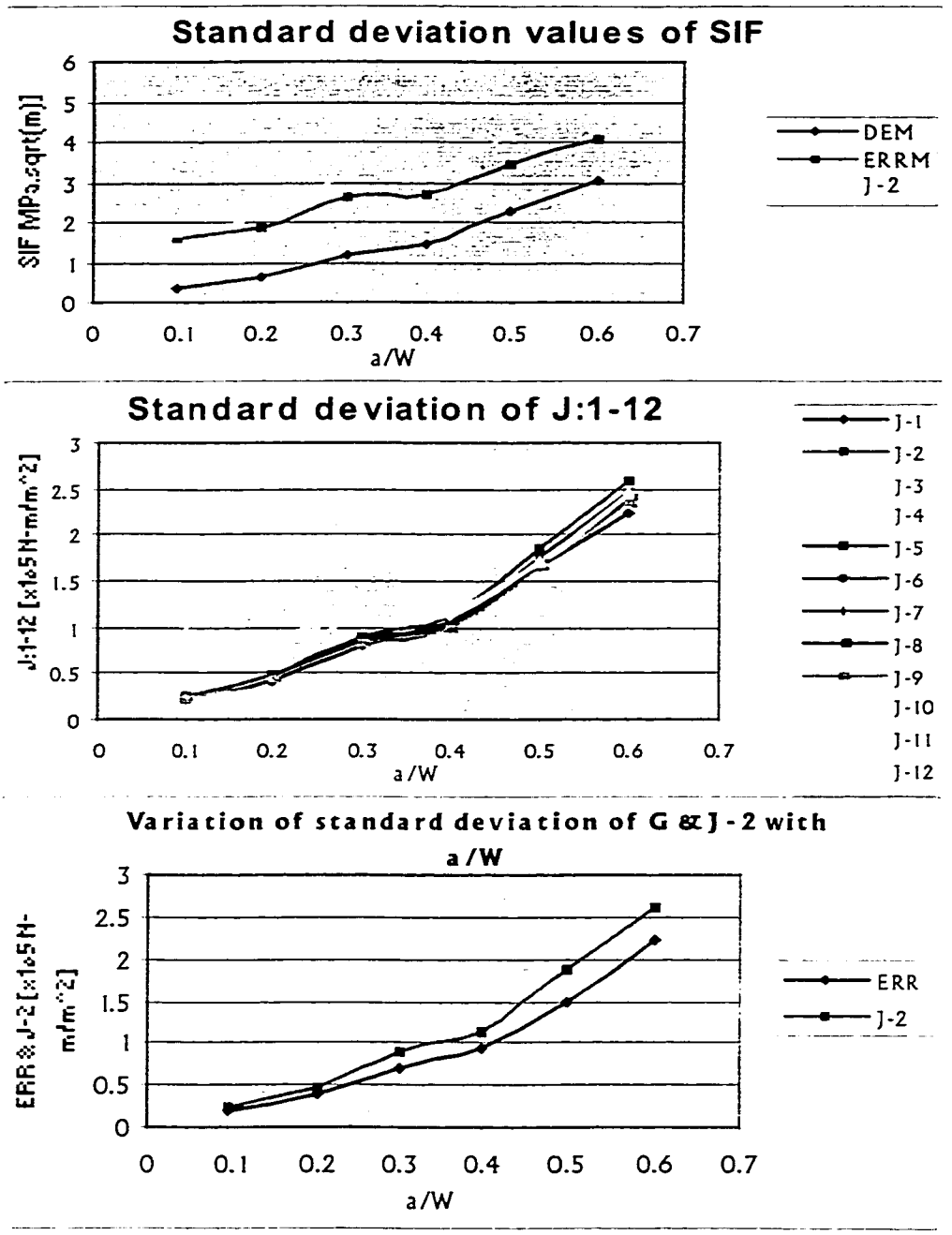

Figure 4.16 Fracture analysis of angle-ply ($[\pm 45]_{6s}$) laminate: (a) Variations of the standard deviation values of *SIF* with an increase in the crack length. (b) Variations in the standard deviation values of the *J*-integral values with increase in the crack length. (c)Comparison of the standard deviations of *ERR* and *J-max* (i.e. J_2) with increasing crack length.

4.4.2 Effect of Finite Plate Size on the SIF

As in the previous cases of orthotropic and quasi-isotropic laminates, the effects of the geometry of plate on the *SIF* for symmetric angle plied laminates are also investigated thoroughly. The various results of the analysis (the mean values and standard deviations of the *SIF*, *ERR* and *J*-integral) are obtained and represented below in a graphical form. In this section, the effect of the variation of the width and the length of the plate on the stochastic behavior of symmetric angle-plied laminates is presented. The individual effects of the plate geometry on the various fracture parameters have been investigated separately.

It can be observed from Figure 4.17-a that the *SIF* obtained from *DEM* increases in an approximately linear manner. The mean values of *SIF* obtained from the *ERR* and the maximum value of *J*-integral (J_2) remain constant until an *a/W* ratio of 0.85 and then onwards increase in an approximately linear manner. Also, a *distinct similarity* can be noticed between Figures 4.5, 4.11 and 4.17. Just one glance at these three figures is enough for one to notice that these three figures have something in common. The explanation that has been offered in section 4.2.2 regarding the increase in the *SIF* applies here too. One more very important point worthy of notice is the striking similarity between variations in the standard deviations (in Figure 4.18) of the various fracture parameters with change in length for the quasi-isotropic laminate ($[0/\pm45/90]_{3s}$) and for the case presently under consideration. *It must be noted that while the graphs (and variation trends) obtained are very similar, the individual values differ from each other quite substantially.*

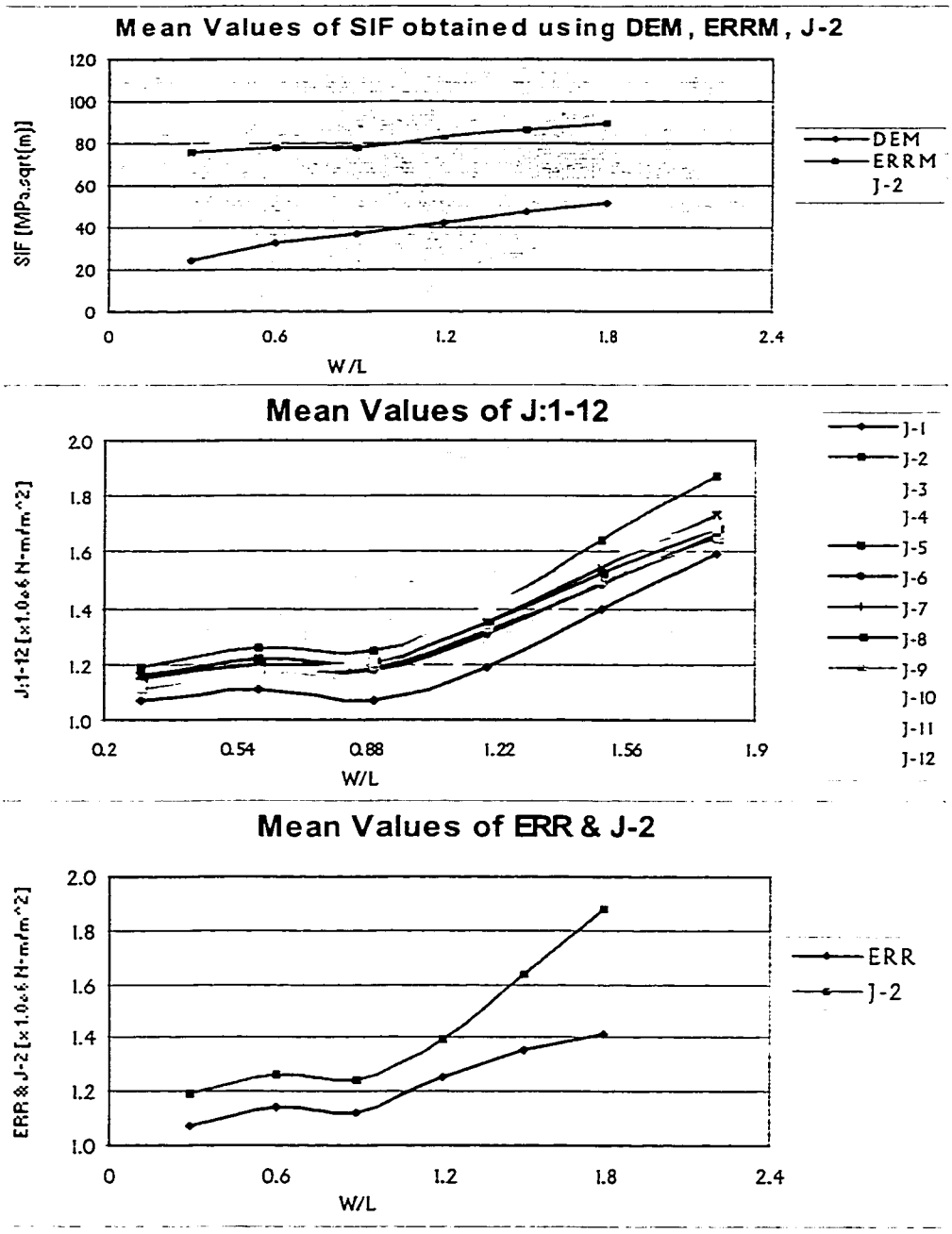

Figure 4.17 Fracture analysis of angle-ply ($[\pm 45]_{6s}$) laminate: (a) Variations of the mean values of the *SIF* with change in the length of the plate. (b) Variations of the mean values of the *J*-integral with change in the length of the plate. (c) Comparison of variations in the mean values of the *ERR* and maximum *J*-integral.

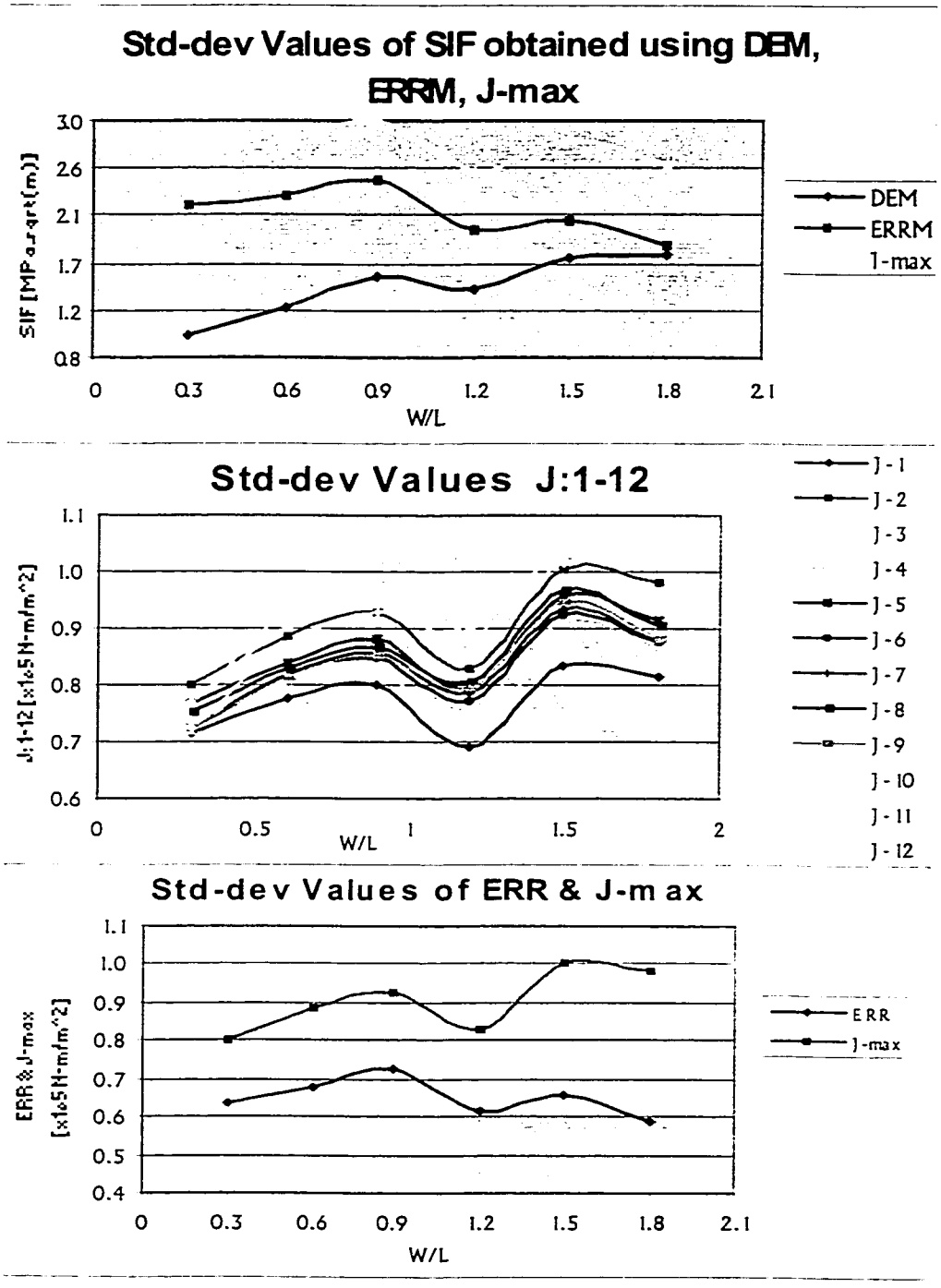

Figure 4.18 Fracture analysis of angle-ply ($[\pm 45]_{6s}$) laminate: (a) Variations of the mean values of the *SIF* with change in the length of the plate. (b) Variations of the mean values of the *J*-integral with change in the length of the plate. (c) Comparison of variations in the mean values of the *ERR* and maximum *J*-integral.

In a similar manner, the effect of the change in the width of the plate on the mean values and the standard deviation values of the various fracture parameters of symmetric angle-ply laminates is found and the values are presented in Figures 4.19 and 4.20. From Figure 4.19 it can be noticed that the variation of the mean values of the *SIF* obtained using *DEM*, *ERRM* and the maximum value of the *J*-integral is approximately linear while the mean values of the *J*-integral values and the *ERR* increase in an approximately parabolic manner. Interestingly, from Figure 4.20-a it can be observed that the variations in the standard deviation values of the *SIF* obtained using *DEM*, *ERRM* and the maximum value of the *J*-integral method increase in an inverted parabolic manner with an increase in the *W/L* ratio. Further, it can be observed from Figures 4.20-b and 4.20-c that while the standard deviation values of *ERR* increase in an inverted parabolic manner with an increase in the *W/L* ratio, the corresponding values of the various *J*-integral values increase linearly.

The variations in the mean values follow a trend which suggests a similarity with the behavior of the quasi-isotropic laminate presented in Figure 4.13 with the exception that *in this case the individual values of various fracture parameters are much higher suggesting a relatively weaker structure*, while the variations in the standard deviation values (Figure 4.20) suggest an entirely different behavior in terms of parameter variability. While the mean values of the *SIF* (Figure 4.17-a) don't change considerably with a decrease in the plate length, its value approaches the deterministic value because the standard deviation decreases (Figure 4.18-a). Also, while the *ERR* values approach the deterministic case, the J_2 values tend to be more and more random.

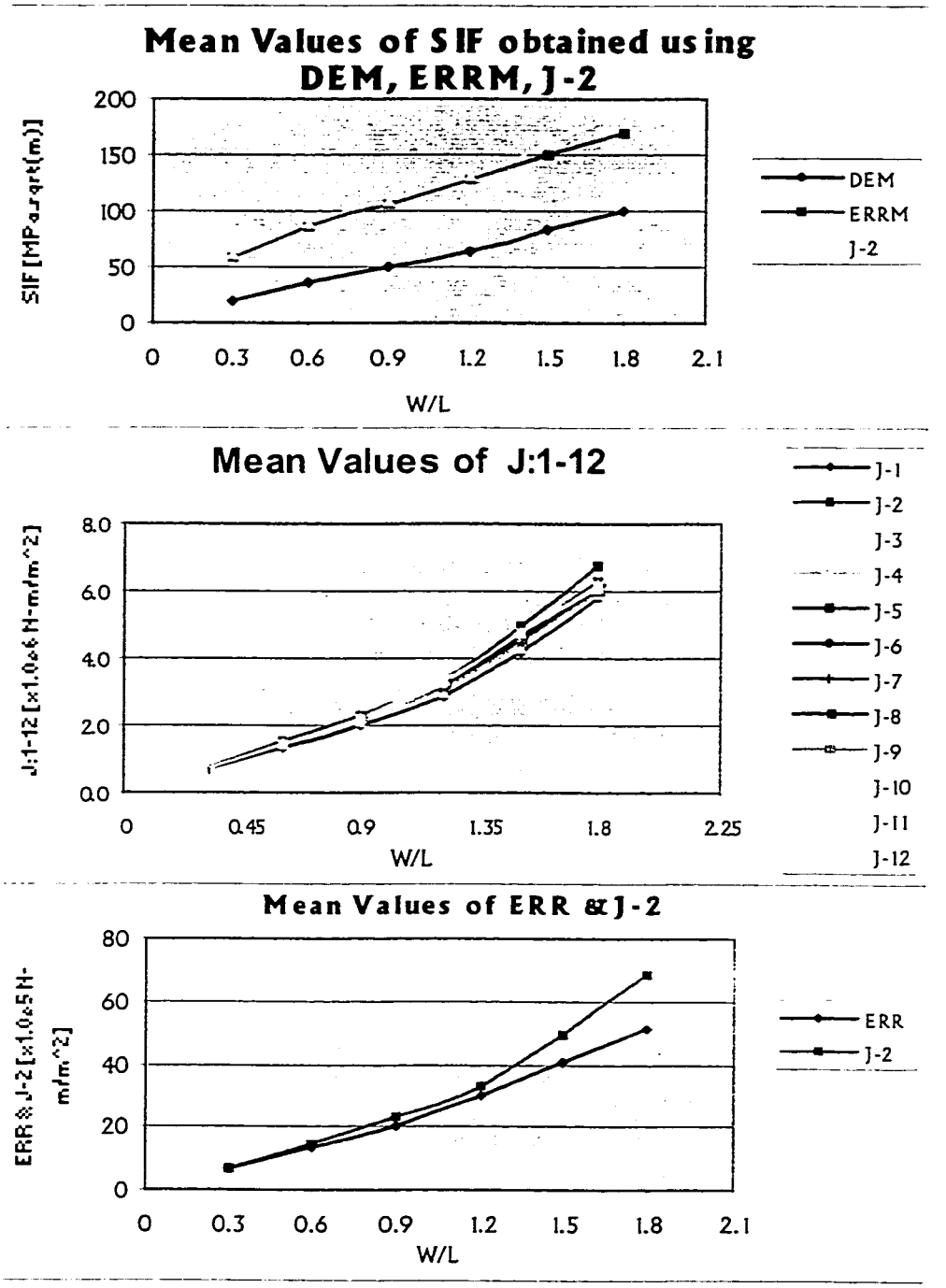

Figure 4.19 Fracture analysis of angle-ply ($[\pm 45]_{6s}$) laminate: (a) Variations of the mean values of the *SIF* with the width of the plate. (b)Variations of the *J*-integral values with the plate width. (c) Comparison between the values of *ERR* and the maximum value of *J*-integral.

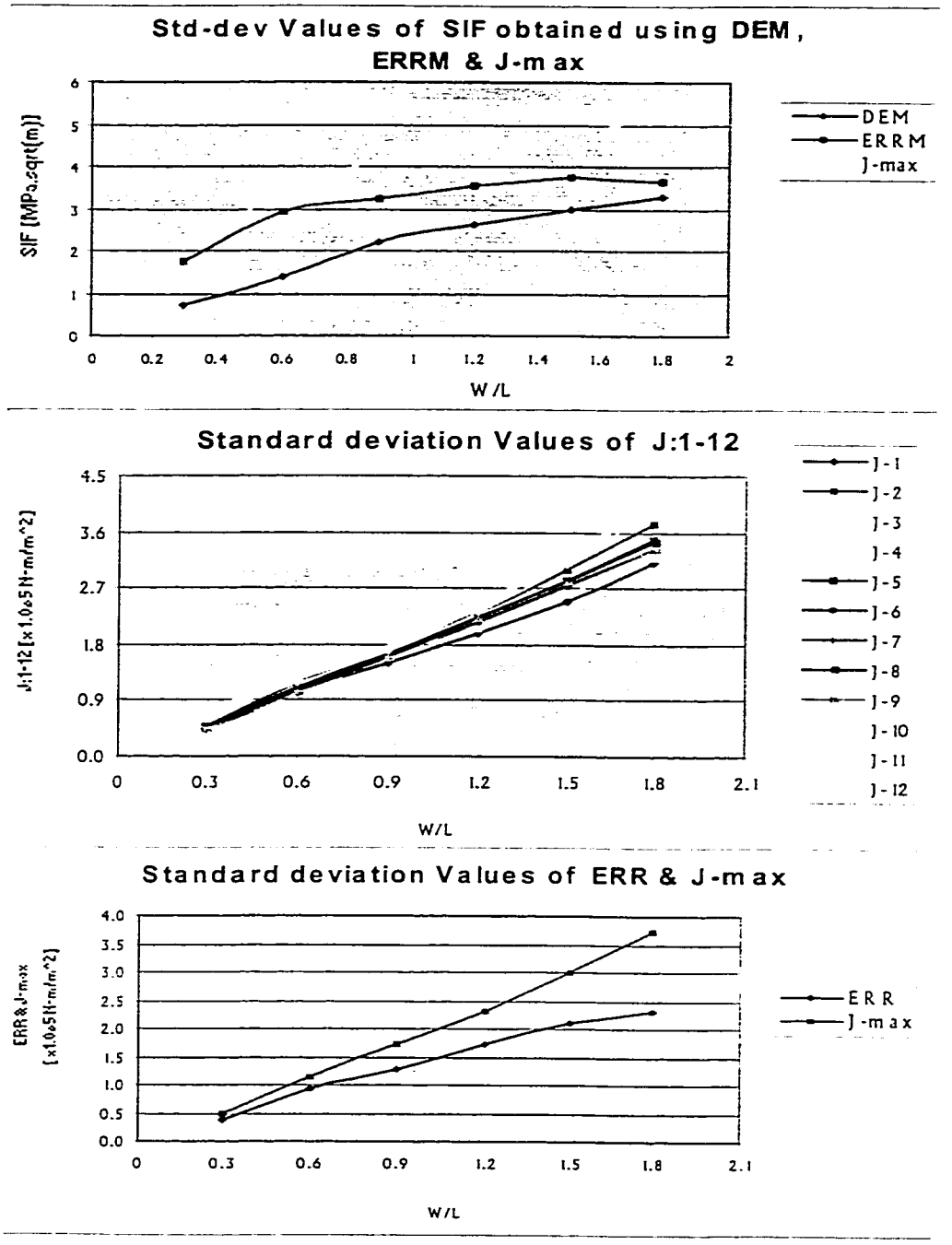

Figure 4.20 Fracture analysis of angle-ply ($[\pm 45]_{6s}$) laminate: (a) Variations of the standard deviation values of *SIF* with an increase in the width of plate. (b) Variations of the standard deviation values of *J*-integral with an increase in the plate width. (c) Comparison of *ERR* with the maximum value of the *J*-integral.

4.5 Conclusions and Discussions

In the present chapter, a thorough analysis has been performed using the stochastic finite element analysis formulation to find out the effects of the crack size and the plate geometry on the various fracture parameters: *SIF*, *ERR* and *J*. These analyses have been performed for three basic types of laminates (orthotropic, quasi-isotropic and symmetric angle-ply laminates) and the results have been represented in a graphical form. Appropriate discussions have been offered for the results obtained at each stage. Also the use of stochastic finite element analysis formulation in determining the minimum number of simulations to be performed for obtaining consistent results has been illustrated.

From the parametric study that has been conducted and presented in Sections 4.2 – 4.4, the following conclusions can be summarized.

- Regarding the effect of the number of simulations on the stochastic fracture analysis of $[0/90]_{6S}$:

Though the mean values tend to be a constant after the number of simulations is equal to 450, the standard deviation values vary stochastically throughout the entire range of the number of simulations. Also the variation of the mean values of *SIF* is approximately 3% of the mean value, while the variation in the mean values of the *ERR* and J_2 (maximum value of the *J*-integral) is approximately 2% of their respective mean values. However, considering the simulation time and the distributions (discussed in Chapter 5) of various fracture parameters, the number of simulations has been selected to be 250.

- Regarding the effect of the crack length and the plate dimensions on the stochastic fracture behavior of $[0/90]_{6s}$:

As the crack length increases, the J_2 (maximum value of the J-integral) and the *SIF* obtained from J_2 yield the maximum values throughout the analysis. As the crack length increases, the standard deviation values also increase suggesting that the plate behaves in a more probabilistic manner. In contrast to this behavior, as the length (dimension perpendicular to the crack) of the plate is reduced (*W/L* ratio is increased) the plate behaves in a deterministic manner. On the other hand, as the width of the plate increases, J_2 always yields the maximum values of the fracture parameters. It can be observed that the width of the plate, crack length and the length of the plate have most significant influence on the probabilistic fracture behavior, in that order. Thus it can be seen that the stochastic J-integral provides a better representation of the effects of various factors on the fracture behavior. Also, for most part in this case, the J_2 can be used as the design parameter.

- Regarding the effect of the crack length and the plate dimensions on the stochastic fracture behavior of $[0/\pm45/90]_{3s}$:

In this case when the crack length is approximately 50% of the width of the plate, the *ERRM* yields higher estimates of the mean values than the J_2 which remains to be the maximum value of the J-integral. Also, the laminate behaves in a more probabilistic manner. The effect of the *W/L* ratio when the length is changed is very minimal while the effect of the plate width on the fracture behavior is maximum. Here too the J_2 can be used as the critical design parameter. Also, it can be observed that the orthotropic laminate is

relatively weaker than the quasi-isotropic laminate (under tensile loading). The probabilistic behavior of the laminate in fracture increases as the plate length decreases but the behavior tends to be more deterministic as the width of the laminate increases.

- Regarding the effect of the crack length and the plate dimensions on the stochastic fracture behavior of $[\pm 45]_{6s}$:

As the crack length increases, the probabilistic behavior of the laminate increases and J_2 yields the maximum values. In this case the effects of increasing the crack length and the plate width have an almost equal effect on various fracture parameters. However, the effect of the length of the plate is almost none. In the cases of increasing the crack length and the plate width, the probabilistic behavior is more pronounced. As the crack length increases, this laminate exhibits the *weakest* behavior of all the three laminates considered. Considering the increase in the width of the laminate, the strength of this laminate is intermediate between the orthotropic and the quasi-isotropic laminates. However, this laminate manifests a very strong behavior as the *SIF* is unaffected by the reduction in the length of the plate.

In this chapter, the stochastic characteristics of the *J*-integral have been pointed out. Even though in the deterministic case the *J*-integral is supposed to be a constant irrespective of the position of the contour over which it is evaluated, the material properties and hence the stresses computed vary stochastically in the present case, and so does the *J*-integral. Thus, the description of the stochastic *J*-integral has been put forth and illustrated through various examples. The *J*-integral method also brings out the variations in the fracture

behavior of the laminate at various locations in the laminate. The *J*-integral method provides a better representation and gives a better description of the probabilistic fracture behavior than the conventional *ERRM* and *DEM*. Also, in all the three cases described in this chapter, the J_2 can be considered as the critical design parameter as it gives the maximum value of the *SIF*.

From the results of analyses, it can be concluded that the crack size and the width of the plate have the most profound effect on various fracture parameters and their variability in the cases of all the three kinds of laminates. Given a particular cracked plate configuration with uniformly distributed load, the quasi-isotropic laminate gives the minimum value for any fracture parameter in all analyses. For analyses based solely on the crack size, the orthotropic laminates give the highest values for any fracture parameter. For analyses based on the geometry of the plate (both the plate length and the plate width), the symmetric angle ply laminates give the highest values for any fracture parameter.

The results of above analyses can be used to develop *data charts* providing the values of factors f_1 and f_2 for various ratios of *a/W* and *W/L* similar to those available for isotropic materials (for the deterministic case). For composite materials these types of charts would be a major contribution to the probabilistic design process in reducing the time taken to select suitable values for the factors, f_1 and f_2.

Chapter 5

Reliability Analysis of Composite Laminates

5.1 Introduction

The ultimate purpose of any analysis is to predict the failure of a structure in operation and avert it by making necessary modifications in the design parameters. In the case of failure by fracture there are several methods that can be employed to avoid failure. These methods range from employing crack-arrest techniques, adding reinforcements, localized heat treatment techniques, crack-path diversion techniques, etc. to replacing the component itself. Reliability is a very important concept in the mass production of various components. Also, reliability and safety are inseparable from one another.

Procedures for determining the reliability of anisotropic laminates by taking into account the various aspects of the subject under analysis are of interest in this chapter. It is very important to incorporate all the factors that effect the performance of a structure while performing an analysis to yield parameters representing the entire class of the structure. In the third chapter the role of stochastic finite element analysis in computing the various fracture parameters by taking into account the various aspects that are characteristic to composite laminates was discussed in detail. In order to evaluate the reliability of any structure, two parameters are required, for instance, one representing the strength and the other representing the stress developed due to the external loading. A successful attempt has been made to incorporate these parameters into the analysis and develop an innovative technique that calculates the probabilistic reliability of anisotropic laminates.

In the next few sections, the various steps involved in the probabilistic reliability calculation are discussed in detail. In this chapter, the *SIF* is used as the parameter for evaluating the reliability of anisotropic laminates. For demonstration purposes, only orthotropic laminates are considered. As it has been stated earlier, in order for us to calculate the reliability, one needs to have two parameters; in this case they are the *SIF* and the *fracture toughness*. The *fracture toughness* can be evaluated by testing the orthotropic laminates but a standardized test procedure for evaluation of *fracture toughness* of composite laminates has not been designed so far. Several methods and procedures have been described so far for evaluating the *fracture toughness* of composite laminates. The evaluation of *fracture toughness* as proposed by Kageyama [129] has been employed in the present thesis.

In the first few sections of this chapter, the manufacturing and testing of orthotropic laminates is described. In the last few sections, the *Maximum Entropy Method* (*MEM*) for obtaining the exact distribution followed by a set of sample data is described. Further, the evaluation of the fracture toughness from failure loads is described; and the *SIF* is evaluated for the same. Then the reliability is computed from both these parameters by numerical integration.

5.2 Manufacturing of Composite Laminates

The manufacturing of composite laminates can be categorized into two phases:

(1) Fabrication and

(2) Processing

In the fabrication phase the fiber reinforcement and accompanying matrix material are placed or shaped into a structural form such as a flat or curved plate, a cylinder or other body of revolution, and the like. In the present study, a flat plate is manufactured using layers, or plies, of preimpregnated NCT-301 graphite/epoxy material. During the processing phase, an autoclave is used which provides the proper levels of heat and pressure to solidify and consolidate the structure.

5.2.1 Fabrication

Tooling:

All fabrication methods require tools to provide the shape of the composite structure during the processing. A flat aluminum tool is used to support the laminates for applying hand pressure during the manufacturing of the flat composite plate.

Specialty Materials:

Many secondary or specialty materials are used in composites manufacturing such as release coating, peel plies, release films, bleeder plies, breather plies, vacuum bags and sealant tape. Each of these materials serves a specific function [148]. A cross section of typical lay-up of a composite structure prepared for autoclave processing is shown in Figure 5.1.

Hand Lay-up:

The lay-up of preimpregnated material by hand is the oldest and most common fabrication method for advanced composite structures. Each step in the hand lay-up of a flat composite laminate must follow in successive fashion in order to obtain a high-

quality composite laminate after final processing. A description of these steps is given in Ref. [148].

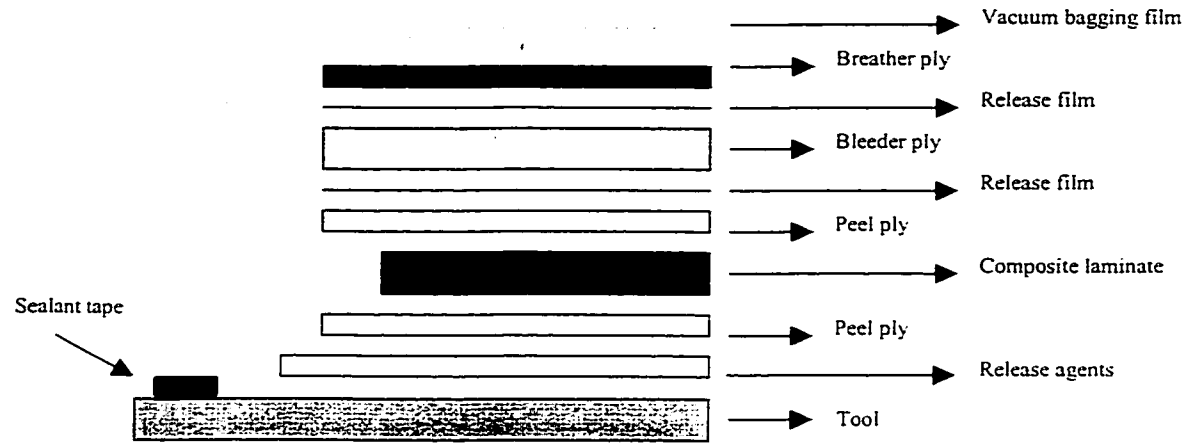

Figure 5.1 Typical cross section of autoclave lay-up

At first the surface of the tool is cleaned and a release agent is applied and then, a peel ply is placed on the top of the tool. The preimpregnated plies are cut according to design specifications, i.e. 12 inch by 12 inch. The first prepreg ply is oriented and placed upon the tool. Subsequent plies are placed one upon another according to the laminate configuration; a roller is used to compact the plies and to remove entrapped air that could later lead to voids or layer separations. After that, a peel ply, a sheet of porous release film, the bleeder plies, another release film and the breather plies are placed on top of the laminate one by one according to Figure 5.1.When the laminate fabrication is completed the sealant tape is placed around the entire periphery of the tool and the vacuum bag is placed over the entire tool.

It is important to ensure that the bag is adequately sealed before proceeding to the processing cycle. The vacuum port is installed through the bag and the contents are evacuated by vacuum pump.

5.2.2 Processing

Once the composite plies are put together so as to get the desired shape and orientation, it is necessary to apply the proper temperature and pressure for specific periods of time to produce the fiber-reinforced laminate. The temperature cycle is usually referred to as the cure cycle, since it is the heating of the resin that initiates the cure reaction. The overall cycle, which indicates pressurization and the temperature cycle, is referred to as the process cycle. The best quality laminates are cured using an autoclave. An autoclave consists of a large cylindrical metal pressure vessel with end enclosures that is thermally insulated and heated. A typical autoclave is shown in a schematic form in Figure 5.2.

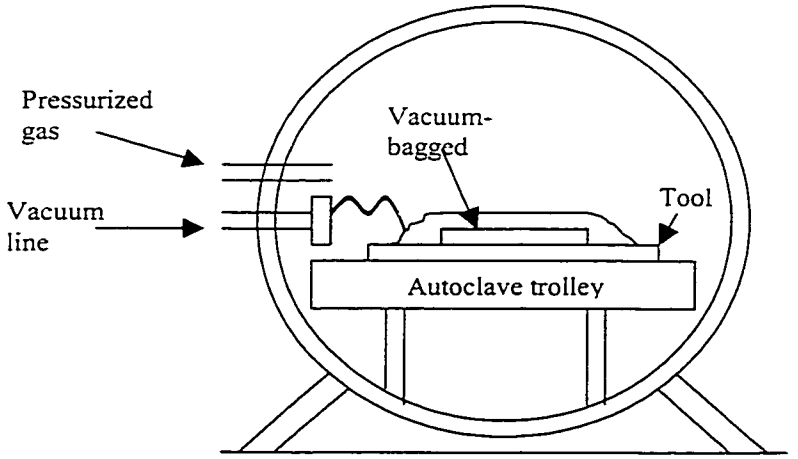

Figure 5.2 Schematic of an autoclave

A typical cure cycle for NCT-301 graphite/epoxy composites is a two step cycle shown in Figure 5.3. In such a cycle the temperature of the material is increased from room temperature to 104° C, and this temperature is held constant for half an hour (first dwell). Afterwards, the temperature is again increased to 140° C, and held constant for one hour (second dwell). After that the part is cooled to room temperature at constant rate.

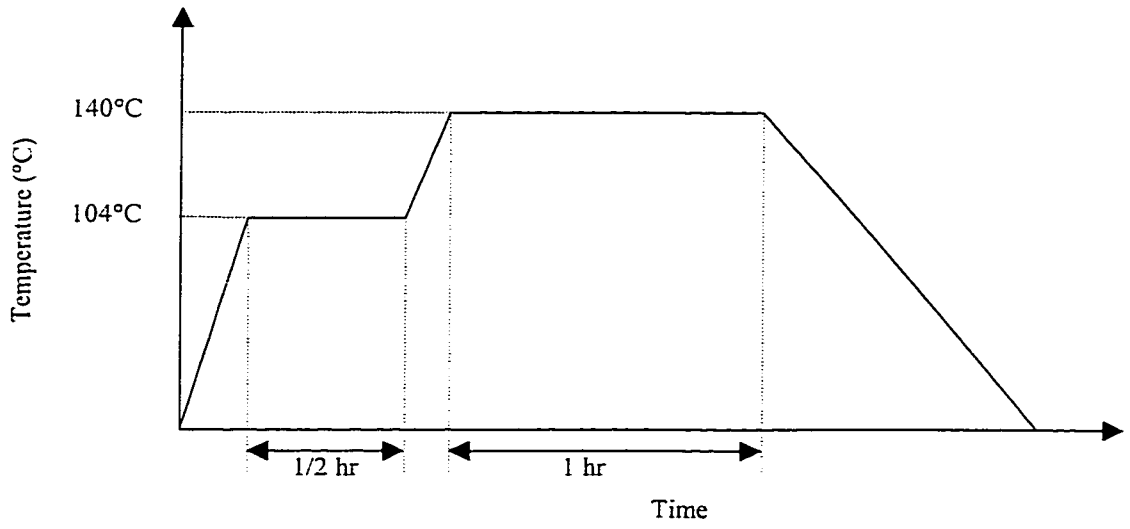

Figure 5.3 Cure cycle for NCT-301 graphite/epoxy composite material

The purpose of the first dwell is to allow gases (entrapped air, water vapor or volatiles) to escape from the matrix material and to allow the matrix to flow, facilitating compaction of the part. The purpose of the second dwell is to allow cross-linking of the resin to take place. The strength and related mechanical properties of the composite are developed during the second dwell. A constant 60 psi pressure is maintained inside the autoclave throughout the processing time. After cooling to room temperature the composite plate is ready for use.

5.3 Fracture Testing of Composite Laminates

The analysis and design of composite structures require the input of reliable experimental data. One of the major objectives of testing composite materials is the determination of the fracture toughness data for individual laminates so that their exact distribution can be determined later by the Maximum Entropy Method (*MEM*). This information together with the distribution of the stress intensity factor (*SIF*) obtained using the stochastic *FEM* can then be used to determine the reliability of the laminate. For determining the *plane strain fracture toughness* (K_{IC}) of isotropic materials the standard test procedure as described in ASTM E399 is to be followed. As it has been mentioned earlier, no such standardized testing procedure exists to date for evaluating the fracture toughness of anisotropic materials. The present work follows the test method proposed by Kageyama [129] but with minor modifications. The reason for adopting the procedure described by Kageyama [129] with minor modifications is explained below. One look at the specimen geometry used for determining the fracture toughness of metallic specimens gives us an idea of the philosophy of the test. The test is aimed at finding out the maximum amount of load that a particular material can withstand prior to failure by fracture. In the case of isotropic materials, the crack tip (Figure 5.4) is subjected to both a point load and a moment that pull apart the top and bottom portions of the test coupon. Comparing this loading with the loading applied on the composite test coupons in the work of Kageyama [129] it can be observed that the loading is uniformly distributed in the case of the composite test coupon. In the present work, the length of the specimen is increased and a hole is drilled through the tabs (Figure 5.5), which is used for the application of point load. Also, the length of the tab is increased so that the stress distribution inside the

effective specimen length is uniform.

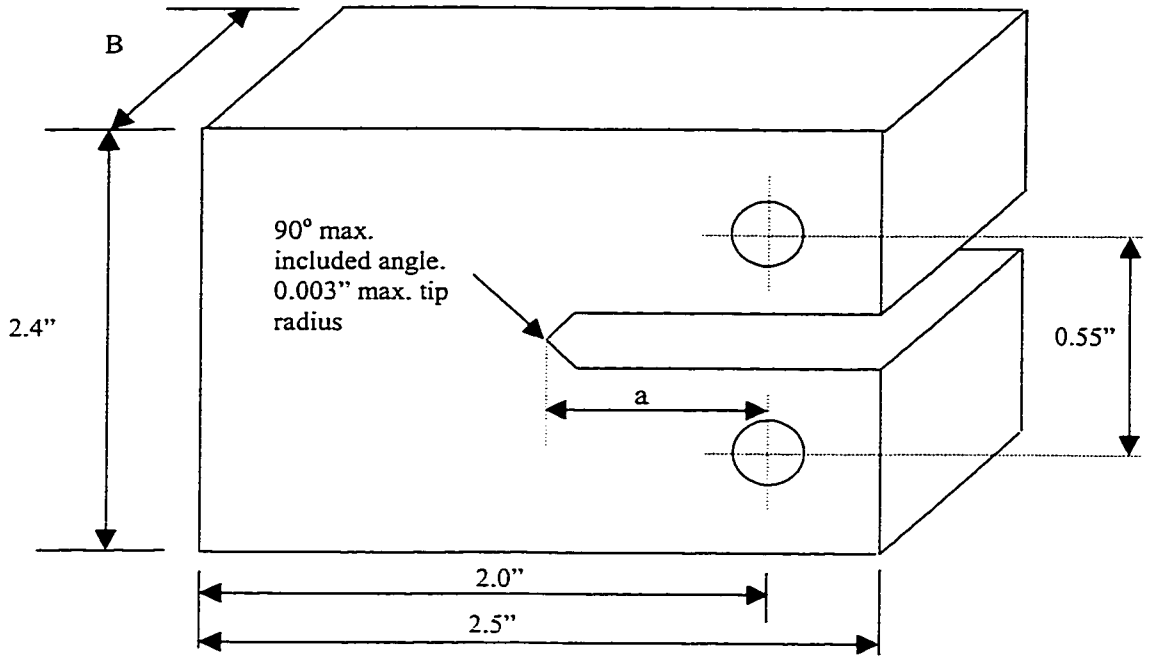

Figure 5.4 ASTM fracture test specimen for isotropic materials

In the case of fracture test specimen for isotropic materials, the loading is applied through pins inserted into the two holes shown in Figure 5.4. This load is equivalent to a combination of a point load and a moment at the crack tip, both of which tend to pull both the halves apart. This is the worst possible loading that can be applied at the crack tip. In the present work, a point load is applied at the crack tip. The geometry of the specimen is shown below in Figure 5.5. The length of the tab is chosen based on the widely used stress analysis result that, the effect of a concentrated load applied at a circle of radius r is smoothened out at a distance of more than three times the radius of the circle. In the present work, forty-two test specimens with the geometry as shown in Figure 5.5 have been prepared.

The crack geometry and all the relevant details for each specimen are summarized in table 5.1.

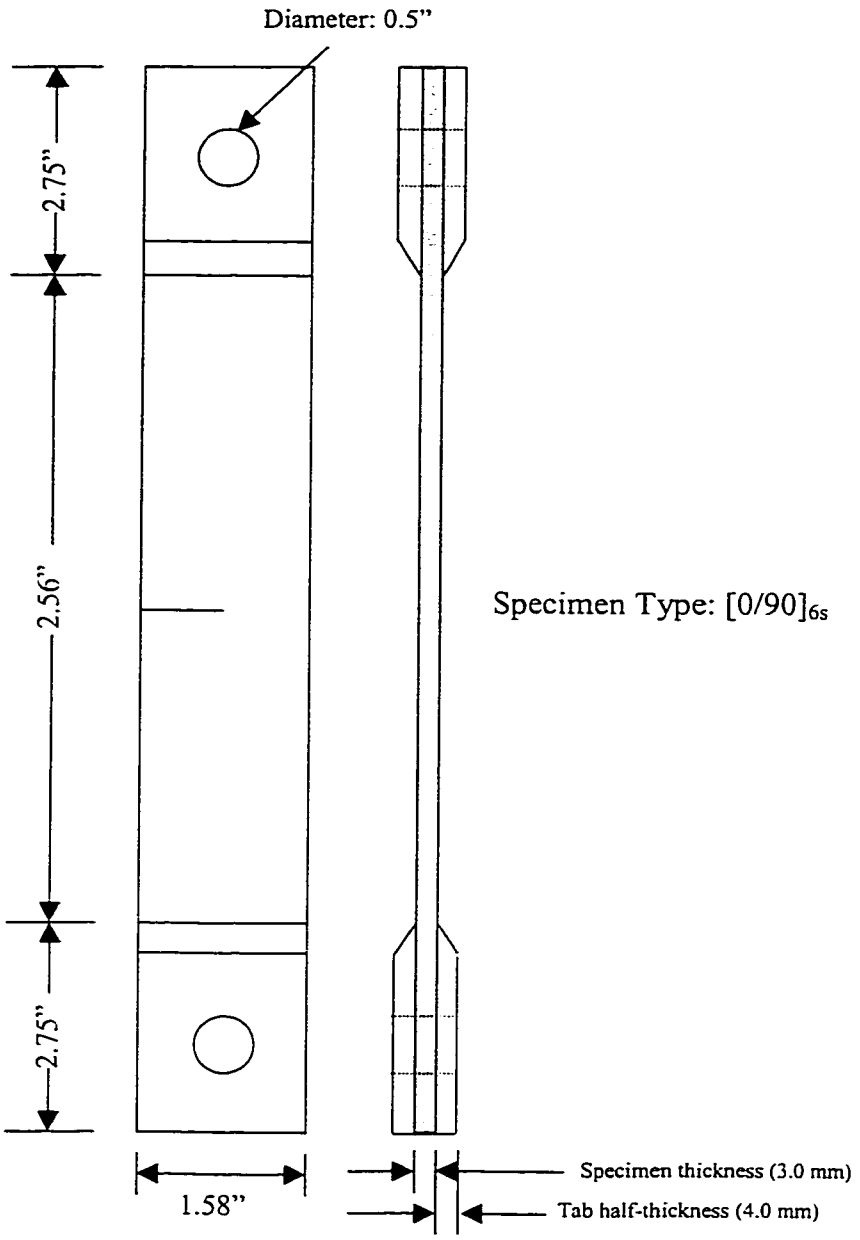

Figure 5.5 Schematic of the fracture test specimen

A digital photograph of the actual test specimen is also provided in Figure 5.6.

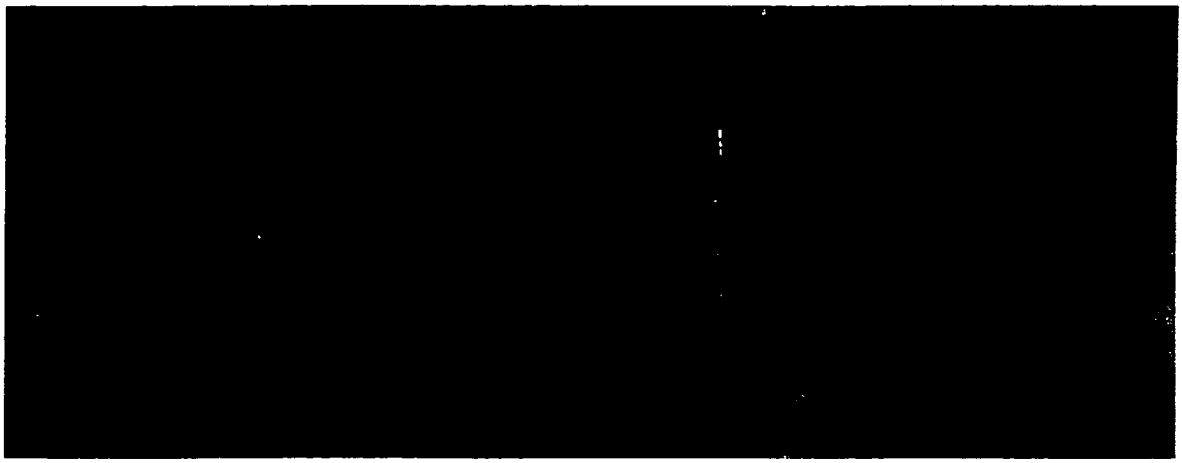

Figure 5.6 A photograph of the fracture test specimen

The *crack* is introduced into the specimen by using a diamond slicing wheel mounted on a vertical milling machine. Holes for applying the load, are drilled in the specimen for applying the load by a half-inch diameter drill-bit. The crack is approximately 50% of the width of the specimen, which is about 40 mm. The tabs are fabricated using glass fibers and epoxy resin. The layers of glass-epoxy material were placed one over the other, and were held together by Araldite (resin-epoxy adhesive). The same adhesive is used to bond the tabs together with the test specimen.

By following the laminate manufacturing process described above, six laminate plates of $[0/90]_{6s}$ configuration have been manufactured using *NCT-301* graphite-epoxy composite material. From each plate specimens with the above configuration have been obtained by using a diamond wheel mounted on a rotating horizontal handsaw. The final finishing is performed on a vertically rotating rough-surfaced belt. And then finally, the crack is cut into the specimen by a diamond slicing wheel which is 12 thou (0.3mm approx.) thick.

In this manner, a total of 42 specimens have been manufactured. At this stage, the specimen as it is, is not yet ready for the fracture test. This is because the specimen has to be properly aligned between the grips of the tensile testing machine so that the load is applied directly over the crack tip. The schematic of the set-up is shown in Figure 5.7.

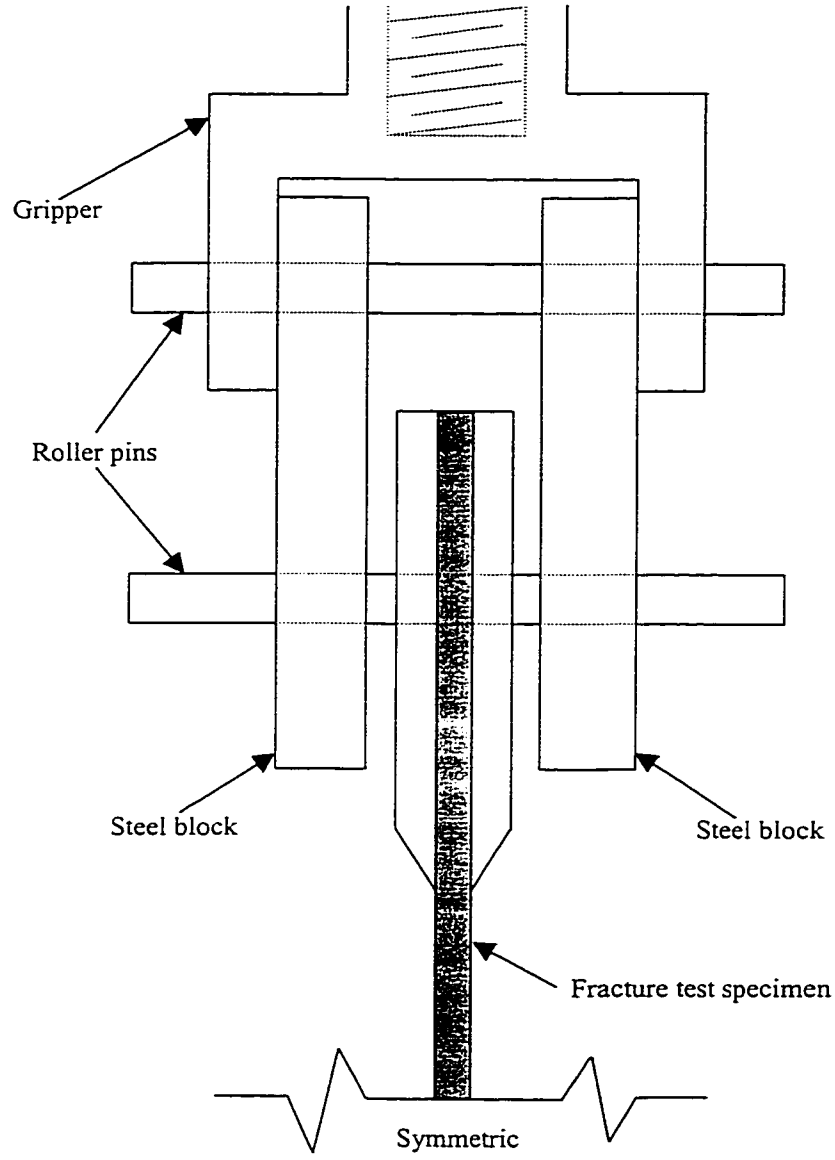

Figure 5.7 Schematic view of the test set-up near the grip

For this purpose two blocks of steel are employed that act as connectors between the specimen and the grips. Roller pins serve three important purposes: providing the connection, facilitating the load transfer from the grips to the specimen and perfectly aligning the specimen with the direction of loading. Thus, it is ensured through the above set-up that the loading is applied directly over the crack tip, which is crucial to the fracture toughness test. Also a digital photograph is presented below in Figure 5.8.

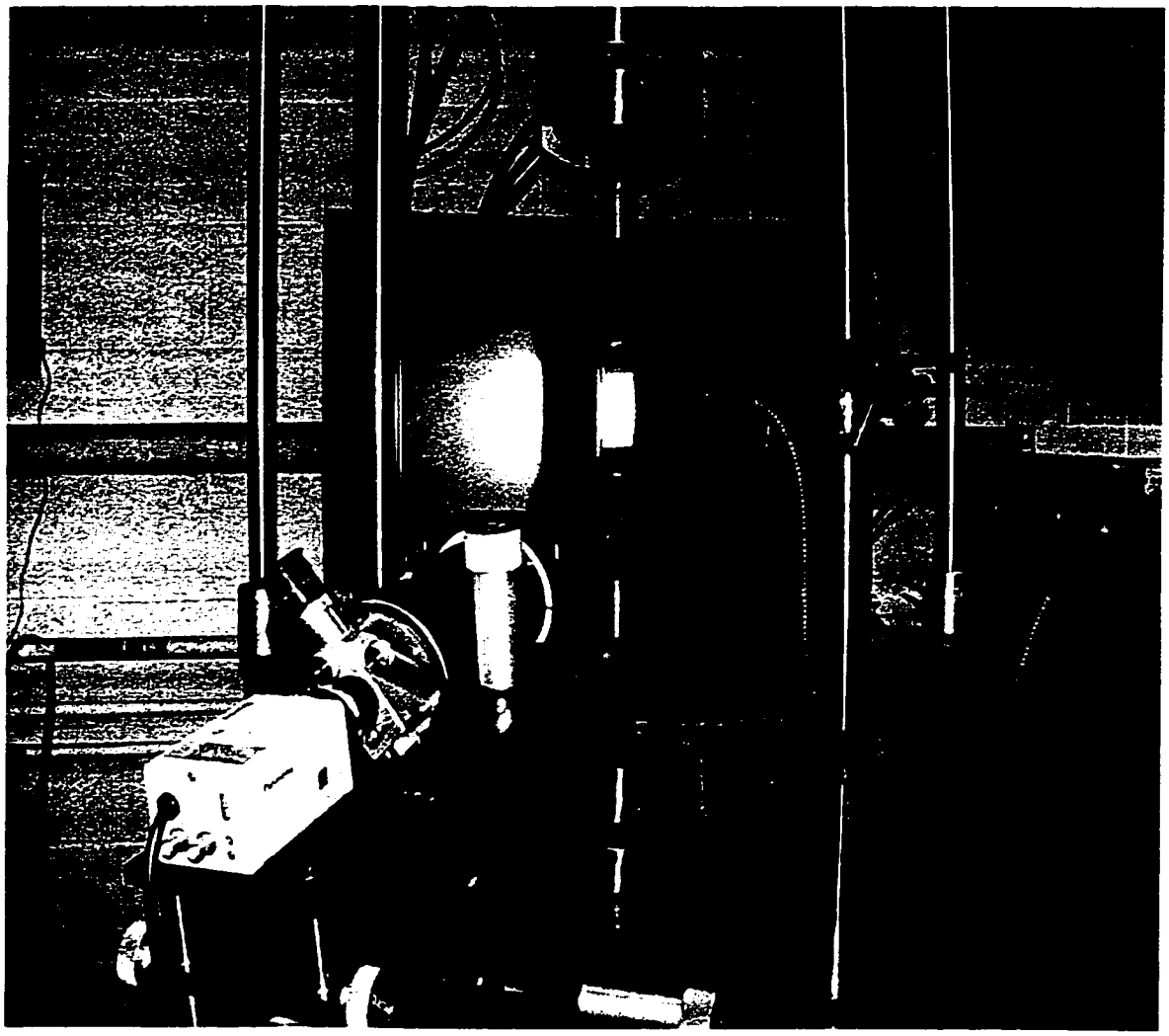

Figure 5.8 A photograph of the test set-up

5.3.1 Results of the Fracture Toughness Tests

Specimen Number	Crack width, a (mm)	Specimen Width, B (mm)	Specimen Length, 2L (mm)	Load at failure, P (Newtons)
1	20.15	41.08	65.08	8495.323
2	20.19	40.68	66.55	6183.037
3	20.23	40.89	65.38	7861.254
4	20.05	40.66	65.78	8664.179
5	20.34	41.02	65.77	8533.230
6	19.81	40.29	64.14	9670.420
7	19.79	40.35	64.01	8167.951
8	19.98	40.53	65.06	7392.594
9	20.07	40.20	65.40	7768.211
10	20.01	39.82	66.26	7161.710
11	19.97	40.31	66.01	7209.954
12	20.01	40.56	65.28	7844.024
13	20.15	40.46	66.03	6744.740
14	19.89	40.45	65.92	7516.651
15	20.10	40.66	64.92	8257.548
16	19.84	40.51	65.78	9239.666
17	20.04	41.35	64.64	9060.473
18	20.04	41.15	64.39	7365.025
19	20.08	41.10	65.45	8057.678
20	20.07	41.66	65.61	9057.027
21	20.10	40.76	65.62	9477.441
22	19.78	40.59	64.16	8205.857
23	20.17	40.76	64.88	8209.303
24	20.07	40.84	65.45	8088.692
25	20.05	40.61	66.17	9398.184
26	20.04	40.65	65.06	8581.184
27	19.93	40.76	65.59	9122.501
28	20.07	40.82	65.84	8223.087
29	20.34	41.13	66.04	9232.773
30	20.06	41.06	65.57	7695.844
31	19.91	41.13	64.97	7933.621
32	20.23	41.04	65.35	9232.773
33	19.95	40.83	65.71	8174.843
34	20.11	40.82	66.20	6865.351
35	20.07	40.99	65.05	8023.217
36	20.06	41.29	65.12	8198.965
37	20.20	40.96	65.34	8409.173
38	20.11	40.92	64.22	8223.087
39	20.05	40.93	65.53	9515.349
40	20.05	40.88	65.33	10469.900
41	20.16	40.81	64.48	10955.790
42	20.21	40.88	64.73	8002.542

Table 5.1 Results of fracture toughness tests

Initially, it has been tried to find out if the duplication of the test as in the case of isotropic materials is possible. It has been tried to fatigue the specimen so as to create a fatigue crack at the crack tip. Even though the specimen was fatigued for 15,000 cycles of loading, no visible fatigue crack has been created. In the case of the standard Aluminum fracture test specimen, a crack of 1 - 2 mm could be detected at 10,000 cycles of loading. Also, it is worth noting that the fracture toughness of *NCT-301* graphite-epoxy composite is not affected by the pre-cracking of the specimen through fatigue cycling. Hence the test has been carried out without fatiguing the specimen.

It has been found that the average failure load is around 8440 Newtons, which, as can be seen from the Table 5.1 is a representative value of the test data. The test has been monitored and further, the data and the load-displacement data for each specimen have been recorded using a data-acquisition system. A typical load-displacement curve is shown below in Figure 5.9. It can be observed that the curve is linear until failure occurs by fracture.

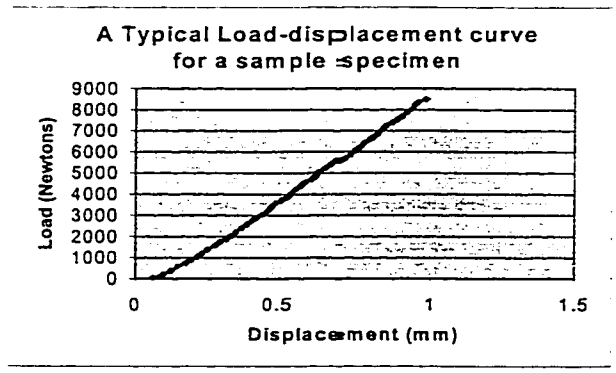

Figure 5.9 A typical load-displacement curve for a sample test specimen shown in Figure 5.6

5.3.2 Evaluation of Fracture Toughness from Failure Load data

The specimen length, width and the crack length are used as inputs to the program developed in chapter 4. Now for each specimen the above parameters are modified and the failure load is also provided as an input. The stochastic J-integral is evaluated for each specimen and the least value of J, i.e. J_{min}, is considered for evaluating the fracture toughness. It should be recalled that the maximum value of the stochastic J-integral is used for calculating the *SIF* (which is analogous to the stress) whereas the minimum value of the J-integral is used for computing the *fracture toughness* (which is analogous to the strength). Since the material is orthotropic with the crack on the plane of symmetry, the J-integral can be used to determine the *fracture toughness* by the relation

$$K_{IC} = \sqrt{E^{\cdot} J} \tag{5.1}$$

in which the *effective Young's modulus* is defined as [113]

$$E^{\cdot} = \frac{1}{\sqrt{2E_x E_y}} \sqrt{\frac{E_x}{2G_{xy}} - \nu_x + \sqrt{\frac{E_x}{E_y}}} \tag{5.2}$$

For the program developed earlier in chapter 5, another function: *CALC_EFF_YUNG.m* is added which performs the functions of calculating the effective Young's modulus and the fracture toughness as in Equations (5.1 – 5.2). The fracture toughness data for each of the test specimens is presented below in Table 5.2.

Specimen Number	Failure Load (N)	K1C (MPa√m)
1	8495.323	27.80
2	6183.037	24.86
3	7861.254	27.79
4	8664.179	30.77
5	8533.230	28.15
6	9670.420	32.44
7	8167.951	29.89
8	7392.594	24.97
9	7768.211	28.54
10	7161.710	26.07
11	7209.954	23.84
12	7844.024	27.76
13	6744.740	23.11
14	7516.651	26.34
15	8257.548	28.39
16	9239.666	31.15
17	9060.473	30.36
18	7365.025	26.38
19	8057.678	28.49
20	9057.027	30.47
21	9477.441	34.25
22	8205.857	29.68
23	8209.303	30.28
24	8088.692	27.63
25	9398.184	31.07
26	8581.475	30.70
27	9122.501	31.01
28	8223.087	27.57
29	9232.773	32.47
30	7695.844	25.34
31	7933.621	28.44
32	9232.773	32.09
33	8174.843	28.44
34	6865.351	23.77
35	8023.217	28.64
36	8198.965	27.45
37	8409.173	29.49
38	8223.087	28.42
39	9515.349	33.55
40	10469.898	37.51
41	10955.789	37.88
42	8002.542	27.58

Table 5.2 Fracture toughness data corresponding to the failure loads

5.4 Application of the Maximum Entropy Method

As stated earlier at the beginning of this chapter, the ultimate aim of the engineer might be to determine the reliability of a particular laminate. Fracture tests could be performed on a few samples from a batch, and failure loads and hence the K_{IC} data can be obtained by using the MATLAB® program developed in section 5.3.2. Now, if the service load is known, the *SIF* can also be calculated using the same program. If the probability distributions of the above two quantities are known, then the reliability can be calculated which is a representative of the entire batch. The *Maximum Entropy Method* (*MEM*) [168] can be used to determine the probability density functions of both the *SIF* and the *fracture toughness* data. In this section this method is described in sufficient detail.

The Jayne's principle [149] can be used to generate a probability density function from sample data. It can initially be assumed that no information is available in order that one is convinced about the presence of physical arguments that would suggest a particular distribution. Therefore, maximizing the entropy (information required for estimating a particular sample value) of the variable's distribution should lead to the least biased estimate of its form. A convenient way to use the sample information is by evaluation of the sample moments. For a continuous random variable the objective function, the entropy denoted by S is given by

$$S = -\int_R f(x)\ln[f(x)]dx \qquad (5.3)$$

in which

$$\int f(x)dx = 1 \tag{5.4}$$

and the central moments are given by

$$\int x^i f(x)dx = m_i;\ i = 1,\ldots,m \tag{5.5}$$

in which m is the number of moments to be used and m_i is the i^{th} moment about the origin, determined numerically from the sample. It has been shown that the density function inherently has a specific analytical form [149]. Hence, instead of using the numerical optimization techniques to solve Equation (5.3), classical methods of calculus have been employed. Let $\bar{S}$ represent the modified function which is expressed using the Lagrangian multipliers $\lambda_0, \lambda_1,\ldots, \lambda_m$, as

$$\bar{S} = S + (\lambda_0 + 1)\left[\int_R f(x)dx - 1\right] + \sum_{i=1}^{m} \lambda_i \left[\int_R x^i f(x)dx - m_i\right] \tag{5.6}$$

The multiplier, (λ_0+1), is actually used rather than λ_0 in order to obtain a more accurate result [149]. Now, in order to maximize $\bar{S}$, the derivative of $\bar{S}$ is obtained and set to be equal to zero.

$$\frac{d\bar{S}}{df(x)} = -\int_R \{ln[f(x)]+1\}dx - (\lambda_0 + 1)\int_R dx - \sum_{i=1}^{m} \lambda_i \left(\int_R x^i dx\right) = 0 \tag{5.7}$$

Combining the terms under the integral sign leads to the equation

$$\int_R \left\{ -ln[f(x)] - 1 + \lambda_0 + 1 + \sum_{i=1}^{m} \lambda_i x^i \right\} dx = 0 \tag{5.8}$$

For this equation to be true, the argument must be equal to zero.

$$ln[f(x)] = \lambda_0 + \sum_{i=1}^{m} \lambda_i x^i \tag{5.9}$$

or

$$f(x) = exp\left(\lambda_0 + \sum_{i=1}^{m} \lambda_i x^i \right) \tag{5.10}$$

This is the analytical form of the maximum entropy density function. Now the problem is to determine the values of the λ_i's. To achieve this one needs two expressions developed as follows. Substituting Equation (5.10) into Equation (5.4), one gets the following equation:

$$\int_R exp\left(\lambda_0 + \sum_{i=1}^{m} \lambda_i x^i \right) dx = 1 \tag{5.11}$$

Multiplying throughout by $e^{-\lambda_0}$ gives

$$e^{-\lambda_0} = \int_R exp\left(\sum_{i=1}^{m} \lambda_i x^i\right) dx \tag{5.12}$$

which leads to the first expression required.

$$\lambda_0 = -ln\left[\int_R exp\left(\sum_{i=1}^{m} \lambda_i x^i\right) dx\right] \tag{5.13}$$

The second equation is obtained by differentiating Equation (5.12) with respect to λ_i.

$$-e^{-\lambda_0} \frac{\partial \lambda_0}{\partial \lambda_i} = \int_R x^i \, exp\left(\sum_{i=1}^{m} \lambda_i x^i\right) dx \tag{5.14}$$

or

$$\frac{\partial \lambda_0}{\partial \lambda_i} = -\int_R x^i \, exp\left(\lambda_0 + \sum_{i=1}^{m} \lambda_i x^i\right) dx \tag{5.15}$$

This reduces to Equation (5.5), which is the second equation.

$$\frac{\partial \lambda_0}{\partial \lambda_i} = -m_i \tag{5.16}$$

In order to solve for the λ's one must set up a set of simultaneous equations. This is done by differentiating Equation (5.13) with respect to λ_i.

$$\frac{\partial \lambda_0}{\partial \lambda_i} = -\frac{\int_R x^i \exp\left(\sum_{i=1}^{m} \lambda_i x^i\right) dx}{\int_R \exp\left(\sum_{i=1}^{m} \lambda_i x^i\right) dx} = -m_i \tag{5.17}$$

The above equation represents m simultaneous equations to be solved for $\lambda_1, \lambda_2, \ldots, \lambda_m$. Having these, λ_0 is obtained from Equation (5.13). The above equations are put in a form more convenient for numerical solution as follows:

$$1 - \frac{\int_R x^i \exp\left(\sum_{i=1}^{m} \lambda_i x^i\right) dx}{m_i \int_R \exp\left(\sum_{i=1}^{m} \lambda_i x^i\right) dx} = R_i \tag{5.18}$$

In the above equation the R_i's are the residuals that are reduced to near zero values by a numerical technique. A solution can be obtained by using nonlinear programming to obtain the minimum of the sum of the squares of the residuals.

$$\mathrm{R} = \sum_{\mathrm{i}=1}^{\mathrm{m}} \mathrm{R}_{\mathrm{i}}^2 \tag{5.19}$$

is minimum. Convergence is achieved when $R < \varepsilon$, or all $|R_i| < \varepsilon$ in which ε is the specified acceptable error. The integrals in Equation (5.18) are evaluated numerically, and it is apparent that the bounds of the unknown density function must be known or assumed.

Because x^m must be evaluated in Equation (5.18) there exists a risk of overflow in the computation. To circumvent this the domain of x is transformed to lie in between 0 and 1. Also, the algorithm requires a starting value in order to begin the nonlinear programming solution. A good starting value is important for successful convergence, and therefore four alternative methods for determining a starting value are provided. The desired method can be pre-selected, or by default the algorithm will try the methods given one by one automatically in the order given until one of them succeeds. The methods used for finding a starting value for each of the Lagrangian multipliers are given below.

1. The distribution of λ_i is assumed to be normal, in which case the parameters are estimated by

$$\lambda_1 = \frac{c_1}{c_2}, \lambda_2 = -\frac{1}{2c_2}, \lambda_3 = \lambda_4 = \ldots = \lambda_m = 0 \tag{5.20}$$

2. The distribution of λ_i is assumed to be uniform. This works better for density functions whose shapes are similar to the uppercase alphabets, *J* and *U*.

$$\lambda_1 = \lambda_2 = \ldots = \lambda_m = 0 \tag{5.21}$$

3. A collocation method is used to calculate the values for the x's. Numerical integration forms of Equations (5.4 – 5.5) are written using $(m+1)$ stations.

$$\sum_{j=1}^{m+1} a_j f(x_j) = 1 \tag{5.22}$$

$$\sum_{j=1}^{m+1} a_j x_j^i f(x_j) = m_i ; i = 1,...,m \tag{5.23}$$

in which the a_j's are numerical integration multipliers. These are the $(m+1)$ linear equations for the $(m+1)$ unknown $f(x_j)$'s that are solved and the results are applied to Equation (5.10).

$$f(x_j) = exp(\lambda_0 + \lambda_1 x_j + ... + \lambda_m x_j^m), j = 1,...,(m+1) \tag{5.24}$$

3. A step-by-step start is used which begins using method *1* but with *m* set to be equal to *3*. The algorithm then iterates with the values obtained for λ_0, λ_1, and λ_2, and with λ_3 equal to zero. This is repeated until *m* starting λ's are obtained.

The algorithm can be summarized as follows:

1. Input the moments and bounds.
2. Calculate the moments about the origin.
3. Transform the domain.
4. Set up the expressions for the residuals as in Equation (5.18).
5. Select a starting method and calculate starting values.
6. Call the optimization subroutine.
7. Check if convergence has been achieved ?
8. *YES*: Go to step 12.
9. *NO*: Check if all the methods have been tried ?

10. *YES*: Exit with failure.

11. *NO*: Select next method and go to step 5.

5. Calculate λ_0.

13. Calculate the values of other λ's corresponding to the original domain.

14. Output the results.

Also it has been proved [149] that the Maximum Entropy Method is based on a global optimum value.

5.5 Probability Distributions of the Lagrangian Multiplier Constants

The following parametric study has been performed to find out how the Lagrangian multiplier constants λ_i's vary with the number of simulations. The number of moments used, m is taken to be equal to four. The variation of the Lagrangian multipliers with the number of simulations (within the range 50 - 650) has been investigated and the variations are presented graphically below in Figure (5.10).

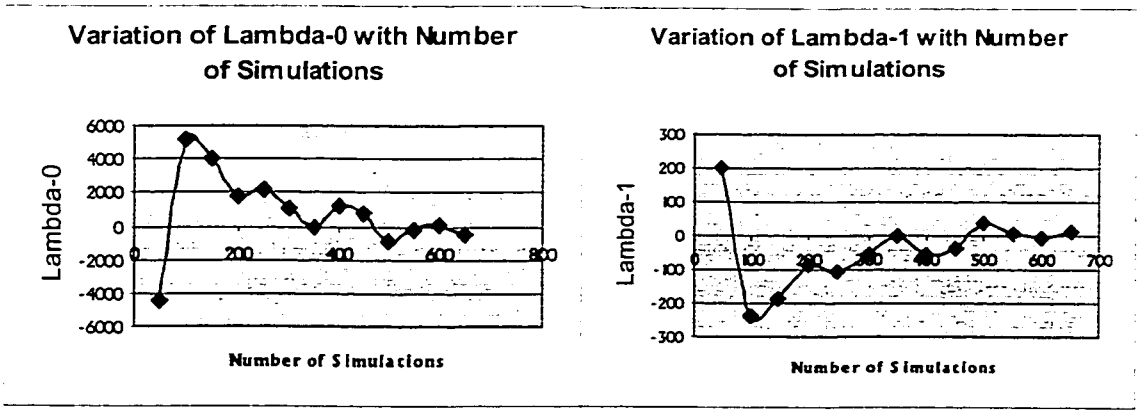

Figure 5.10 (a) Variation of λ_0 with the number of simulations; (b) Variation of λ_1 with the number of simulations.

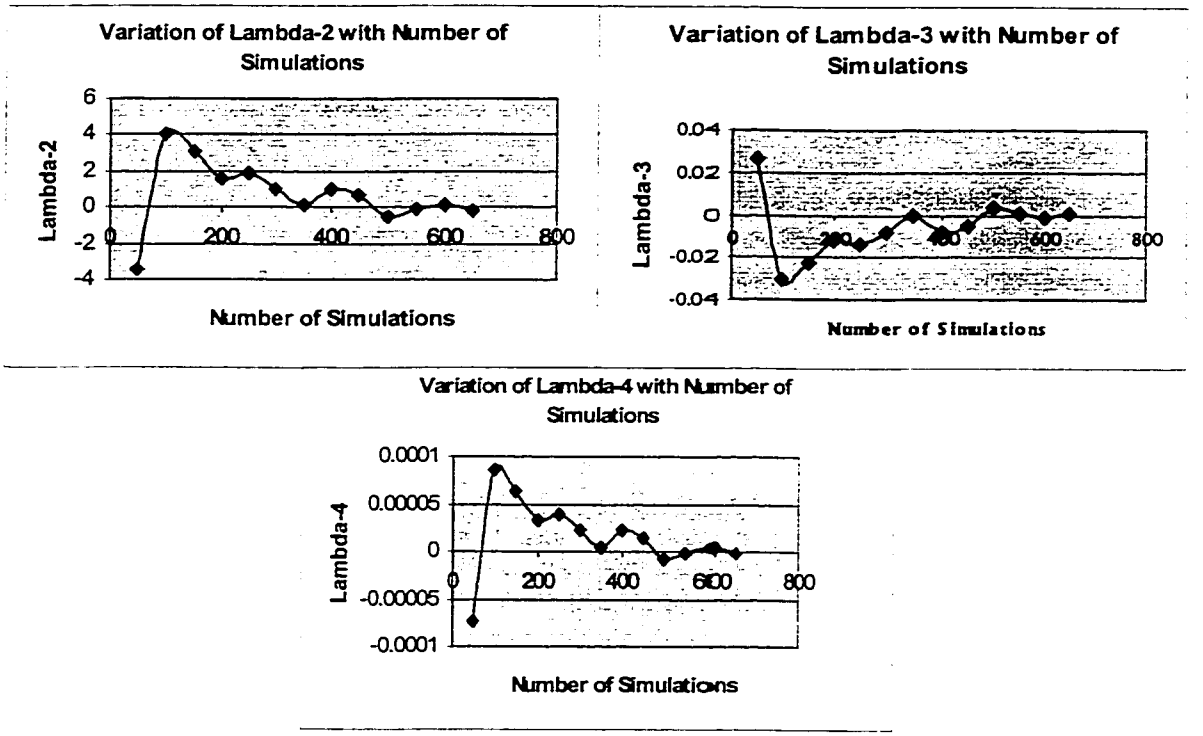

Figure 5.10 (contd.) (c) Variation of λ_2 with the number of simulations. (d) Variation of λ_3 with the number of simulations. (e) Variation of λ_4 with the number of simulations.

From the above graphs it can be observed that variations in values of each of the Lagrangian constants follow a *certain trend* that is compatible with the analytical formulation as obtained in the previous section (5.4). It can be observed that while λ_0 starts with a negative value and alternatively takes a positive and negative value, the same trend is followed by alternate λ_i's i.e., λ_2 and λ_4 with their individual values having entirely different ranges. A mirror image of this trend is followed by the other set of λ_i's i.e., λ_1 and λ_3.

5.6 Reliability of Composite Laminates in Fracture

As pointed out earlier in the beginning of this chapter, the main purpose of stochastic analysis when both the factors, that are the *SIF* and the *fracture toughness*, are involved is to determine the *reliability* with both the distributions known at a critical location in the component. The distributions followed by each of these two representatives might be quite different from each other and they can be represented as

$$K_I = A\left(\mu_{K_I}, \sigma_{K_I}\right) \quad and \quad K_{IC} = B\left(\mu_{K_{IC}}, \sigma_{K_{IC}}\right) \tag{5.25}$$

in which A and B represent the two different distributions followed by the *SIF* and the *fracture toughness* respectively. A general method has been described below which is capable of solving the above problem. In the following, the subscript *1* is used to represent the *fracture toughness* distribution and the subscript *2* is used to designate the *SIF* distribution. These two distributions are shown below in Figure (5.11) so that a single cursor, x, can be used to identify points on both distributions.

$$\begin{pmatrix} Probability\ that \\ the\ SIF \\ is\ less\ than\ K_{IC} \end{pmatrix} = dp\left(K_I < K_{IC}\right) = dR = F_2(x)dF_1(x) \tag{5.26}$$

By substituting $(1 - R_2)$ for F_2 and $-dR_1$ for dF_1, Equation (5.26) reduces to

$$dR = -[1 - R_2(x)]dR_1(x) \tag{5.27}$$

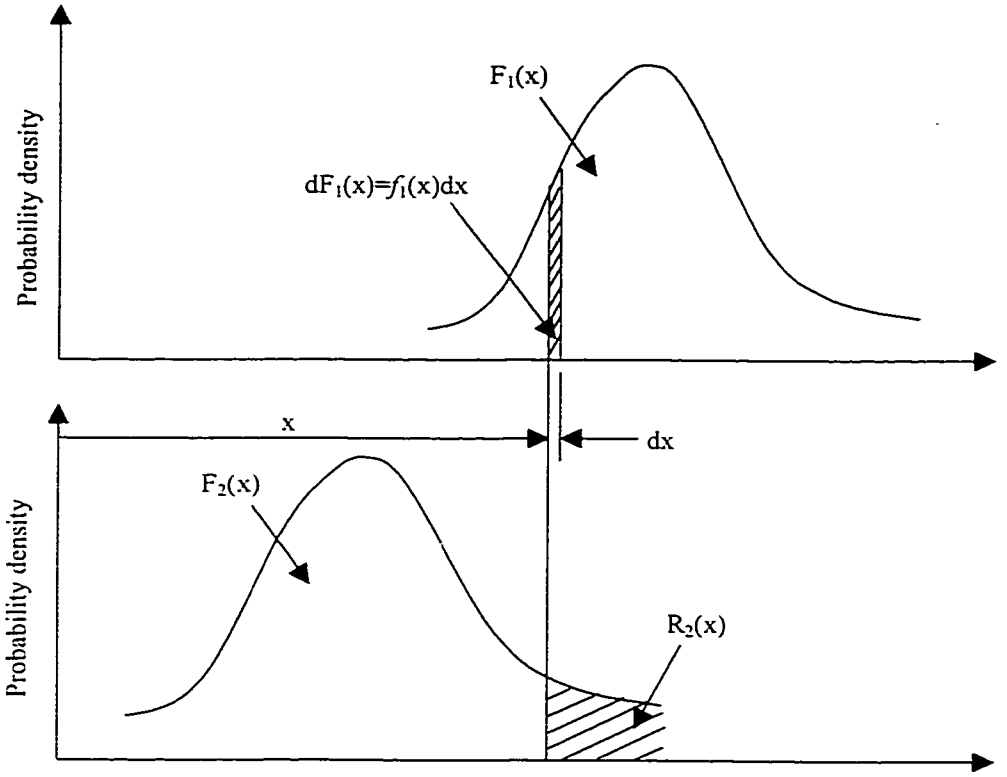

Figure 5.11 Probability distribution functions of K_{IC} (denoted by F_2) and K_I (denoted by F_1).

The reliability is obtained by considering all possible locations of the cursor and integrating x from -∞ to +∞; but this corresponds to an integration from 1 to 0 on the reliability R_I. Therefore,

$$R = -\int_1^0 [1 - R_2(x)]dR_1(x) \tag{5.28}$$

which can be rewritten as

$$R = 1 - \int_0^1 R_2 dR_1 \tag{5.29}$$

In a form that can be evaluated numerically, the above Equation (5.29) can be expressed as

$$(1-R) = \int_0^1 R_2 dR_1 = \int_{x=L_{K_{IC}}}^{U_{K_{IC}}} \left[\int_x^{U_{K_I}} f_2(x)dx \right] f_1(x)dx \tag{5.30}$$

in which

$$R_1(x) = \int_x^{\infty} f_1(K_{IC})dK_{IC} \tag{5.31}$$

and $$R_2(x) = \int_x^{\infty} f_2(K_I) \tag{5.32}$$

The one-third Simpson's rule has been used to expand the right hand side of Equation (5.30), which is given by

$$\int_a^b f(x)dx = \frac{h}{3}\left[(y_0 + y_{2n}) + 4(y_1 + y_3 + \ldots + y_{2n-1}) + 2(y_2 + y_4 + \ldots + y_{2n-2})\right] \tag{5.33}$$

in which $y_0, y_1, ..., y_{2n}$ are the values of $y = f(x)$ evaluated at $x = a, a+h, a+2h, ..., a+2nh$. Also, the interval between the extreme limits, a and b is divided into an even ($2n$) number of intervals.

Also, $L_{K_{IC}}$, $U_{K_{IC}}$ and U_{K_I} represent the lower limit of the *fracture toughness*, upper limit of the *fracture toughness* and the upper limit of the *SIF*, respectively. The distribution followed by the *fracture toughness* that has been obtained by testing as presented in table 5.2, is shown in Figure 5.12.

The above programs have been tested for validity by applying it to an example problem [149] for a particular case of Gaussian distribution. The problem description is as follows: The load induced stress at a critical location of a part in simple tension is given by $\sigma \sim N(40,5)$ and the yield strength is given by $S \sim N(60,4)$. It is required to estimate the reliability against failure by yielding.

The reliability obtained using the above-developed program is 0.998787, which compares very well with the reliability obtained using the normal distribution tables.

The distribution followed by the *fracture toughness* data that has been obtained by testing is presented below in Figure 5.12. The distribution of the *SIF* of a 24-ply orthotropic laminate, of dimensions 240mm x 120mm, and made of *NCT-301* graphite-epoxy composite material that is subjected to a total tensile load of 17.5 KN which is distributed throughout the edge, is obtained and presented below in Figure 5.13.

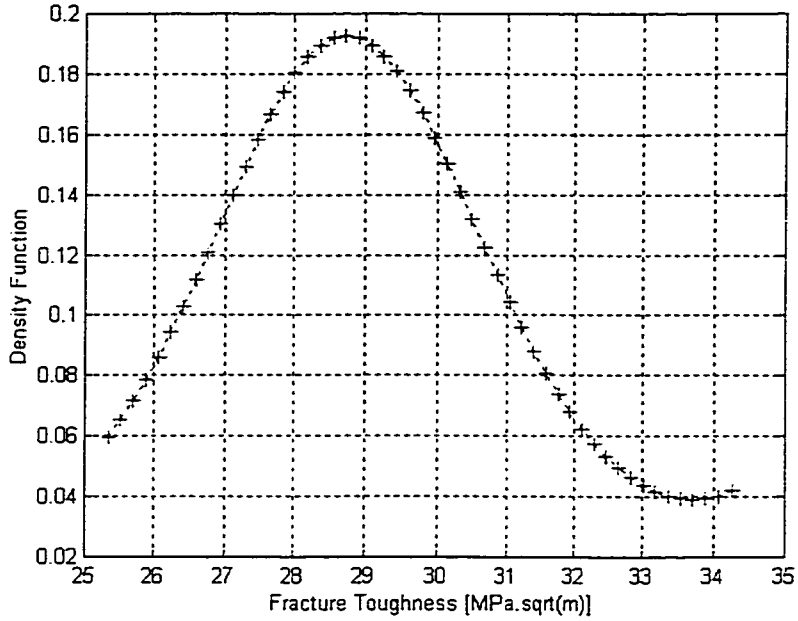

Figure 5.12 Probability distribution of the fracture toughness data obtained by testing.

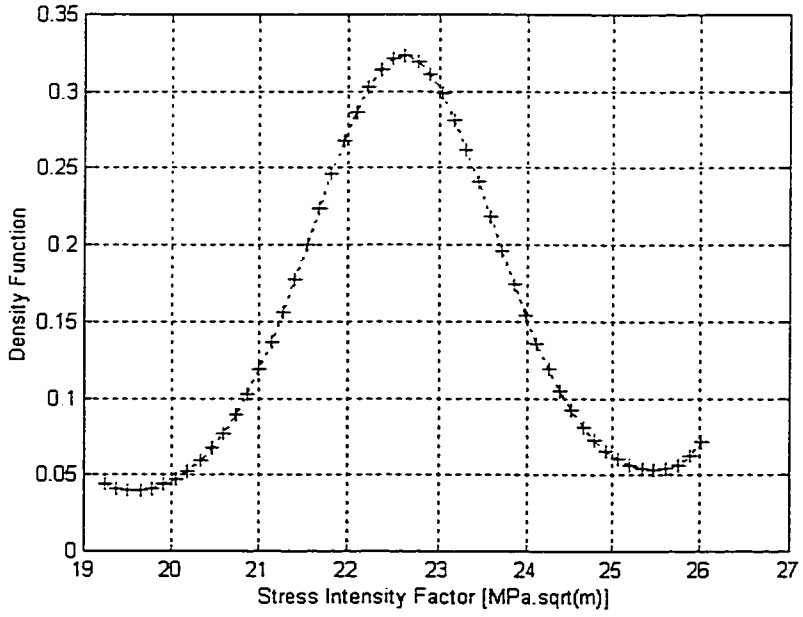

Figure 5.13 Probability distribution of the *SIF* of a 24-ply orthotropic laminate.

The values of the *SIF* generated by the stochastic finite element analysis of an orthotropic laminate with a configuration of $[0/90]_{6s}$ and subjected to a load of 17.5 KN, are provided as input to the *MEM*. The values of the Lagrangian constants obtained corresponding to the maximum entropy are tabulated in the second column of table 5.3. Similarly, the values of the K_{IC} (provided in table 5.2) are provided as input to the *MEM* and the values of the Lagrangian constants obtained are provided in the first column of table 5.3.

	Lagrangian constants for K1C	Lagrangian constants for SIF
Lambda-0	1597.80678	6335.75566
Lambda-1	-230.48845	-1144.06015
Lambda-2	12.3119354	76.9805699
Lambda-3	-0.2891476	-2.28859302
Lambda-4	0.00252005	0.02536805

Table 5.3 Values of the Lagrangian constants for the distributions of K_{IC} and *SIF* obtained by the maximum entropy method (17.5 KN)

Each of the corresponding sets of Lagrangian constants for *SIF* and K_{IC} are substituted into Equation 5.24 and the resulting expressions for $f(K_{IC})$ and $f(K_I)$ are inserted into Equation 5.30, which is evaluated using the Simpson's rule (Equation 5.33). In the Equation 5.30, the corresponding values for the upper and lower limits of the K_{IC} are taken as 37.88 MPa$\sqrt{m}$ and 23.11 MPa$\sqrt{m}$ respectively, and the upper limit for the *SIF* is considered to be 26.03 MPa$\sqrt{m}$ as obtained from the stochastic finite element analysis. The right hand side of the Equation 3.30 has been evaluated to be 0.0009679. This value

is equivalent to (1-*R*), in which *R* denotes the reliability. Thus, the reliability (*R*) of the laminate has been calculated and has been found to be 0.9990321.

The distribution of the *SIF* of a 24-ply orthotropic laminate ([0/90]), of dimensions 240 mm x 120 mm, and made of *NCT-301* graphite-epoxy composite material that is subjected to a total tensile load of 22.0 KN which is distributed throughout the edge, is obtained, as in the earlier case. Now, the values of the *SIF* obtained by the stochastic *FEA* are provided as input to the *MEM*. The values of the Lagrangian constants obtained from the *MEM* are presented in the second column of table 5.4.

	Lagrangian constants for K1C	Lagrangian constants for SIF
Lambda-0	1597.80678	3941.5732
Lambda-1	-230.48845	-556.1222
Lambda-2	12.3119354	29.200653
Lambda-3	-0.2891476	-0. 676742
Lambda-4	0.00252005	0.005842

Table 5.4 Values of the Lagrangian constants for the distributions of K_{IC} and *SIF* obtained by the maximum entropy method (22.0 KN)

Using these values of the Lagrangian constants the right hand side of Equation (3.30) is calculated as 0.547313 and the reliability is 0.452687. Thus, it can be seen that the reliability decreases as the applied load (and hence the *SIF*) increases. Reliability is the measure of safety of the system (or structure) against failure. The reliability obtained in this case is based on stochastic *FEA* and the exact variations of the *SIF*s and the K_{IC}s.

The reliability can also be represented graphically and is presented below. Considering the first case in which the applied load is 17.5 KN, the distributions of the *SIF*s and the K_{IC}s are represented (approximately) below in figure 5.14 on a single plot.

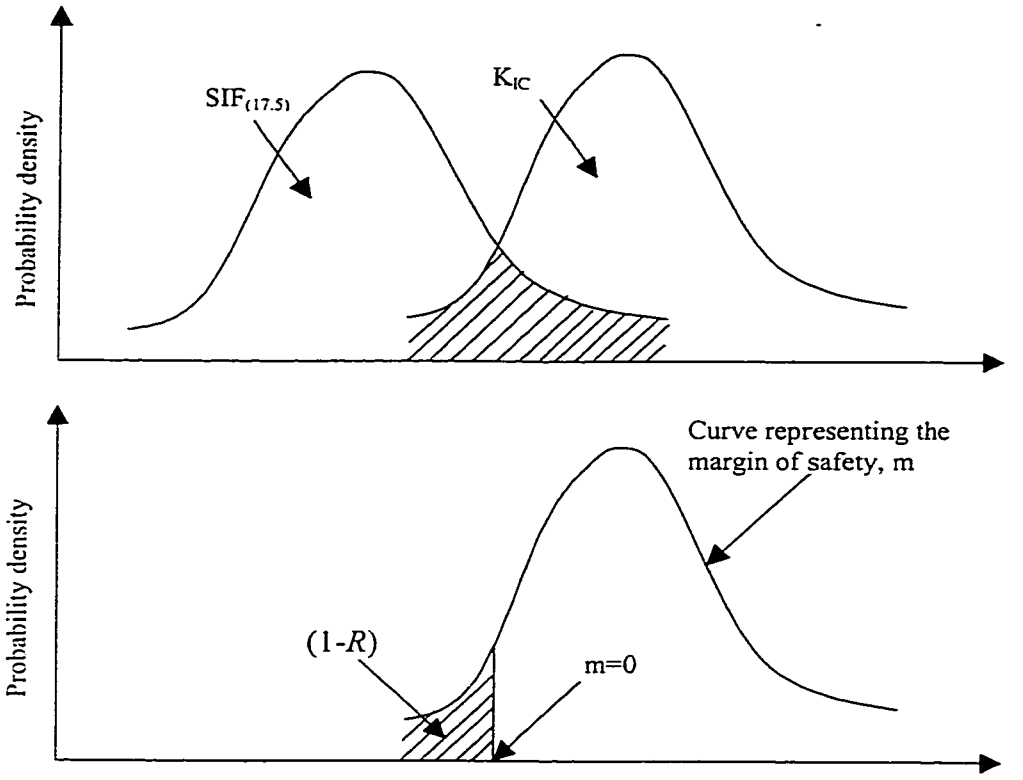

Figure 5.14 (a) Plot of the density functions showing how the interference between the K_{IC} and *SIF* (for an applied load of 17.5 KN) is used to obtain the safety margin. (b) Curve representing the probability density distribution of the margin of safety.

It can be observed from Figure 5.14 that the curve representing the probability distribution of the margin of safety can be used to obtain the reliability. In this case, the total area below the margin of safety curve is equal to one and the shaded area represented by (1-*R*) is equal to 0.0009679, from which the reliability, (*R*) can be calculated to be 0.9990321.

Now considering the second case in which the applied load is equal to 22.0 KN, the distributions of the *SIF*s and the K_{IC}s are represented (approximately) below in Figure 5.15 on a single plot.

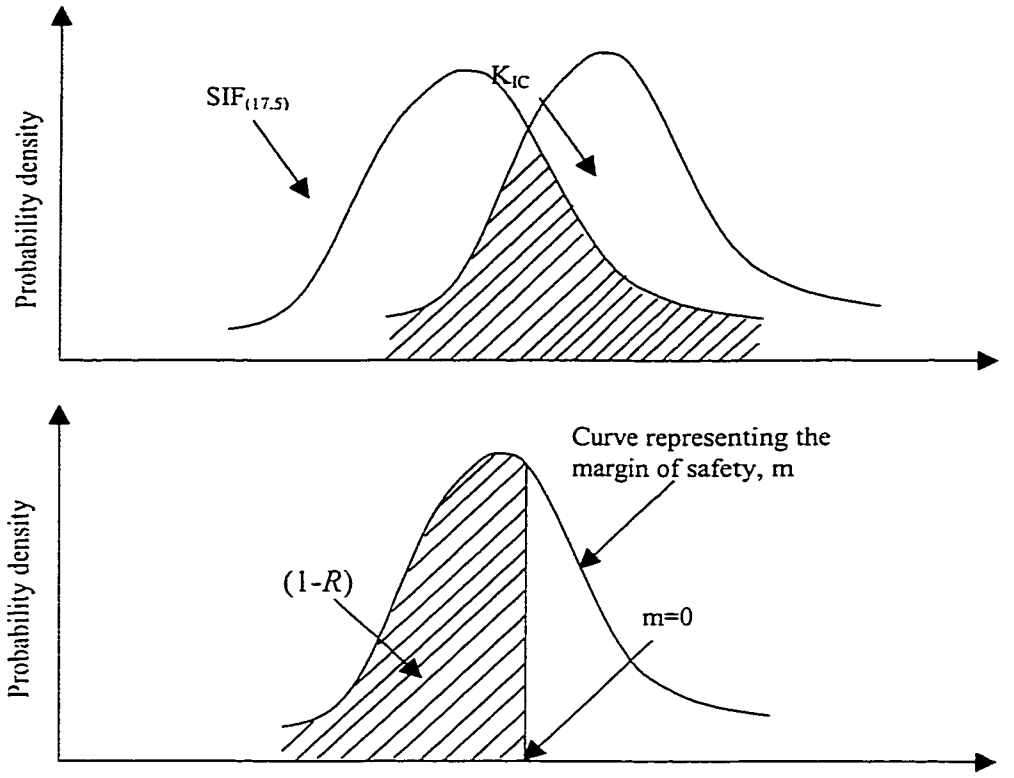

Figure 5.15 (a) Plot of the density functions showing how the interference between the K_{IC} and *SIF* (for an applied load of 22.0 KN) is used to obtain the safety margin. (b) Curve representing the probability density distribution of the margin of safety.

In this case, the total area below the margin of safety curve in Figure (5.15) is equal to one and the shaded area represented by (1-*R*) is equal to 0.547313, from which the reliability, (*R*) can be calculated to be 0.452687.

Proceeding in a similar manner, the reliability has been calculated corresponding to various applied loads. The variation of the reliability of the laminate with an increase in the applied load is plotted below in Figure 5.16.

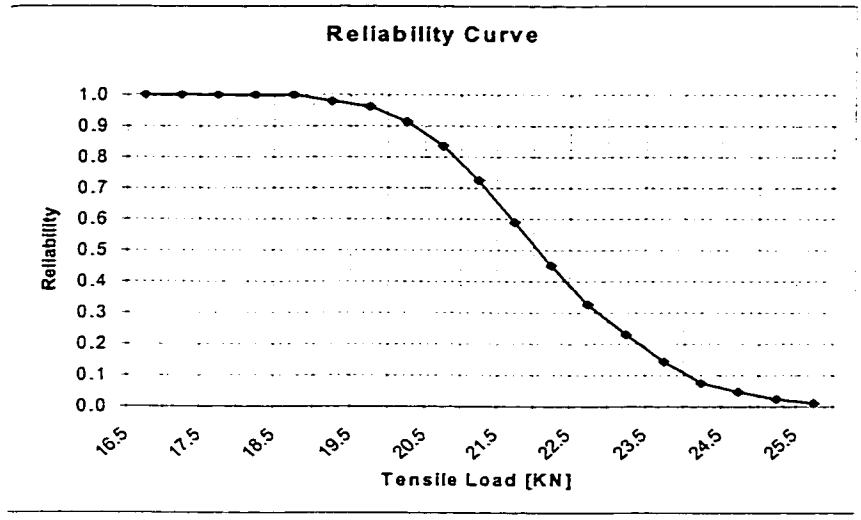

Figure 5.16 Plot of reliability versus the tensile load for a $[0/90]_{6s}$ laminate ($a/W = 1/3$ and $W/L = 1/2$) subjected to tensile loading

It can be observed from Figure 5.16 that the (downward) slope of the curve first increases and then remains constant for some time before it starts to decrease. Based on the trend of the slope of the curve, it can broadly be divided into three regions. In the first one-third portion of the graph (until 19.0 KN) that is shown in Figure 5.16, it can be observed that reliability of the orthotropic laminate does not decrease much with an increase in the applied load (the curve resembles an inverted parabola). In the central portion of the graph (until 23.0 KN), it can be observed that the gradient of the curve stabilizes and the variation follows an almost linear trend. In the last portion of the graph, it can be observed that the (upward) gradient increases with an increase in the applied load and the

curve is nearly parabolic. The reliability approaches the value of zero in an asymptotic manner. It has been seen from various parametric studies in chapter 4 that the standard deviation values of any fracture parameter increase with an increase in the mean values of the respective fracture parameter. As the standard deviation values increase, the slope of the flanges of the K_I curve keeps on decreasing which means that the slope of the reliability curve also keeps on decreasing towards the end, which can be seen in Figure 5.16. The numerical values corresponding to Figure 5.16 are presented below in table 5.5.

Applied Load (KN)	Reliability
16.5	0.9999
17.0	0.9999
17.5	0.9993
18.0	0.9991
18.5	0.9988
19.0	0.9786
19.5	0.9612
20.0	0.9136
20.5	0.8346
21.0	0.7242
21.5	0.5890
22.0	0.4511
22.5	0.3263
23.0	0.2293
23.5	0.1431
24.0	0.0746
24.5	0.0465
25.0	0.0233
25.5	0.0106

Table 5.5 Variation of reliability with the applied tensile load

5.7 Conclusions and Discussions

In the Section 5.2 of this chapter, the manufacturing of composite laminates has been discussed in detail. The detailed procedure to be followed for evaluating the *fracture toughness* of composite laminates has been described. Further, in Section 5.3, the testing

for *fracture toughness* has been conducted successfully. It has been found from literature survey that graphite-epoxy composite laminates with a configuration of [0/90] typically have a *fracture toughness* value of around 30 MPa$\sqrt{m}$. This confirms the validity of the test results presented in table 5.2.

The purpose of, and the need for the Maximum Entropy Method (*MEM*) in relation to determining the reliability of composite laminates based on the stochastic finite element analysis (*FEA*) have been described. The details of the mathematical and computational aspects of *MEM* have also been described. The use of the *MEM* in obtaining the analytical distributions of any sample data obtained from the stochastic *FEA* (described in chapter 3) has also been illustrated.

Further, the mathematical formulation and the computational procedure for computing the reliability of composite laminates based on a stochastic field modeling has been illustrated by means of an example problem. Also, the variation of the reliability with an increase in the applied load, for a particular orthotropic laminate has been determined and presented.

Chapter 6

Conclusions and Recommendations

In the present thesis, a stochastic finite element methodology (using MATLAB® software) for evaluating the various fracture parameters such as the stress intensity factor (*SIF*), the energy release rate (*ERR*) and the values of the *J*-integral at various locations in both the isotropic plates as well as composite laminates has been developed and demonstrated by means of examples, wherever appropriate. The model has the capability to accommodate the inherent variations in the material properties, ply angles and ply thicknesses.

The program that has been developed in Chapters 2 and 3, performs the analysis for 250 simulated laminates and gives the mean and standard deviation values of the various fracture parameters. It has been found that the *J*-integral when computed at various locations in the laminate keeps track of the stochastic variations in the various material properties and gives the stochastic values of the *J*-integral at each of these locations. For this purpose, an advanced and complex finite element mesh is required. Such a mesh has been developed and presented in chapter 3.

The program has been used to relatively compare the fracture behavior of three different composite laminates: orthotropic laminate ($[0/90]_{6s}$), quasi-isotropic laminate ($[0/\pm45/90]_{3s}$) and symmetric angle-ply laminate ($[\pm45]_{6s}$). It has been demonstrated that the *J*-integral can be used to bring out the stochastic characteristics of the variations in

fracture parameters at various locations in the composite laminates. Thus the *J*-integral method has been proven to give a better and more complete description of fracture in composite laminates than the conventional *ERRM* and *DEM*. It has also been shown that the maximum value of the stochastic *J*-integral can be used as a valid critical design parameter. It has been found that the length of the crack and the dimension of the plate parallel to the crack surface (in 2-D case, it is the width of the plate) have the most profound effect on all the fracture parameters.

Quasi-isotropic laminates have been found to be the *strongest* laminates. The crack size has a more pronounced effect on the orthotropic laminates. The symmetric angle-ply laminates have been found to be subjected to a more pronounced effect by the plate dimensions. Further, the results of the analyses can be used in creating *data charts* that can aid the analysts in quantifying the variations in the fracture parameters of various composite laminates with different crack sizes and plate dimensions.

Tests have been conducted in order to obtain the plane-strain fracture toughness values of *NCT*-301 graphite-epoxy orthotropic laminates with 24 plies. The Maximum Entropy Method (*MEM*) has been used to obtain the true analytical probability distribution of a set of randomly distributed values. The distributions thus obtained have been used to compute the reliability of the orthotropic laminates under various uniformly distributed tensile loads (corresponding to mode-I). Similarly the developed stochastic finite element model can be used for any loading in mode-II also. Thus the *reliability graph* depicting the variation in the reliability of the component with the change in the applied load has

been obtained. This greatly assists the design engineers in avoiding over-design and yet ensuring the safe operation of the component in practical situations.

The following related works are suggested for future research:

- A three-dimensional model can be developed so as to accommodate a combination of loads in all the three modes of fracture. The existing program(s) can be used for this purpose.
- Further research needs to be carried out for developing efficient models (similar to the present one) for accommodating the stochastic variations in the material and laminate properties that demand much less computational time.
- Reliability charts need to be developed for various laminates considering varying loads and various combinations of loads that are commonly encountered in practice.
- Tests have to be conducted in order to obtain the experimental values of the critical *ERR* (i.e., G_C) and the critical value of the stochastic J-integral (i.e., J_C). Based on these, the reliabilities of various laminates have to be computed.

References

[1] Anderson, T. L., "*Fracture Mechanics*", CRC Press, Ann Arbor, 1991.

[2] Rice, J.R., "*Some Remarks on Elastic Crack-tip Stress Fields*", Int. J. Solid Structures, Vol. 8, 1972, pp. 751-758.

[3] Owen, D.R.J., and Fawkes, A.J., "*Engineering Fracture Mechanics: Numerical Methods and Applications*", Pineridge Press, Swansea, 1983.

[4] Hull, D., "*Introduction to Composite Materials*", Cambridge University Press, Cambridge, 1981.

[5] Roulin-Moloney, A.C., "*Fractography and Failure Mechanisms of Polymers and Composites*", Elsevier Applied Science Publishers, Barking, 1989.

[6] Hoa, S.V., Ed., "*Computer-Aided Design of Polymer-Matrix Structures*", Marcel Dekker, 1995.

[7] Lakshminarayana, H.V., "*Stress Distribution around a Semi-circular Edge-notch in a Finite Laminated Composite Plate under Uniaxial Tension*", Journal of Composite Materials, Vol. 17, 1983, pp. 357-367.

[8] Wang, C.M.S. and Matthews, F.L., "*A Finite Element Analysis of Single and Two-hole Bolted Joints in Fiber Reinforced Plastic*", Journal of Composite Materials, Vol. 15, 1981, pp. 484-491.

[9] Hori, M., "*Statistical Theory of Effective Electrical, Thermal and Magnetic Properties of Random Heterogeneous Materials-II*", J. of Math. Phys., Vol. 14, 1973, pp. 1942-1948.

[10] Borri, A., "*Stochastic Behavior of Special Materials: The Composite Material in Dynamic Motion: Chaotic and Stochastic Behavior*", Ed.:F. Casciati, Springer-Verlag, 1993, pp. 171-202.

[11] Haugen, E. B., "*Probabilistic Approaches to Design*", John Wiley & Sons, Inc., 1968.

[12] Chell, G.G., "*Developments in Fracture Mechanics*", edited by Chell, G. G., Applied Science Publishers Limited, 1980.

[13] Knott. J. F., and Elliott, D., "*Worked examples in fracture mechanics*", The Institution of Metallurgists Monograph No. 4, 1979.

[14] Buchalet, C. B. and Bramford, W. H., "*Stress intensity factor solution for continuous surface flaws in reactor pressure vessels*", ASTM STP 590, 1976.

[15] Hearmon, R.F.S., "*An Introduction to Applied Anisotropic Elasticity*", Oxford University Press, Oxford, 1969.

[16] Lekhnitskii, S.G., "*Theory of Elasticity of an Anisotropic Elastic Body*", Trans. P. Fern, Holden Day, San Francisco, 1963.

[17] Muskhelishvili, N.I., "*Some Basic Problems of the Mathematical Theory of Elasticity*", Noordhoff, Groningen, The Netherlands, 1953.

[18] Barrell, J.D., "*Effect of Crack-Front Width on Fracture Toughness of Douglas-Fir*", Engineering Fracture Mechanics, Vol. 9, 1976, pp. 711-717.

[19] Chen, P.E., "*Stress Fields Around Parallel Edge Cracks*", Journal of Composite Materials, Vol. 1, 1967, pp. 82-90.

[20] Davies, P. and Benzeggagh, M.L., "*Interlaminar Mode-I Fracture Testing*", Application of Fracture Mechanics to Composite Materials, Ed.: K. Friedrich,

Composite Materials Series, Vol. 6, Elsevier Science Publishers B.V., 1989, pp. 81-157.

[21] Charalambides, M., Kinlock, A.J., Wang, Y. and Williams, J.G., "*On the Analysis of Mixed-Mode Fracture*", International Journal of Fracture, Vol. 54, 1992, pp. 269-291.

[22] Williams, J.G., "*Fracture Mechanics of Anisotropic Material*", Application of Fracture Mechanics to Composite Materials, Edited by K. Friedrich, 1989, pp. 3-38.

[23] Choi, N.S., Kinloch, A.J. and Williams, J.G., "*Delamination Fracture of Multidirectional Carbon-Fiber/Epoxy Composites under Mode-I, Mode-II and Mixed-Mode-I/II Loading*", Journal of Composite Materials, Vol. 33, 1999, pp. 73-100.

[24] Whitcomb, J.D., "*Finite Element Analysis of Instability Related Delamination Growth*", Journal of Composite Materials, Vol. 15, 1981, pp. 403-426.

[25] Waszczak, J.P. and Cruse, T.A., "*Failure Mode and Strength Predictions of Anisotropic Bolt Bearing Specimens*", Journal of Composite Materials, Vol. 5, 1971, pp. 421-425.

[26] Tang, S., "*Failure of Composite Joints under Combined Tension and Bolt Loads*", Journal of Composite Materials, Vol. 15, 1981, pp. 329-335.

[27] York, J.L., Wilson, D.W. and Pipes, R.B., "*Analysis of Tension Failure Mode in Composite Bolted Joints*", Journal of Reinforced Plastics and Composites, Vol. 1, 1982, pp. 141-153.

[28] Tsujimoto, Y. and Wilson, D., "*Elasto-Plastic Fracture Analysis of Composite Bolted Joints*", Journal of Composite Materials, Vol. 20, 1985, pp. 236-251.

[29] Eisenmann, J.R., "*Bolted Joint Static Strength Model for Composite Materials*", NASA TM-X-3377, pp. 563-602.

[30] Wong, C.M.S. and Matthews, F.L., "*A Finite Element Analysis of Single and Two-Hole Bolted Joints in Fiber Reinforced Plastic*", Journal of Composite Materials, Vol. 15, 1981, pp. 481-490.

[31] Kurt, C.S. and Paul, F.P., "*A Tension-Mode Fracture Model for Bolted Joint in Laminated Composites*", Journal of Composite Materials, Vol. 29, 1995, pp. 37-58

[32] Whitney, J.M. and Nuismer, R.J., "*Stress Fracture Criteria for Laminated Composites Containing Stress Concentrations*", Journal of Composite Materials, Vol. 8, 1974, pp. 253-265.

[33] Waddoups, M.E., Eisenmann, J.R. and Kaminski, B.E., "*Microscopic Fracture Mechanics of Advanced Composite Material*", Journal of Composite Materials, Vol. 5, 1971, pp. 446-454.

[34] Pipes, R.B., Wetherhold, R.C. and Gillespie, J.W., Jr., "*Notched Strength of Composite Materials*", Journal of Composite Materials, Vol. 12, 1979, pp. 1151-1155.

[35] Karlak, R.F., "*Hole effects in a Related Series of Symmetrical Laminates*", Proceedings of Fracture Modes in Composites, IV, Metallurgical Society of American Inst. of Mining Metallurgical and Petroleum Engineers, Chicago, IL, 1977, pp. 105-117.

[36] Awerbuch, J. and Madhukar, M.S., "*Notched Strength of Composite Laminates: Prediction and Experiments-A Review*", Journal of Reinforced Plastics and Composites, Vol. 4, 1985, pp. 3-15.

[37] Rajesh, S.V. and Sun, C.T., "*Fracture Criterion for Notched Thin Composite Laminates*", AIAA Journal, Vol. 35, 1997, pp. 311-316.

[38] Guofang, S., "*Fracture of Fiber glass Reinforced Composites*", Journal of Composite Materials, Vol. 15, 1981, pp. 521-530.

[39] Aronsson, C., and Backluwd, J., "*Tensile Fracture of Laminates with Cracks*", Journal of Composite Materials, Vol. 20, 1986, pp. 287-307.

[40] Wang, J.Z. and Darrell, F.S., "*Failure Strength and Damage Mechanisms of E-Glass/Epoxy Laminates under In-plane Biaxial Compressive Deformation*", Journal of Composite Materials, Vol. 27, 1993, pp. 40-58.

[41] Lee, L.J. and Wang, C.H., "*Stress Intensity Factor by Weight Function Method for Cracked Composite Laminates*", Engineering Fracture Mechanics, Vol. 48, No. 2, 1994, pp. 267-279.

[42] Ruijia, M. and Reddy, D.V., "*Stress Intensity Factor and Weight Function for Semi-Elliptical Crack using Finite Element Alternating Method*", Engineering Fracture Mechanics, Vol. 48, No. 3, 1994, pp. 305-323.

[43] Tan, P.W. and Bigelow, C.A., "*Analysis of Cracked Laminates with Holes Using The Boundary Force Method*", AIAA Journal, Vol. 26, No. 9, 1988, pp. 1094-1099.

[44] Nairn, J. A., "*Fracture Mechanics of Unidirectional Composites Using the Shear-Lag Mode I: Theory*", Journal of Composite Materials, Vol.22, 1988, pp. 561-588.

[45] Case, S.W., Carman, G.P., Lesko, J.J., Fajardo, A.B. and Peifsnider, K.L., "*Fiber Fracture in Unidirection Composite*", Journal of Composite Materials, Vol. 29, 1995, pp. 208- 228.

[46] Snyder, M.D. and Cruse, T.A., "*Crack Tip Stress Intensity Factor in Finite Anisotropic Plates*", Air Force Material Laboratory, AFML-TR-73-209, 1973.

[47] Yeh, J.R., "*Fracture Analysis of A Stiffened Orthotropic Sheet*", Engineering Fracture Mechanics, Vol. 46, No. 5, 1993, pp. 857-866.

[48] Mandell, J.F., McGarry, F.J., Wang, S.S. and Im, J., "*Stress Intensity Factors for Anisotropic Fracture Test Specimens of Several Geometry*", Journal of Composite Materials, Vol. 8, 1974, pp. 106-116.

[49] Phillips, D.C., "*The Fracture Mechanics of Carbon Fiber Laminates*", Journal of Composite Materials, Vol. 8, 1974, pp. 130-141.

[50] Victor, E.S. and Efthimios, S.S., "*Stress Intensity Factor in Anisotropic Bodies Using Singular Isoparametric Elements*", Engineering Fracture Mechanics, Vol. 25, No. 1. 1986, pp. 115-121.

[51] Hutchinson, J. W., "*Singular behavior at the end of a tensile crack tip in a Hardening Material*", Journal of the Mechanics and Physics of Solids, Vol. 16, 1968, pp. 13-31.

[52] Rice, J. R. and Rosengren, G. F., "*Plane Strain Deformation near a Crack Tip in a Power-Law Hardening Material*", Journal of Mechanics and Physics of Solids, Vol. 16, 1968, pp. 1-12.

[53] McMeeking, R. M., "*Estimates of the J-Integral for Elastic-Plastic Specimens in Large Scale Yielding*", Journal of Engineering Materials and Technology, Vol. 106, 1984, pp. 278-284.

[54] Derbalian, G., "*J-Integral Estimation Procedures*", Journal of Pressure Vessel Technology, Vol. 105, 1984, pp. 299-308.

[55] Klepaczko, J. R., "*Determination of the Critical Value of the J-Integral at High Loading Rates Using the Wedge-Loaded Specimen*", Journal of Testing and Evaluation, Vol. 13, 1985, pp. 441-445.

[56] Zahoor, A., "*J-Integral Analysis of the Compact Tension Specimen*", Journal of Engineering materials and Technology, Vol. 111, 1989, pp. 138-144.

[57] Zahoor, A., "*J-Integral Analysis for Notched Round Bar in Tension*", Journal of Pressure Vessel Technology, Vol. 109, 1987, pp. 155-158.

[58] Zahoor, A., "*J-Integral Analysis of Three-Point Bend Specimen*", Journal of Engineering materials and Technology, Vol. 111, 1989, pp. 132-137.

[59] Lubarda, V. A., "*A Simplified Determination of the J-Integral and Some Estimates of Elastic Stress Intensity Factors*", Journal of Applied Mechanics, Vol. 60, 1993, pp. 29-32.

[60] Joyce, J. A, and Smudz, R., "*Evaluation of Elastic Stress Intensity using J-Integral Specimen Geometries*", Journal of Testing and Evaluation, Vol. 20, 1992, pp. 1-5.

[61] Faucher, Bernard, "*Crack Length and J-Integral Expressions for Specimens Loaded in Tension*", Journal of Testing and Evaluation, Vol. 22, pp. 30-35.

[62] Gennady P. Nishikov, Jurgeb Heerens, and Dieter Hellmann, "*Effect of Crack Front Curvature and Side Grooving on CTOD δ_5 and J-integral in CT and 3PB Specimens*", Journal of Testing and Evaluation, Vol. 27, 1999, pp. 312-319.

[63] Yuhara, T., and Kortshot, M., "*A simplified determination of the J-integral for paper*", Journal of Materials Science, Vol. 28, 1993, pp. 3571-3580.

[64] Westerlind, B. S., Carlsson, L. A., and Andersson, Y. H., "*Fracture toughness of liner board evaluated by the J-integral*", Journal of Materials Science, Vol. 26, 1991, pp. 2630-2636.

[65] Crouch, B. A., and Huang, D. D., "*The J-integral technique applied to toughened nylons under impact loading*", Journal of Materials Science, Vol. 29, 1994, pp. 861-864.

[66] Roos, E., and Eisele, U., "*Determination of Material Characteristic Values in Elastic-Plastic Fracture Mechanics by Means of J-Integral Crack Resistance Curves*", Journal of Testing and Evaluation, Vol. 16, 1988, pp. 132-137.

[67] Tian, Z. and Swanson, S.R., "*The Fracture Behavior of Carbon/Epoxy Laminates Containing Internal Cut Fibers*", Journal of Composite Materials, Vol. 25, 1991, pp. 1427-1444.

[68] Ko, W.L., "*Finite Element Microscopic Stress Analysis of Cracked Composite Systems*", Journal of Composite Materials, Vol. 12, 1978, pp. 97-109.

[69] Heppler, G.R., Frisken, S. and Hansen, J.S., "*Stress Intensity Factor Calculation for Designing with Fiber-Reinforced Composite Materials*", AIAA Journal, Vol. 23, No. 6, 1985, pp. 893-901.

[70] Heppler, G. and Hansen, J.S., "*Mixed Mode Fracture Analysis of Rectilinear Anisotropic Plates by High Order Finite Elements*", International Journal for Numerical Methods in Engineering, Vol. 17, 1981, pp. 445-464.

[71] Zhu, H. and Sankar, B.V., "*Evaluation of Failure Criteria for Fiber Composites Using Finite Element Micro-mechanics*", Journal of Composite Materials, Vol. 32, 1998, pp. 766-782.

[72] Yeh, J.H., "*Stress Singularity in Composite Laminates by Finite Element Method*", Journal of Composite Materials, Vol. 20, 1986, pp. 347-364.

[73] Chen, A.T. and Yang, T.Y., "*Static Dynamic and Buckling Formulation of a Symmetrically Laminated Plate Finite Element for a Microcomputer*", Journal of Composite Materials, Vol. 21, 1987, pp. 441-453.

[74] Nassehi, V., Kinsella, M. and Mascia, L., "*Finite Element Modeling of the Stress Distribution in Polymer Composites with Coated Fiber Interlayers*", Journal of Composite Materials, Vol. 27, 1993, pp. 195-214.

[75] Thomas, J.B., Paul, A.W. and Anthony, R.I., "*Finite Element Modelling of Fracture Propagation in Orthotropic Materials*", Engineering Fracture Mechanics, Vol. 26, No. 2, 1987, pp. 185-201.

[76] Tasu, L.R. and Plunkett, R., "*Finite Element Analysis of Progressive Failure for Laminated FRP Plates with Inplane Loading*", Engineering Fracture Mechanics, Vol. 45, No. 4, 1993, pp. 529-546.

[77] Tsai, S.W. and Wu, E.M., "*A General Theory of Strength for Anisotropic Materials*", Journal of Composite Materials, Vol. 5, 1971, pp. 58-80.

[78] Sih, G.C., Chen, E.P., Huang, S.L. and McQuillen, E.J., "*Material Characterization on the Fracture of Filament-Reinforced Composites*", Journal of Composite Materials, Vol. 9, 1975, pp. 167-186.

[79] Buczek, M.B. and Herakovich, C.T., "*A Normal Stress Criterion for Crack Extension Direction in Orthotropic Composite Materials*", Journal of Composite Materials, Vol. 19, 1985, pp. 544-553.

[80] Kadi, H.E., Ellyin, F., "*Crack Extension in Unidirectional Composite Laminate*", Engineering Fracture Mechanics, Vol. 51, No. 1, 1995, pp. 27-36.

[81] Ellyin, F. and Kadi, H.E., "*Predicting Crack Growth Direction in Unidirectional Composite Laminates*", Engineering Fracture Mechanics, Vol. 36, 1990, pp. 27-37.

[82] Krawczak, P. and Pabiot, J., "*Fracture Mechanics Applied to Glass Fiber/Epoxy Matrix Interface Characterization*", Journal of Composite Materials, Vol. 29. 1995, pp. 2230-2253.

[83] Sih, G.C. and Chen, E.P., "*Fracture Analysis of Unidirectional Composites*", Journal of Composite Materials, Vol. 7, 1973, pp. 230-244.

[84] Gu, Y.H., "*Fracture Behavior of Continuous Alumina Fiber Reinforced Epoxy*", Journal of Composite Materials, Vol. 28, 1994, pp. 1227-1236.

[85] William, W.F., "*A Failure Criterion for Composite Materials*", Journal of Composite Materials, Vol. 25, 1991, pp. 88-100.

[86] Ovchinskii, A.S., "*Fracture Process in Composite Materials: Computer Imitation of Micro and Macromechanisms*", Nauka, Moscow, 1988, (in Russian)

[87] Stock, T.A., Bellini, P.X., Murthy, L.N. and Chamis, C.C., "*Probabilistic Composite Micromechanics*", Proceeding of the AIAA/ASME/ASCE/AHS/ASC 29th Structures, Srtuctural Dynamics and Materials Conference (Williamsburg, VA), AIAA, Washington, DC, April 1988, Pt. 3, pp. 1289-1293.

[88] Fukuda, H., "*Monte Carlo Simulation of the Strength of Hybrid Composite*", Journal of Composite Materials, Vol. 16, 1982, pp. 371-385.

[89] Dzenis, Y.A., Joshi, S.P. and Bogdanovich, A.E., "*Damage Evaluation Modeling in Orthotropic Laminated Composites*", AIAA Journal, Vol. 32, No. 2, 1994, pp.357-364.

[90] Joshi, S.P. and Frantziskonis, G., "*Damage Evaluation in Laminated Advanced Composites*", Composite Structures International Journal, Vol. 17, No. 2, 1991, pp. 127-139.

[91] Larder, R.A., "*The Stochastic Finite Element Simulation of Parallel Fiber Composites*", Journal of Composite Materials, Vol. 10, 1976, pp. 21-31.

[92] Wang, A.S.D., Chou, P.C. and Lei, S.C., "*A Stochastic Model for the Growth of Matrix Crack in Composite laminates*", Journal of Composite Materials, Vol. 18, 1984, pp. 239-254.

[93] Cassenti, B.N., "*Probabilistic Static Failure of Composite Material*", AIAA Journal, Vol. 22, No. 1, 1984, pp. 103-110.

[94] Fukunaga, H. and Chou, T.W., "*Probabilistic Failure Strength Analysis of Graphite/Epoxy Cross-Ply laminates*", Journal of Composite Materials, Vol. 18, 1984, pp. 339-351.

[95] Rosen, B.W., "*Tensile Failure of Fibrous Composite*", AIAA Journal, Vol. 2, No. 11, 1964, pp. 1985-1991.

[96] Zweben, C., "*Tensile failure of Fiber Composite*", AIAA Journal, Vol. 6, No. 12, 1968, pp. 2325-2332.

[97] Harlow, D.G. and Phoenix, S.L., "*The Chain of Bundles Probability Model for the Strength of Fibrous materials I: Analysis and Conjectures*", Journal of Composite Materials, Vol. 12, 1978, pp. 195-214.

[98] Harlow, D.G. and Phoenix, S.L., "*The Chain of Bundles Probability Model for the Strength of Fibrous materials II: A Numerical Study of Convergence*", Journal of Composite Materials, Vol. 12, 1978, pp. 314-334.

[99] Batdorf, S.B., "*Tensile Strength of Unidirectionally Reinforced Composites-I*", Journal of Reinforced Plastics and Composites, Vol. 1, 1982, pp. 153-164.

[100] Tamuzs, V.P., "*Some Peculiarities of Fracture in Heterogeneous Materials*", Fracture of Composite Materials, Edited by G.C. Sih and V.P. Tamuzs, Martinus Hijhoff, Boston, MA, 1982, pp. 131-137.

[101] Yushanov, S.P. and Joshi, S.P., "*Stochastic Modeling of Fracture Processes in Fiber Reinforced composites*", AIAA Journal, Vol. 33, No. 9, 1995, pp. 1689-1697.

[102] Contreras, H., "*The Stochastic Finite Element Method*", Int. J. for Computers and Structures, Vol. 12, 1980, pp. 341-348.

[103] Vanmarcke, E., Shinozuka, M., Nakagiri, S., Schueller, G.I., and Grigoriu, M., "*Random Fields and Stochastic Finite elements*", Structural Safety, Vol. 3, 1986, pp. 143-166.

[104] Benaroya, H., and Rehak, M., "*Finite Element Methods in Probabilistic Structural Analysis: A Selective Review*", Appl. Mech. Rev., Vol. 41, No. 5, May 1988, pp. 201-213.

[105] Yamazaki, F., Shinozuka, M., and Desgupta, G., "*Neumann Expansion for Stochastic Finite Element Analysis*", Journal of Engineering Mechanics, Vol. 114, No. 8, 1986, pp. 1335-1354.

[106] Ostoja-Starzewski, M., "*Micromechanics as a basis of Stochastic Finite Elements and Differences: An Overview*", Appl. Mech. Rev., Vol. 46, No. 2, November 1993, pp. S136-S147.

[107] Vanmarcke, E.H., "*Stochastic Finite Elements and Experimental Measurements*", Probabilistic Engineering Mechanics, Vol. 9, 1994, pp. 103-114.

[108] Bucher, C.G., and Brenner, C.F., "*Stochastic Response of Uncertain Systems*", Archives of Applied mechanics, Vol. 62, 1992, pp. 507-516.

[109] Iwan, W.D., and Jensen, H., "*On the Dynamic Response of Continuous Systems Including Model Uncertainty*", Journal of Applied Mechanics, Vol. 60, 1993, pp. 484-490.

[110] Koyluoglu, H.U., Nielsen, S.R.K., and Cakmak, A.S., "*Stochastic Dynamics of Geometrically Non-Linear Structures with Random Properties Subject to Stationary Random Excitation*", Journal of Sound and Vibration, Vol. 190, 1996, pp. 821-841.

[111] Ramu, S.A., and Ganesan, R., "*A Galerkin Finite Element Technique for Stochastic Field Problems*", Computer Methods in Applied Mechanics and Engineering, Vol. 105, 1993, pp. 315-331.

[112] Zhu, W.Q., Ren, Y.J., and Wu, W.Q., "*Stochastic FEM Based on Local Averages of Random vector Fields*", Journal of Engineering Mechanics, Vol. 118, No. 3, 1992, pp. 496-511.

[113] Jensen, H., and Iwan, W.D., "*Response of Systems with Uncertain Parameters to Stochastic Excitation*", Journal of Engineering Mechanics, Vol. 118, No. 5, 1992, pp. 1012-1025.

[114] Liu, W.K., Belytschko, T., and Mani, A., "*Applications of Probabilistic Finite Element Methods in Elastic/Plastic Dynamics*", Journal of Engineering for Industry, Vol. 109, 1987, pp. 2-8.

[115] Ghanem, R., and Spanos, P.D., "*Polynomial Chaos in Stochastic Finite Elements*", Journal of Applied Mechanics, Vol. 57, 1990, pp. 197-202.

[116] Ganesan, R., Sankar, T.S., and Ramu, S.A., "*Non-Conservatively Loaded Stochastic Columns*", Int. J. Solids Structures, Vol. 30, No. 17, 1993, pp. 2407-2424.

[117] Shinozuka, M., Kako, T., and Tsurui, A., "*Random Vibration Analysis in Finite Element Formulation*", Random vibration – status and recent development, Ed. I. Elishakoff and R.H. Lyon, Elsevier, NewYork, 1986.

[118] Ramu, S.A., and Ganesan, R., "*Free Vibration of a Stochastic Beam-Column using Stochastic FEM*", Int. J. for Computers and Structures, Vol. 41, No. 5, 1991, pp. 987-994.

[119] Ren, Y.J., Elishakoff, I., and Shinozuka, M., "*Finite Element Method for Stochastic Beams based on Variational Principles*", Journal of Applied Mechanics, Vol. 64, 1997, pp. 664-669.

[120] Sankar, T.S., Ramu, S.A., and Ganesan, R., "*Variability of SIF and COD of Stochastic Structural Systems*", Int. J. for Computers and Structures, Vol. 43, No. 6, 1992, pp. 1135-1145.

[121] Sankar, T.S., Ramu, S.A., and Ganesan, R., "*Stochastic Finite Element Analysis for High Speed Rotors*", Journal of Vibration and Acoustics, Vol. 115, 1993, pp. 59-64.

[122] Liaw, D.G., and Yang, H.T.Y., "*Reliability of Initially Compressed uncertain Laminated Plates in Supersonic Flow*", AIAA Journal, Vol. 29, No. 6, 1991, pp. 952-945.

[123] Ganesan, R., and Hoa, S.V., "*Stochastic Finite Element Analysis of Composite Structures*", CANCAM 95, 15th Canadian Congress of Applied Mechanics, May 95, Victoria, Canada.

[124] Nakagiri, S., Takabatake, H., and Tani, S., "*Uncertain Eigenvalue Analysis of Composite Laminated Plates by the Stochastic Finite Element Method*", Journal of Engineering for Industry, Vol. 109, 1987, pp. 9-12.

[125] Engelstad, S.P., and Reddy, J.N., "*Probabilistic Nonlinear Finite Element Analysis of Composite Structures*", AIAA Journal, Vol. 31, No. 2, 1993, pp. 362-369.

[126] Chang, C., and Yang, H.T.Y., "*Reliability of Uncertain Flexible Laminated Skewed Plates under Random Compressions*", AIAA Journal, Vol. 30, No. 2, 1992, pp. 464-472.

[127] Slattery, K., "*A Random-damage Finite Element for Modeling Failure in Advanced Composite Materials*", Composite Materials: Fatigue and Fracture, Vol. 5, Ed. R.H. Martin, ASTM, Philadelphia, 1995, pp. 231-245.

[128] Roebuck, B., and Lord, K., "*Plane strain fracture toughness test for particulate metal matrix composites*", Materials Science and Technology, Vol. 6., 1990, pp. 1199-1209.

[129] Kageyama, K., "*Fracture Mechanics of Notched Carbon/Epoxy Laminates*", Application of Fracture Mechanics to Composite Materials, Edited by K. Friedrich, 1989, pp. 327-396.

[130] Chatterjee, Sailendra N., "*Analysis of Test Specimens for Interlaminar Mode II Fracture Toughness, Part I. Elastic Laminates*", Journal of Composite Materials, Vol. 25, 1991, pp. 470-511.

[131] Yokoyama, T., "*Determination of Dynamic Fracture-Initiation Toughness Using a Novel Impact Bend Test Procedure*", Journal of Pressure Vessel Technology, Vol. 115, 1993, pp. 389-397.

[132] Kumar, A. M., Hirth, J. P., Hoagland, R., and Feng, X., "*A Suggested Test Procedure to Measure Mixed Mode I-III Fracture Toughness of Brittle Materials*", Journal of Testing and Evaluation, Vol. 22, 1994, pp. 327-334.

[133] Ono, T., and Kaji, M., "*Fracture Toughness of Structural Ceramics Under Biaxial Stress State by Anticlastic Bending Test*", Journal of Engineering for Gas Turbines and Power, Vol. 119, 1997, pp. 7-14.

[134] Shivkumar, K. N., Crews, J. H. : Jr., and Avva, V. S., "*Modified Mixed-Mode Bending Test Apparatus for Measuring Delamination Fracture Toughness of*

Laminated Composites", Journal of Composite Materials, Vol. 32, 1998, pp. 804-828.

[135] Iwadate, T., Tanaka, Y., and Takemata, H., "*Prediction of Fracture Toughness K_{IC} Transition Curves of Pressure Vessel Steels From Charpy V-Notch Impact Test Results*", Journal of Pressure Vessel Technology, Vol. 116, 1994, pp. 353-358.

[136] Sriharsha, H. K., Anantharaman, S., and Chatterjee, S., "*A Computer Program to Aid in Fatigue Precracking of Fracture Toughness Test Specimens*", Journal of testing and Evaluation, Vol. 26, 1998, pp. 513-518.

[137] Miki, M., Murotsu, Y., Tanaka, T., and Shao, S., "*Reliability of Unidirectional Fibrous Composites*", AIAA Journal, Vol. 28, 1990, pp. 1980-1986.

[138] Miki, M., and Murotsu, Y., Tanaka, T., "*Optimum Fiber Angle of Unidirectional Composites for Load with Variations*", AIAA Journal, Vol. 30, 1992, pp. 189-196.

[139] Shao, S., Miki, M., and Murotsu, Y., "*Optimum Fiber Orientation Angle of Multiaxially Laminated Composites Based on Reliability*", AIAA Journal, Vol. 31, 1993, pp. 919-920.

[140] Miki, M., Murotsu, Y., and Murayama, N., "*Application of Lamination Parameters to Reliability-Based Stiffness Design of Composites*", AIAA Journal, Vol. 31, 1993, pp. 1938-1945.

[141] Kogiso, N., Shao, S., and Murotsu, Y., "*Effect of Correlation on Reliability-Based Design of Composites Plate for Buckling*", AIAA Journal, Vol. 36, no. 9, 1998, pp. 1706-1713.

[142] Thomas, D. J., and Wetherhold, R. C., "*Reliability Analysis of Ceramic Matrix Composite Laminates*", Journal of Engineering for Gas Turbines and Power, Vol. 115, 1993, pp. 117-121.

[143] Cohen, David, "*Application of Reliability and Fiber Probabilistic Strength Distribution Concepts to Composite Vessel Burst Strength Design*", Journal of Composite Materials, Vol. 26, 1992, pp. 1984-2014.

[144] Haque, Md. Zaki-ul, "*A combined experimental and stochastic finite element analysis methodology for the probabilistic fracture behavior of composite laminates*", Concordia University, 1999.

[145] Rice, J. R., "*A Path Independent Integral and some Approximate Analysis of Strain Concentration by Notches and Cracks*", Journal of Applied Mechanics, Vol. 35, 1968, pp. 379-386.

[146] Reddy, J.N., "*An Introduction to the Finite Element Method*", 2nd edition, McGraw-Hill, New York, 1993.

[147] Daniel, I.M., and Ishai, O., "*Engineering Mechanics of Composite Materials*", Oxford University Press, Oxford, 1994.

[148] Hyer, M.W., "*Stress Analysis of Fiber-Reinforced Composite Materials*", McGraw-Hill, New York, 1998.

[149] Siddall, J. N., "*Probabilistic engineering design : principles and applications*", M. Dekker, New York, , 1983.

[150] Richard, W.H., "*Deformation and Fracture Mechanics of Engineering Materials*", 4th Ed., John Wiley, NewYork, 1996.

[151] Ewalds, H.L., and Wanhill, R.J.H., "*Fracture Mechanics*", Edward Arnold Publishers, Maryland, 1986.

[152] Barsoum, R.S., "*On the use of Isoparametric Finite Elements in Linear Fracture Mechanics*", Int. J. Num. Meth. Engng., Vol. 10, 1976, pp. 537-545.

[153] Henshell, R.D., and Shaw, K.G., "*Crack Tip Elements are Unnecessary*", Int. J. Num. Meth. Engng., Vol. 9, 1975, pp. 495-509.

[154] Hellen, T.K., "*On the Method of Virtual Crack Extensions*", Int. J. Num. Meth. Engng., Vol. 9, 1975, pp. 187-208.

[155] D3039, "*Standard Test Method for Tensile Properties of Fiber-Resin Composites*", Annual Book of ASTM Standard, 1989, pp. 118-122.

[156] D3518, "*Standard Practice for In-Plane Shear Stress-Strain Response of Unidirectional Polymer matrix Composite*", Annual Book of ASTM Standard, 1991, pp. 114-148.

[157] Vanmarcke, E., "*Random Fields: Analysis and Synthesis*", MIT Press, Cambridge, 1983.

[158] Shigley, J.E., and Mischke, C.R., "*Mechanical Engineering Design*", 5th edition, McGraw-Hill, NewYork, 1989.

[159] Chang-Sik Ha, Youngkyoo Kim, and Won-Jei Cho, "*Fracture toughness investigation of dynamically vulcanized EPDM/PP/ionomer ternary blends using the J-integral via the locus method*", Journal of Materials Science, Vol. 31, 1996, pp. 2917-2924.

[160] Li Dongming, Zheng Wenge, and Qi Zongneng, "*The J-integral fracture toughness of PP/$CaCO_3$ composites*", Journal of Materials Science, Vol. 29, 1994, pp. 3754-3758.

[161] Eck, S. J., and Ardell, A. J., "*Fracture Toughness of Polycrystalline NiAl from Finite-Element Analysis of Miniaturized Disk-Bend Test Results*", Metallurgical and Materials Transactions. Part A, Physical Metallurgy and Materials Science, Vol. 28A, 1997, pp. 991-996.

[162] Kam, T. Y., Chu, K. H., and Chang, E. S., "*Reliability Assessment of Laminated Composite Plates with Random Strength Parameters*", AIAA Journal, Vol. 37, no. 12, 1999, pp. 1648-1655.

[163] Mahadevan, S., and Liu, X., "*Probabilistic Optimum Design of Composite Laminates*", Journal of Composite Materials, Vol. 32, no. 1, 1998, pp. 68-82.

[164] Thomas, D. J., and Wetherhold, R. C., "*Reliability Analysis of Composite Laminates with Load Sharing*", Journal of Composite Materials, Vol. 25, 1991, pp. 1459-1475.

[165] Mishra, K. B., "*Reliability Analysis and Prediction*", Elsevier, 1992.